

Transition Metal Complexes of Tridentate Bisphenol Ligands and Their Reactivity towards Organic Substrates

Dissertation for the degree of
Doktor der Naturwissenschaft
in the Fakultät für Naturwissenschaften
(Department Chemie)
at the Universität Paderborn

presented by

Tapan Kanti Paine

Mülheim an der Ruhr 2002

To the memory of my mother

This work was independently carried out between December 1999 and November 2002 at the
Max-Planck-Institut für Strahlenchemie, Mülheim an der Ruhr, Germany.

Papers published:

1. T. K. Paine, T. Weyhermüller, K. Wieghardt, P. Chaudhuri;
The Methanol-Methanolate $\text{CH}_3\text{OH}\dots\text{OCH}_3^-$ Bridging Ligand: Tuning of Exchange Coupling
by Hydrogen Bonds in Dimethoxo-Bridged Dichromium(III) Complexes.
Inorg. Chem. **2002**, 41, 6538.

2. T. Weyhermüller, T. K. Paine, E. Bothe, E. Bill, P. Chaudhuri;
Complexes of an Aminebis(phenolate) [O,N,O] Donor Ligand and EPR Studies of
Isoelectronic, Isostructural Cr(III) and Mn(IV) Complexes.
Inorg. Chim. Acta **2002**, 337, 344.

Examination Committee:

Prof. Dr. K. Huber

Prof. Dr. N. Risch

Prof. Dr. G. Henkel

Prof. Dr. P. Chaudhuri

Examination: January 10th, 2003

Acknowledgements

I would like to acknowledge everyone who extended their support and help during the course of this work. My deep sense of gratitude goes to:

- Prof. Dr. P. Chaudhuri, who introduced me to the research area of coordination chemistry and taught me the way of scientific thinking, for his encouragement, invaluable guidance, continuous support and hour-long discussions. He shared his wealth of experience in numerous occasions and this had provided me with a great learning experience.
- Prof. Dr. K. Wieghardt, for the opportunity of working in his research group, for providing me with all laboratory facilities when needed.
- Dr. T. Weyhermüller and Mrs. H. Schucht for their elegant work with the X-ray crystallography.
- Dr. E. Bothe and Mrs. P. Höfer for their help during electrochemical measurements.
- Dr. E. Bill, Mr. A. Göbels, Mr. F. Reikowski and Mr. B. Mienert for discussions and measurements of EPR, SQUID and Mössbauer.
- Dr. E. Rentschler for assistance with the fitting of magnetochemical data.
- Dr. F. Neese, for help with his EPR simulation program.
- Mr. U. Pieper and Mrs. R. Wagner for their help in the laboratory.
- Mrs. U. Westhoff, Mrs. G. Schmidt and Mrs. M. Trinoga for skilful GC and LC analyses.
- Dr. U. Beckmann, Dr. C. N. Verani, Dr. R. Schumacher, Dr. S. Kimura, Dr. L. Slep, Dr. H. Chun, Dr. D. R. Van Staveren for their interest, friendship and good suggestions during this work.
- Mr. S. Mukherjee, Mr. K. Ray, Dr. D. Ray, Mr. S. Khanra, Mrs. R. Kapre, Mr. K. S. Min for a nice atmosphere in- and outside the laboratory.
- My father, brothers, sister-in-laws for their constant inspiration and encouragement.
- My nephew Suparno and niece Tanisha for their smiling face.
- My wife Sudipta for her understanding, inspiration, invaluable support and having faith in me.
- Deutsche Forschungsgemeinschaft (DFG) and Max-Planck-Gesellschaft (MPG) for financial support.

CONTENTS

Chapter 1

OBJECTIVES AND LIGANDS INVOLVED

| | | |
|-----|------------------------|----|
| 1.1 | OBJECTIVES | 03 |
| 1.2 | THEORETICAL BACKGROUND | 05 |
| 1.3 | LIGAND SYNTHESIS | 11 |
| | References | 16 |

Chapter 2

NON-OXO VANADIUM (IV) AND OXO-VANADIUM(V) COMPLEXES OF BISPHENOL LIGANDS

| | | |
|-------|--|----|
| 2.1 | INTRODUCTION | 23 |
| 2.2 | SYNTHESIS | 24 |
| 2.3 | INFRARED SPECTROSCOPY | 27 |
| 2.4 | MASS SPECTROSCOPY | 28 |
| 2.5 | X-RAY CRYSTAL STRUCTURE | 29 |
| 2.5.1 | Molecular structure of VL^S_2 (1) | 29 |
| 2.5.2 | Molecular structure of VL^{Se}_2 (2) | 31 |
| 2.5.3 | Molecular structure of VL^P_2 (3) | 31 |
| 2.5.4 | Molecular structure of VL^{PO}_2 (4) | 32 |
| 2.5.5 | Molecular structure of VL^N_2 (5) | 34 |
| 2.5.6 | Molecular structure of VL^{N1}_2 (6) | 36 |
| 2.5.7 | Molecular structure of $[VO(L^{PO})(HL^{PO})]$ (7) | 36 |
| 2.5.8 | Molecular structure of $[VOL^{Se}(\mu-OH)]_2$ (8) | 38 |
| 2.6 | ELECTRONIC SPECTROSCOPY | 39 |
| 2.7 | MAGNETISM | 41 |
| 2.8 | ELECTRO- AND SPECTROELECTROCHEMISTRY | 42 |
| 2.9 | EPR SPECTROSCOPY | 50 |
| 2.10 | ^{51}V NMR SPECTROSCOPY | 55 |
| | References | 57 |

Chapter 3

COORDINATION PROPERTIES OF BISPHENOLATE LIGANDS

WITH TRANSITION METAL IONS (Cr^{III} , Mn^{III} , Mn^{IV} , Fe^{III} AND Ni^{II})

| | |
|--|-----------|
| 3.1 INTRODUCTION | 61 |
| 3.2 CHROMIUM(III) COMPLEXES OF $\text{H}_2\text{L}^{\text{X}}$ ($\text{X} = \text{S}, \text{Se}$) | 61 |
| 3.2.1 SYNTHESIS | 62 |
| 3.2.2 INFRARED AND MASS SPECTROSCOPY | 62 |
| 3.2.3 X-RAY CRYSTAL STRUCTURE | 63 |
| 3.2.3.1 Molecular structure of $[\text{CrL}^{\text{Se}}(\mu\text{-OMe})(\text{MeOH})]_2$ (9) | 63 |
| 3.2.3.2 Molecular structure of | |
| $\text{Bu}_4\text{N}[\text{Cr}_2\text{L}^{\text{Se}}_2(\mu\text{-OMe})_2(\text{MeOH})(\text{OMe})]$ (10) | 65 |
| 3.2.3.3 Molecular structure of $[\text{CrL}^{\text{S}}(\mu\text{-OMe})(\text{MeOH})]_2$ (11) | 66 |
| 3.2.3.4 Molecular structure of | |
| $\text{Bu}_4\text{N}[\text{Cr}_2\text{L}^{\text{S}}_2(\mu\text{-OMe})_2(\text{MeOH})(\text{OMe})]$ (12) | 68 |
| 3.2.4 ELECTRONIC SPECTROSCOPY | 68 |
| 3.2.5 MAGNETISM | 70 |
| 3.3 MANGANESE(III/ IV) AND IRON(III) COMPLEXES | |
| OF $\text{H}_2\text{L}^{\text{X}}$ ($\text{X} = \text{S}, \text{Se}$) | 72 |
| 3.3.1 SYNTHESIS | 72 |
| 3.3.2 INFRARED AND MASS SPECTROSCOPY | 74 |
| 3.3.3 X-RAY CRYSTAL STRUCTURE | 74 |
| 3.3.3.1 Molecular structure of $[\text{Mn}^{\text{III}}\text{L}^{\text{Se}}(\mu\text{-OMe})(\text{MeOH})]_2$ (13) | 75 |
| 3.3.3.2 Molecular structure of $[\text{Mn}^{\text{IV}}\text{L}^{\text{Se}}_2]$ (15) | 76 |
| 3.2.3.3 Molecular structure of $[\text{Mn}^{\text{IV}}\text{L}^{\text{S}}_2]$ (17) | 78 |
| 3.3.3.4 Molecular structure of $[\text{Fe}^{\text{III}}\text{L}^{\text{Se}}(\mu\text{-OMe})(\text{MeOH})]_2$ (18) | 79 |
| 3.3.3.5 Molecular structure of $\text{Bu}_4\text{N}[\text{Fe}^{\text{III}}\text{L}^{\text{Se}}_2]$ (19) | 81 |
| 3.3.3.6 Molecular structure of $\text{Bu}_4\text{N}[\text{Fe}^{\text{III}}\text{L}^{\text{Se}}\text{L}^{\text{Se}'}]$ (20) | 83 |
| 3.3.4 ELECTRONIC SPECTROSCOPY | 84 |
| 3.3.5 MAGNETISM | 86 |
| 3.3.6 ELECTROCHEMISTRY | 89 |
| 3.3.7 EPR SPECTROSCOPY | 95 |
| 3.3.8 MÖSSBAUER SPECTROSCOPY | 97 |
| 3.3.9 REACTIVITY STUDIES | 98 |

| | |
|--|------------|
| 3.4 POLYNUCLEAR NICKEL(II) COMPLEXES OF BISPHENOL LIGANDS | 100 |
| 3.4.1 SYNTHESIS | 100 |
| 3.4.2 INFRARED AND MASS SPECTROSCOPY | 101 |
| 3.4.3 X-RAY CRYSTAL STRUCTURE | 102 |
| 3.4.3.1 Molecular structure of | |
| $[\text{Ni}_4\text{L}^{\text{Se}}_2(\mu\text{-OMe})_4(\text{MeOH})_4(\text{MeCN})_2]$ (23) | 102 |
| 3.4.3.2 Molecular structure of | |
| $[\text{Ni}_5\text{L}^{\text{N}}_4(\mu_3\text{-OH})_2(\mu\text{-H}_2\text{O})_2(\text{EtOH})_2]$ (24) | 104 |
| 3.4.3.3 Molecular structure of | |
| $[\text{Ni}_6\text{L}^{\text{N}}_4(\mu\text{-MeOH})(\mu_3\text{-OMe})_2(\text{MeOH})_2(\text{MeCN})_2]$ (25) | 107 |
| 3.4.4 MAGNETISM | 109 |
| References | 118 |

Chapter 4

SYNTHESIS, CHARACTERIZATION AND REACTIVITY STUDY OF COPPER(II) COMPLEXES OF SELENOBISPHENOL LIGAND

| | |
|--|------------|
| 4.1 INTRODUCTION | 123 |
| 4.2 SYNTHESIS | 123 |
| 4.3 INFRARED AND MASS SPECTROSCOPY | 126 |
| 4.4 X-RAY CRYSTAL STRUCTURE | 126 |
| 4.4.1. Molecular structure of $[\text{CuL}^{\text{Se}}(\text{Et}_3\text{N})]$ (26) | 126 |
| 4.4.2. Molecular structure of $[\text{CuL}^{\text{Se}}(\text{Et}_2\text{NH})]$ (27) | 127 |
| 4.4.3. Molecular structure of $[\text{CuL}^{\text{Se}}(\text{PhCH}_2\text{NH}_2)]_2$ (29) | 128 |
| 4.4.4. Molecular structure of $[\text{L}^{\text{Se}}_2(\text{HL}^{\text{Se}})\text{Cu}_3(\mu\text{-OH})(\text{MeCN})]$ (30) | 130 |
| 4.4.5. Molecular structure of $[\text{L}^{\text{Se}}_2(\text{HL}^{\text{Se}})\text{Cu}_3(\mu\text{-OMe})(\text{MeOH})]$ (31) | 133 |
| 4.4.6. Molecular structure of $[\text{L}^{\text{Se}1}_2\text{Cu}_2]$ (32) | 134 |
| 4.5 ELECTRONIC SPECTROSCOPY | 136 |
| 4.6 MAGNETISM | 137 |
| 4.7 EPR SPECTROSCOPY | 140 |
| 4.8 REACTIVITY STUDIES | 142 |
| 4.8.1 Amine oxidation | 144 |
| 4.8.2 Alcohol oxidation | 146 |
| References | 149 |

Chapter 5

TRANSITION METAL COMPLEXES OF AN AMINE BISPHENOL LIGAND WITH [O,N,O] DONOR SET

| | |
|--|------------|
| 5.1 INTRODUCTION | 153 |
| 5.2 SYNTHESIS | 153 |
| 5.3 INFRARED SPECTROSCOPY | 154 |
| 5.4 MASS SPECTROSCOPY | 154 |
| 5.5 ELECTRONIC SPECTROSCOPY | 155 |
| 5.6 X-RAY CRYSTAL STRUCTURE | 156 |
| 5.6.1 Molecular structure of $[\text{Mn}^{\text{IV}}\text{L}_2^{\text{N}}]$ (34) | 156 |
| 5.6.2 Molecular structure of $[\text{Mn}^{\text{III}}\text{L}_2^{\text{N}}]^-$ (35) | 158 |
| 5.6.3 Molecular structure of $\text{Bu}_4\text{N}[\text{Cr}^{\text{III}}\text{L}_2^{\text{N}}]$ (36) | 160 |
| 5.7 ELECTROCHEMISTRY | 162 |
| 5.8 MAGNETISM | 164 |
| 5.9 EPR SPECTROSCOPY | 165 |
| 5.10 SOLUTION STUDY | 168 |
| References | 173 |

Chapter 6

| | |
|-------------------------------------|------------|
| CONCLUSIONS AND PERSPECTIVES | 175 |
|-------------------------------------|------------|

Chapter 7

EQUIPMENT AND EXPERIMENTAL WORK

| | |
|-----------------------------------|------------|
| 7.1 METHODS AND EQUIPMENTS | 185 |
| 7.2 SYNTHESIS | 188 |
| 7.2.1 LIGANDS | 188 |
| 7.2.2 COMPLEXES | 196 |
| 7.3 REACTIVITY STUDIES | 228 |

Appendices

| | |
|---------------------------------|------------|
| 1) Crystallographic data | 233 |
| 2) Magnetochemical data | 244 |
| 3) Curriculum Vitae | 278 |

Abbreviations:

technical terms:

AF : antiferromagnetic

Ag / AgNO₃ : reference electrode

av. : average

B : magnetic field

CT : charge transfer

D : zero-field splitting

deg. : degree (°)

e⁻ : electron

E : total energy

exp. : experimental

F : ferromagnetic

fac. : facial

Fc⁺/Fc : internal electrochemical standard

g : Landé factor

H : Hamiltonian

h.s. : high-spin

I : nuclear spin

J : coupling constant (cm⁻¹)

KD : Kramer doublet

LF : ligand field

m/z : mass per charge

[M]⁺: molecular ion peak

mer.: meridional

MP : melting point

PI : paramagnetic impurity

RT : room temperature (293K)

S : electron spin

SCE : standard calomel electrode

sh. : shoulder

sim. : simulated

TIP : temperature independent paramagnetism

TON : turnover number

techniques:

CV : cyclic voltammetry

EA : elemental analysis

EI : electron ionisation

EPR : electron paramagnetic resonance

ESI : electrospray ionisation

GC : gas chromatography

HPLC : high performance liquid chromatography

IR : infrared spectroscopy

LC : liquid chromatography

MS: mass spectroscopy

NMR : nuclear magnetic resonance

SQUID : superconducting quantum interface device

SW : square wave voltammetry

TLC : thin layer chromatography

UV-Vis : ultraviolet-visible spectroscopy

units:

Å : angstrom (10^{-10} m)

cm : centimetre

emu : electromagnetic unit

G : gauss

h : hour

K : Kelvin

m : meter

M : molar

min. : minute

mm : millimeter

nm : nanometer (10^{-9} m)

ppm : part per million

s : second

T : tesla

V : volts

μ_B : bohr magnetron

latin expressions:

ca. : around

et al : and coworkers

e.g. : for example

i.e. : namely

tert- : tertiary

vs. : versus, against

symbols:

λ : wavelength (nm)

ϵ : extinction coefficient ($\text{M}^{-1}\text{cm}^{-1}$)

μ_{eff} : magnetic moment (μ_{B})

ΔE_{Q} : quadrupole splitting (mm/s)

δ : isomer shift (mm/s)

solvents and reagents:

acac : acetylacetone

PhCH_2NH_2 : benzylamine

$^t\text{BuNH}_2$: *tert*-butylamine

Bu_4NOMe : tetrabutylammoniummethoxide

Bu_4NOH : tetrabutylammoniumhydroxide

BuLi : butyllithium

cat.: catechol

CH_2Cl_2 : dichloromethane

CHCl_3 : chloroform

Et_2O : diethylether

Et_2NH : diethylamine

$\text{EtN}(\text{}^i\text{Pr})_2$: diisopropylethylamine

Et_3N : triethylamine

EtOH : ethanol

HCl : hydrogen chloride

H_2O_2 : hydrogen peroxide

KBr : potassium bromide

LiOMe : lithium methoxide

LiOEt : lithium ethoxide
 MeCN : acetonitrile
 MeNH₂ : methylamine
 MeOH : methanol
ⁱPrOH : isopropanol
 sal. : salicaldehyde
 TBAPF₆ : tetrabutylammonium hexafluorophosphate
 THF : tetrahydrofuran
 TMS : trramethylsilane
 [9]-aneN₃ : triazacyclononane

ligands used in this work:

H₂L^{Se} : 2, 2'-Selenobis(4, 6-di-*tert*-butylphenol)
H₂L^S : 2, 2'-Thiobis(4, 6-di-*tert*-butylphenol)
H₂L^P : 2, 2'-Phenylphosphinebis(4, 6-di-*tert*-butylphenol)
H₂L^{PO} : 2, 2'-Phenylphosphineoxidebis(4, 6-di-*tert*-butylphenol)
H₂L^N : Methylamino-N, N-bis(2-methylene 4, 6-dimethylphenol)
H₂L^{N1} : Methylamino-N, N-bis(2-methylene 4, 6-di-*tert*-butylphenol)
H₂L^{Se-Se} : 2, 2'-Diselenobis(4, 6-di-*tert*-butylphenol)
H₂L^{S-S} : 2, 2'-Dithiobis(4, 6-di-*tert*-butylphenol)

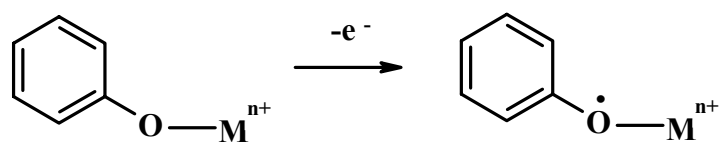
List of complexes synthesized with their numbers:

| | |
|--|------------|
| VL^S₂ | (1) |
| VL^{Se}₂ | (2) |
| VL^P₂ | (3) |
| VL^{PO}₂ | (4) |
| VL^N₂ | (5) |
| VL^{N1}₂ | (6) |
| [VO(L^{PO})(HL^{PO})] | (7) |
| [VOL^{Se}(μ-OH)₂] | (8) |
| [CrL^{Se}(μ-OMe)(MeOH)₂] | (9) |

| | |
|---|-------------|
| Bu₄N[Cr₂L^{Se}₂ (μ-OMe)₂(MeOH)(OMe)] | (10) |
| [CrL^S(μ-OMe)(MeOH)]₂ | (11) |
| Bu₄N[Cr₂L^S₂ (μ-OMe)₂(MeOH)(OMe)] | (12) |
| [MnL^{Se}(μ-OMe)(MeOH)]₂ | (13) |
| Bu₄N[MnL^{Se}₂] | (14) |
| [MnL^{Se}₂] | (15) |
| [MnL^S(μ-OMe)(MeOH)]₂ | (16) |
| [MnL^S₂] | (17) |
| [FeL^{Se}(μ-OMe)(MeOH)]₂ | (18) |
| Bu₄N[FeL^{Se}₂] | (19) |
| Bu₄N[FeL^{Se}L^{Se'}] | (20) |
| Bu₄N[FeL^SL^{S'}] | (21) |
| [Ni₄L^S₂ (μ-OMe)₄(MeOH)₄(MeCN)₂] | (22) |
| [Ni₄L^{Se}₂ (μ-OMe)₄(MeOH)₄(MeCN)₂] | (23) |
| [Ni₅L^N₄ (μ₃-OH)₂(μ-H₂O)₂(EtOH)₂] | (24) |
| [Ni₆L^N₄ (μ-MeOH)(μ₃-OMe)₂(MeOH)₂(MeCN)₂] | (25) |
| [Cu L^{Se}(Et₃N)] | (26) |
| [CuL^{Se}(Et₂NH)] | (27) |
| [CuL^{Se}(^tBuNH₂)] | (28) |
| [CuL^{Se}(PhCH₂NH₂)]₂ | (29) |
| [L^{Se}₂ (HL^{Se})Cu₃(μ-OH)(MeCN)] | (30) |
| [L^{Se}₂ (HL^{Se})Cu₃(μ-OMe)(MeOH)] | (31) |
| [L^{Se1}₂Cu₂] | (32) |
| Bu₄N[FeL^N₂] | (33) |
| [MnL^N₂] | (34) |
| Bu₄N[MnL^N₂] | (35) |
| Bu₄N[CrL^N₂] | (36) |

Chapter 1

OBJECTIVES AND LIGANDS INVOLVED



1.1 OBJECTIVES

The study of the binding modes of biologically relevant ligands to various transition metals has proved to be one of the hottest areas of research in bioinorganic chemistry. It is well known that transition metal ions comprise the active sites of certain enzymes, providing good binding site for substrates and thereby activating the appropriate bonds of the substrates. They have the unique property of attaining variable oxidation states, can act as a reservoir for electrons by accepting and donating electrons during redox cycles and stabilize appropriate amino acid radicals, e.g., phenoxyl radical in tyrosine residue, thiyl radical in cysteine residue etc.

The realization of the widespread occurrence of amino-acid radicals in enzyme catalysis has recently been documented in the literature.¹ Among the catalytically essential redox-active amino acids glycyl (e.g., anaerobic class III ribonucleotide reductase² and pyruvate formate lyase³), tryptophanyl (e.g., cytochrome peroxidase⁴), cysteinyl (class I and II ribonucleotide reductase¹), tyrosyl (e.g., class I ribonucleotide reductase,⁵ photosystem II,⁶ prostaglandin H synthase⁷) and modified tyrosyl (e.g., cytochrome c oxidase,⁸ galactose oxidase,⁹ glyoxal oxidase¹⁰) are the most prevalent.

Enzymes containing amino acid radicals are generally associated with transition metal ions, such as iron, manganese, cobalt or copper. In some instances, the metal is absent; it is apparently replaced by redox-active organic cofactors such as S-adenosylmethionine or flavins. Functionally, their role is analogous to that of the metal ions in metalloproteins.

The metal ions in active sites help to generate and stabilize the amino acid radicals and the radical in turn initiates catalysis by abstracting a hydrogen atom from the substrate. The function of the metal site in the oxygen-dependent radical enzymes galactose oxidase, ribonucleotide reductase and cytochrome c oxidase is *inter alia* to bind O₂ in their reduced forms which undergo the appropriate redox-chemistry to generate a metal-bound, activated oxygen species of variable nature.

The recent continuing development in the coordination chemistry of phenol containing ligands¹¹ is mainly because of the discovery of the tyrosine radicals in various metalloproteins involved in oxygen dependent enzymatic catalysis.¹² The synthetic analogue of the tyrosine radical is the phenoxyl radical, and phenol containing ligand systems have potential ability to form one-electron oxidized phenoxyl radical complexes.

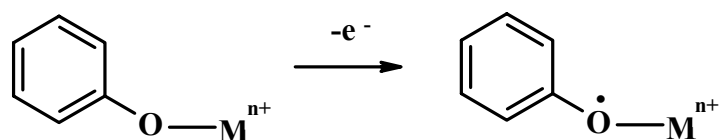


Figure 1.1.1 Formation of phenoxyl radical.

This led the bioinorganic chemists to design and synthesize transition metal complexes of different phenol-containing ligands in developing homogeneous catalysts¹³ and sometimes mimicking the structural and/or functional aspect of metalloenzymes. One of the major advantages of homogeneous catalysis is the possibility of fine-tuning the catalyst by varying the ancillary ligand. In this way, chemo-, regio- and stereo-selectivity can be directed toward the desired products. One way to achieve this is by changing the donor atoms in ligands, e. g. nitrogen, oxygen, phosphorus, sulphur etc, and a more subtle way is to change the substituents on the ligands, influencing the metal center of the complexes electronically and/or sterically. An additional advantage of the ligands with heterodonor sets is that the hardness/softness of the ligand can be adjusted so as to accommodate variations in the hardness/softness property of the metal ion.

The major objective of this thesis is to study the different heterodonor containing bisphenol ligands in stabilizing various chelate rings with transition metal ions. Different heterodonor and ring substituents have profound effects on the electrode potential and chelate ring size to form a variety of complexes. First row transition metal complexes of different heterodonor (N, S, Se, P, PO) bisphenol ligands have been studied in this work to establish the coordinating properties of the ligand system. Phenoxyl radicals are generally transient reactive species and the metal-oxygen bond of a coordinated phenoxyl is expected to be significantly weaker than the corresponding metal-oxygen bond of a bound phenolate because the π -donating properties of neutral phenoxyls are reduced as compared to those of anionic phenolates. With increasing electron density and tendency to form less covalently bonded complexes from left to right of the first row transition metal ions, ease of formation of phenoxyl radical complexes decreases. This tendency is established by studying the reactivity of the complexes with suitable substrates.

This work presents an in-depth study of transition metal complexes of bisphenol ligands and their reactivity study to explain their unique structural, electronic and magnetochemical properties. A part of this work explains the effect of π -donation of ligands to stabilize the higher oxidation state of the early transition metal ions and subsequent effect of ring size on

the electrode potential and electronic state. Similarly the ligation property of the bisphenolate ligand with other first row transition metal ions also provides a diverse output. The last part of this thesis demonstrates the formation of phenoxyl radicals as reactive intermediates by their reactions with various substrates. This work is undertaken to represent a fundamental research having implications for the understanding of the ligating properties of bisphenolate ligands towards 3d transition metal ions as well as to mimic some biological functions.

1.2 THEORETICAL BACKGROUND

Prior to 1975, reports of complexes with ‘non-innocent’ ligands such as quinones, semiquinones and catechols were rare. More recently, polyradical complexes have started to be used in the field of molecular magnets.¹⁴ Phenoxyl metal ion complexes now constitute a well-established class of coordination compounds because of the involvement of the phenoxyl radical in catalytic biological functions of some metalloenzymes. This has inspired the bioinorganic chemists to synthesize most successfully the functional and/or structural mimics of the related metalloenzymes.¹² One of the most intensively investigated biomolecules is Galactose Oxidase, which catalyses the oxidation of primary alcohols to aldehydes in the presence of aerial oxygen. The phenoxyl radical is stabilized as an essential component, forming an antiferromagnetically (AF) coupled phenoxyl radical-copper active site. Nature has designed the active site in the enzyme in order to perform a hydrogen-atom abstraction reaction from the α -carbon atom of an O-bound alcoholate.

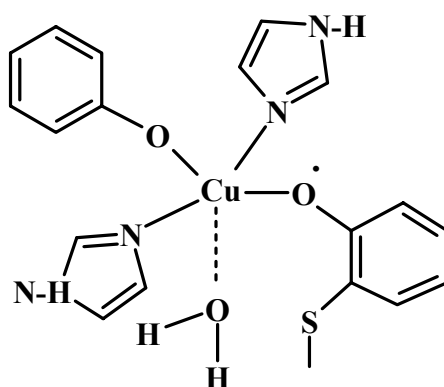


Figure 1.2.1 Schematic representation of the active site of Galactose Oxidase (GO).

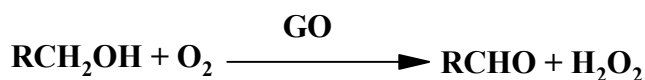


Figure 1.2.2 Reactivity of Galactose Oxidase.

The search for low molecular weight phenoxyl Cu(II) complexes as functional models for GO, which would mimic this reactivity, had a promising start in 1996 when Tolman and co-workers^{11a} reported a stoichiometric oxidation of benzyl alcohol to benzaldehyde by a phenoxyl radical complex. In the same year Wang and Stack^{11b} reported first a truly catalytic system, which in presence of a base and an oxidizing agent oxidizes benzyl alcohol to benzaldehyde up to 10 turnovers. A different system has been described by Pierre and co-workers in 1998.^{11c} They showed that the electrochemically one-electron oxidized phenoxyl radical complex electrocatalyzes, in the presence of KOH, the oxidation of primary alcohols to the corresponding aldehydes (where > 30 turnovers were observed).

A breakthrough was reported by Stack and coworkers¹⁵ in 1998 by describing the first biomimetic catalytic system for the oxidation of primary alcohols by air. Independently, in the same year Chaudhuri *et al*^{13a} reported efficient aerobic oxidation of primary and secondary alcohols.

Very recently, a structural and functional model of GO appeared in literature¹⁶ using a phenol containing tripodal ligand. The model mimics the native enzyme structurally and also the functional aspect by oxidizing primary alcohols to the corresponding aldehydes with moderate turnover numbers.

Recent studies, together with this work on bisphenol ligand systems having different hetero-donor atoms in developing homogeneous catalysts, can be expressed in a general way in the following table.

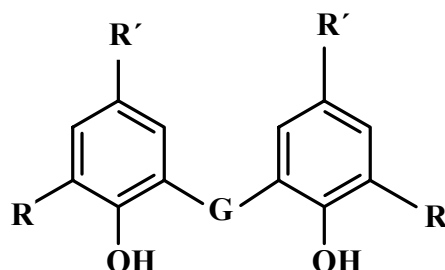


Figure 1.2.3 Bisphenol ligand system.

| G | R | R' | Ligand |
|--|-----------------|-----------------|---------------------------------------|
| NH | ^t Bu | ^t Bu | L ¹ |
| S | H | H | L ^{2a} |
| S | ^t Bu | CH ₃ | L ^{2b} |
| S | ^t Bu | ^t Bu | H₂L^S |
| SO | ^t Bu | CH ₃ | L ³ |
| CH ₂ | ^t Bu | CH ₃ | L ⁴ |
| S-S | ^t Bu | ^t Bu | H₂L^{S-S} |
| S-S | ^t Bu | CH ₃ | L ^{4a} |
| Se | H | H | L ⁵ |
| Se | ^t Bu | ^t Bu | H₂L^{Se} |
| Se-Se | ^t Bu | ^t Bu | H₂L^{Se-Se} |
| O | H | H | L ⁶ |
| PPh | H | H | L ⁷ |
| PPh | ^t Bu | ^t Bu | H₂L^P |
| POPh | ^t Bu | ^t Bu | H₂L^{PO} |
| CH ₂ N(CH ₃)CH ₂ | CH ₃ | CH ₃ | H₂L^N |
| CH ₂ N(CH ₃)CH ₂ | ^t Bu | ^t Bu | H₂L^{N1} |

Until recently, the non-innocent ligand system L¹ has been used to study the polyradical metal complex system, their magnetic and electrochemical properties.¹⁷ Very recently, Chaudhuri *et al* used this system in a series of studies investigating ligand-based catalyst.^{13b} The Cu(II) complex of this ligand can oxidize alcohols to aldehydes aerobically at room temperature in an organic solvent. A strongly AF-coupled radical/Cu(II) complex is believed to take part in the rate-determining C-H abstraction process from substrates.

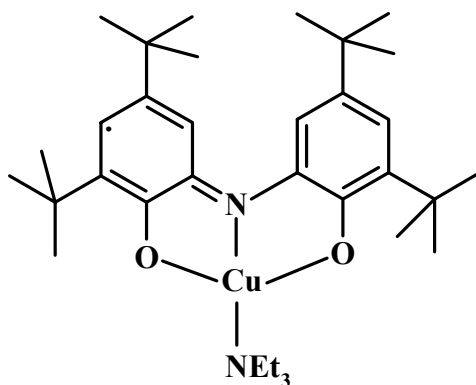


Figure 1.2.4 Chaudhuri et al's functional model complex of GO (A).

The same approach was taken by the group to make another homogeneous catalyst using ligand system H_2L^S .^{13a}

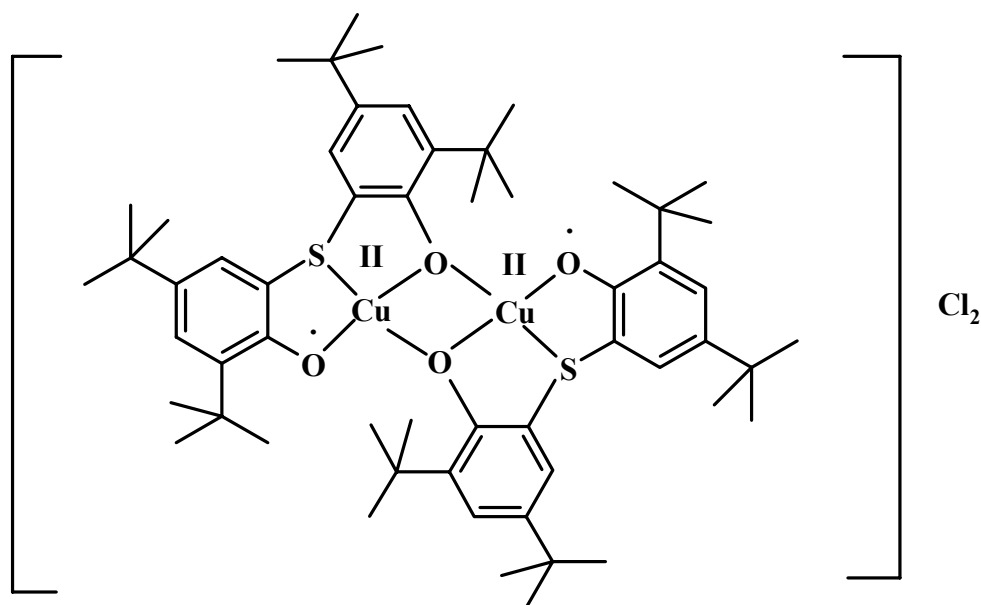


Figure 1.2.5 Chaudhuri et al's functional model complex of GO (B).

Both model complexes (A and B) are capable of oxidizing alcohols to the corresponding carbonyl compounds and the oxidized phenoxyl radical intermediates are proved to be the active species involved in C-H abstraction from the coordinated alcoholate anion in the rate-determining step. The basic difference between the two model complexes is the nuclearity involved in the active form. The ligand H_2L^S forms a dinuclear Cu(II) complex which is oxidized aerobically to its diradical form (B), and both Cu(II) centers can be involved in the oxidation process forming radical coupled products from substrates.

This type of bisphenol ligand system has also been used for making P-complexes in studying the heterocyclic ring systems containing trivalent phosphorus with special rigid stereochemistry at the P-centre in the ring.¹⁸ Also, it is the ring substituents and the different

functionalities at the phosphorous centers that make the heterocycles fascinating with respect to both structural and electronic properties. Heterocycles with P-C, P-N, P-O, P-S^{19a} and P-P^{19b} bonds, in addition to their great biochemical and commercial importance, play a major role in some substitution mechanisms as intermediates or as transition states.²⁰ A few such phosphorus containing heretocycles have been found to be potentially carcinostatic²¹ among other pharmacological activities. The introduction of tervalent phosphorus centers into the ring enhances the versatility of the heterocycles in complexing with both hard and soft metals. Since the tervalent phosphorus centers can stabilize transition metals in low oxidation states, such complexes can be potential homogeneous or phase transfer catalysts in various organic transformations.

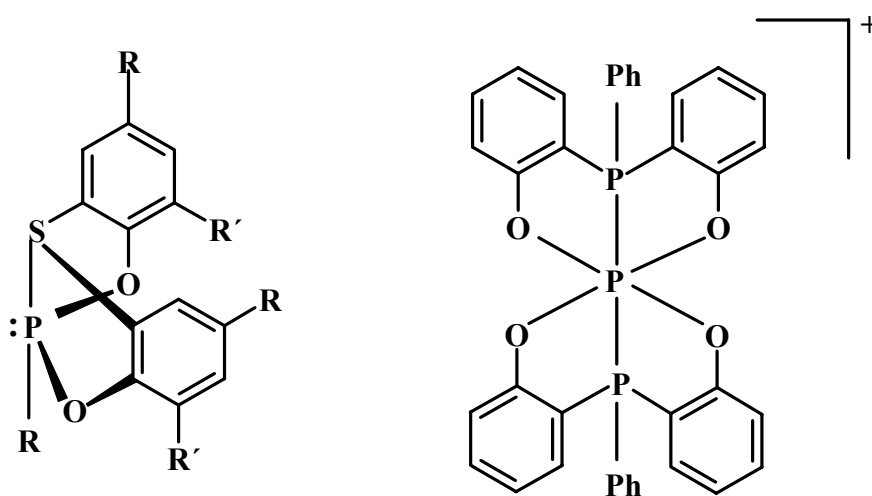


Figure 1.2.6 Bonding mode of bisphenolate ligands (L^{2b} and L^7) with phosphorus.

Comparable with phosphorus, silicon complexes are applicable as models for activated states or intermediates in nucleophilic substitution reactions of silicon.²² The silicon complex of ligand L^{2b} shown below is one of such model complexes.

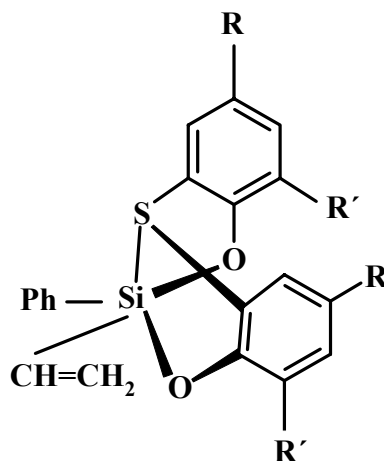


Figure 1.2.7 Bonding mode of bisphenolate ligand (L^{2b}) with silicon.

Bisphenolate complexes of group IV transition metals in combination with MAO (methylaluminoxane) as co-catalyst have been reported recently to polymerize olefins and diolefins. Of particular interest are the catalysts prepared from 2, 2'-thiobis(4-methyl-6-*tert*-butylphenoxy)MX₂ (with ligand L^{2b}) and 2,2'-methylenebis(4-methyl-6-*tert*-butylphenoxy)-MX₂ (with ligand L⁴).²³

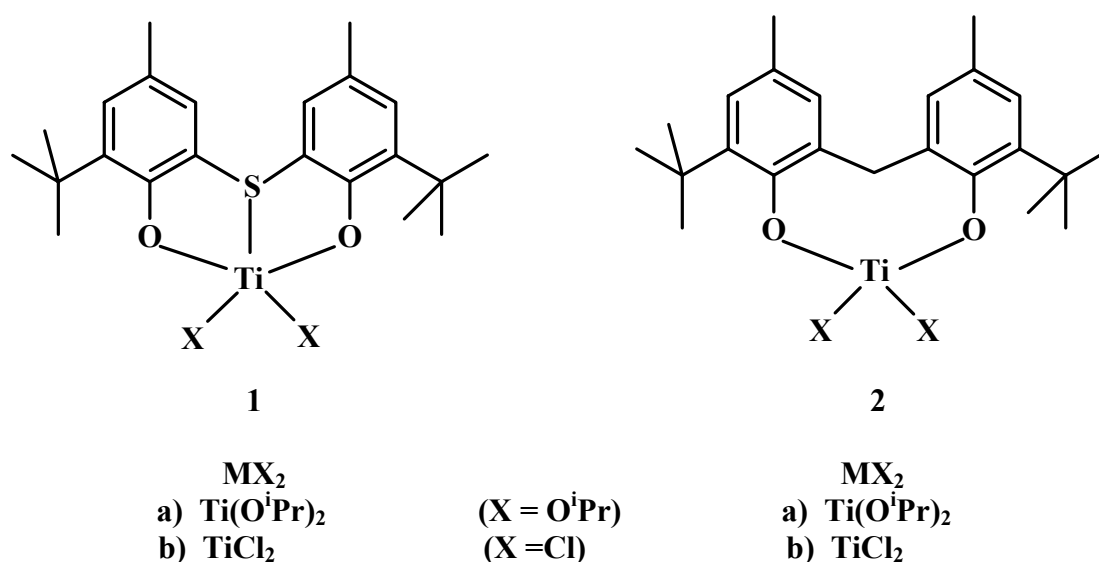


Figure 1.2.8 Bonding mode of bisphenolate ligand with Ti, (a polymerization catalyst).

The catalyst prepared from **1** have been found to be more active than that prepared from **2** in the polymerization of styrene, ethylene and 1,3-dienes. It has been speculated that this difference of activity may be due to an increased ligand flexibility and effects of possible π -donation from S to Ti in **1**. The incorporation of bulky olefins depends upon the ring size of the Ti-complex and as a result the rate of polymerization increases which is evident from recent reports using ligands, L³ and L^{4a}.²⁴ Such tuning of the catalyst by changing the donor atom reflects the importance of bisphenol ligand system in homogeneous catalysis.

The 3d-metal coordination chemistry of bisphenol ligands is not well established until now. Extensive study of metal complexes with L¹ ligand revealed the importance of polyradical system by exploring their spectral, magnetic and electrochemical properties. On the other hand, only a few complexes have been studied with the ligands mentioned above other than those described earlier and used as homogeneous catalysts. A few studies on bisphenol ligands tabulated above have appeared in literature. Among those the mononuclear homoleptic Co(II) complex of L^{2a},^{25a} Co(III) complex of L⁵,^{25b} Cu(II) complex of L^{2a},^{25c} trinuclear μ -oxo tris W(VI) complex of L^{2a},^{25d} square planar mononuclear Ni(II) complex,

Co(III) complex and Rh(III) complex of H_2L^P , dinuclear Co(II) complex of H_2L^{PO} ,²⁶ Ge(IV) complexes of H_2L^S ^{27a} and H_2L^{Se} ^{27b} are structurally well characterized.

Summarily, the main theme of this work is to explore the transition metal coordination complexes of bisphenol ligands containing an additional heterodonor atom like N, S, Se, P, PO, and possible application in homogeneous catalysis of the prepared complexes.

1.3 LIGAND SYNTHESIS

The synthesis of ligands H_2L^S ,^{28a} H_2L^P , H_2L^{PO} ²⁶ and H_2L^N ^{28b} are well documented in literature and so only the synthetic outlines are discussed here.

The ligand H_2L^S is synthesized by the substitution reaction of 2,4-di-*tert*-butylphenol with sulfur dichloride in petroleum ether using zinc chloride as catalyst. Removal of HCl gas by argon flow and then usual work-up procedure results in a white compound with moderate yield. Spectral (IR, NMR and MS) characterizations confirm the compound as 2,2'-thiobis(4,6-di-*tert*-butylphenol).

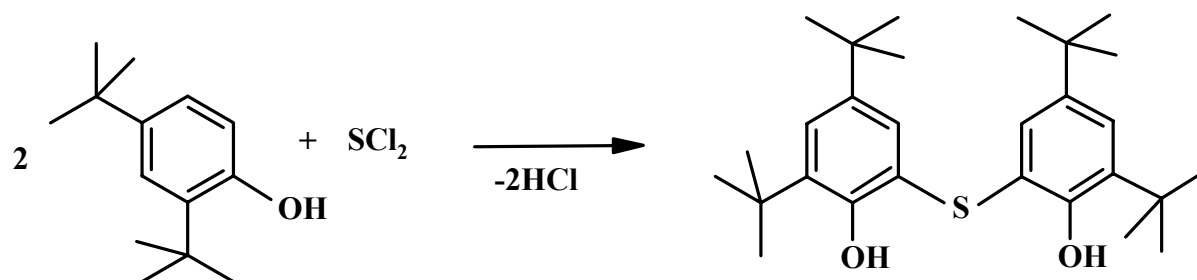


Figure 1.3.1 Synthesis of ligand H_2L^S .

On the other hand, ligand H_2L^P is synthesized by the reaction of 2-bromo-4,6-di-*tert*-butylphenol with butyllithium followed by the addition of dichlorophenylphosphine in ether. Care should be taken during the work-up process to avoid the oxidation of the ligand to H_2L^{PO} . A very similar method is used for the preparation of H_2L^{PO} by using dichlorophenylphosphineoxide instead of dichlorophenylphosphine. H_2L^{PO} can also be prepared by treating H_2L^P with H_2O_2 and purified by thin layer chromatography in very good yield.

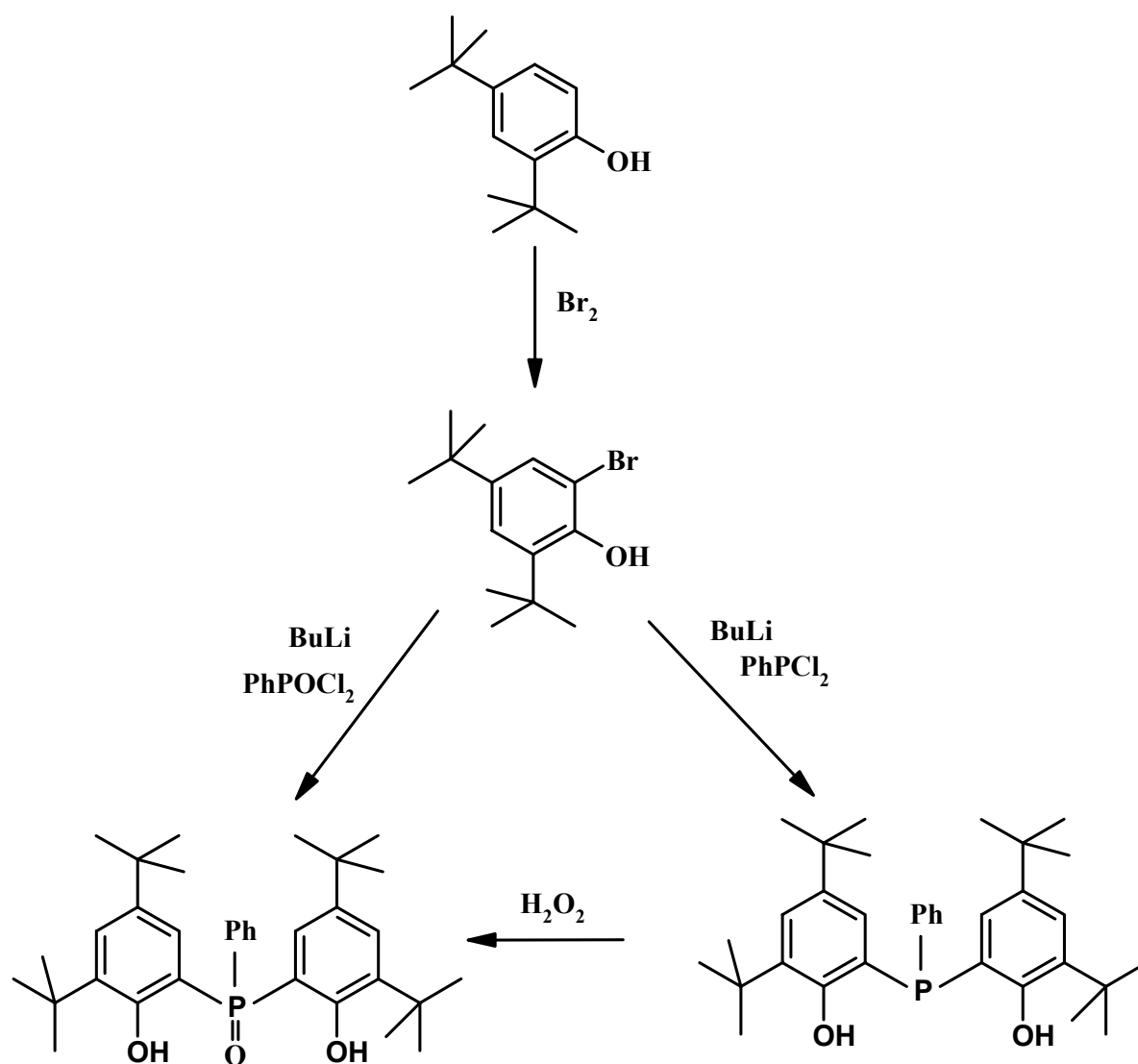
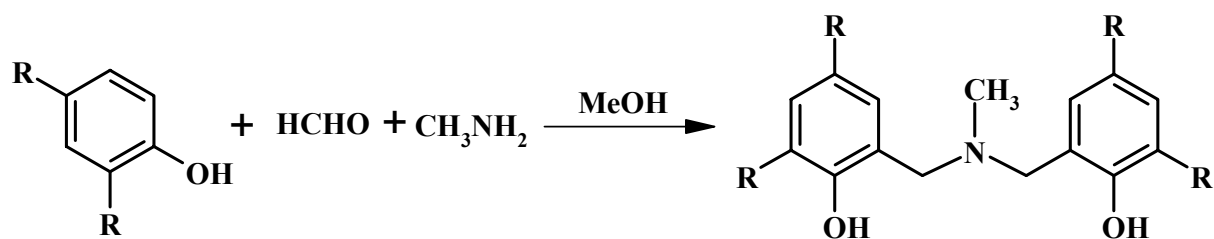


Figure 1.3.2 Synthesis of ligands H_2L^P and H_2L^{PO} .

The ligands H_2L^N and H_2L^{N1} are prepared by the Mannich condensation reaction of 2,4-dimethylphenol and 2,4-di-*tert*-butylphenol, respectively with aqueous formaldehyde and $MeNH_2$ in $MeOH$. Work-up procedure yields a white solid from the heterogeneous liquid phase. The compounds are stable under air and soluble in organic solvents.



When, R = ^tBu; H₂L^{N1}

R = Me; H₂L^N

Figure 1.3.3 Syntheses of ligands H₂L^N and H₂L^{N1}.

The single literature report on the H₂L^{Se} ligand^{27b} involves basically the same chemistry but the overall yield reported is very low. The reaction between phenol and SeOCl₂ in CHCl₃ for 2 h yields the ligand with only 18% conversion. During the course of this work the method was modified to improve the yield and handling.

SeO₂ and conc. HCl are used as reagent in this work. In conc. HCl, SeO₂ forms SeOCl₂ at moderate temperature (at high temperature Se₂Cl₂ is also formed, which ultimately leads to diselenium as product) *in situ*, which reacts further with phenol to give the desired ligand in 25% yield.

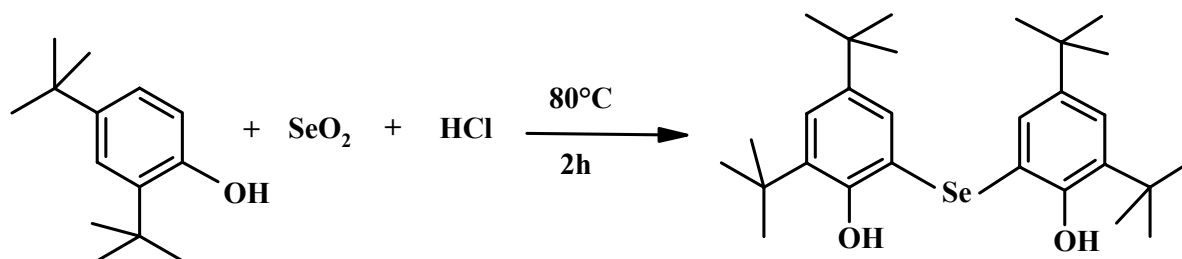


Figure 1.3.4 Synthesis of ligand H₂L^{Se}.

The ligand was characterized by different spectral techniques. The melting point of the ligand is 141°C. The IR spectrum shows a strong free phenol –OH stretching frequency at 3406 cm⁻¹, and strong C-H stretches of *tert*-butyl groups in the range 2868-2858 cm⁻¹. The ¹H-NMR spectrum in CDCl₃ shows peaks: δ (ppm) 1.2 (s, 18H), 1.38 (s, 18H), 6.25 (s, 2H, OH) and 7.24 (m, 4H, aromatic H). In the EI mass spectrum the desired molecular ion peak is observed at m/z = 490 in the ratio calculated for the naturally abundant isotope mixture of Se-74, 76, 77, 78, 80 and 82.

The ligand was also structurally characterized. Figure 1.3.5 shows the ORTEP diagram of the molecule with atom labeling scheme along with the bond parameters in Table 1.3.1.

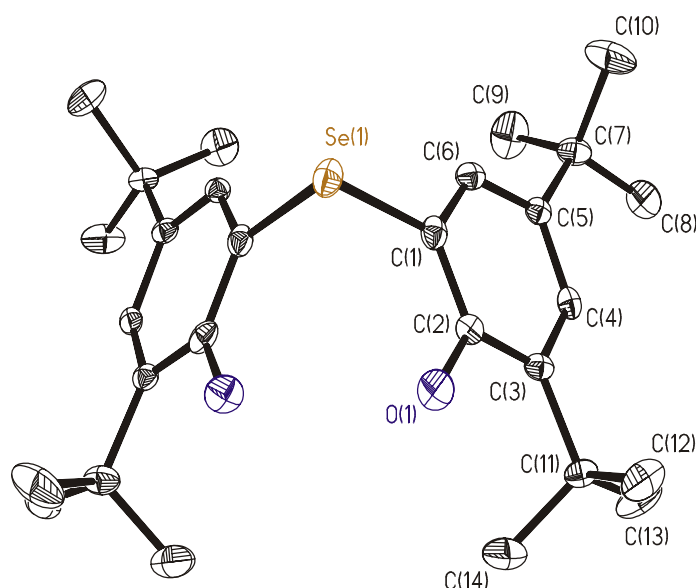


Figure 1.3.5 The ORTEP and atom labeling scheme for H_2L^{Se} .

Table 1.3.1 Selected bond distances (Å) and angles (deg) for ligand H_2L^{Se}

| | | | |
|-------------------|----------|------------|----------|
| Se(1)-C(1)#1 | 1.942(4) | Se(1)-C(1) | 1.942(4) |
| C(1)-C(2) | 1.384(6) | C(2)-C(3) | 1.392(6) |
| C(1)-C(6) | 1.394(5) | C(3)-C(4) | 1.406(5) |
| C(3)-C(11) | 1.536(5) | C(4)-C(5) | 1.387(5) |
| C(5)-C(6) | 1.391(5) | C(5)-C(7) | 1.530(5) |
| C(1)#1-Se(1)-C(1) | | 95.7(2) | |
| C(2)-C(1)-Se(1) | | 119.9(3) | |
| C(6)-C(1)-Se(1) | | 119.8(3) | |

Both phenyl rings attached to phenolic oxygen atoms are planar and are, as expected, aromatic in nature.

The ligand H_2L^{Se-Se} can be prepared following a similar reaction protocol used for the ligand H_2L^S , using Se_2Cl_2 and 2,4-di-*tert*-butylphenol. But the yield is very low. So, a similar strategy as was used in case of the H_2L^{Se} is applied by preparing Se_2Cl_2 *in situ* and by concomitant reaction with phenol. At high temperature SeO_2 reacts with conc. HCl to form Se_2Cl_2 . The reaction should be performed for 4 h. After working up, the crude product is washed with MeOH forming the ligand in good yield (70%). Washing thoroughly with MeOH can separate the side product, H_2L^{Se} .

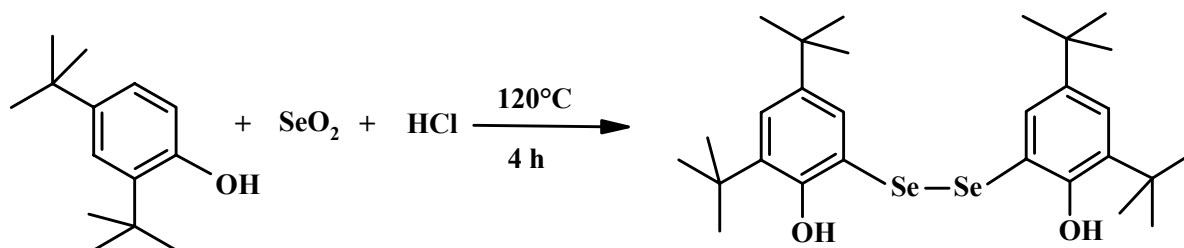


Figure 1.3.6 Synthesis of ligand H_2L^{Se-Se} .

The EI-mass spectrum shows a molecular ion peak at $m/z = 570$, whereas the IR spectrum displays two sharp bands at 3416 and 3444 cm^{-1} , which are assigned to two different phenolate O-H stretching bands. The Se-Se bond affects the planarity of the molecule and two O-H groups are in different planes and appear at different stretching frequencies in the IR spectrum.

The ligand H_2L^{S-S} is synthesized in a similar way by the condensation of 2,4-di-*tert*-butylphenol with disulfur dichloride in toluene at room temperature. The orange brown crude product is dissolved in hot EtOH and recrystallization from MeOH results in light yellow solid in moderate yield (32%).

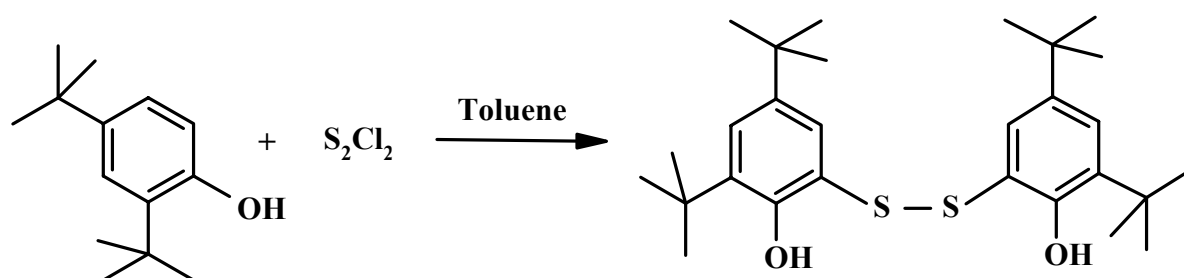


Figure 1.3.7 Synthesis of ligand H_2L^{S-S} .

The ligand was also characterized using different analytical techniques. The EI-mass spectrum shows a molecular ion peak at $m/z = 474$, whereas the IR spectrum displays two sharp bands at 3436 and 3464 cm^{-1} , which are assigned to two different phenolate O-H stretching bands.

References

1. (a) J. Stubbe, *Annu. Rev. Biochem.* **1989**, 58, 257. (b) P. A. Frey, *Chem. Rev.* **1990**, 90, 1343. (c) J. W. Whittacker in H. Sigel and A. Sigel, Eds., *Metalloenzymes Involving Amino Acid-Residue and Related Radicals*, Marcel Dekker, New York, **1994**, Vol. 30, pp.315-360. (d) J. Z. Pederson, A. Finazzi-Agro, *FEBS Lett.* **1993**, 325, 53. (e) R. C. Prince, *Trends Biochem. Sci.* **1988**, 13, 152. (f) G. T. Babcock, M. Espe, C. Hoganson, N. Lydakis-Simantiris, J. McCracken, W. Shi, S. Styring, C. Tommos, K. Warncke, *Acta Chem. Scand.* **1997**, 51, 533. (g) M. M. Fontecave, J.-L. Pierre, *Bull. Soc. Chim. Fr.* **1996**, 133, 653. (h) E.-I. Ochiai, *J. Chem. Ed.* **1993**, 70, 128. (i) J. Stubbe, W.A. van der Donk, *Chem. Rev.* **1998**, 98, 705. (j) R. H. Holm, E. I. Solomon, Guest Editors, *Chem. Rev.* **1996**, 96, 7.
2. D. K. Logan, J. Anderson, B.-M. Sjöberg, P. Nordlund, *Science* **1999**, 283, 1499.
3. (a) J. W. Kozarich, E. J. Brush, in *The Enzymes*, D. S. Sigman, Ed., Academic, San Diego, **1992**, Vol. XX, p. 317. (b) J. Knappe, G. Sawers, *FEMS Microbiol. Rev.* **1990**, 75, 383. (c) H. Contradt, H. Hohmann-Berger, H. Hohmann, H. P. Blaschkowski, J. Knappe, *Arch. Biochem. Biophys.* **1984**, 228, 133.
4. (a) J. E. Huyett, P. E. Doan, R. Gurbiel, A. L. P. Housemann, M. Sivaraja, D. B. Goodin, B. Hoffman, *J. Am. Chem. Soc.* **1995**, 117, 9033. (b) M. Sivaraja, D. B. Goodin, M. Smith, B. Hoffman, *Science* **1989**, 245, 738. (c) T. Yonetani, H. Schleyer, A. Ehrenberg, *J. Biol. Chem.* **1966**, 241, 3240.
5. (a) M. Fontecave, P. Nordlund, H. Eklund, P. Reichard, in *Advances in Enzymology and Related Areas of Molecular Biology*, A. Meister, Ed., Wiley, New York, **1992** Vol. 65, p. 147. (b) J. Stubbe, in *Advances in Enzymology and Related Areas of Molecular Biology*, A. Meister, Ed., Wiley, New York, **1990** Vol. 63, p. 349. (c) B. M. Sjöberg, in *Nucleic Acids and Molecular Biology*, F. Eckstein, D. M. Lilley, Eds., Springer Verlag, Berlin, **1995** Vol. 9, p. 192.
6. (a) B. A. Barry, G. T. Babcock, *Proc. Natl. Acad. Sci. USA* **1987**, 84, 7099. (b) R. Debus, *Biochim. Biophys. Acta* **1992**, 1102, 269.
7. (a) A. L. Tasi, R. L. Kulmacz, G. Palmer, *J. Biol. Chem.* **1995**, 270, 10503. (b) D. Picot, P. J. Loll, R. M. Garavito, *Nature (London)* **1994**, 367, 243. (c) A. L. Tasi, G. Palmer, R. L. Kulmacz, *J. Biol. Chem.* **1992**, 276, 17753. (d) A. L. Tasi, G. Palmer, G. Xiao, D. C. Swinney, R. L. Kulmacz, *J. Biol. Chem.* **1998**, 273, 3888. (e) L. C. Hsi, C.

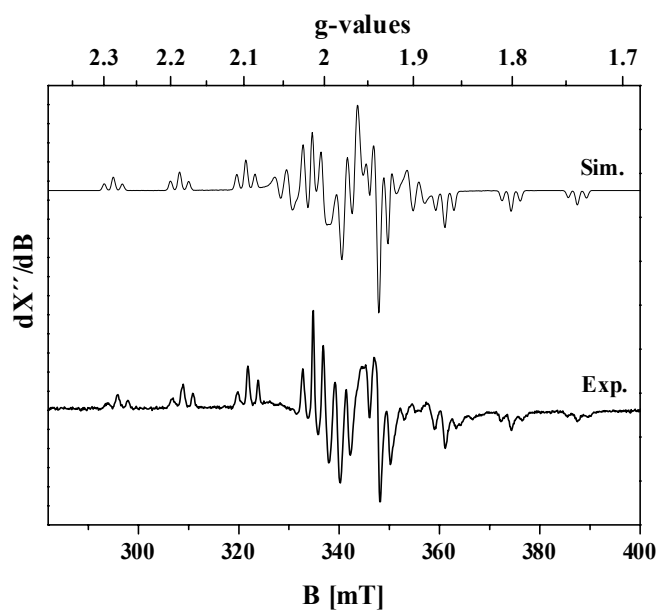
- W. Hoganson, G. T. Babcock, W. L. Smith, *Biochem. Biophys. Res. Commun.* **1994**, 202, 1592.
8. (a) Y.-R. Chen, M. R. Gunther, R. P. Mason, *J. Biol. Chem.* **1999**, 274, 3308. (b) F. MacMillan, A. Kannt, J. Behr, T. Prisner, H. Michel, *Biochemistry* **1999**, 38, 9179.
 9. (a) G. A. Landum, C. A. Ekberg, J. W. Whittaker, *Biophys. J.* **1995**, 69, 674. (b) M. M. Whittaker, C. A. Ekberg, J. Peterson, M.S. Sendova, E. P. Day, J. M. Whittaker, *J. Mol. Cat. B: Enzymatic* **8**, **2000**, 3.
 10. M. M. Whittaker, P. J. Kersten, N. Nakamura, J. Sander-Loehr, E. S. Schweizer, J. M. Whittaker, *J. Biol. Chem.* **1996**, 271, 681.
 11. (a) J. A. Halfen, B. A. Jazdzewski, S. Mahapatra, L. M. Berreau, E. C. Wilkinson, L. Que, Jr., W. B. Tolman, *J. Am. Chem. Soc.* **1997**, 119, 8217. (b) Y. Wang, T. D. P. Stack, *J. Am. Chem. Soc.* **1996**, 118, 13097. (c) D. Zurita, I. Gautier-Luneau, S. Menage, J. L. Piere, E. Saint-Aman, *J. Biol. Inorg. Chem.* **1997**, 2, 46. (d) E. Bill, J. Müller, T. Weyhermüller, K. Wieghardt, *Inorg. Chem.* **1999**, 38, 5795. (e) M. A. Halcrow, L. M. Lindy Chia, X. Liu, E. J. L. McInnes, L. J. Yellowlees, F. E. Mabbs, I. J. Scowen, M. McParrlin, J. E. Davies, *J. Chem. Soc., Dalton Trans.* **1999**, 1753. (f) S. Itoh, S. Takayama, R. Arakawa, A. Furuta, M. Komatsu, A. Ishida, S. Takamuku, S. Fukujumi, *Inorg. Chem.* **1997**, 36, 1407. (g) K. Yamato, T. Inada, M. Doe, A. Ichimura, T. Takui, Y. Kojima, T. Kikunaga, S. nakamura, N. Yanagihara, T. Onaka, S. Yano, *Bull. Chem. Soc. Jpn.* **2000**, 73, 903. (h) Y. Shimazaki, S. Huth, A. Odani, O. Yamauchi, *Angew. Chem., Int. Ed.* **2000**, 112, 1666.
 12. (a) *Metal Ions in Biological Systems*, eds. H. Sigel, A. Sigel, Marcel-Dekker, New York, **1994**, vol. 30. (b) D. P. Goldberg, S. J. Lippard, *Adv. Chem. Ser.* **1995**, 246, 59.
 13. (a) P. Chaudhuri, M. Hess, U. Flörke, K. Wieghardt, *Angew. Chem., Int. Ed.* **1998**, 37, 2217. (b) P. Chaudhuri, M. Hess, T. Weyhermüller, K. Wieghardt, *Angew. Chem., Int. Ed.* **1999**, 38, 1095. (c) P. Chaudhuri, M. Hess, J. Müller, K. Hildenbrand, E. Bill, T. Weyhermüller, K. Wieghardt, *J. Am. Chem. Soc.* **1999**, 121, 9599.
 14. (a) A. Caneschi, D. Gatteschi, R. Sessoli, *Acc. Chem. Res.* **1989**, 22, 392. (b) M. Vaz, L. Pinheiro, H. Stumpf, A. Alcantara, S. Golhen, L. Quahab, O. Cador, C. Mathoniere, O. Kahn, *Chem. Eur. J.* **1999**, 5, 1487. (c) A. Aukauloo, X. Ottenwaelder, R. Ruiz, S. Poussereau, Y. Pei, Y. Jorneaux, P. Fleurat, F. Volatron, B. Cervera, M. C. Munoz, *Eur. J. Inorg. Chem.* **1999**, 1067.
 15. Y. Wang, J. L. DuBois, B. Hedman, K. O. Hodgson, T. D. P. Stack, *Science* **1998**, 279, 537.

16. F. Thomas, G. Gellon, I. G.-Luneau, E. S.-Aman, J.-L. Pierre, *Angew. Chem. Int. Ed.* **2002**, *41*, 3047.
17. S. K. Larsen, C. G. Pierpont, *J. Am. Chem. Soc.* **1998**, *110*, 1827.
18. (a) K. Dimroth, *Heterocyclic Rings containing Phosphorus*, Pergamon: Elmsford, NY, **1984**. (b) H. G. Heal, *The Inorganic Chemistry of Sulfur, Nitrogen and Phosphorus; Academic Press: London*, **1980**. (c) A. M. Caminade, J. P. Majoral, *Chem. Rev.* **1994**, *94*, 1183.
19. (a) D. E. C. Corbridge, *Phosphorus: An Outline of its Chemistry, Biochemistry and Technology, 5 th ed.*; Elsevier: Amsterdam, 1995. (b) H. Luo, R. McDonald, R. G. Cavell, *Angew. Chem. Int. Ed.* **1998**, *37*, 1098.
20. (a) F. Ramirez, *Acc. Chem. Res.* **1968**, *1*, 168. (b) F. H. Westheimer, *Acc. Chem. Res.* **1968**, *1*, 70. (c) S. L. Buchwald, D. H. Pliura, J. R. Knowles, *J. Am. Chem. Soc.* **1982**, *104*, 845.
21. (a) N. Gurusamy, K. D. Berlin, V. D. Helm, M. B. Hossain, *J. Am. Chem. Soc.* **1982**, *104*, 3107. (b) N. Gurusamy, K. D. Berlin, *J. Am. Chem. Soc.* **1982**, *104*, 3114.
22. (a) R. R. Holmes, *Chem. Rev.* **1990**, *90*, 17 and references cited therein. (b) C. Chuit, R. J. P. Corriu, C. Reye, J. C. Young, *Chem. Rev.* **1993**, *93*, 1371 and references cited therein.
23. (a) T. Miyatake, K. Mizunuma, Y. Seki, M. Kakugo, *Makromol. Chem. Rapid Commun.* **1989**, *10*, 349. (b) M. Kakugo, T. Miyatake, K. Mizunuma, *Proc. Int. Symp. On Recent Developments in Olefin Polymerization Catalysts*, Tokyo, October 23-25, **1989**. (c) T. Miyatake, K. Mizunuma, M. Kakugo, *Makromol. Chem., Macromol. Symp.* **1993**, *66*, 203. (d) C. J. Schaverien, A. van der Linden, A.G. Orpen, *Am. Chem. Soc., Polym. Div., Polym. Prep.* **1994**, *35*, 362. (e) A. van der Linden, C. J. Schaverien, N. Meijboom, C. Ganter, G. Orpen, *J. Am. Chem. Soc.* **1995**, *117*, 3008.
24. (a) J. Okuda, S. Fokken, T. Kleinhenn, T. P. Spaniol, *Eur. J. Inorg. Chem.* **2000**, 1321. (b) J. Okuda, S. Fokken, H-C. Kang, W. Massa, *Polyhedron* **1998**, *17*, 943. (c) S. Fokken, T. P. Spaniol, H-Chul Kang, W. Massa, J. Okuda, *Organometallics* **1996**, *15*, 5069.
25. (a) H. Müller, A. Holzmann, W. Hinrichs, G. Klar, *Z. Naturforsch., Teil B* **1982**, *37*, 341. (b) P. Berges, W. Hinrichs, A. Holzmann, J. Wiese, G. Klar, *J. Chem. Res.* **1986**, *12*, 245. (c) A. Holzmann, P. Berges, W. Hinrichs, G. Klar, *J. Chem. Res.* **1987**, *42*, 328. (d) P. Berges, W. Hinrichs, A. Holzmann, J. Wiese, G. Klar, *J. Chem. Res.(s)* **1986**, 201.

26. R. Siefert, T. Weyhermüller, P. Chaudhuri, *J. Chem. Soc., Dalton Trans.* **2000**, 4656.
27. (a) S. D. Pastor, V. Huang, D. NabiRahni, S. A. Koch, H-F. Hsu, *Inorg. Chem.* **1997**, *36*, 5966 (b) T. Thompson. S. D. Pastor, G. Rihs, *Inorg. Chem.* **1999**, *38*, 4163.
28. (a) S. D. Pastor, J. D. Spivack, L. P. Steinhuebel, *J. Heterocycl. Chem.* **1984**, *21*, 1285.
(b) N. V. Timosheva, A. Chandrasekaran, R. O. Day, R. R. Holmes, *Inorg. Chem.* **1998**, *37*, 4945.

Chapter 2

NON-OXO VANADIUM(IV) AND OXO-VANADIUM(V) COMPLEXES OF BISPHENOL LIGANDS



2.1 INTRODUCTION

Vanadium is a trace element in biosystem, but our understanding of its biological role is still in its infancy.¹ In order to know the function of vanadium in a complex biomolecule, it is first necessary to develop its basic coordination chemistry with biologically relevant ligands. The binding of vanadium to protein side chains by tyrosinate, serinate, aspartate, glutamate, cysteinate, methionine and histidine is modelled by complexes with ligand sets containing phenolate, alkoxide, carboxylate, thiolate, thioether and enamine functions. The complexes mimic the possible intermediates and structural motifs of the coordination environment of vanadium enzymes.²

Vanadium is present at the active site of certain enzymes, including haloperoxidases in sea algae and lichens and some nitrogenase, in nitrogen-fixing *Azobacter*.³

Amavadin is a vanadium containing small molecule natural product isolated from *Amanita muscaria* mushrooms.⁴ Amavadin is a non-oxo vanadium(IV) complex having coordination environment shown in Figure 2.1.1.

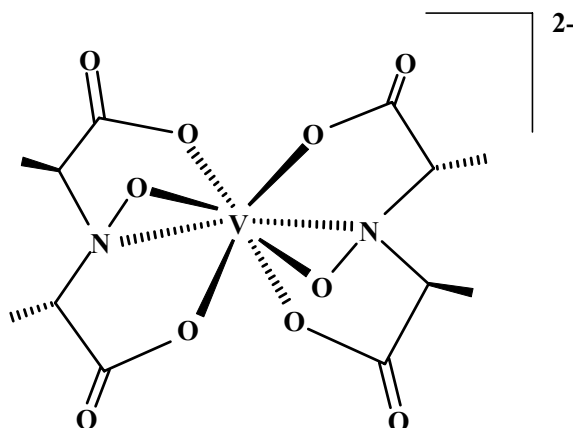


Figure 2.1.1 Amavadin's coordination environment.

The lack of vanadium-oxo bond in both vanadium(IV) and (V) forms of this molecule makes it quite unique. It can be reversibly oxidized ($E^0 = 0.53$ V vs. SCE in H_2O)⁵ and structural changes between the vanadium(IV) and (V) forms are minimal, making it an ideal candidate for one-electron oxidant. It has recently been demonstrated⁶ that certain thiols can be oxidized to disulfides using an amavadin model complex. The model complex $[V^{IV}(HIDA)_2]^{2-}$ is the same (HIDA = N-Hydroxy-iminodiacetate), except the chiral methyl group of the ligand. Subsequent electrochemical reduction of $[V^V(HIDA)_2]^-$ regenerated the active oxidant, $[V^{IV}(HIDA)_2]^{2-}$, allowing for multiple turnovers. The complex anion, which is the first example of a vanadium(IV) eightfold coordinated to nitrogen and oxygen atoms, has an approximate C_2 point symmetry. Due to the geometry and the tetradentate chelating character

of the ligand, the coordination around the vanadium exhibits a distorted dodecahedral configuration.

More recent studies suggest that amavadin may act as a vanadium iodoperoxidase (VIPO). The impetus of these experiments was the realization that the bidentate hydroxylamine coordination to vanadium is analogous to peroxide coordination. Studies of the oxidized model complex $[V^V(\text{HIDA})_2]^-$ show significant rates for iodide oxidation.

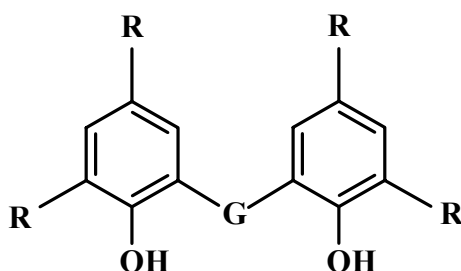
Other than amavadin, vanadium ions are also bound to tyrosinate residues in vanadium-modified transferrin and certain sea squirts or tunicates (polyphenol ascidians) are able to store vanadium in high concentration. Tunichromes, ascidians pigments may be responsible for the reduction of vanadium in the process of uptake of vanadate(V) from sea water to its storage as vanadium(III).⁷

In view of the interaction of vanadium(III), (IV) and (V) with tyrosinate residues⁸ in those vanadium enzymes, vanadium-phenolate chemistry is receiving considerable attention.⁹ However, in contrast to the well known vanadium(IV)/(V) phenolate complexes containing VO^{2+} or VO^{3+} units, only a few non-oxo vanadium(IV) complex, the so-called ‘bare’ complexes have been reported and structurally characterized.^{10, 11a-j}

Keeping an eye to this problem it was important to explore the non-oxo V(IV) chemistry of the bisphenol ligands which primarily stabilizes that unit. A series of structurally characterized non-oxo V(IV) along with two oxo-vanadium(V) complexes of bisphenol ligands are reported in this chapter.

2.2 SYNTHESIS

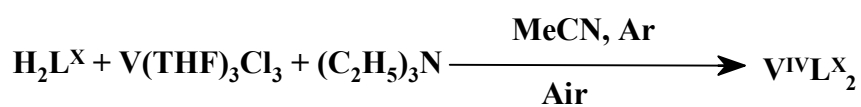
The synthesis of a series of non-oxo vanadium(IV) complexes reported in this chapter involves more or less a general synthetic approach. The ligands used here are as follows:



| G | Heterodonor (X) | R | Ligand (H₂L^X) |
|--|----------------------------|-----------------------|--|
| S | S | ^tBu | H₂L^S |
| Se | Se | ^tBu | H₂L^{Se} |
| PPh | P | ^tBu | H₂L^P |
| POPh | PO | ^tBu | H₂L^{PO} |
| CH₂N(CH₃)CH₂ | N | Me | H₂L^N |
| CH₂N(CH₃)CH₂ | N | ^tBu | H₂L^{N1} |

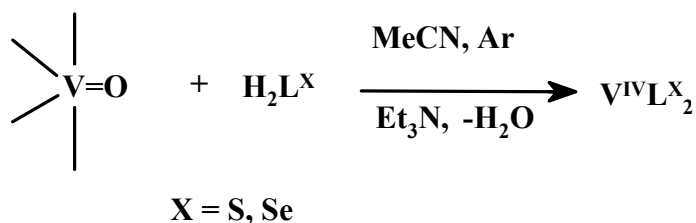
Scheme 2.2.1 Ligands used.

Two general methods allow the synthesis of non-oxo V(IV) complexes. The first and more general approach involves the reaction between V(THF)₃Cl₃, H₂L^X and Et₃N(as base) in dry MeCN. After the reaction is completed the solution was exposed to air for a short time to oxidize V(III) to V(IV) and then keeping the solution under slow argon flow (to avoid further oxidation to V(V)), crystalline complexes in high yield were obtained.



Scheme 2.2.2 General method for complex synthesis.

The second method involves the reaction between H₂L^X (X= S, Se) and VO(acac)₂ or VOSO₄ in MeCN using Et₃N as base under anaerobic condition to displace the oxo-group, resulting in the non-oxo biscomplexes. Displacement of the vanadyl oxygen has been reported previously in the synthesis of tris-(catecholate) vanadium(IV) complexes^{11a} and also in the preparation of V(V)(sal-NSO)₂,¹² in which a sulfur donor is incorporated in a tridentate ligand. These reactions are facilitated by the use of ligand in its protonated form and the addition of a mild base (Et₃N). The oxo group may be protonated and released as water or hydroxide.



Scheme 2.2.3 Synthesis of complex by substitution mechanism.

By contrast, in the previous method V(III) was employed as vanadium source, where oxidation to V(IV) occurred.

The use of oxo-vanadium(IV) starting materials in the syntheses of non-oxo vanadium(IV) products depends not only on the appropriate choice of reaction condition but also on the ability of the chosen ligand to donate sufficient electron density (σ and π) to the metal to stabilize the non-oxo species.

Using the above synthetic methodologies, the following V(IV) complexes were synthesized and characterized:



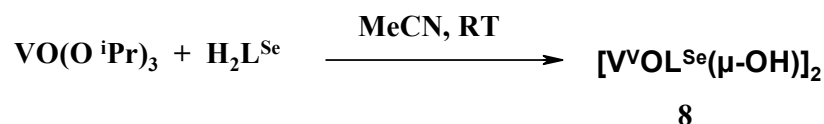
Scheme 2.2.4 Complexes prepared.

All these complexes are stable in the solid state and solution under argon. But when **3** is dissolved in a CH_2Cl_2 and MeCN solvent mixture and kept under air, a V^{VO} monomer **7** is obtained where the ligand L^{P} is oxidized to L^{PO} . The same complex can be isolated by reaction of $\text{VO}(\text{O}^i\text{Pr})_3$ with $\text{H}_2\text{L}^{\text{PO}}$ in MeCN and also by the oxidation reaction of **4** with $[\text{Ni}^{\text{III}}([\text{9}]\text{-aneN}_3)_2](\text{ClO}_4)_3$ in a solvent mixture of CH_2Cl_2 and MeCN.



Scheme 2.2.5 Synthesis of the vanadyl (V) complex.

Interestingly, dimeric complexes are isolated by the same reaction when ligands $\text{H}_2\text{L}^{\text{S}}$ or $\text{H}_2\text{L}^{\text{Se}}$ are used. For X = S system, the complex has been reported in literature.¹³ Synthesis of **8**, $[\text{V}^{\text{VO}}\text{L}^{\text{Se}}(\mu\text{-OH})]_2$ is reported here.



Scheme 2.2.6 Synthesis of the vanadyl (V) dimer.

This difference in reactivity in solution may be because of the structural motif. It is interesting to note that **7** is the main isolated product under the condition that favors the dimer formation for the S- and Se-containing ligands.

Complex **5** exists as a mixture of two isomers (*fac*- and *mer*-isomer) in solid state and in fresh solution. But in CH₂Cl₂ the percentage of the *fac*-isomer decreases with time. This change has been studied by LC (Liquid Chromatography) analyses as a function of time. Detailed analytical data are discussed in **chapter 5** in comparison with the solution behaviour of the Mn(IV) complex.

Each of these complexes was characterized by IR, EA, MS(EI). Their spectroscopic and magnetic behaviour were studied by EPR, susceptibility (SQUID) measurements and their redox behaviour by electrochemical methods.

2.3 INFRARED SPECTROSCOPY

The IR spectra of all complexes (**1-8**) were measured in the region 4000-400 cm⁻¹. The peaks which give more information are those due to ν(OH) which occur as broad peaks in the 3400-3200 cm⁻¹ region, free ligands have sharp peaks in that region. The sharp band is missing in all complexes (**1-8**) indicating the metal complexation with phenolate. The sharp and strong peaks in the region 3000-2800 cm⁻¹ indicate the presence of *tert*-butyl or methyl groups from ligands.

The most important difference between the IR spectra of the bis-complexes **1-6** and the vanadyl(V) complexes **7, 8** is the presence of a strong V=O stretch around 950 cm⁻¹ in **7** and **8**. The V=O stretching frequency is at the low end of the range 935-1035 cm⁻¹ reported for a large set of oxo-vanadium complexes.¹⁴

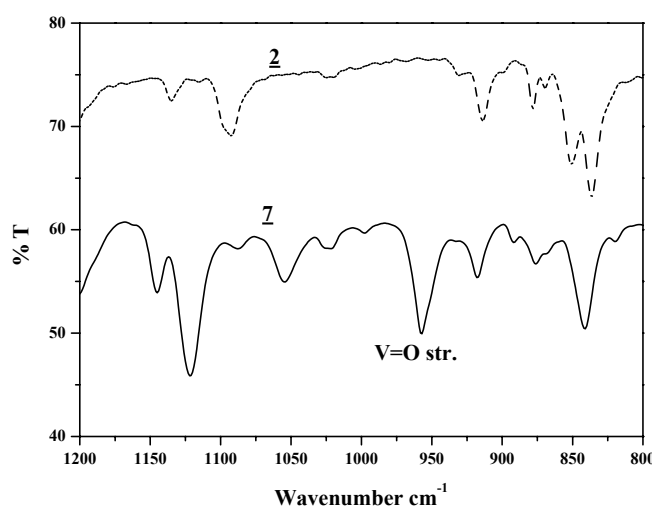


Figure 2.3.1 IR in the region 1200-800 cm⁻¹ for complexes **2** and **7**.

Detailed IR spectra for **1-8** are given in the experimental section. Besides these characteristic peaks, complexes **4** and **7** show strong P=O stretching frequencies at 1118 and 1121 cm^{-1} , respectively.

2.4 MASS SPECTROSCOPY

Complexes **1-7** were analyzed by EI- and ESI-mass spectroscopy, which was found to be very important analytical techniques for the characterization of the complexes, and the molecular ion peaks i.e., the compositions, are in good agreement with elemental analysis.

The EI-mass spectrum of **1** shows the molecular ion peak at 931 with an abundance of 100% with expected isotope pattern. Similarly, complexes **2**, **3** and **4** show the molecular ion peak at 1027, 1083 and 1115 (all with 100% abundance), respectively, with isotopic distribution calculated for those complexes. As a representative example, Figure 2.4.1 shows the comparison of the experimental and theoretical isotope pattern of M^+ ions for **2**. This isotope pattern reflects the natural abundance of metal and ligand atom isotopes.

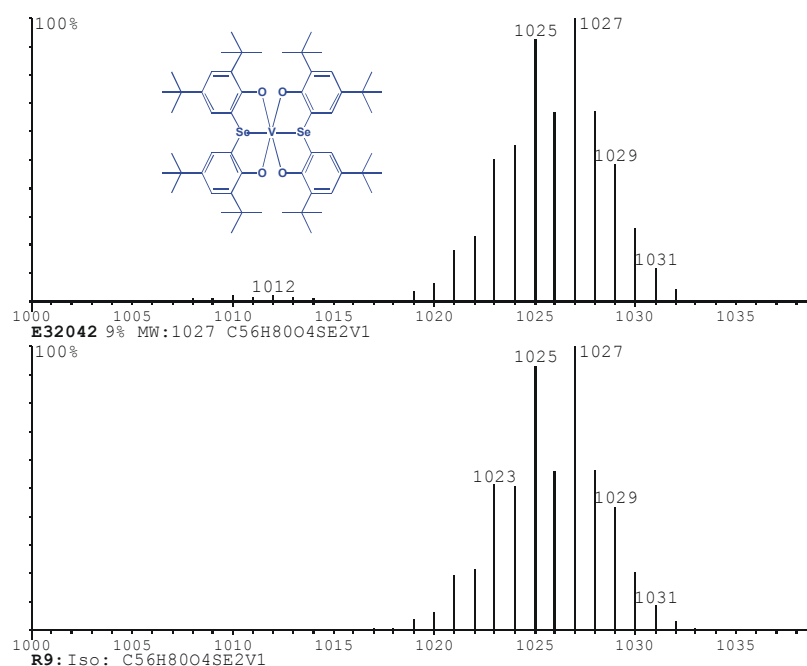


Figure 2.4.1 EI-mass spectrum for complex **2** with experimental (above) and calculated (below) isotopic distribution.

But the EI-mass spectrum of **5** shows a molecular ion peak at m/z 645 with only 42% abundance. The base peak at 377 is a fragmentation product in that condition. The ESI (positive ion mode in CH_2Cl_2) mass spectrum for **6** clearly confirms the composition of the complex showing $m/z = 981(100\%)$. The EI-mass spectrum of **7**, on the other hand, shows a

molecular ion peak at m/z 1133 with an abundance of 56%. The peak at m/z 534 with 100% abundance (base peak) corresponding to ligand H_2L^{PO} is observed as a result of fragmentation. The EI-MS or ESI-MS for **8** does not provide any useful information. In the EI-MS, the peak at m/z 1027 for **8** corresponds to the gas phase decomposition product VL^{Se}_2 , **2**. This is an indication of the removal of the oxo-group from $V=O$ even at a higher oxidation state in gas phase.

2.5 X-RAY CRYSTAL STRUCTURE

Complexes **1-3** are isostuctural with a *fac*- XO_2 donor set (X = hetero donor atom) and, hence, details of them are not discussed here. Only complex **1** as a representative case is discussed below and the others are shown as their ORTEP diagram. Selected bond angles and bond lengths are given together in Table 2.5.1 for comparison purposes.

2.5.1 Molecular structure of VL^{S}_2 (**1**)

Single crystals of **1** were isolated from a MeCN solution and analysed by the single crystal X-ray diffraction method. The analysis confirms that a vanadium complex with $M:L = 1:2$ is formed. The resulting unit cell contains two independent molecules with a nearly identical environment and almost similar bond distances and bond angles.

The figure below shows the ORTEP diagram of VL^{S}_2 with the atom-labeling scheme. A detailed table (2.5.1) containing selected bond distances and angles is also given. The complex consists of a neutral unit composed of a central pseudo-octahedral vanadium ion surrounded by two tridentate ligands bound in a facial manner (*fac*-OSO donor set). Pyramidal sulfur favors facial coordination.

The ligands coordinate through the phenolate oxygen and thioether sulfur atoms. All the phenols are deprotonated, indicating +4 oxidation state of the vanadium center. It clearly shows that the vanadium (IV) ion is hexacoordinated by two deprotonated ligands using O,S,O donor sets. Two oxygen and two sulfur atoms (from two ligand sets) form the equatorial plane, where two same donor atoms occupy *cis*-positions with respect to each other. The remaining phenolate oxygen atoms, mutually *trans*, complete the coordination sphere. All the phenyl rings attached to the phenolate oxygen atoms are planar. This indicates the retention of aromaticity of the phenyl rings upon coordination.

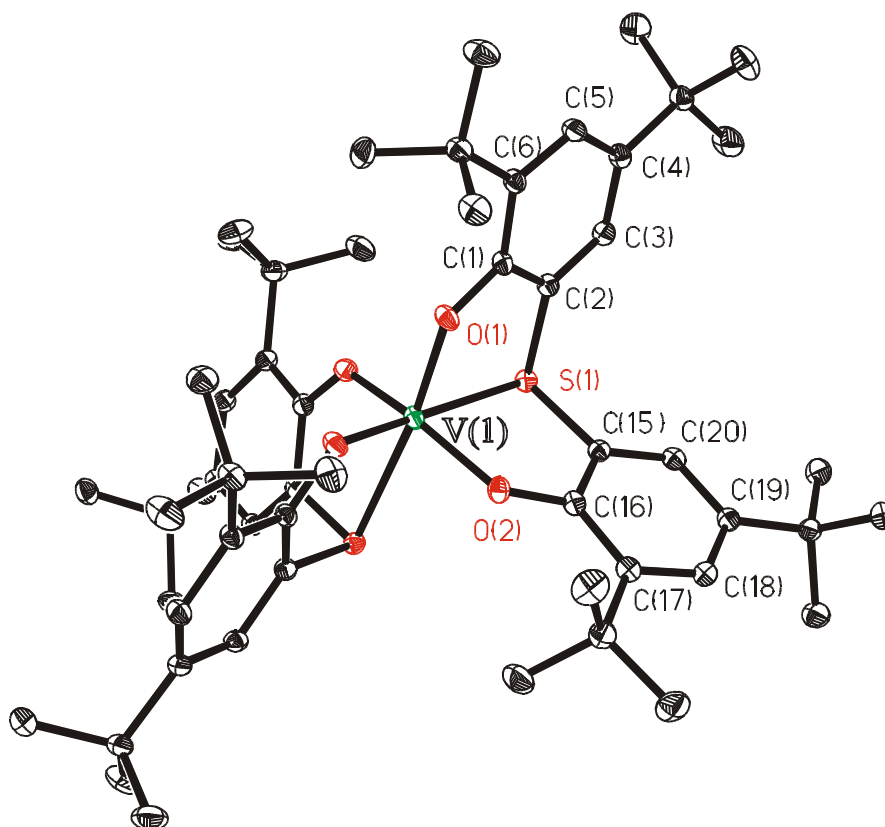


Figure 2.5.1 ORTEP and atom labeling scheme for VL_2^S (**1**).

The mean value of the four V-O bond distances of 1.8535(10) Å in VL_2^S is consistent with the V(IV) oxidation state, although significantly shorter than in the catecholate vanadium(IV) complex $[Et_3NH]_2[V^{IV}(cat)_3].MeCN$ (av. 1.930(3) Å)^{11a} and somewhat longer than in the $[V^{IV}L][BPh_4]$ complex (L = 1,4,7-tris (5-tert-butyl-2-hydroxybenzyl)-1,4,7-triazacyclononane) (av. 1.827(5) Å)^{11b}.

2.5.2 Molecular structure of VL^{Se}₂ (2)

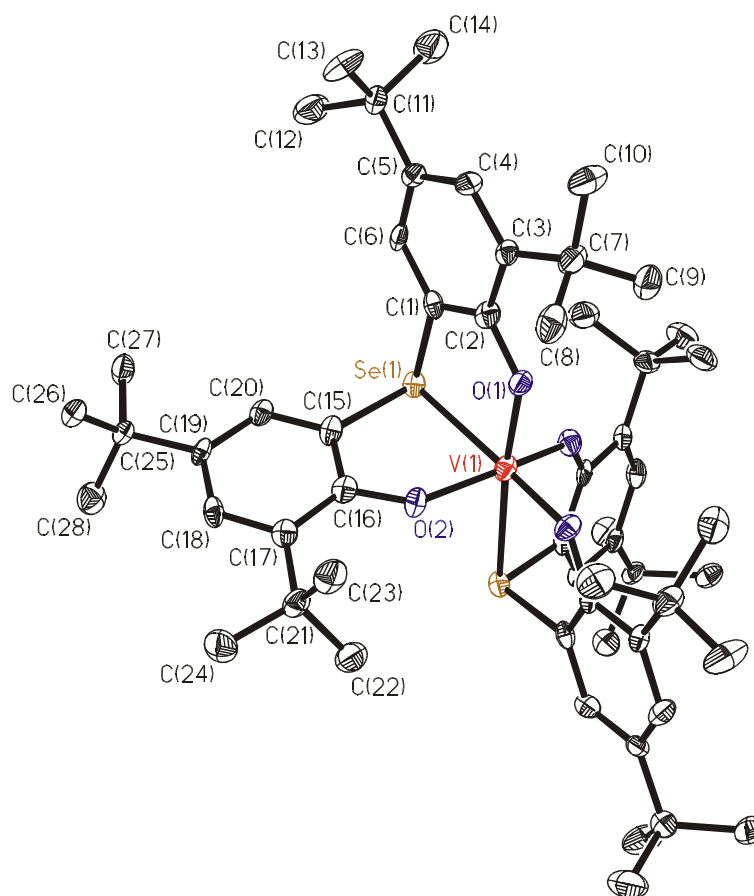


Figure 2.5.2 ORTEP and atom labeling scheme for VL^{Se}₂ (2)

2.5.3 Molecular structure of VL^P₂ (3)

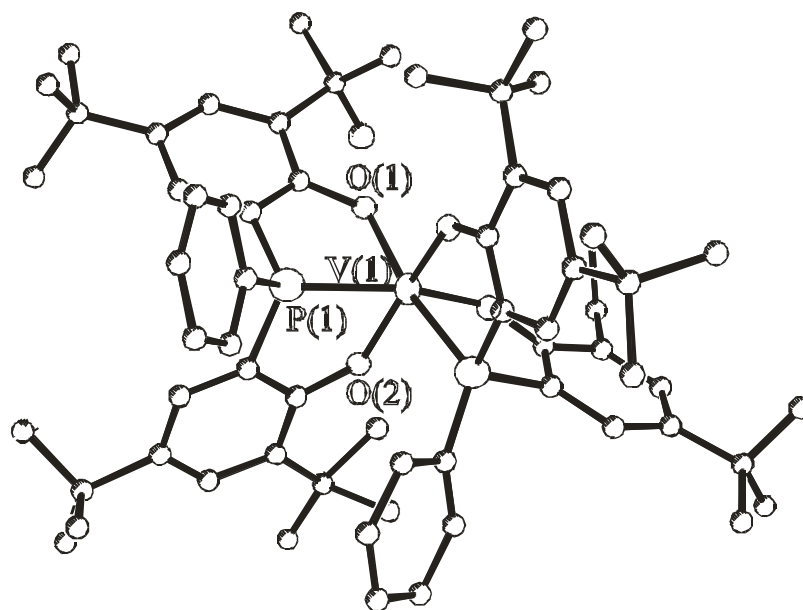


Figure 2.5.3 Ball and stick diagram of VL^P₂ (3).

Table 2.5.1 Selected bond distances (Å) and angles (deg) for complexes **1-3**

| Bond parameters | 1 (X = S) | 2 (X = Se) | 3 (X = P) |
|--------------------|---------------------|----------------------|---------------------|
| V(1)-O(1)#1 | 1.8487(10) | 1.846(3) | 1.909(10) |
| V(1)-O(1) | 1.8488(10) | 1.846(3) | 1.904(10) |
| V(1)-O(2)#1 | 1.8583(10) | 1.859(3) | 1.872(10) |
| V(1)-O(2) | 1.8584(10) | 1.859(3) | 1.921(10) |
| V(1)-X(1) | 2.5306(4) | 2.6373(9) | 2.476(5) |
| V(1)-X(1)#1 | 2.5306(4) | 2.6374(9) | 2.475(5) |
| O(1)#1-V(1)-O(1) | 93.23(6) | 93.5(2) | 102.88(43) |
| O(1)#1-V(1)-O(2)#1 | 100.34(5) | 100.19(14) | 103.48(43) |
| O(1)-V(1)-O(2)#1 | 96.28(4) | 96.22(14) | 91.17(43) |
| O(1)#1-V(1)-O(2) | 96.29(4) | 96.22(14) | 89.44(43) |
| O(1)-V(1)-O(2) | 100.34(5) | 100.19(14) | 98.47(42) |
| O(2)#1-V(1)-O(2) | 155.72(6) | 156.0(2) | 161.52(43) |
| O(1)#1-V(1)-X(1) | 82.42(3) | 83.29(10) | 79.83(33) |
| O(2)#1-V(1)-X(1) | 85.14(3) | 84.72(10) | 76.60(33) |
| O(2)-V(1)-X(1) | 79.68(3) | 79.92(10) | 75.76(32) |
| O(1)#1-V(1)-X(1)#1 | 82.42(3) | 83.29(10) | 80.20(32) |
| O(1)-V(1)-X(1)#1 | 173.38(3) | 174.46(10) | 165.51(34) |
| O(2)#1-V(1)-X(1)#1 | 79.69(3) | 79.92(10) | 90.52(33) |
| O(2)-V(1)-X(1)#1 | 85.15(3) | 84.72(10) | 75.76(32) |
| X(1)-V(1)-X(1)#1 | 102.34(3) | 100.21(5) | 101.19(18) |

2.5.4 Molecular structure of VL^{PO}₂ (**4**)

Single crystals of *fac-cis*(O,O)-[VL^{PO}₂] were obtained from a MeCN solution by slow evaporation of the solvent. The ORTEP diagram for the structure of compound **4** is displayed in Figure 2.5.4, while selected bond lengths and angles are summarized in Table 2.5.2.

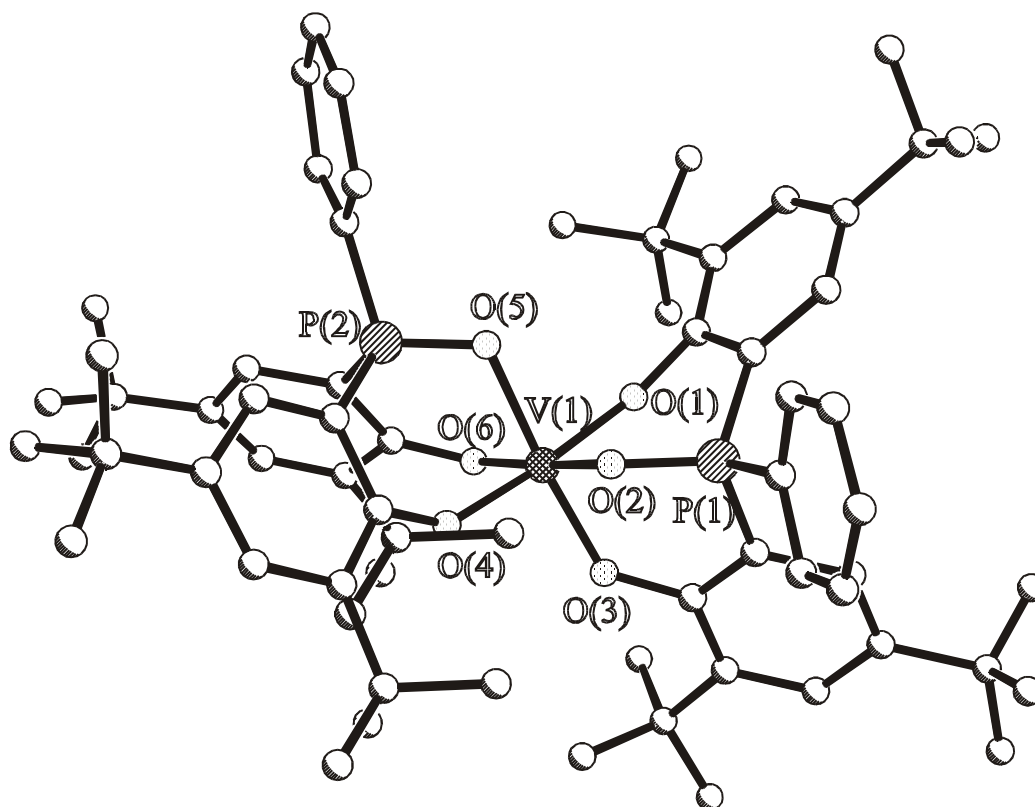


Figure 2.5.4 Ball and stick diagram of $VL^{PO}_2 (4)$.

The complex consists of a neutral unit composed of a distorted octahedral vanadium ion surrounded by two ligands with O, O, O donor set in a facial manner. The basic structural difference between this complex and other complexes discussed previously is the bonding mode of the ligand. Although the ligands are facially coordinated, the axial plane consists of two different types of oxygen donor. This makes the system more distorted tetragonally along the axial direction. Three phenolate oxygens from two ligands and one phosphoryl oxygen from one ligand make the equatorial plane, whereas the remaining phenolate oxygen from one ligand and phosphoryl oxygen from another ligand are *trans* to each other. Different V-O bond distances, V(1)-O(5) [1.996(10)Å] and V(1)-O(3) [1.883(10)Å] make the system distorted resulting in a O(3)-V(1)-O(5) angle at 174.53(45)°. The V(1)-O(3) bond distance is longer than the other V-O(phenolate) bond distances because of the distortion along O(3)-V(1)-O(5), which is a direct outcome of the Jahn-Teller distortion, expected for d^1 systems. All the phenols are deprotonated and aromatic rings are planar, confirming the formal oxidation state of the central vanadium ion to be +4, which was further established by EPR and magnetic measurements.

Table 2.5.2 Selected bond distances (Å) and angles (deg) for **4**

| | | | |
|----------------|------------|-----------|-----------|
| V(1)-O(1) | 1.831(11) | V(1)-O(3) | 1.883(10) |
| V(1)-O(4) | 1.810(10) | V(1)-O(6) | 1.868(10) |
| V(1)-O(2) | 1.980(10) | V(1)-O(5) | 1.996(10) |
| O(1)-V(1)-O(3) | 90.75(43) | | |
| O(1)-V(1)-O(4) | 171.47(50) | | |
| O(3)-V(1)-O(4) | 94.56(44) | | |
| O(6)-V(1)-O(4) | 91.15(46) | | |
| O(6)-V(1)-O(3) | 95.68(45) | | |
| O(1)-V(1)-O(6) | 94.98(46) | | |
| O(1)-V(1)-O(2) | 87.57(43) | | |
| O(2)-V(1)-O(3) | 89.13(40) | | |
| O(2)-V(1)-O(4) | 85.83(42) | | |
| O(5)-V(1)-O(4) | 88.39(43) | | |
| O(5)-V(1)-O(6) | 88.86(41) | | |
| O(2)-V(1)-O(2) | 86.48(40) | | |
| O(6)-V(1)-O(2) | 174.52(41) | | |
| O(1)-V(1)-O(5) | 85.81(43) | | |
| O(5)-V(1)-O(3) | 174.53(45) | | |

2.5.5 Molecular structure of VL^N₂ (**5**)

Single crystals of deep blue *mer-trans*(N,N)-[VL^N₂]_{2/3} MeCN were obtained from acetonitrile solution by slow evaporation of the solvent. As no substantial differences in bond lengths and angles are found between the crystallographically nonequivalent molecules, only one ORTEP diagram for the structure of compound **5** is displayed in Figure 2.5.5, while selected bond lengths and angles are summarized in Table 2.5.3.

The overall geometry around the vanadium ion V(1) is best described as a distorted meridional octahedron with two *trans* positioned nitrogens N(7) and N(27) of the amine bisphenolate ligand. The doubly deprotonated ligand with O, N, O donor set is bound in a meridional manner, the facial mode being sterically unavailable. All the phenyl rings attached to the phenolate oxygen atoms are found to be planar, indicating that upon coordination the aromaticity of the phenyl rings are retained. The small distortion from octahedral geometry is mainly caused by the acute bite angles between the phenolate O atom and the N atom of the

[ONO]²⁻ ligand: N(7)-V(1)-O(10) 88.00(11)°, N(7)-V(1)-O(30) 93.31(11)°. The O(30)-V(1)-O(21) and O(10)-V(1)-O(1) angles are 168.88(11)° and 178.51(11)°, respectively, while the corresponding N(27)-V(1)-N(7) angle at 173.88(11)° deviates from linearity. All the C-O bond lengths found in compound **5** are normal, the average is 1.345(4) Å. The average V-O and V-N distances of 1.879(3) and 2.185(3) Å fall in the range reported for other structurally characterized mononuclear vanadium (IV) complexes, the V-O bond is a little shorter.^{11a} The V-N and V-O bond lengths are in accord with those of a d¹ V(IV) complex, which corroborates also with the EPR measurements.

Table 2.5.3 Selected bond distances (Å) and bond angles (deg) for **5**

| | | | |
|--------------------|------------|--------------------|------------|
| V(1)-O(30) | 1.851(2) | O(21)-C(21) | 1.353(4) |
| V(1)-O(21) | 1.835(2) | O(30)-C(30) | 1.344(4) |
| V(1)-O(10) | 1.919(2) | O(10)-C(10) | 1.339(4) |
| V(1)-O(1) | 1.916(3) | O(1)-C(1) | 1.346(4) |
| V(1)-N(27) | 2.209(3) | V(1)-N(7) | 2.160(3) |
| O(30)-V(1)-O(21) | 168.88(11) | O(30)-V(1)-O(10) | 91.46(11) |
| O(21)-V(1)-O(10) | 92.20(11) | O(30)-V(1)-O(1) | 87.71(11) |
| O(21)-V(1)-O(1) | 88.84(11) | O(10)-V(1)-O(1) | 178.51(11) |
| O(30)-V(1)-N(27) | 83.12(11) | O(21)-V(1)-N(27) | 86.59(11) |
| O(10)-V(1)-N(27) | 87.13(11) | O(1)-V(1)-N(27) | 94.00(11) |
| O(30)-V(1)-N(7) | 83.12(11) | O(21)-V(1)-N(7) | 97.31(11) |
| O(10)-V(1)-N(7) | 88.00(11) | O(1)-V(1)-N(7) | 90.81(11) |
| N(27)-V(1)-N(7) | 173.88(11) | | |
| V(2)-O(41) | 1.921(3) | O(41)-C(41) | 1.342(4) |
| V(2)-O(41)# | 1.921(3) | O(50)-C(50) | 1.357(4) |
| V(2)-O(50) | 1.849(2) | V(2)-O(50)# | 1.849(2) |
| V(2)-N(47)# | 2.167(3) | V(2)-N(47) | 2.167(3) |
| O(50)-V(2)-O(50)# | 180.0 | O(41)#-V(2)-O(50)# | 90.40(11) |
| O(41)#-V(2)-O(50) | 89.60(11) | O(41)-V(2)-O(50)# | 89.60(11) |
| O(50)-V(2)-O(41) | 90.40(11) | O(41#)-V(2)-O(41) | 180.0 |
| O(50)#-V(2)-N(47)# | 85.35(11) | O(50)-V(2)-N(47)# | 94.65(11) |
| O(41#)-V(2)-N(47)# | 91.29(11) | O(41)-V(2)-N(47)# | 88.71(11) |
| O(50)#-V(2)-N(47) | 94.65(11) | O(50)-V(2)-N(47) | 85.35(11) |
| O(41)#-V(2)-N(47) | 88.71(11) | O(41)-V(2)-N(47) | 91.29(11) |
| N(47)#-V(2)-N(47) | 180.00 | | |

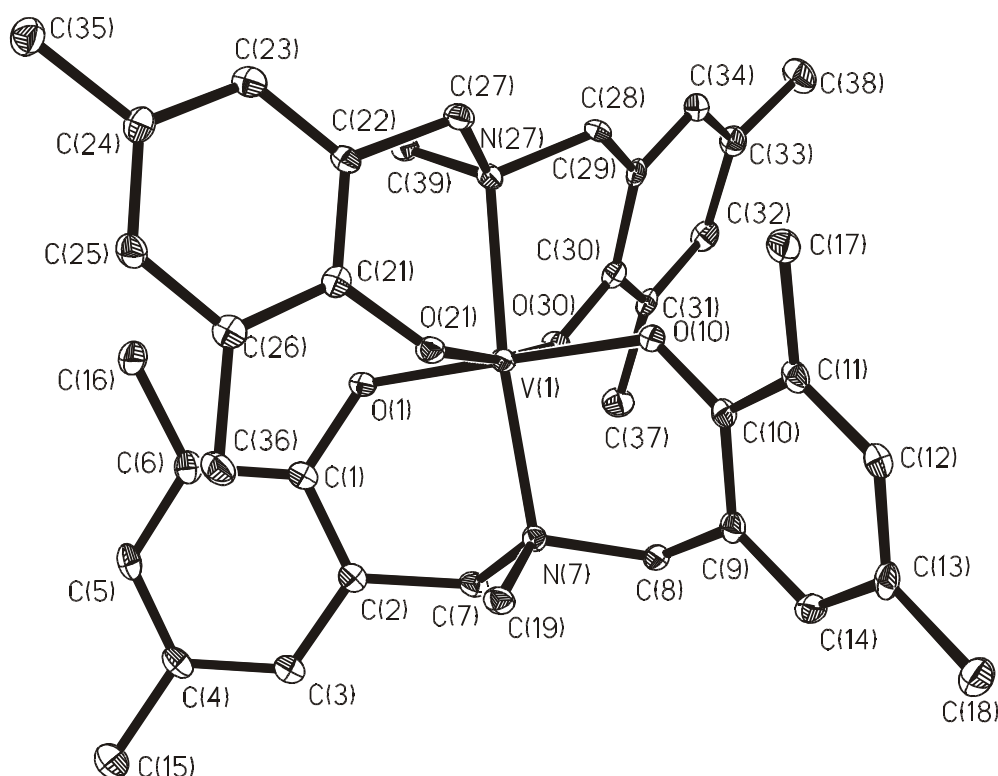


Figure 2.5.5 ORTEP and atom labeling scheme for VL^N_2 (**5**).

2.5.6 Molecular structure of VL^{N1}_2 (**6**)

This complex is isostructural with complex **5** having overall distorted octahedral geometry around the vanadium ion with two meridionally spanning ligands and two *trans* positioned nitrogens. Because of poor crystal quality no detailed structural aspect is described here.

2.5.7 Molecular structure of $[V^V O(L^{PO})(HL^{PO})]$ (**7**)

The ORTEP diagram of the complex is shown in Figure 2.5.6. Important bond distances and angles are given in Table 2.5.4.

The complex can be described as a distorted octahedron with two ligands per oxovanadium(V) unit. One $[L^{PO}]^{2-}$ is coordinated facially through O,O,O donor set. The second ligand occupies the remaining equatorial sites using phenolate oxygen and phosphoryl oxygen. The phosphoryl oxygen O(10) is bonded *trans* to vanadyl oxygen O(30) making the axial plane having a O(10)-V(1)-O(30) angle at $176.33(8)^\circ$. The second phenol of that ligand is uncoordinated and remains protonated, forming a hydrogen bond with phosphoryl oxygen. The V-O(phenolate) bond distances for the facially coordinated ligand are V(1)-O(1) 1.864(2)Å, V(1)-O(2) 1.859(2)Å whereas the similar V(1)-O(3) distance for the other ligand

is longer at 1.895(2)Å. The V-O distances are within the range of normal V-O(phenolate) distances. The V(1)-O(30) bond distance [1.60482)Å] clearly indicates the V=O character and the system is a genuine V(V) system, as is also evident from the electroneutral molecular formula with one protonated ligand. The aromatic rings are planar and hence they retain their aromatic character after complexation.

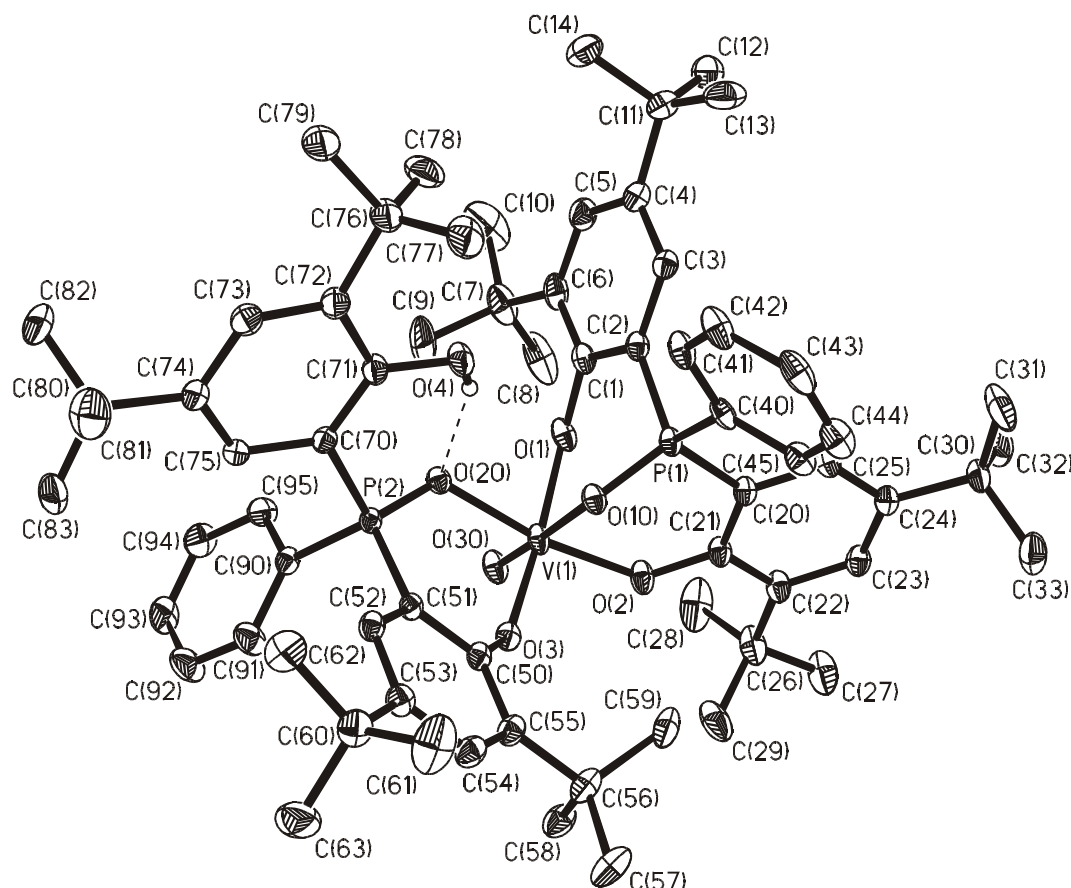


Figure 2.5.6 ORTEP and atom labeling scheme for $[V^VO(L^{PO})(HL^{PO})]$ (7).

Table 2.5.4 Selected bond lengths (Å) and angles (deg) for complex 7

| | |
|------------------|-----------|
| V(1)-O(30) | 1.604(2) |
| V(1)-O(2) | 1.859(2) |
| V(1)-O(1) | 1.864(2) |
| V(1)-O(10) | 2.190(2) |
| V(1)-O(3) | 1.895(2) |
| V(1)-O(20) | 2.054(2) |
| O(30)-V(1)-O(2) | 97.80(8) |
| O(30)-V(1)-O(1) | 96.05(9) |
| O(30)-V(1)-O(10) | 176.33(8) |
| O(30)-V(1)-O(3) | 95.10(9) |

| | |
|------------------|-----------|
| O(30)-V(1)-O(20) | 98.28(8) |
| O(2)-V(1)-O(1) | 92.02(9) |
| O(2)-V(1)-O(10) | 85.52(7) |
| O(2)-V(1)-O(3) | 94.26(8) |
| O(2)-V(1)-O(20) | 163.69(7) |
| O(1)-V(1)-O(10) | 85.37(7) |
| O(1)-V(1)-O(3) | 166.35(7) |
| O(1)-V(1)-O(20) | 83.65(7) |
| O(10)-V(1)-O(3) | 83.05(7) |
| O(10)-V(1)-O(20) | 78.48(6) |
| O(3)-V(1)-O(20) | 86.97(7) |

2.5.8 Molecular structure of $[V^V O(\mu-OH)L^{Se}]_2$ (**8**)

The dinuclear oxovanadium complex was recrystallized from a solvent mixture of CH_2Cl_2 and toluene. The unit cell contains a dinuclear unit, which is shown in the ORTEP diagram with the atom labeling scheme in Figure 2.5.7. Selected bond parameters are given in Table 2.5.5.

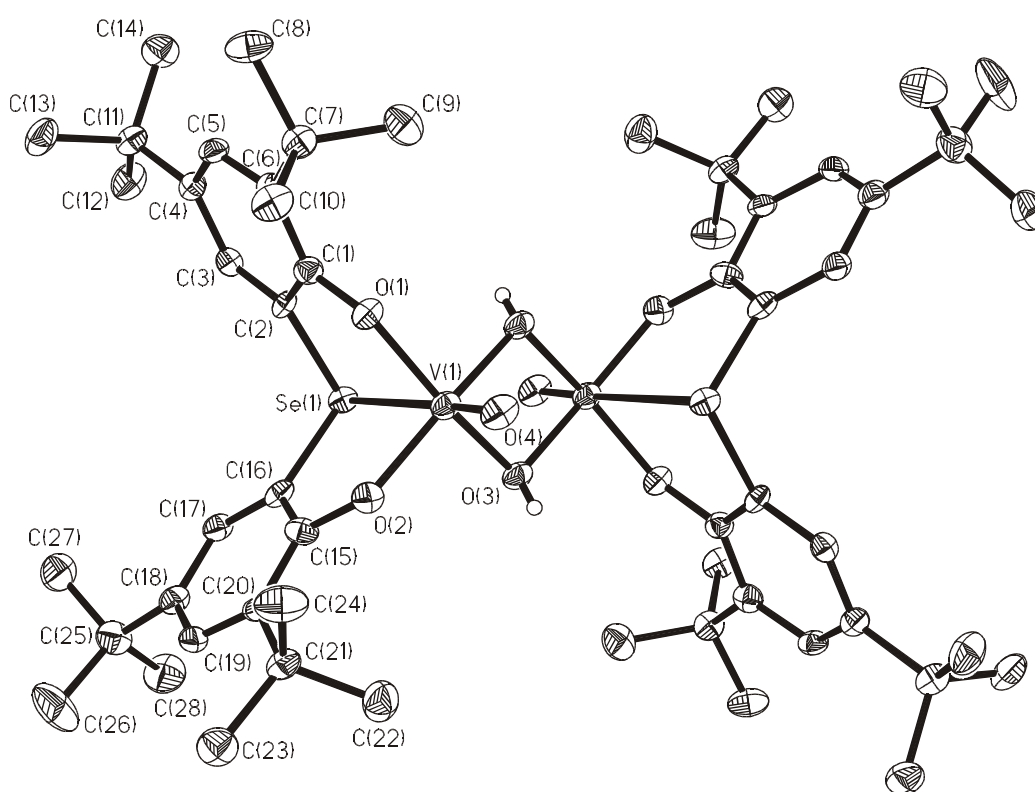


Figure 2.5.7 ORTEP and atom labeling scheme for $[V^V O(\mu-OH)L^{Se}]_2$ (**8**).

This complex is composed of two edge-shared octahedra in which the ligand $[L^{Se}]^{2-}$ coordinates facially with the selenium atom trans to the oxo-donor atom and which are related by a crystallographic center of symmetry and pseudo two-fold axis of symmetry. Two vanadium atoms are bridged by two hydroxide ligands. Two bridging hydroxide oxygens and two phenolates from the ligand form the equatorial plane. The axial Se(1)-V(1)-O(4) angle $174.64(12)^\circ$ makes both vanadyl-centered octahedra slightly distorted. The hydroxide bridge is symmetric with V(1)-O(3) and V(1)-O(3)# distances at $1.964(3)\text{\AA}$ and $1.969(3)\text{\AA}$, respectively. The axial V(1)-Se(1) and V(1)-O(4) distances are $2.8857(9)\text{\AA}$ and $1.585(3)\text{\AA}$ respectively, clearly indicating the unit as a V=O unit and the oxidation state of the metal center as (+5), which is in accord with the ^{51}V NMR spectroscopy. V-O(phenolate) bond distances are also in the normal range of V(V)-O distances.

Table 2.5.5 Selected bond lengths (\AA) and angles (deg) for complex 8

| | | | |
|-----------------|------------|------------------|-----------|
| V(1)-O(4) | 1.585(3) | V(1)-O(3) | 1.964(3) |
| V(1)-O(3)# | 1.969(3) | V(1)-O(1) | 1.850(3) |
| V(1)-O(2) | 1.842(3) | V(1)-Se(1) | 2.8857(9) |
| V(1)-V(1)# | 3.141(3) | | |
| O(4)-V(1)-O(3) | 101.3(2) | O(4)-V(1)-O(3)# | 100.4(2) |
| O(4)-V(1)-O(1) | 100.90(14) | O(4)-V(1)-O(2) | 98.3(2) |
| O(4)-V(1)-Se(1) | 174.64(12) | O(3)-V(1)-O(3)# | 74.0(2) |
| O(3)-V(1)-O(1) | 154.4(2) | O(3)-V(1)-O(2) | 91.74(3) |
| O(3)-V(1)-Se(1) | 81.96(10) | O(3)#-V(1)-O(1) | 89.68(14) |
| O(3)#-V(1)-O(2) | 158.32(14) | O(3)#-V(1)-Se(1) | 84.53(10) |
| O(1)-V(1)-O(2) | 97.37(13) | O(1)-V(1)-Se(1) | 76.95(9) |
| O(2)-V(1)-Se(1) | 77.21(9) | V(1)-O(3)-V(1)# | 106.0(2) |

2.6 ELECTRONIC SPECTROSCOPY

Electronic spectra for complexes **1-8** were measured over the range 200-1200 nm in CH_2Cl_2 solution and are shown in Figures 2.6.1 and 2.6.2. In the analyzed region intra-ligand transitions at higher energies and charge transfer (CT) transitions at intermediate energies are expected to be found. The long tail of CT bands obscures low energy ligand field transitions.

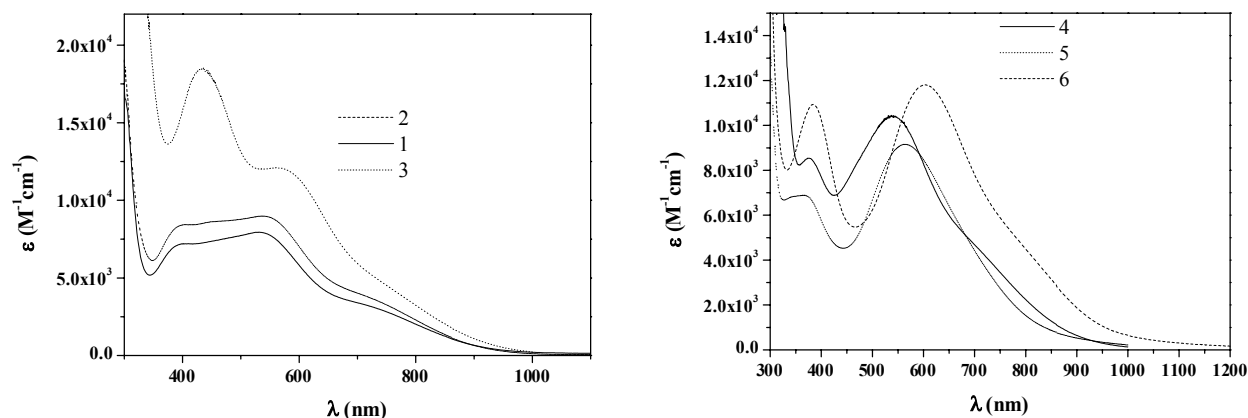


Figure 2.6.1 UV-vis spectra for complexes **1-6** at room temperature in CH_2Cl_2 .

The electronic spectra of complexes **1-6** in CH_2Cl_2 solution consist of the following transitions: a band around 550 nm and another band around 400 nm. The lowest energy bands around 550 nm is assigned, by analogy with other reported ‘bare’ vanadium(IV) complexes,¹¹ as being phenolate-to-vanadium(IV) CT transitions. The higher energy transitions at around 400 nm, which are absent in the free ligands, are also assigned to the phenolate-to-vanadium(IV) CT transition. There is also a shoulder at ~700 nm for complexes **1-6**.

Table 2.6.1 Room temperature electronic spectral (1200-200 nm) data for complexes **1-8**

| Complex | λ_{max} , nm (ϵ , $\text{M}^{-1}\text{cm}^{-1}$) |
|----------|--|
| 1 | 400sh (7190), 531 (7950), 700sh (3430) |
| 2 | 400sh (8370), 536 (8950), 700sh (4100) |
| 3 | 436 (18560), 562 (12130), 700sh (5930) |
| 4 | 375 (8280), 542 (10110), 700sh (4510) |
| 5 | 362 (6890), 562 (9160) |
| 6 | 383 (10900), 603 (11830), 814sh (4120) |
| 7 | 395 (5750), 537 (7120), 721 (3400) |
| 8 | 511 (15120), 788 (8520) |

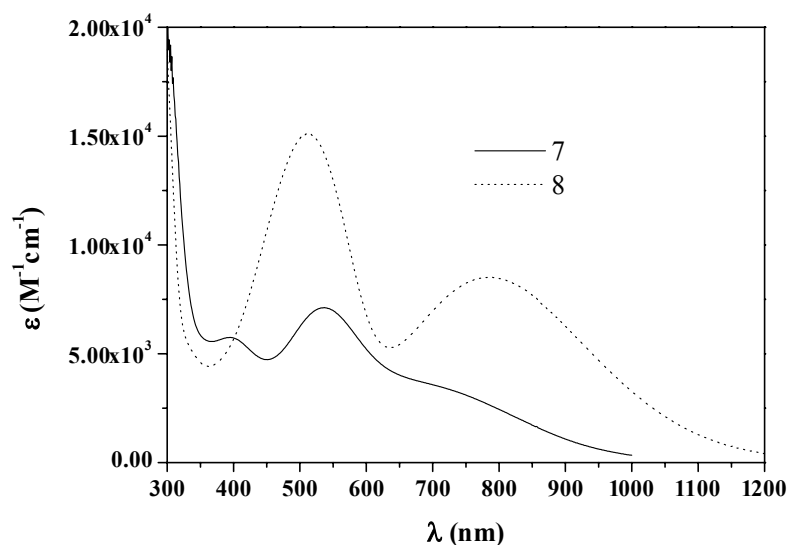


Figure 2.6.2 UV-vis spectra for complexes **7-8** at room temperature in CH_2Cl_2 .

The purple color of the complexes **7** and **8** along with their high ϵ value, is presumably due to phenolate-to-vanadium charge transfer, as is seen for other oxovanadium(V) complexes of phenolate derived ligands. The absence of the low-energy transitions, (i.e., >800 nm) suggests that this transition may be due to the *trans*- $\text{Ar}_2\text{Se} \rightarrow \text{VO}$ chromophore.

2.7 MAGNETISM

Magnetic susceptibility data for polycrystalline samples of the complexes **1-6** were collected in the temperature range 2 - 290 K in an applied magnetic field of 1 T. The room temperature magnetic moments of solids **1**, **2**, **3**, **4**, **5** and **6** are $1.77 (\pm 0.33)$, $1.76 (\pm 0.33)$, $1.74 (\pm 0.33)$, $1.74 (\pm 0.33)$, $1.75 (\pm 0.33) \mu_{\text{B}}$ and $1.74 (\pm 0.3) \mu_{\text{B}}$, respectively. These results are consistent with the formulation of the complexes as vanadium(IV) d^1 species (spin-only $\mu_{\text{eff}} = 1.73\mu_{\text{B}}$) with no or very small intermolecular coupling and are in complete agreement with X-ray and EPR results. Simulations of the experimental magnetic moment data yield $g_{\text{v}} = 1.96$, $\text{TIP} = 90 \times 10^{-4}$ emu for **1**, $g_{\text{v}} = 1.95$, $\text{TIP} = 90 \times 10^{-4}$ emu for **2**, $g_{\text{v}} = 1.97$, $\text{TIP} = 40 \times 10^{-6}$ emu for **3**, $g_{\text{v}} = 1.94$ for **4**, $g_{\text{v}} = 1.89$, $\text{TIP} = 145 \times 10^{-4}$ emu for **5** and $g_{\text{v}} = 1.92$, $\text{TIP} = 200 \times 10^{-6}$ emu for **6**.

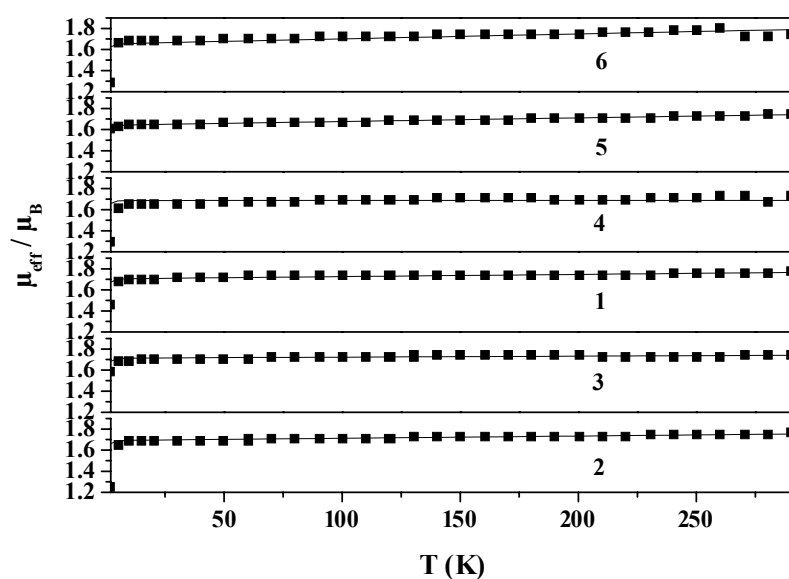


Figure 2.7.1 Magnetic susceptibility measurements for complexes 1-6.

Complexes 7 and 8 are diamagnetic as expected for vanadium(V) with d^0 electronic configuration.

2.8 ELECTRO- AND SPECTROELECTROCHEMISTRY

Cyclic and square wave voltammograms of the complexes were measured in CH_2Cl_2 solution. A three electrode cell was employed with a glassy carbon working electrode, a 0.01 M Ag/AgNO_3 reference electrode, a Pt wire as auxiliary electrode and TBAPF_6 as supporting electrolyte. All potentials were referenced vs ferrocene, which was used as internal standard. The results for the complexes are outlined below:

Table 2.8.1 Electrochemical results for the complexes 1-8

| Complex | $E_{1/2}^{\text{red}}$ (V) | $E_{1/2}^{\text{ox}}$ (V) vs Fc^+/Fc | Fc^+/Fc (V) |
|---------|----------------------------|--|-----------------------------|
| 1 | -0.929 | 0.595 | 0.233 |
| 2 | -0.951 | 0.464 | 0.233 |
| 3 | -1.060 | -0.175 | 0.233 |
| 4 | -0.987 | 0.193 | 0.233 |
| 5 | -0.882 | 0.177, 0.950 (ir.) | 0.244 |
| 6 | -0.72 (ir.) | 0.226, 0.875 | 0.240 |
| 7 | -0.890 | 0.726(ir.) | 0.230 |
| 8 | -0.630, -0.488 | 0.867(ir.) | 0.230 |

Complex **1** exhibits two redox processes at -0.929 and 0.595 V vs Fc^+/Fc . Controlled potential coulometry at 0.85 V vs Fc^+/Fc revealed that the species is oxidized by one electron per vanadium center. The CV of the oxidized solution is identical to that of the starting material under the same conditions and the spectrum of the starting material can be regenerated with re-reduction at 0.0 V vs Fc^+/Fc . Similarly, coulometry at an appropriate potential establishes the wave at -0.929 V corresponding to a one-electron reduction process.

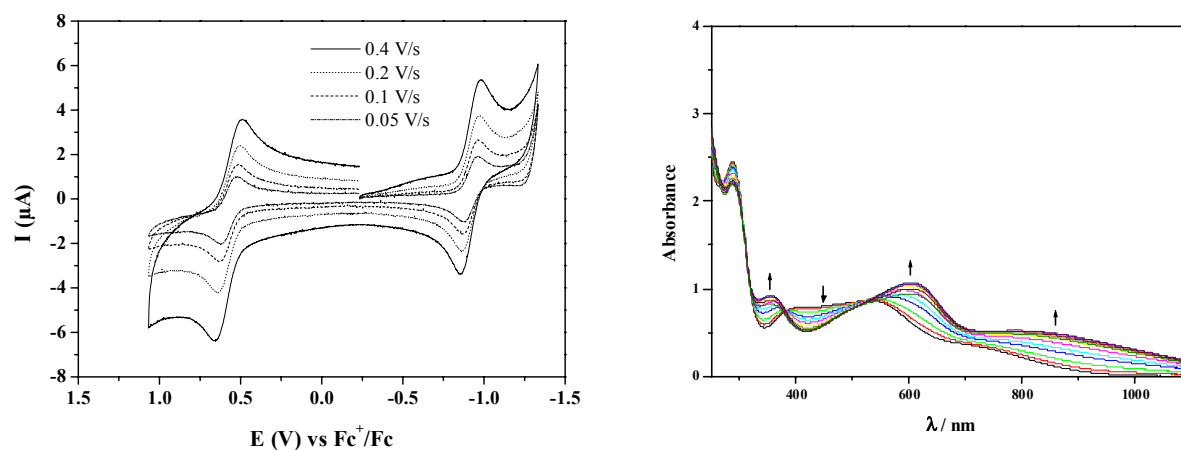


Figure 2.8.1 Left: Cyclic voltammogram of VL^{S}_2 (**1**). Right: Optical spectral change during $1e^-$ -oxidation.

The UV-vis spectra above (Figure 2.8.1) exhibit the modification caused by the electrochemical oxidation of the complex. It can be seen that it consists of an increase in the intensity of the bands at around 600 nm and a shift to lower energy. This peak corresponds to a phenolate \rightarrow V(V) charge transfer. So the oxidation is metal-centered.

During electrochemical reduction the band at 500 nm vanishes, yielding finally a colorless solution (Figure 2.8.2). This one electron reduction may be assigned to V(IV) to V(III) reduction.

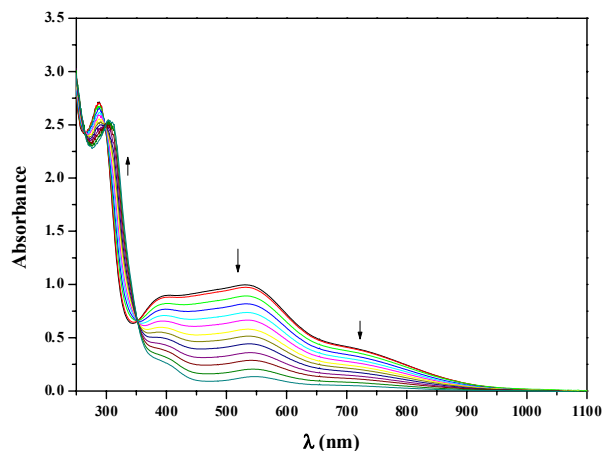


Figure 2.8.2 Electronic spectra of VL^S_2 (**1**) and its electrochemically $1 e^-$ reduced species.

Complex **2**, like complex **1**, shows two reversible redox processes at -0.951 and 0.464 V vs Fc^+/Fc , as shown in Figure 2.8.3. According to coulometric experiments at fixed potentials, the wave at -0.951 V is attributed to a one-electron reduction process and the wave at 0.464 V to a one-electron oxidation process.

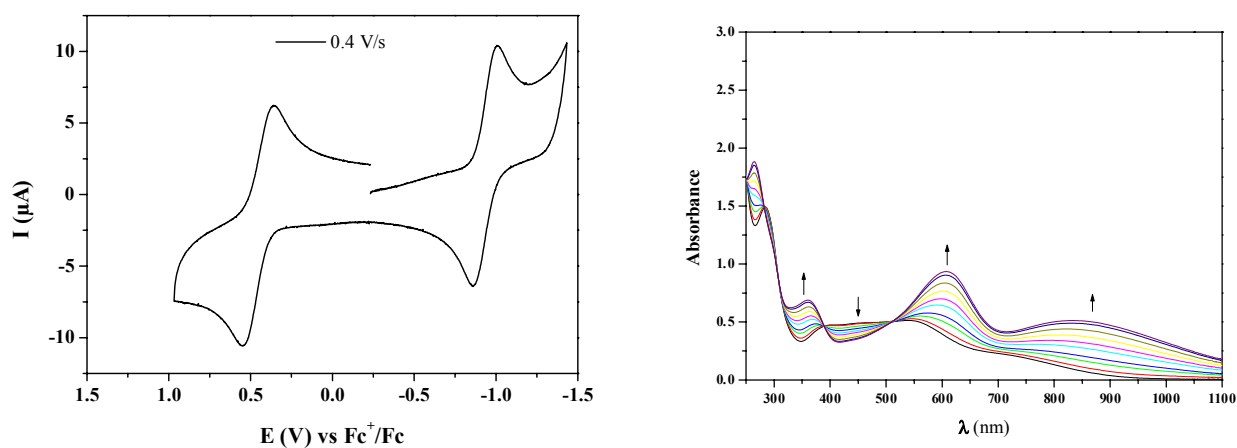


Figure 2.8.3 Left: Cyclic voltammogram of VL^{Se}_2 (**2**). Right: Optical spectral change during $1 e^-$ oxidation process.

The spectral changes upon oxidation and reduction of **2** are similar to those of **1** (Figure 2.8.3 shows the oxidation process).

Complex **3** exhibits two redox processes at -1.060 V and -0.175 V vs Fc^+/Fc . Clearly one-electron reversible oxidation (at -0.175 V) and one electron reversible reduction (at -1.060 V) is observed, as established by coulometry at fixed potentials.

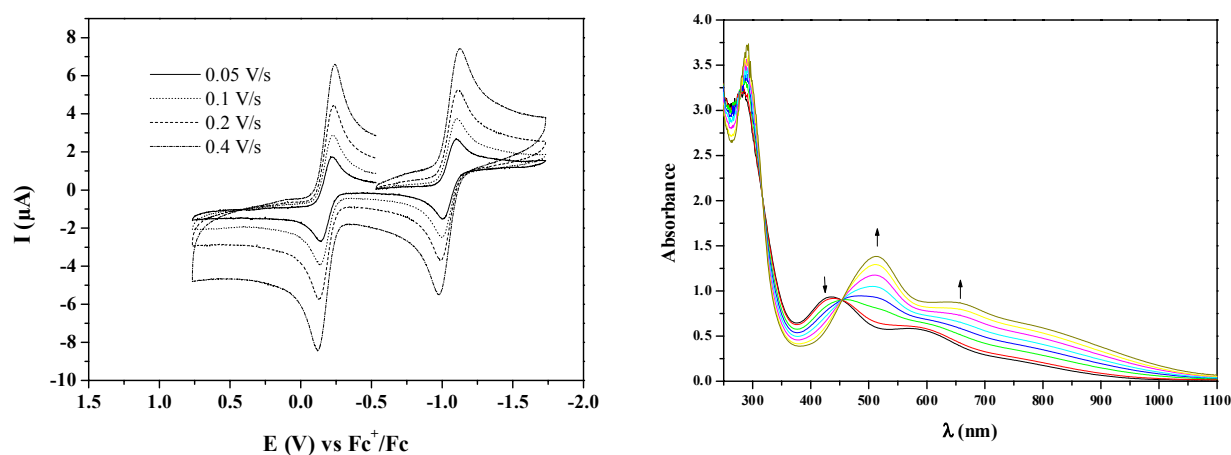


Figure 2.8.4 Left: Cyclic voltammogram of VL^{P}_2 (**3**). Right: Optical spectral change during $1e^-$ -oxidation.

The spectral changes caused by both oxidative and reductive coulometry show the same trend as observed with **1** and **2**. The peak intensity at 500 nm increases during the oxidation process and the peak at 450 nm diminishes during the reduction.

Very similar to complex **3**, complex **4** exhibits two redox processes at -0.987 V and 0.193 V vs Fc^+/Fc . Clearly one-electron reversible oxidation (at 0.193 V) and one electron reversible reduction (at -0.987 V) is observed, as established by coulometry at fixed potentials.

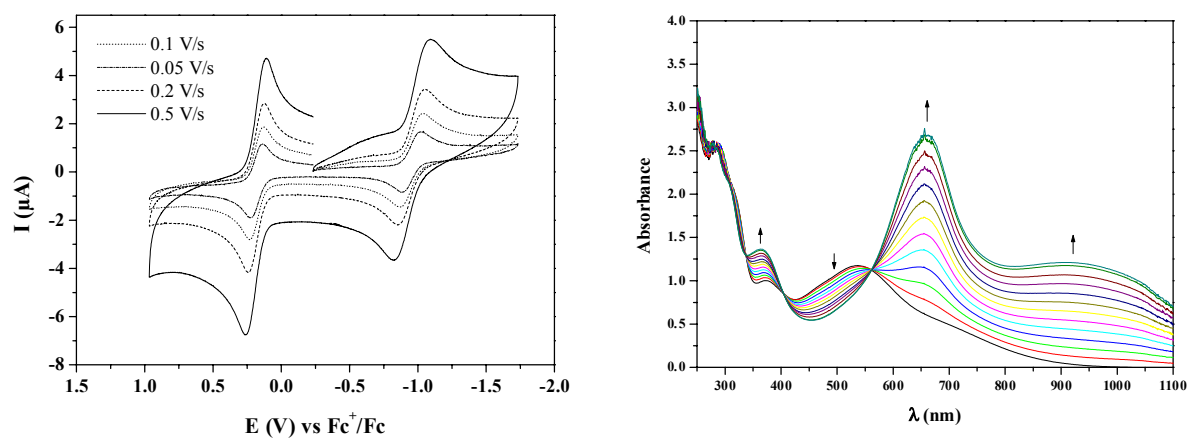


Figure 2.8.5 Left: Cyclic voltammogram of VL^{PO}_2 (**4**). Right: Optical spectral change during $1e^-$ -oxidation.

Again the spectral changes caused by both oxidative and reductive coulometry show the same features. The peak at 650 nm increases during the oxidation process and the peak at 550 nm diminishes during the reduction.

Complex **5** exhibits two reversible redox processes at -0.882 and 0.177 V and one irreversible redox process at 0.950 V vs Fc^+/Fc . Coulometry at an appropriately fixed potential establishes that the redox process at -0.882 V is a one electron reduction whereas that at 0.177 V is a one-electron oxidation process.

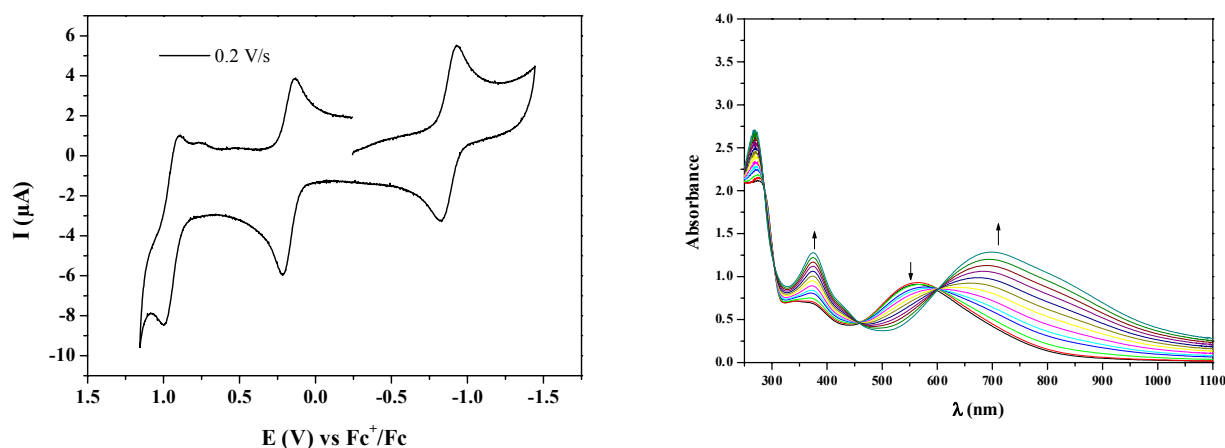


Figure 2.8.6 Left: Cyclic voltammogram of VL^{N}_2 (**5**). Right: Optical spectral change during $1e^-$ -oxidation.

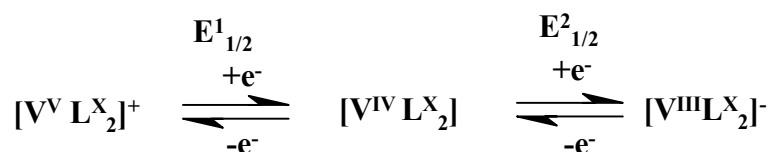
The irreversible oxidation peak at 0.950 V corresponds to another oxidation process, which may be assigned to ligand-centered oxidation leading to the formation of a phenoxyl radical. But because of its irreversible nature the coulometric oxidation does not provide a stable species. The spectral change during the one-electron oxidation, where the peaks at 700 and 380 nm increase their absorbance (typical for phenolate to V(V) charge transfer band) indicates the first oxidation to be metal-centered.

But there is still an inherent ambiguity in assigning the redox waves for the system having phenolate ligated to the metal center because of their tendency to form phenoxyl radical complexes. All the non-oxo vanadium complexes are in a formal oxidation state of $+4$ as is evidenced from magnetic and EPR measurements. But in CV there are two possibilities for the assignment of redox-waves, particularly the oxidative wave. One is the metal-centered oxidation giving rise to V(V) species; a second possibility is the formation of an AF-coupled V(IV) radical system. Both systems are EPR silent and no other analytical tools are available

to confirm directly the way of oxidation. But a few observations and experimental results discard the second possibility:

- From the table of the potentials of the complexes given above it is clear that complex **3** is easily oxidizable. In air it is oxidized to the oxovanadium(V) complex **7** where oxidation of P(III) to P(V) also occurs. Electrochemically oxidized species from all the non-oxo vanadium complexes are very much air-sensitive.
- Complex **4** can also be oxidized by Ni(III) salt to complex **7** indicating that oxovanadium(V) is more stable than its non-oxo congener.
- Chemically and electrochemically oxidized species of all the complexes are EPR-silent in the temperature range 2 – 30 K.
- No peak corresponding to characteristic π - π^* transition of the phenoxyl radical is observed in the coulometry during exhaustive oxidation and the peaks appearing are rather similar to other reported ligand \rightarrow V(V) charge transfer species.

At scan rates of 50 - 500 mV s⁻¹ two well-defined reversible one-electron transfer waves were detected. These data are consistent with the redox-process:



On the other hand, complex **6** shows two reversible oxidation peaks (at 0.226 and 0.875 V vs Fc⁺/Fc) and one irreversible reductive peak in CH₂Cl₂ as established by coulometry at -20°C.

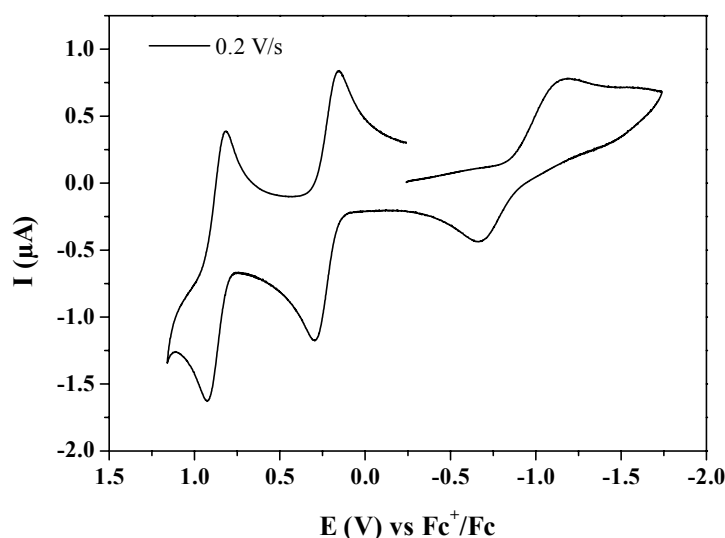


Figure 2.8.7 Cyclic voltammogram of VL^{NI}₂ (**6**).

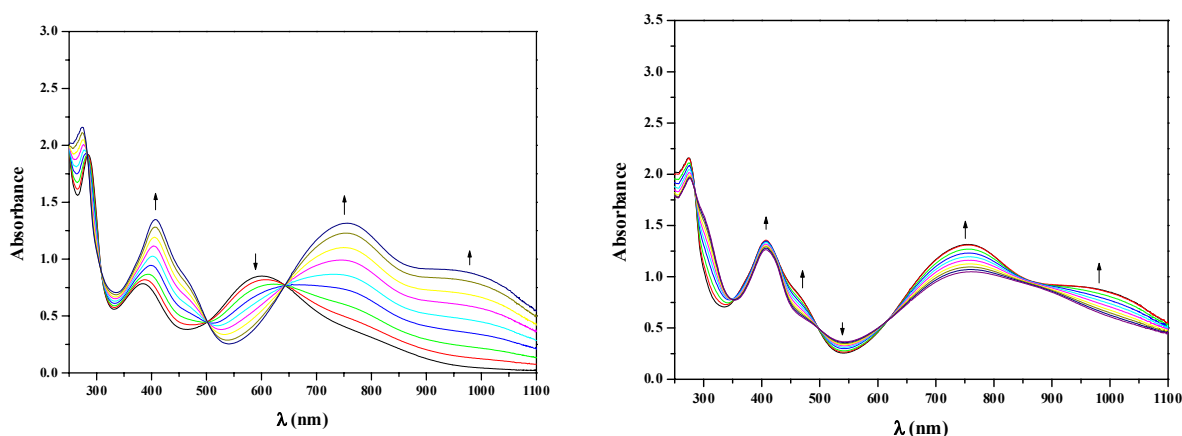
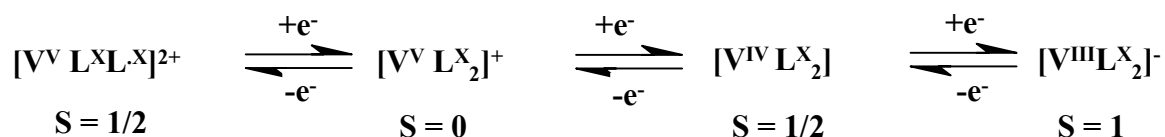


Figure 2.8.8 Optical spectral change of VL^{NI}_2 (**6**) during $1e^-$ -first oxidation (left) and second oxidation (right).

The first oxidation is metal-centered while the second oxidation is ligand-centered, as is evidenced from the EPR spectrum of the electrochemically oxidized species ($S = \frac{1}{2}$ signal) where no vanadium hyperfine coupling is observed, confirming the formation of the phenoxyl radical. These data are consistent with the redox-process:



Mononuclear oxo-vanadium(V) complex **7** shows only one reduction wave corresponding to a V(V)/V(IV) equilibrium, is reversible in nature and has one irreversible oxidative wave. Because of the slow oxidation process and the irreversible nature, the oxidized product could not be characterized by EPR spectroscopy but can be assigned to ligand-based oxidation, i.e. phenolate to phenoxyl radical formation.

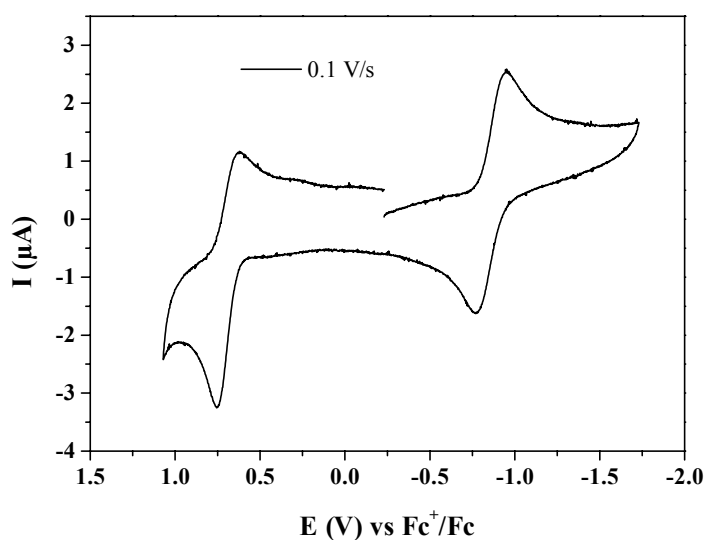


Figure 2.8.9 Cyclic voltammogram of $[V^VO(L^{PO})(HL^{PO})]$ (**7**) in CH_2Cl_2 at room temperature.

By contrast, dinuclear oxo-vanadium(V) complex **8** shows two reversible reductive waves (corresponding to a V(V)/V(IV) couple) with one irreversible oxidative wave.

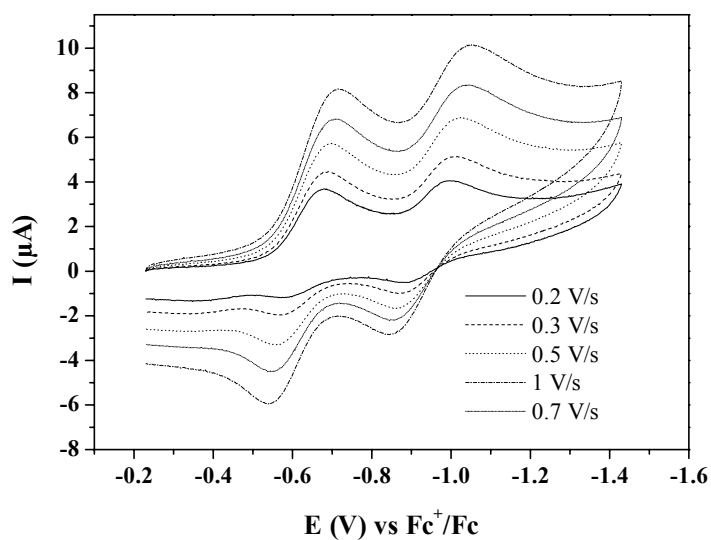


Figure 2.8.10 Cyclic voltammogram of $[V^VO(\mu-OH)L^{Se}]_2$ (**8**) in CH_2Cl_2 at room temperature.

2.9 EPR SPECTROSCOPY

EPR spectra of complexes **1-6** were measured at the X-band frequency at low temperature in a variety of solvents or solvent mixtures. The EPR spectra of the complexes display the typical eight-line pattern of vanadium (^{51}V ; $I = 7/2$) and the corresponding anisotropic g and $A(10^{-4} \text{ cm}^{-1})$ values are given in Table 2.9.1.

Table 2.9.1 EPR parameters for complexes **1-6**

| Complex | g_x | g_y | g_z | A_x (10^{-4} cm^{-1}) | A_y (10^{-4} cm^{-1}) | A_z (10^{-4} cm^{-1}) |
|----------|--------|--------|--------|--|--|--|
| 1 | 1.9611 | 1.9573 | 1.9911 | 49.96 | 129.25 | 13.08 |
| 2 | 1.9559 | 1.9584 | 1.9818 | 49.66 | 128.45 | 19.33 |
| 3 | 1.970 | 1.970 | 1.975 | 43.3 | 43.3 | 126.76 |
| | | | | | ($A_{\text{VP}} = 21.68$) | |
| 4 | 1.9350 | 1.9350 | 1.7900 | 70.00 | 70.00 | 173.00 |
| 5 | 1.9341 | 1.9663 | 1.9588 | 44.52 | 14.52 | 147.40 |
| 6 | 1.9200 | 1.9450 | 1.9540 | 50.00 | 10.00 | 146.00 |

For systems having d^1 electronic configuration covalent bonding becomes progressively more important as the charge on the ion increases. The resultant transfer of charge to the ligands lower the effective value of spin-orbit coupling parameter and in some cases may reverse the expected relative magnitudes of g components. According to LF-theory, $g_z > g_x = g_y$. The correct ordering of g factors is obtained when the ligands are considered explicitly in the MO calculation.¹⁵ This calculation indicates that g_z is affected only by bonding in the equatorial plane, while axial bonding on the Z-axis affects g_x, g_y .

Six coordinated vanadium(IV) complexes have been shown¹⁶ from previous EPR studies to fall into two classes: those with a $d_{x^2-y^2}$ ground state, which display all $g < 2$ and a large A_z , and those with a d_{z^2} ground state which display $g_z \sim 2$, $g_x, g_y < 2$ and $A_z \ll A_x, A_y$. The latter parameter can be associated with geometry that is distorted from octahedral toward trigonal prismatic.

The EPR parameters for complexes **1** and **2** clearly place themselves into the category with a d_{z^2} ground state. This ground state is only observed with complexes having five-membered rings incorporating the central metal ion. Obviously the extra strain in the ring compared with that for six-membered rings must have a dramatic effect upon the structure with consequent

reordering of the energy levels. Complexes **1**, **2** and **3** form five-membered rings through facially coordinated ligands, where two donor atoms of the same type are *trans* to each other along the axial plane (from X-ray structure). They are in the same category with other six-coordinate vanadium(IV) complexes with d_z^2 ground state, $[\text{V}(\text{mnp})_3]^{17}$, $[\text{V}(\text{cat})_3]^{2-18}$, $[\text{V}(\text{mnt})_3]^{2-19}$ (mnp = 2-mercapto-4-methylphenolate, cat = catecholate, mnt = maleonitriledithiolate).

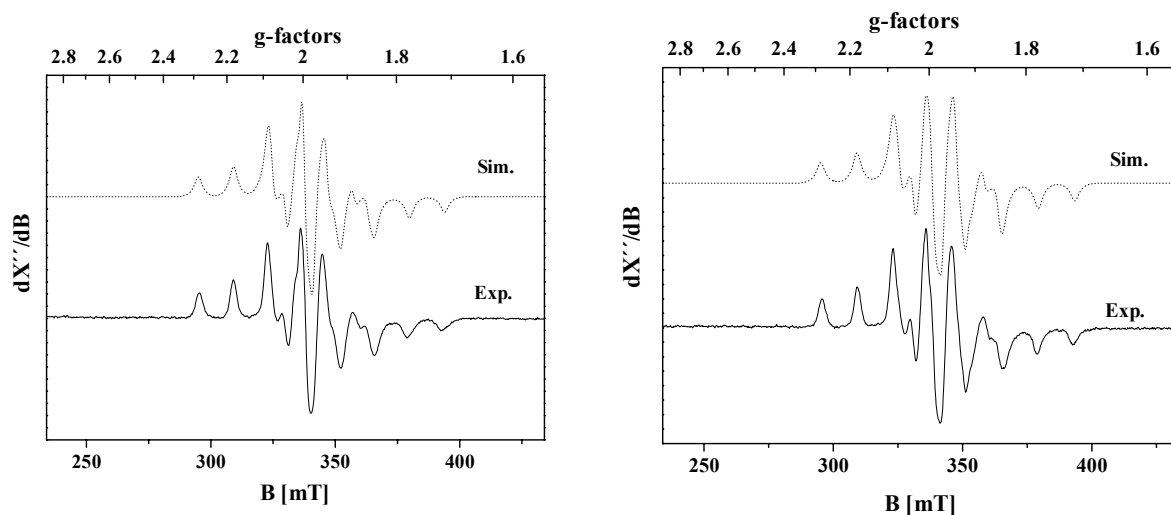


Figure 2.9.1 X-band EPR spectra for complexes **1** (left) and **2** (right) in CH_2Cl_2 at 60K. Experimental conditions (—): microwave frequency 9.44 GHz (**1**); 9.44 GHz (**2**), microwave power 0.1 mW (**1**); 1 μW (**2**), modulation amplitude 12.5 G (**1**); 12.5 G (**2**). The simulations (---): $g = \{1.9611, 1.9573, 1.9911\}$, $A = \{49.96, 129.25, 13.08\} \times 10^{-4} \text{ cm}^{-1}$ for **1** and $g = \{1.9559, 1.9584, 1.9818\}$, $A = \{49.66, 128.45, 19.33\} \times 10^{-4} \text{ cm}^{-1}$ for **2**; Lorentzian line with angular-dependent line width $W = \{38, 49, 54\} \text{ G}$ (**1**); $W = \{38, 48, 49\} \text{ G}$ (**2**).

Interestingly, the EPR spectrum of complex **3** in a 1:1 solvent mixture of CH_2Cl_2 /toluene exhibits superhyperfine coupling from P ($I = \frac{1}{2}$) for each eight-line pattern due to vanadium. Phosphorus is directly bonded to the central vanadium giving rise to five-membered rings and subsequent distortion toward a trigonal prismatic structure. The solvent dependent observed hyperfine coupling from phosphorus and the resulting coupling with vanadium is novel and the first of this kind. The value of g_z decreases compared to complexes **1** and **2**. The decrease in the g_z value is due to equatorial in-plane π -back bonding from phosphorus increasing the covalency in the equatorial plane.

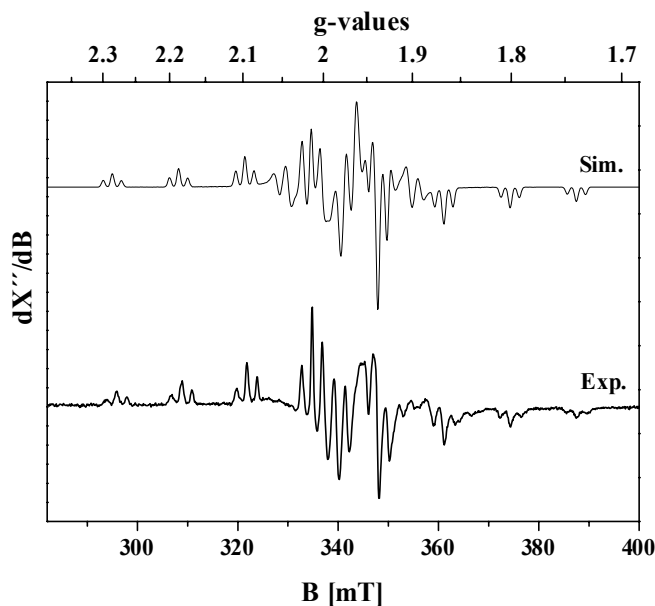


Figure 2.9.2 X-band EPR spectrum for complex **3** in $\text{CH}_2\text{Cl}_2/\text{toluene}$ at 60K. Experimental conditions (—): microwave frequency 9.44 GHz, microwave power 0.1 mW, modulation amplitude 4.96 G. The simulations (—): $g = \{1.970, 1.970, 1.975\}$, $A = \{43.3, 43.3, 126.76\} \times 10^{-4} \text{ cm}^{-1}$, $A_{VP} = 21.68 \times 10^{-4} \text{ cm}^{-1}$.

In case of complex **4** different g-values are obtained. From its structure it is clear that two different types of oxygen are *trans* to each other forming the axial plane. This leads to a tetragonal distortion along the Z-axis as well as along the XY-plane. This is seen from the solid-state crystal structure analysis and the complex shows a higher degree of g - anisotropy. Simulation of the experimental spectrum yields the parameters $g_x = g_y = 1.935$, $g_z = 1.79$ and $A_{xx} = A_{yy} = 70 \times 10^{-4} \text{ cm}^{-1}$, $A_{zz} = 173 \times 10^{-4} \text{ cm}^{-1}$. For a d^1 octahedral system with tetragonal distortion, $g_z = g_e - 8\lambda/\Delta_1$ and $g_x = g_y = g_e - 2\lambda/\Delta_2$ [Δ_1 = energy separation between $d_{x^2-y^2}$ and d_{xy} and Δ_2 = energy separation between d_{xz}, d_{yz} and d_{xy}].

From simulation parameters of complex **4** $g_e - g_z = 8\lambda/\Delta_1$, so $\Delta_1 = 9448 \text{ cm}^{-1}$ (λ of $\text{V}^{4+} = 248 \text{ cm}^{-1}$). Similarly, Δ_2 is found to be 7630 cm^{-1} . The magnitude of Δ_1 and Δ_2 can be explained in terms of the orbital splitting shown in Figure 2.9.3. The d_{xy} orbital is stabilized more than d_z^2 . Although the geometry corresponding to this orbital splitting does not fit with that of the crystal structure but qualitatively explains the ‘unusually’ low g_z value. An alternative explanation is the mixing of orbitals in the ligand field resulting in same Δ values. Absence of

any d-d band in the UV-vis spectrum of the complex does not allow any correlation between the Δ values and EPR parameters.

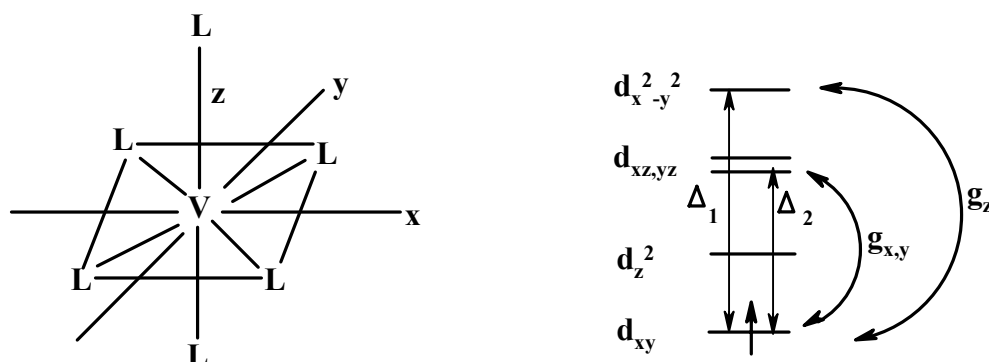


Figure 2.9.3 Relative energies of the metal orbitals in **4** with axis-notation.

Thus the drop in g_z value reflects the increased covalency and stability of the equatorial σ bonds.

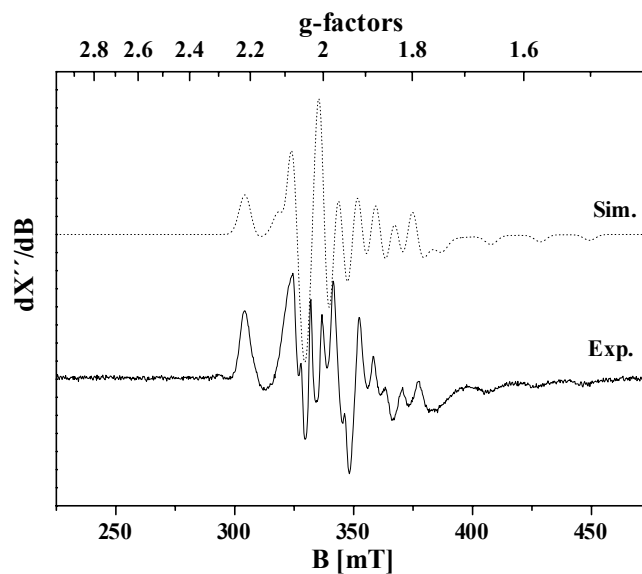


Figure 2.9.4 X-band EPR spectrum for complex **4** in CH_2Cl_2 at 10K. Experimental conditions (—): microwave frequency 9.45 GHz, microwave power 0.25 μW , modulation amplitude 5 G. The simulations (----): $g = \{1.935, 1.935, 1.79\}$, $A = \{70, 70, 173\} \times 10^{-4} \text{ cm}^{-1}$; Gaussian line with frequency-dependent line width $W_f = 120 \text{ G}$.

Complexes **5** and **6** can be placed in the class with a $d_{x^2-y^2}$ ground state. This is due to the structural difference observed for the other complexes. Six-membered ring formation and steric availability favors the coordination of the ligand in meridional manner. This results in a small increase in the equatorial σ bonding and considerable increase in the in-plane π -bonding. So a σ bonding d_{xy} orbital will be stabilized slightly, whereas the π -bonding $d_{x^2-y^2}$ orbital is strongly stabilized.

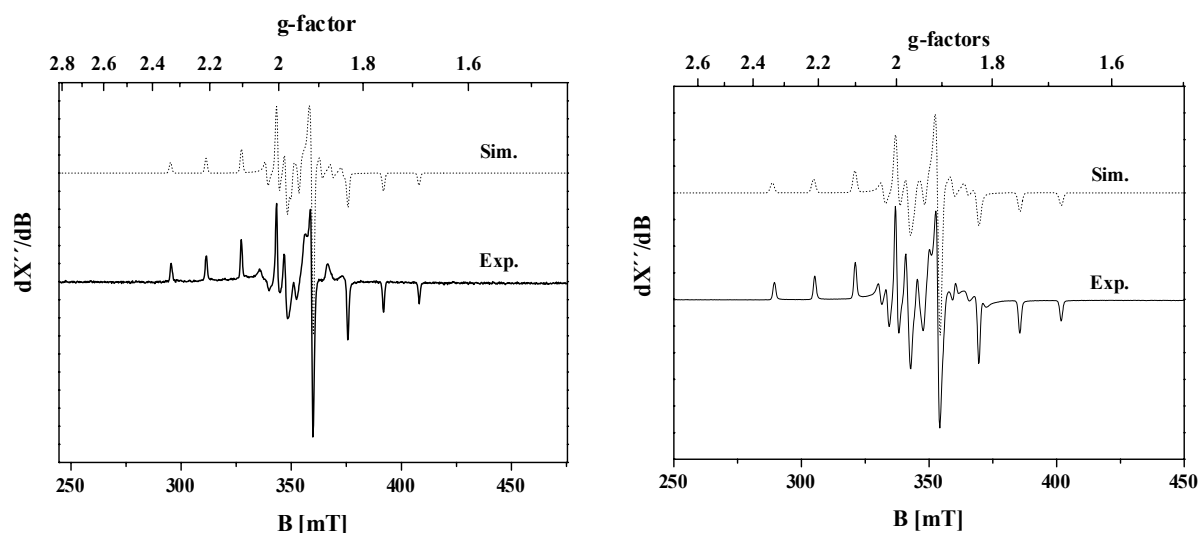


Figure 2.9.5 X-band EPR spectra for complexes **5** (left) at 33.8K and **6** (right) at 18K in CH_2Cl_2 + toluene. Experimental conditions (—): microwave frequency 9.64 GHz (**5**); 9.44 GHz (**6**), microwave power 0.2 μW (**5**); 0.2 mW (**6**), modulation amplitude 5 G (**5**); 11 G (**6**). The simulations (----): $g = \{1.9341, 1.9663, 1.9588\}$, $A = \{44.52, 14.52, 147.4\} \times 10^{-4} \text{ cm}^{-1}$ for **5** and $g = \{1.92, 1.945, 1.954\}$, $A = \{50, 10, 146\} \times 10^{-4} \text{ cm}^{-1}$ for **6**; Gaussian line with frequency-dependent line width $W_f = 30 \text{ G}$ (**5**) and 40 G (**6**).

This clearly correlates between the structural and electronic properties (covalency) from EPR measurements. And the measurements fully confirm the complexes to be genuine V(IV) with a d^1 electronic configuration. This is the first general study with a series of non-oxo vanadium(IV) complexes which establishes such correlation.

Complex **6**, on two-electron oxidation, forms the V(V) phenoxyl radical complex, as has already been discussed. The one-electron oxidized species is EPR silent, but at low temperature in CH_2Cl_2 , the electrochemically two-electron oxidized species exhibits an isotropic signal typical for an organic radical ($S = 1/2$). Simulation of the spectrum yields

parameters $g_x = g_y = 2.0078$, $g_z = 2.0027$ ($g_{iso} = 2.0061$). This confirms again the formation of the phenoxyl radical in the V(V) complex.

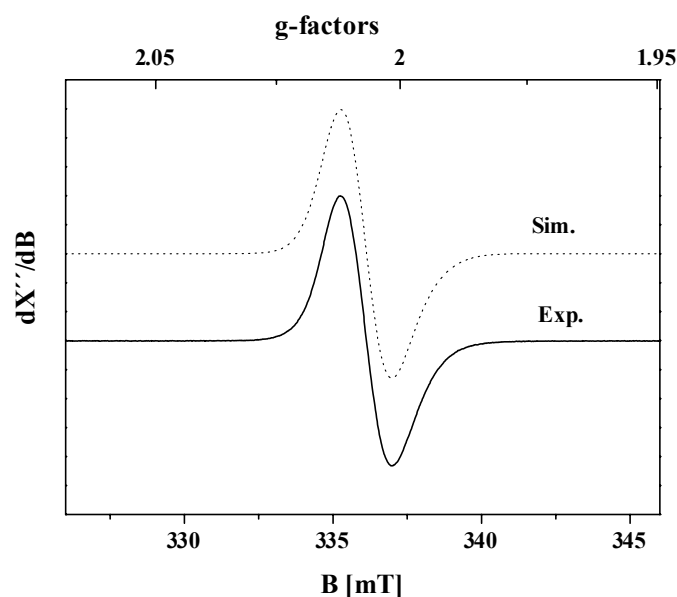


Figure 2.9.6 X-band EPR spectrum for the electrochemically $2e^-$ oxidized species of complex **6** at 30K in CH_2Cl_2 . Experimental conditions (—): microwave frequency 9.44 GHz, microwave power 0.16 mW, modulation amplitude 6G. The simulations (----): $g_{iso} = 2.0061$; Gaussian line with angular-dependent line width $W = \{18, 22, 26\}$ G.

Complexes **7** and **8** are, as expected, EPR silent with d^0 electronic configuration.

2.10 ^{51}V NMR SPECTROSCOPY

Complexes **7** and **8** show well resolved ^{51}V NMR spectra as expected for diamagnetic V(V) complexes. In CD_2Cl_2 solution (~ 1 mM) at ambient temperature, at least two species are present for each complex. Complex **7** shows two ^{51}V NMR resonances with a major peak at -430.31 ppm and a peak at -479.92 ppm having significantly higher line width. This increased line width may be because of a combination of quadrupolar broadening and chemical exchange effects. The phenolate and phosphoryl equatorial donors of **7** should impose a greater electric field gradient at the vanadium centers.

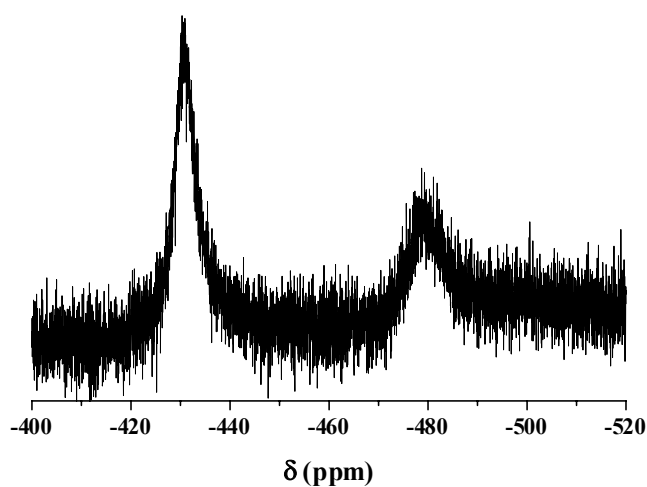


Figure 2.10.1 ^{51}V NMR spectrum of **7** in CD_2Cl_2 .

Complex **8** shows four resonances at - 387.93, - 393.34, -400.56 and - 404.55 ppm. These four resonances are more likely due to syn/anti and ligand exchange isomers. Addition of excess EtOH to a CH_2Cl_2 solution of **8** yields a complex with an ethoxide bridge, indicating that the hydroxide bridging ligands are labile.

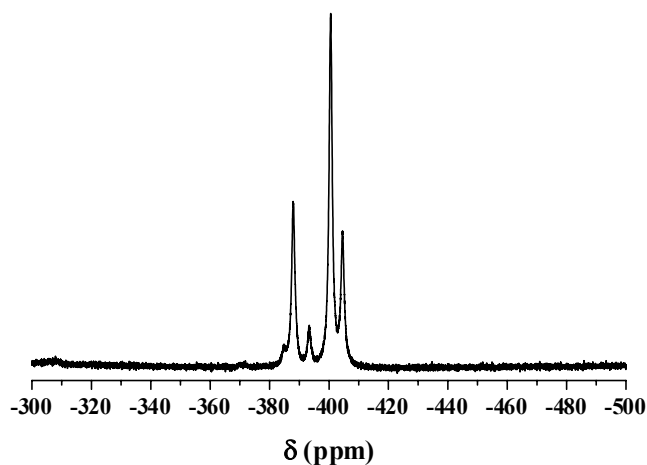


Figure 2.10.2 ^{51}V NMR spectrum of **8** in CD_2Cl_2 .

^{51}V NMR, thus, is a very useful tool to characterize the V(V) complexes and to study their isomerization behaviour in solution.

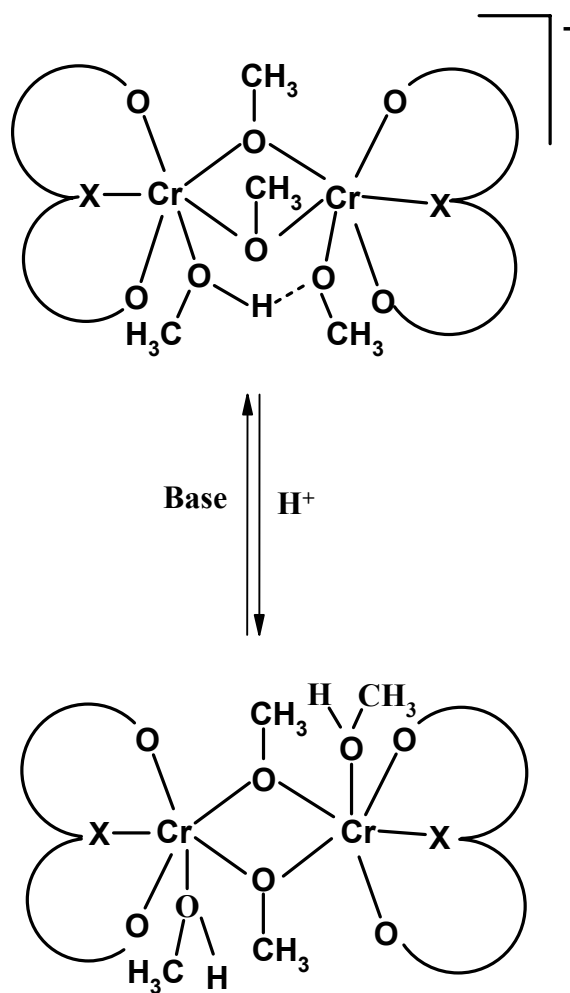
References

1. *Metal Ions in Biological Systems*, ed. H. Siegel, A. Siegel, Marcel Dekker, New York, **1995**, vol. 31.
2. D. Rehder, *Coordination Chemistry Reviews* **1999**, 82, 297.
3. (a) R. L. Robson, R. R. Eady, T. H. Richardson, R. W. Miller, M. Hawkins, J. R. Postgate, *Nature* (London) **1986**, 322, 388. (b) B. J. Hales, E. E. Case, J. E. Morningstar, M. F. Dzeda, L. A. Manterrer, *Biochemistry* **1986**, 25, 7251.
4. (a) H. Kneifel, E. Bayer, *Angew. Chem. Intl. Ed. Engl.* **1973**, 12, 508. (b) E. Bayer, H. Kneifel, *Z. Naturforsch.* **1972**, 27B, 20.
5. E. M. Armstrong, R. L. Beddoes, L. J. Calviou, J. M. Charnock, D. Collison, N. Ertok, J. H. Naismith, C. D. Garner, *J. Am. Chem. Soc.* **1993**, 115, 807.
6. M. F. C. Guedes da Silva *J. Am. Chem. Soc.* **1996**, 118, 7568.
7. S. W. Taylor, B. Kamerer, E. Bayer, *Chem. Rev.* **1997**, 97, 333.
8. (a) W. R. Harris, C. J. Carrano, *J. Inorg. Biochem.* **1984**, 22, 201. (b) M. J. Smith, D. Kim, B. Horenstein, K. Nakanishi, K. Kustin, *Acc. Chem. Res.* **1991**, 24, 117.
9. (a) J. A. Bonadies, C. J. Carrano, *J. Am. Chem. Soc.* **1986**, 108, 4088. (b) J. A. Bonadies, W. M. Butler, V. L. Pecorara, C. J. Carrano, *Inorg. Chem.* **1987**, 26, 1218. (c) M. Mazzanti, S. Gambarotta, C. Floriani, A. Chiesi-Villa, C. Guastini, *Inorg. Chem.* **1986**, 25, 2308.
10. (a) A. A. Diamantis, M. R. Snow, J. A. Vanzo, *J. Chem. Soc., Chem. Commun.* **1976**, 264. (b) P. Comba, L. M. Engelhardt, J. M. Harrowfield, G. A. Lawrance, L. L. Martin, A. M. Sargeson, A. H. White, *J. Chem. Soc., Chem. Commun.* **1985**, 174. (c) A. A. Diamantis, M. Manikas, M. A. Salam, M. R. Snow, E. R. T. Tiekink, *Aust. J. Chem.* **1988**, 41, 453.
11. (a) S. R. Cooper, Y. B. Koh, K. N. Raymond, *J. Am. Chem. Soc.* **1982**, 104, 5092. (b) U. Auerbach, B. S. P. C. Della Vedova, K. Wieghardt, B. Nuber, J. Weiss, *J. Chem. Soc., Chem. Commun.* **1990**, 1004. (c) A. Neves, A. Ceccato, I. Vencato, Y. P. Mascarenhas, C. Erasmus-Buhr, *J. Chem. Soc., Chem. Commun.* **1992**, 652. (d) S. Bruni, A. Caneschi, F. Cariati, C. Delfs, A. Dei, D. Gatteschi, *J. Am. Chem. Soc.* **1994**, 116, 1388. (e) V. Vergopoulos, S. Jantzen, D. Rodewald, D. Rehder, *J. Chem. Soc., Chem. Commun.* **1995**, 377. (f) T. A. Cabanos, A. M. Z. Slawin, D. J. Williams, J. D. Woollins, *J. Chem. Soc., Dalton Trans.* **1992**, 1423. (g) M. Farahbakhsh, H. Schimdt, D. Rehder, *J. Chem. Soc., Chem. Commun.* **1998**, 2009. (h) T. A. Cabanos, A. J. P. White, D. J. Williams, J. D. Woollins, *J. Chem. Soc., Chem. Commun.* **1992**, 17. (i) E.

- Ludwig, H. Hefele, E. Uhlemann, F. Weller, W. Kläui, *Z. anorg. allg. Chem.* **1995**, 621, 23. (j) H. Hefele, E. Ludwig, E. Uhlemann, F. Weller, *Z. anorg. allg. Chem.* **1995**, 621, 1973. (k) M. Farahbakhsh, H. Nekola, H. Schimdt, D. Rehder, *Chem. Ber.* **1997**, 130, 1129.
12. J. C. Dutton, G. D. Fallon, K. S. Murray, *Inorg. Chem.* **1988**, 27, 34.
13. C. R. Cornman, K. M. Geiser-Bush, J. W. Kampf, *Inorg. Chem.* **1999**, 38, 4303.
14. (a) J. Selbin, *Chem. Rev.* **1965**, 65, 153. (b) J. Selbin, *Coord. Chem. Rev.* **1966**, 1, 293.
15. B. R. McGarvey, in R. L. Carlin (ed.), *Transition Metal Chemistry*, vol. 3, p. 150, Marcel Dekker, New York, **1966**.
16. A. Jezierski, J. B. Raynor, *J. Chem. Soc., Dalton Trans.* **1981**, 1.
17. P. R. Klich, A. T. Danider, P. R. Challen, *Inorg. Chem.* **1996**, 35, 347.
18. (a) S. R. Cooper, Y. B. Koh, K. N. Raymond, *J. Am. Chem. Soc.* **1982**, 104, 5092. (b) M. Branca, G. Micera, A. Dessi, D. Sanna, K. N. Raymond, *Inorg. Chem.* **1990**, 29, 1586.
19. W.-L. Kwik, E. I. Stiefel, *Inorg. Chem.* **1973**, 12, 2337.

Chapter 3

COORDINATION PROPERTIES OF BISPHENOLATE LIGANDS WITH TRANSITION METAL IONS



3.1 INTRODUCTION

This chapter is concerned with the study of tridentate bisphenol ligands containing heterodonor atoms (S, Se and N) to scrutinize the effect of chelate ring size on the ligating properties with transition metal ions. The ligands studied here are H_2L^S , H_2L^{Se} and H_2L^N . Ligating properties of these ligands were extensively examined with first row transition metal ions. They stabilize different nuclearity and oxidation states depending upon the metal ion and the ring size, which is somewhat dependent on the particular synthetic protocol. It is well established that bisphenolate ligands stabilize the enigmatic oxidation state of V(IV), which has already been discussed in the case of a series of non-oxo V(IV) complexes of bisphenol ligands in chapter 2. In this chapter unique ligating properties of the bisphenolate ligands are discussed along with their interesting structural, magnetic and electrochemical properties. Sections 3.2, 3.3 and 3.4 deal with the complexes of Cr(III), Mn(III/IV), Fe(III) and Ni(II), respectively.

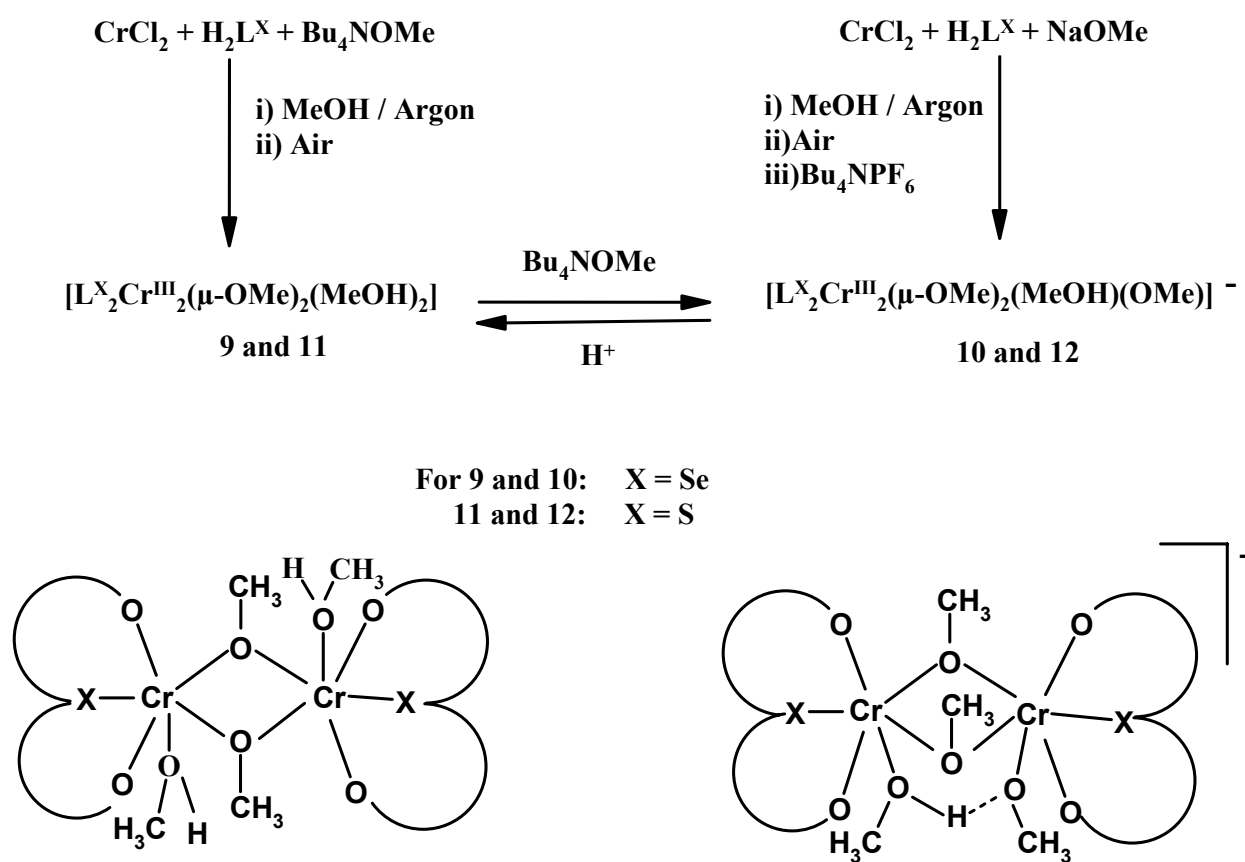
3.2 CHROMIUM(III) COMPLEXES OF H_2L^X (X = S, Se)

The importance of hydrogen bonds in modifying physical and chemical properties of active sites in biological systems is well known.¹ On the other hand, it has been recently recognized that hydrogen bonds play a major role in the transmission of *ferromagnetic* interactions in organic ferromagnets.²

The hydrogen-oxide bridging ligand, $H_2O \cdots OH^- [H_3O_2]^-$, formed by means of a strong and symmetrical hydrogen bond between a hydroxo-ligand coordinated to a metal center and an aqua ligand of a neighbouring metal ion, plays a fundamental role in the hydrolysis of aquated metal ions.³ A similar important role is envisagable for the analogous methanol-methanolate, $CH_3OH \cdots OCH_3^-$, bridging anion in the methanolysis reactions of metal ions. Any example of such a bridging mode is lacking in the literature. Here four complexes containing the bis(μ -methoxo)dichromium(III) complex core **9-12**, of which in **9** and **11** two coordinated methanol molecules are disposed in trans position, whereas **10** and **12** contain a bridging $CH_3OH \cdots OCH_3^-$ ligand. **9**, **10**, **11** and **12** exhibit the effect of the hydrogen-bond on the exchange coupling interactions between the chromium(III) centers in two forms, which are otherwise identical. These four complexes represent first examples of coordination compounds in tuning intramolecular spin coupling interactions by hydrogen-bonds.

3.2.1 SYNTHESIS

The complexes have been prepared by the general synthetic route shown in scheme 3.2.1.1. Treatment of the ligands with CrCl_2 in the presence of methoxide base in methanol yields bis(μ -methoxo) complexes **9** and **11**. On the other hand, if the same reaction is carried out in the presence of excess methoxide base and then subsequent treatment with ionic salt with big counterion, hydrogen-bonded complexes **10** and **12** are isolated. Treatment of the complexes **9** and **11** with base in CH_2Cl_2 and MeOH solvent mixture yields the complexes **10** and **12**, respectively, in high yield.



Scheme 3.2.1.1 Synthetic scheme for Cr(III) dimers.

3.2.2 INFRARED AND MASS SPECTROSCOPY

Two isomers were initially identified by IR spectroscopy. The most characteristic peaks are those due to $\nu(\text{C-H})$ of *tert*-butyl groups from the ligands at $2850\text{--}2960\text{ cm}^{-1}$ indicating the complexation. For the complexes **10** and **12**, $\nu(\text{OMe})$ peaks are symmetric at 1062 cm^{-1} and at 550 cm^{-1} . But for complexes **9** and **11**, those peaks are asymmetric and shifted to lower energy. Other peaks appear at normal ranges as expected.

In EI mass spectrometry, the complexes **9** and **11** show molecular ion peaks at $m/z = 1140$ and at 1047 respectively, with the expected isotopic distributions. They correspond to the molecular mass $[M-\text{MeOH}]$. High temperature gas phase decomposition products are also seen in the EI mass spectra for the complexes **10** and **12**.

Mass spectrometry in ESI mode for complexes **10** and **12** does not leave any doubt about the composition. Two single peaks, one in positive mode at m/z 242 and the second in negative mode at m/z 1172 or 1077 with the expected isotope distribution pattern, correspond to $[\text{Bu}_4\text{N}]^+$ and $[M-\text{MeOH}]^-$ for **10** and **12**, respectively.

3.2.3 X-RAY CRYSTAL STRUCTURE

3.2.3.1 Molecular Structure of $[\text{CrL}^{\text{Se}}(\mu\text{-OMe})(\text{MeOH})]_2$ (**9**)

The single crystal X-ray structure analysis of **9** substantiates the dinuclear structure, where two roughly octahedral chromium(III) ions are symmetrically bridged by two methoxy ligands, as shown in the ORTEP drawing of **9** in Figure 3.2.3.1 with selected bond parameters in Table 3.2.3.1.

The six coordination sites of the chromium ions are occupied by two *cis*-methoxy bridging groups, one facially coordinated $[\text{L}^{\text{Se}}]^{2-}$ ligand providing the donor atoms O,Se,O and a methanol molecule. Two methanol molecules are *trans* relative to each other. The Cr(1)-Cr(1A) and Cr(1)-O(3) (methoxide) distances and the Cr(1)-O(3)-Cr(1A) angle of the bridging moiety are 3.093(2), 1.972(2) Å and 103.58(6)°, respectively, which are comparable to the similar bis(alkoxy)-bridged dichromium(III) complexes.⁴ The Cr_2O_2 bridging unit is strictly planar, there being a crystallographic inversion center in the middle of the dimer. The methoxy carbon atoms C(29) and C(29A) are almost planar with C(29) lying 0.055 Å above the plane. Although the O-Cr-O angles are in the small range of 95.7(1)-89.9(1)°, the O(3)-Cr(1)-O(3A) angle with 76.4(1)° deviates remarkably from ideal 90°. The oxygen of the methanol molecule, O(4), coordinated to Cr(1), is hydrogen-bonded to a non-coordinated methanol molecule with an O...O distance of 2.652(5) Å.

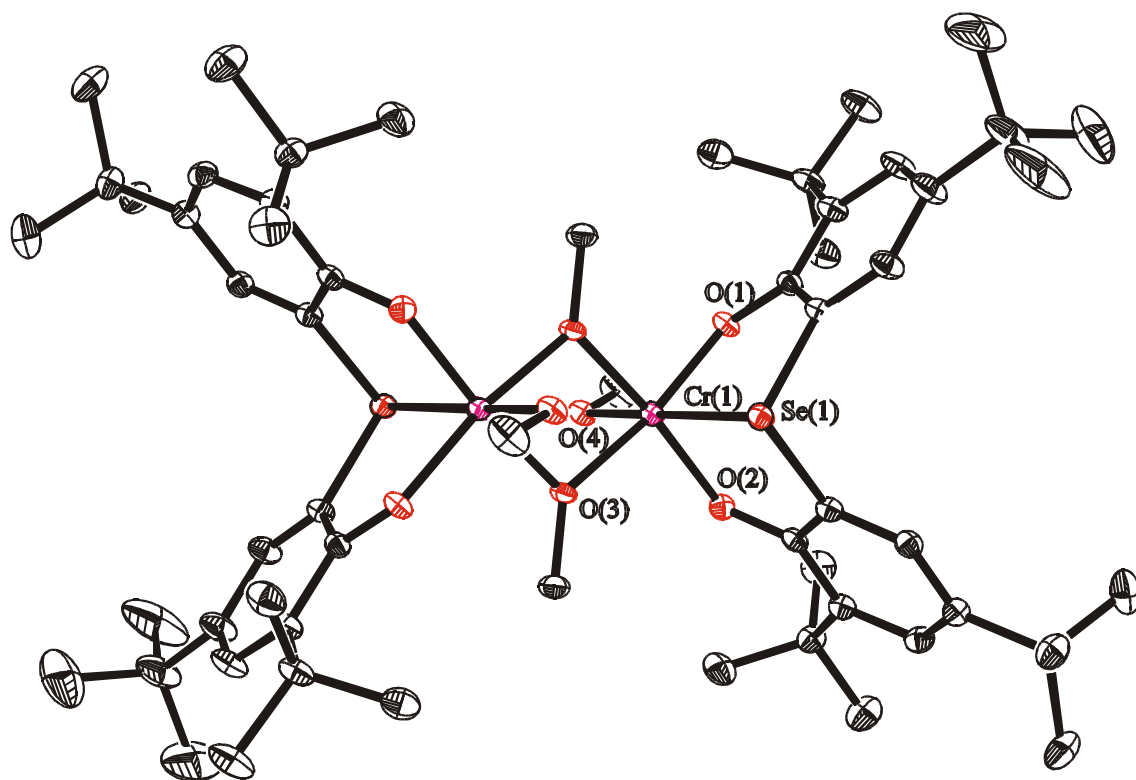


Figure 3.2.3.1 ORTEP and atom labeling scheme for $[\text{CrL}^{\text{Se}}(\mu\text{-OMe})(\text{MeOH})]_2$ (**9**).

Table 3.2.3.1 Selected bond distances (Å) and angles (deg) for complex **9**

| | | | |
|--------------------|------------|--------------------|-----------|
| Cr(1)-O(1) | 1.934(2) | O(1)-Cr(1)-O(2) | 93.71(7) |
| Cr(1)-O(2) | 1.9354(14) | O(1)-Cr(1)-O(3)#1 | 95.70(6) |
| Cr(1)-O(3)#1 | 1.9638(14) | O(2)-Cr(1)-O(3)#1 | 170.55(6) |
| Cr(1)-O(3) | 1.972(2) | O(1)-Cr(1)-O(3) | 171.16(6) |
| Cr(1)-O(4) | 2.036(2) | O(2)-Cr(1)-O(3) | 94.14(6) |
| Cr(1)-Se(1) | 2.5008(5) | O(3)#1-Cr(1)-O(3) | 76.42(6) |
| | | O(1)-Cr(1)-O(4) | 89.94(7) |
| Cr(1)#1-O(3)-Cr(1) | 103.58(6) | O(2)-Cr(1)-O(4) | 90.51(7) |
| C(6)-Se(1)-Cr(1) | 91.26(7) | O(3)#1-Cr(1)-O(4) | 90.27(7) |
| C(7)-Se(1)-Cr(1) | 90.87(7) | O(3)-Cr(1)-O(4) | 94.05(6) |
| C(1)-O(1)-Cr(1) | 124.61(13) | O(1)-Cr(1)-Se(1) | 85.42(5) |
| C(8)-O(2)-Cr(1) | 124.08(13) | O(2)-Cr(1)-Se(1) | 85.03(5) |
| C(29)-O(3)-Cr(1)#1 | 129.47(14) | O(3)#1-Cr(1)-Se(1) | 94.95(5) |
| C(29)-O(3)-Cr(1) | 126.88(13) | O(3)-Cr(1)-Se(1) | 91.22(5) |
| C(30)-O(4)-Cr(1) | 123.0(2) | O(4)-Cr(1)-Se(1) | 173.33(5) |

3.2.3.2 Molecular Structure of $\text{Bu}_4\text{N}[\text{Cr}_2 \text{L}^{\text{Se}}_2 (\mu\text{-OMe})_2(\text{MeOH})(\text{OMe})]$ (**10**)

The structure of the complex anion in **10** containing the dinuclear chromium(III) core is shown in Figure 3.2.3.2, selected bond parameters are given in Table 3.2.3.2.

The coordination geometry of the chromium center Cr(1) is distorted octahedral with three donor atoms, O(1), Se(1) and O(2), from the facially coordinated $[\text{L}^{\text{Se}}]^{2-}$ ligand, two oxygen atoms, O(40) and O(30), from the cis-bridging methoxide groups and a methanol molecule, O(50), resulting in the CrO_5Se core as that in **9**. The presence of the cation $[\text{Bu}_4\text{N}]^+$ in **10** dictates on account of charge-balance, the loss of one proton from the coordination sphere of the chromium(III) centers. The distance between the symmetry-related atoms O(50)-O(50A) of 2.43(1) Å is clearly indicative of a strong hydrogen-bond interaction, suggesting that one of the methanol molecule is deprotonated and coordinates as a methoxide ligand. Indeed, a difference Fourier map in the refinement stages did reveal a peak assignable to a single proton,

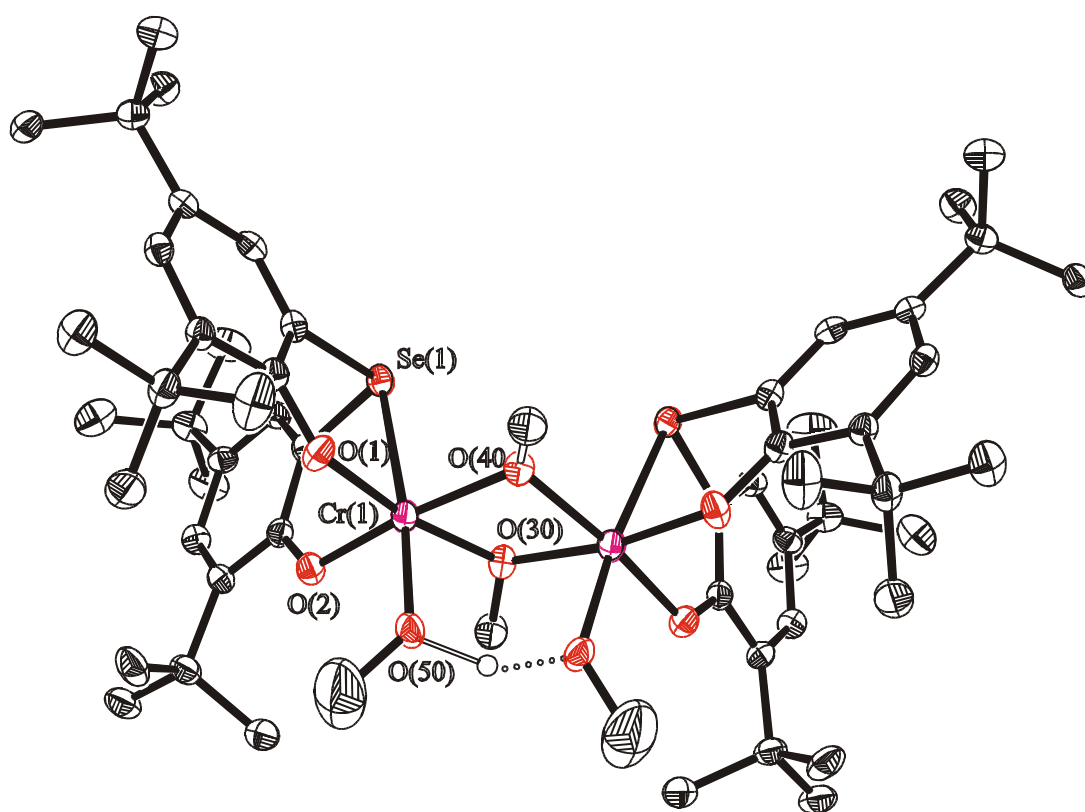


Figure 3.2.3.2 ORTEP and atom labeling scheme for $[\text{Cr}_2 \text{L}^{\text{Se}}_2 (\mu\text{-OMe})_2(\text{MeOH})(\text{OMe})]^-$ (**10**).

Table 3.2.3.2 Selected bond distances (Å) and angles (deg) for complex **10**

| | | | |
|--------------------|------------|--------------------|------------|
| Se(1)-Cr(1) | 2.5390(8) | C(2)-Se(1)-Cr(1) | 90.58(13) |
| Cr(1)-O(2) | 1.923(3) | C(16)-Se(1)-Cr(1) | 91.44(13) |
| Cr(1)-O(1) | 1.930(3) | O(2)-Cr(1)-O(1) | 94.26(14) |
| Cr(1)-O(30) | 1.972(3) | O(2)-Cr(1)-O(30) | 94.99(14) |
| Cr(1)-O(50) | 1.982(3) | O(1)-Cr(1)-O(30) | 170.66(13) |
| Cr(1)-O(40) | 1.989(3) | O(2)-Cr(1)-O(50) | 92.35(13) |
| | | O(1)-Cr(1)-O(50) | 91.28(12) |
| Cr(1)*-O(30)-Cr(1) | 101.7(2) | O(30)-Cr(1)-O(50) | 89.6(2) |
| Cr(1)*-O(40)-Cr(1) | 100.5(2) | O(2)-Cr(1)-O(40) | 170.72(14) |
| O(1)-Cr(1)-O(40) | 93.98(13) | O(30)-Cr(1)-O(40) | 76.69(14) |
| O(50)-Cr(1)-O(40) | 91.7(2) | O(2)-Cr(1)-Se(1) | 83.96(9) |
| O(1)-Cr(1)-Se(1) | 84.26(8) | O(30)-Cr(1)-Se(1) | 95.45(12) |
| O(50)-Cr(1)-Se(1) | 173.97(9) | O(40)-Cr(1)-Se(1) | 92.64(11) |
| C(1)-O(1)-Cr(1) | 125.1(3) | C(15)-O(2)-Cr(1) | 126.0(3) |
| C(30)-O(30)-Cr(1) | 128.68(13) | C(30X)-O(30)-Cr(1) | 125.5(2) |
| C(40)-O(40)-Cr(1) | 124.4(2) | C(50)-O(50)-Cr(1) | 129.5(4) |

appearing equidistant from the two oxygen atoms, and this was included in the final refinement cycle. The oxygen-oxygen separation in the bridging $\text{CH}_3\text{O}^-\cdots\text{H}^+\cdots\text{OCH}_3^-$ anion of 2.43 Å is comparable with that in the $\text{HO}^-\cdots\text{H}^+\cdots\text{OH}^-$ anion, H_3O_2^- , bridging two metal ions (2.44-2.50 Å).⁵ It is noteworthy that the oxygen-oxygen distance is significantly shorter in the non-coordinated H_3O_2^- anion (2.27 Å)^{3,6} or in the cation $(\text{CH}_3\text{OH})_2\text{H}^+$ (2.23 Å).⁷ The Cr(1)-Cr(1A), Cr(1)-O(40) and Cr(1)-O(30) (methoxide) distances and the angles Cr(1)-O(40)-Cr(1A) and Cr(1)-O(30)-Cr(1A) of the bridging moiety are 3.059(2), 1.989(3), 1.972(3) Å, 100.5(2)° and 101.7(2)°, respectively, which are not significantly different from those of **9** and other similar complexes.⁴ The Cr_2O_2 bridging unit is folded with an angle of 24.8° between the two Cr-O-Cr planes. That the coordination geometry of Cr(1) in **10** is very similar to that of the chromium centers in **9** is dictated by the O-Cr-O angles lying in the range 94.3(1)-89.6(2)° and the O(30)-Cr(1)-O(40) angle with 76.7(1)°. Thus the metrical parameters for **9** and **10** are very similar, irrespective of different geometrical dispositions of the methanol / methanolate molecule.

3.2.3.3 Molecular Structure of $[\text{CrL}^{\text{S}}(\mu\text{-OMe})(\text{MeOH})]_2$ (**11**)

This compound is isostructural with compound **9** and hence details are not discussed here. The ORTEP diagram is shown in Figure 3.2.3.3 and the selected bond angles and bond distances are given in the Table 3.2.3.3.

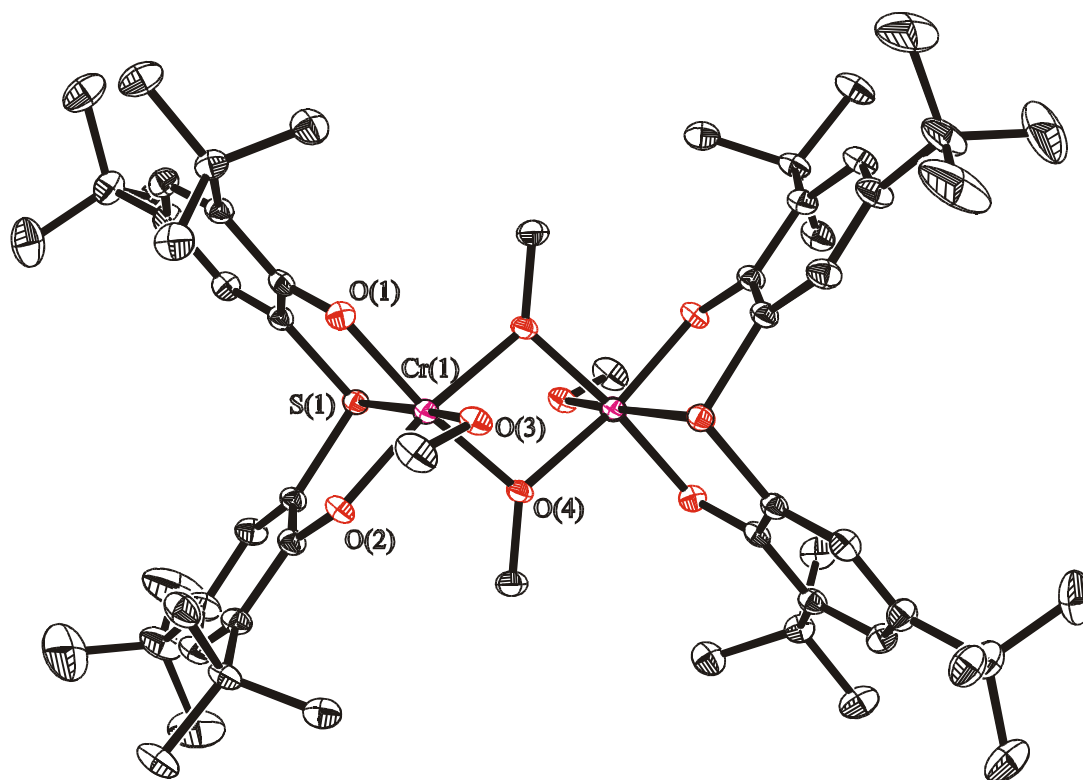


Figure 3.2.3.3 ORTEP and atom labeling scheme for $[\text{CrL}^{\text{S}}(\mu\text{-OMe})(\text{MeOH})]_2$ (**11**).

Table 3.2.3.3 Selected bond distances (\AA) and angles (deg) for complex **11**

| | | | |
|--------------------|-----------|-------------------|-----------|
| Cr(1)-O(1) | 1.927(2) | O(1)-Cr(1)-O(2) | 93.40(9) |
| Cr(1)-O(2) | 1.931(2) | O(1)-Cr(1)-O(4)#1 | 95.33(8) |
| Cr(1)-O(4)#1 | 1.963(2) | O(2)-Cr(1)-O(4)#1 | 171.19(8) |
| Cr(1)-O(4) | 1.972(2) | O(1)-Cr(1)-O(4) | 171.28(8) |
| Cr(1)-O(3) | 2.025(2) | O(2)-Cr(1)-O(4) | 94.31(8) |
| Cr(1)-S(1) | 2.3994(8) | O(4)#1-Cr(1)-O(4) | 76.90(8) |
| | | O(1)-Cr(1)-O(3) | 90.25(8) |
| Cr(1)#1-O(4)-Cr(1) | 103.10(8) | O(2)-Cr(1)-O(3) | 90.18(8) |
| C(6)-S(1)-Cr(1) | 94.70(9) | O(4)#1-Cr(1)-O(3) | 90.99(8) |
| C(7)-S(1)-Cr(1) | 94.47(9) | O(4)-Cr(1)-O(3) | 93.79(8) |
| C(1)-O(1)-Cr(1) | 122.1(2) | O(1)-Cr(1)-S(1) | 84.98(6) |
| C(8)-O(2)-Cr(1) | 121.7(2) | O(2)-Cr(1)-S(1) | 84.47(6) |
| C(30)-O(4)-Cr(1)#1 | 129.8(2) | O(4)#1-Cr(1)-S(1) | 95.07(6) |
| C(30)-O(4)-Cr(1) | 126.8(2) | O(4)-Cr(1)-S(1) | 91.71(6) |
| C(29)-O(3)-Cr(1) | 122.7(2) | O(3)-Cr(1)-S(1) | 172.60(7) |

3.2.3.4 Molecular Structure of $\text{Bu}_4\text{N}[\text{Cr}_2 \text{L}^{\text{S}}_2 (\mu\text{-OMe})_2(\text{MeOH})(\text{OMe})]^-$ (**12**)

This compound is isostructural with compound **10** and hence details are not discussed here. Only the ORTEP diagram of the complex anion is shown in Figure 3.2.3.4 because of the mediocre quality of the crystal structure.

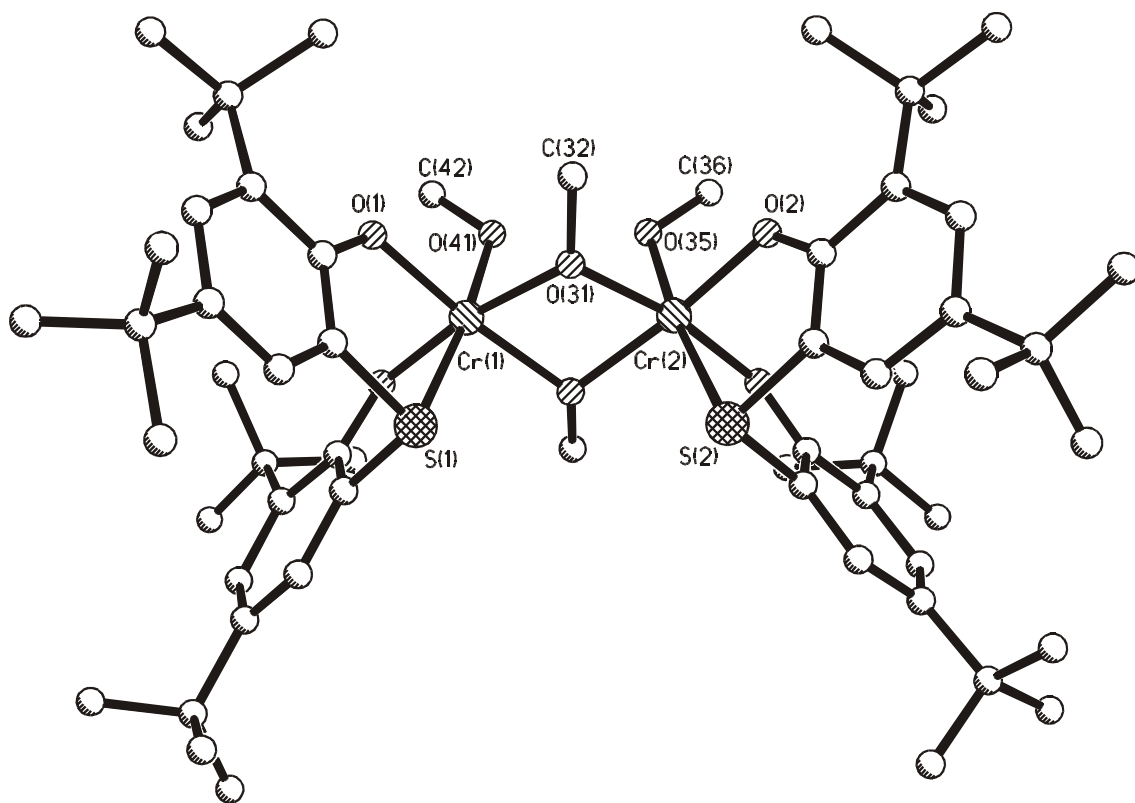


Figure 3.2.3.4 Ball and stick diagram of $[\text{Cr}_2 \text{L}^{\text{S}}_2 (\mu\text{-OMe})_2(\text{MeOH})(\text{OMe})]^-$ (**12**).

3.2.4 ELECTRONIC SPECTROSCOPY

The UV-vis spectra of complexes **9** and **11** in $\text{CH}_2\text{Cl}_2 + \text{MeOH}$ solution are typical of an octahedral Cr(III) complex, showing two spin-allowed transitions, ${}^4\text{A}_{2g} \rightarrow {}^4\text{T}_{2g}$ and ${}^4\text{A}_{2g} \rightarrow {}^4\text{T}_{1g}$ at ~ 560 and ~ 640 nm, respectively. Addition of base changes the spectrum corresponding to **10** and **12**, which shows transition at ~ 620 nm. The spectral changes can be rationalized in term of the conversion of MeOH group to OMe group, i.e. generation of **10** and **12** from **9** and **11**, respectively.

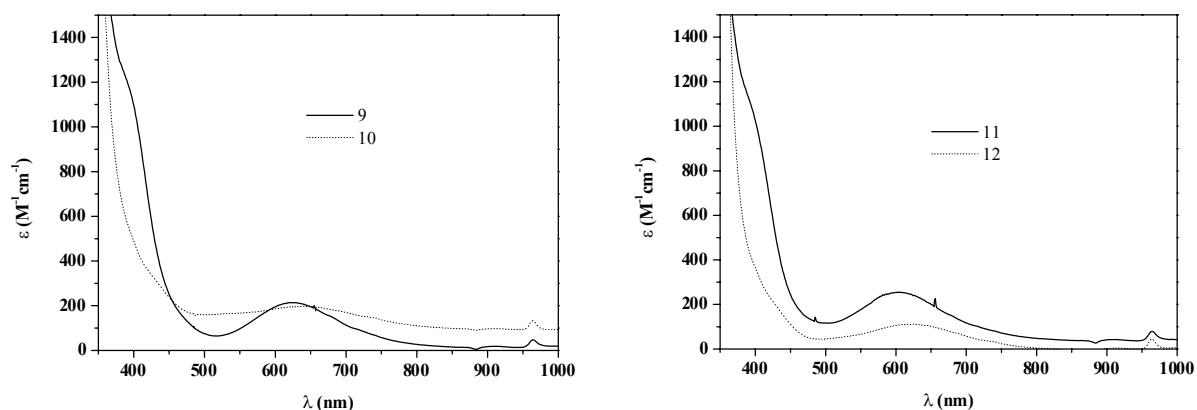


Figure 3.2.4 Optical spectra for complexes **9-12** in $\text{CH}_2\text{Cl}_2 + \text{MeOH}$ solution. The spectra for **9** and **11** were measured in presence of perchloric or trifluoromethane sulfonic acid, whereas the spectra for **10** and **12** were taken in presence of Bu_4OMe .

The spin allowed bands shift to lower energy, as is expected from the ligand field strength of the oxo-ligand. Similar changes in spectrum have been observed on addition of base to other hydroxo-bridged Cr(III) dinuclear complexes.⁸

Table 3.2.4 Optical spectral data for complexes **9-12** in $\text{CH}_2\text{Cl}_2 + \text{MeOH}$

| Complex | λ_{max} , nm (ϵ , $\text{M}^{-1}\text{cm}^{-1}$) |
|-----------|--|
| 9 | 622 (214), 400sh(1190) |
| 10 | 635 (197) |
| 11 | 605 (255), 400sh(1160) |
| 12 | 626 (112) |

An acid-base dependent equilibrium between the two forms has been established by optical spectroscopy.

3.2.5 MAGNETISM

Magnetic data (SQUID) at $H = 1$ T for polycrystalline samples of **9-12** are displayed in Figures 3.2.5.1 and 3.2.5.2 as μ_{eff} vs T . On lowering the temperature, the effective magnetic moments decrease monotonically for both complexes. Representative μ_{eff} and $\chi_{\text{M}} \cdot T$ values for complexes **9** and **10** (given in brackets) are $5.07\mu_{\text{B}}$ and $3.190\text{ cm}^3 \text{ K mol}^{-1}$ ($5.22\mu_{\text{B}}$; $3.37 \text{ cm}^3 \text{ K mol}^{-1}$) at 290K, $4.36\mu_{\text{B}}$ and $2.365 \text{ cm}^3 \text{ K mol}^{-1}$ ($4.98\mu_{\text{B}}$; $3.089 \text{ cm}^3 \text{ K mol}^{-1}$) at 100K, $0.66 \mu_{\text{B}}$ and $0.05457 \text{ cm}^3 \text{ K mol}^{-1}$ ($2.99 \mu_{\text{B}}$; $1.114 \text{ cm}^3 \text{ K mol}^{-1}$) at 2K, indicating a diamagnetic ground state with $S_{\text{T}} = 0$ for both **9** and **10**. This arises from antiparallel spin coupling between two chromium(III) centers with $S = 3/2$. Simulation ($\hat{H} = -2J \hat{S}_1 \cdot \hat{S}_2$) of the data yielded $J = -9.0 \text{ cm}^{-1}$, $g = 1.94$ for **9** and $J = -1.96 \text{ cm}^{-1}$, $g = 1.89$ for **10**. It was not necessary to consider terms for TIP, paramagnetic impurity or a second-order (bi-quadratic) exchange term in the simulation procedure. That an accurate J value can be obtained from the simulation of the magnetic susceptibility data without considering the biquadratic term for {CrCr} pairs has been pointed out earlier in the literature.⁹

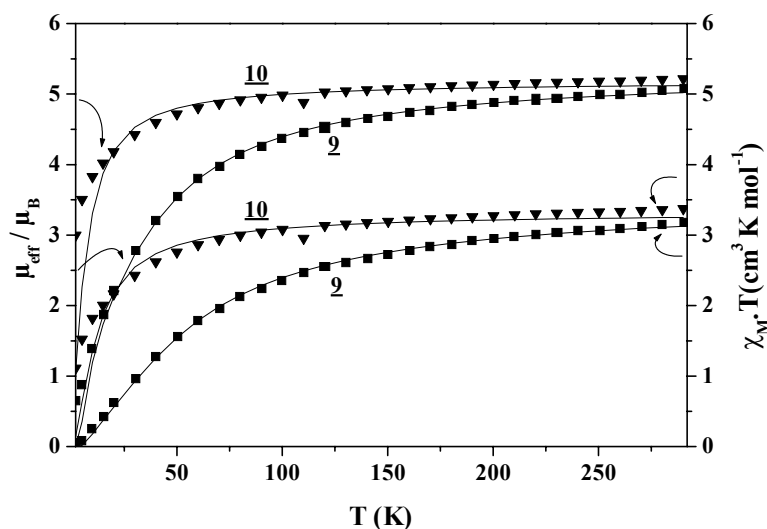


Figure 3.2.5.1 Magnetic measurements for complexes **9** and **10**.

The corresponding sulfur-analogues, **11** and **12**, yield the following evaluated magnetic data: $J = -8.30 \text{ cm}^{-1}$, $g = 1.83$ for **11** and $J = -0.49 \text{ cm}^{-1}$, $g = 1.90$ for **12**. **10** and **12** exhibit the weakest exchange interactions between the chromium(III) centers in bis-alkoxo/ bis-phenoxo-bridged compounds reported until now.⁴

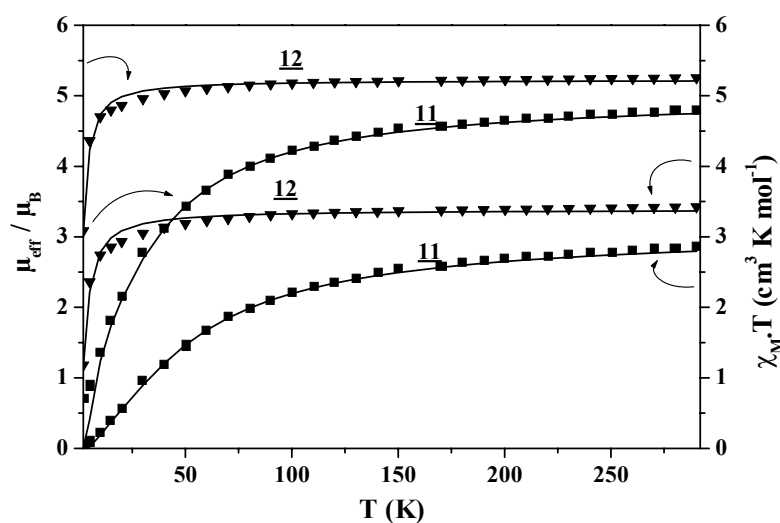


Figure 3.2.5.2 Magnetic measurements for complexes **11** and **12**.

An empirical model relating the magnitude of the coupling to the Cr-O-Cr angle, Cr-O bond length and the angle θ between the bridging plane and the O-R vector of the bridging group, has been proposed to explain antiferromagnetic coupling in edge-shared bioctahedral dichromium(III) complexes.¹⁰ In a second approach¹¹ for magnetostructural correlation in a number of chromium (III) dimers containing a Cr₂O₂ bridging network, the energy separation between the singlet and the triplet levels originating from the exchange interaction was found to be correlated to the ratio between the Cr-O-Cr bond angle (φ) and the Cr-O bond length (r). This correlation was rationalized using a molecular orbital treatment. But none of these models can satisfactorily explain the trend of the exchange interactions in the complexes discussed here.

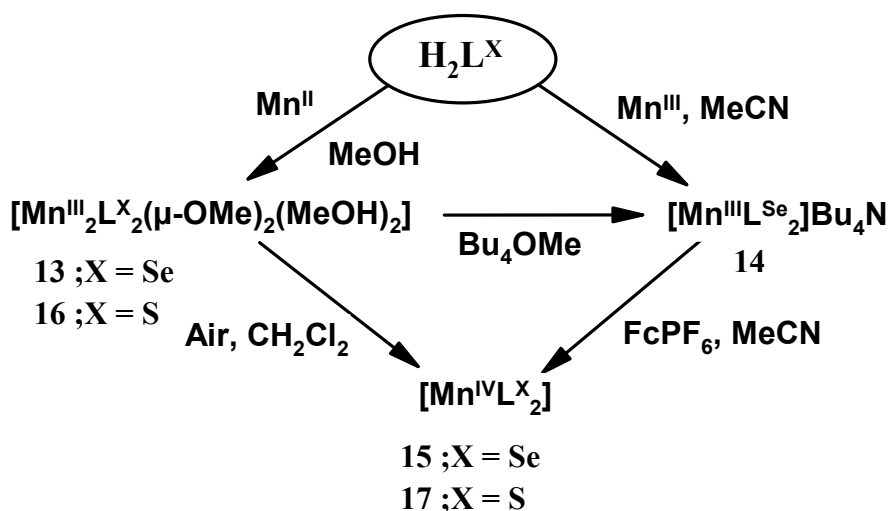
The crystallographic data for the bridging angles and distances in the dimethoxo-bridged complexes **9** and **10** are very similar and therefore do not provide a basis for an explanation of the different magnetic behaviours of **9** and **10**. A qualitative rationale for the trend of the exchange interactions, i.e. the strength of antiferromagnetic coupling is stronger in **9** ($J = -9.0 \text{ cm}^{-1}$) than that in **10** ($J = -1.96 \text{ cm}^{-1}$), can be provided by considering a third bridging unit in **10**, a hydrogen bond between two *cis*-situated methanolates $\text{CH}_3\text{O} \cdots \text{H} \cdots \text{OCH}_3$ which is absent in **9**. The folding of the Cr₂O₂ core in **10** lowers the magnitude of antiferromagnetic interaction in the plane (which dominates exchange coupling between the two Cr(III) units) due to loss of orbital overlap. Comparable complexes with H₃O₂⁻-bridging groups have been intensively studied.³ Evidence for transmission of ferromagnetic interactions through hydrogen bonds in nitroxide radicals has recently been put forward.² Similar arguments can be put forward to explain the magnetic behaviour of complexes **11** and **12**.

3.3 MANGANESE (III/ IV) AND IRON (III) COMPLEXES OF H_2L^X (X = S, Se)

Manganese and iron ions are present at the active site of a variety of enzymes involved in oxidation catalysis. This has inspired the inorganic chemists to synthesize and study of manganese and iron complexes as structural or functional models for these enzymes. Several complexes have been used as bleaching agents or in oxidation reactions of organic substrates.¹² In the biosystem, a recent 3.8 Å resolution X-ray structure of PSII supports a 3+1 motif where one manganese ion is distinct from the other three.¹³ Because of this, renewed attention is being given to both trinuclear manganese and mononuclear Mn(IV) complexes. There are few structurally and spectroscopically well characterized Mn(IV) complexes.¹⁴ This part of the chapter concerns the versatile ligation properties of bisphenolate ligands, H_2L^{Se} and H_2L^S towards manganese stabilizing dinuclear Mn(III), mononuclear Mn(III) and mononuclear Mn(IV) complexes. Similarly, the importance of iron complexes with this bisphenol ligand has also been explored by studying different iron(III) complexes.

3.3.1 SYNTHESIS

The ligands react with different manganese salts in different reaction medium giving a variety of complexes as shown in scheme 3.3.1.1.

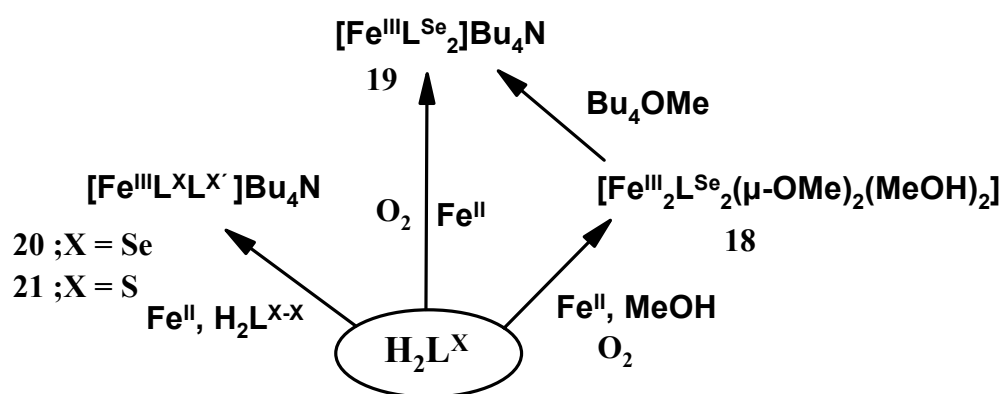


Scheme 3.3.1.1 Synthesis of manganese complexes of bisphenol ligands.

Reaction of metal salts and ligands in a suitable ratio afforded complexes **13-17** in relatively high yield. Both the sulfur and selenium heterodonor containing bis phenolate ligands react with Mn(II)/Mn(III)-salt in alkaline methanol solution to form bis(μ -methoxo)-dimanganese(III) complexes, **13** and **16**, respectively. A MeOH molecule occupies the sixth coordination sphere of each manganese center making them relatively reactive in aprotic or

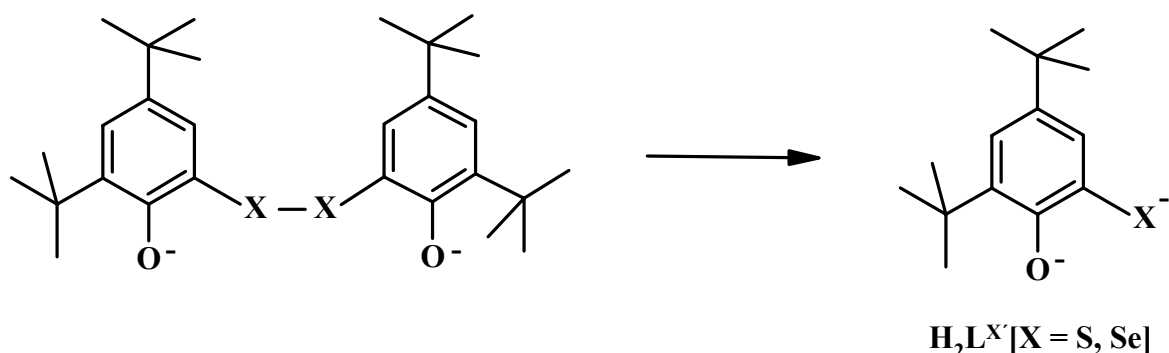
non-coordinating solvents. In CH_2Cl_2 they are easily oxidized by air to the mononuclear bisligand $[\text{Mn}^{\text{IV}}\text{L}_2]$, **15** and **17**, complexes with concomitant formation of MnO_2 . The ligand $\text{H}_2\text{L}^{\text{S}}$ reacts with Mn(III) salt in MeCN using Bu_4NOMe or Bu_4NOH as base to form the $[\text{Mn}^{\text{III}}\text{L}^{\text{Se}}_2]^-$ complex **14**. Treatment of the μ -methoxo dimer **13** with Bu_4NOMe also yields the same complex **14**. Chemical oxidation of this complex by FcPF_6 afforded the mononuclear Mn(IV) complex **15** in high yield.

A variety of Fe(III) complexes were isolated readily (Scheme 3.3.1.2). Like manganese, Fe(II) salts form the μ -methoxodiiron(III) complex **18** in MeOH. Addition of excess base having a large counterion like Bu_4NOMe to a CH_2Cl_2 +MeOH solution of **18** yields the homoleptic bisligand mononuclear Fe(III) complex **19** which can also be synthesized by reaction of ligand and FeCl_2 (2:1) using excess Bu_4NOMe in MeCN and subsequent exposure to air.



Scheme 3.3.1.2 Synthesis of iron complexes of bisphenol ligands.

Interestingly, ligands $\text{H}_2\text{L}^{\text{Se}}$ and $\text{H}_2\text{L}^{\text{S}}$ react with FeCl_2 under argon in MeOH solution in the presence of their di-heterobis analogs, $\text{H}_2\text{L}^{\text{Se-Se}}$ and $\text{H}_2\text{L}^{\text{S-S}}$, respectively, to yield the mononuclear Fe(III) complexes **20** and **21**. During the reaction cleavage of Se-Se and S-S bonds occurs,



Scheme 3.3.1.3 Cleavage of X-X ($\text{X} = \text{S}, \text{Se}$) bond in presence of metal ion.

which then form new ligands $\text{H}_2\text{L}^{\text{Se}'}$ and $\text{H}_2\text{L}^{\text{S}'}$, affording the five-coordinated mononuclear Fe(III) complexes. It is believed that Fe(II) reduces such bond by an electron transfer process, thereby converting to Fe(III) and forming complexes.

3.3.2 INFRARED AND MASS SPECTROSCOPY

IR spectra for all the complexes are given in the experimental section. Presence of the ligands was confirmed by a strong peak in the region $3000\text{-}2800\text{ cm}^{-1}$ due to $\nu(\text{C-H})$ of *tert*-butyl groups in the ligand together with the other $\nu(\text{C-H}, \text{C}=\text{C}, \text{C-O})$ vibrations found in the normal range for these types of linkages. The bands due to $\nu(\text{OH})$ for the free ligands are replaced by a broad peak in the region $3200\text{-}3400\text{ cm}^{-1}$ due to complexation, indicating the loss of phenol character of ligand. Presence of the methanol molecule in the sixth coordination sphere for μ -methoxo manganese(III) and iron(III) dimers sometime show $\nu(\text{OH})$ overlapped by the broad peak in the region $3200\text{-}3400\text{ cm}^{-1}$, along with two symmetric peaks at around 1050 cm^{-1} . This band is absent in the mononuclear complexes.

Except for μ -methoxo complexes, mass spectrometry in the EI and ESI mode has proved to be a very useful analytical tool for the characterization of the complexes and also for the identification of the metal centres, and the compositions are in good agreement with the elemental analysis. EI-mass spectrometry for the μ -methoxo complexes **13**, **16** and **18** does not provide any information. But in the EI-mass spectrum for **17** the parent ion peak with 100% abundance is observed at $m/z = 935$ with the expected isotope pattern, confirming the composition $[\text{Mn}^{\text{IV}}\text{L}^{\text{S}}_2]$. Unfortunately, its selenium-congener does not provide such clear MS in the EI mode.

Mass Spectrometry in ESI mode for **14**, **19**, **20** and **21** does not leave any doubt about the composition. Two single peaks, one at $m/z = 242$ (in positive mode) and the second at $m/z = 1031, 1032, 827$ and 732 (in negative mode) with the expected isotope distribution pattern, correspond to $[\text{Bu}_4\text{N}]^+$ and $[\text{MnL}^{\text{Se}}_2]^-$, $[\text{FeL}^{\text{Se}}_2]^-$, $[\text{FeL}^{\text{Se}}\text{L}^{\text{Se}'}]^-$ and $[\text{FeL}^{\text{S}}\text{L}^{\text{S}'}]^-$ species, respectively.

3.3.3 X-RAY CRYSTAL STRUCTURE

Complexes **13**, **15**, **17**, **18**, **19** and **20** were crystallographically characterized. Other complexes were characterized by other means and in accord with the formulated compositions. Being isostructural with the crystallographically characterized complex **13**

mentioned above, crystal structure analyses were not done for **16**. Similarly complex **21** isostructural with **20** and hence the structure is not reported here.

3.3.3.1 Molecular structure of $[\text{Mn}^{\text{III}}_2\text{L}^{\text{Se}}_2(\mu\text{-OMe})_2(\text{MeOH})_2]$ (**13**)

Crystal structure analysis reveals the complex to be dimeric in nature and consists of two six coordinated Mn(III) ions. The Ball and Stick diagram along with the atom-labeling scheme is shown in Figure 3.3.3.1, selected bond angles and bond lengths are given in Table 3.3.3.1.

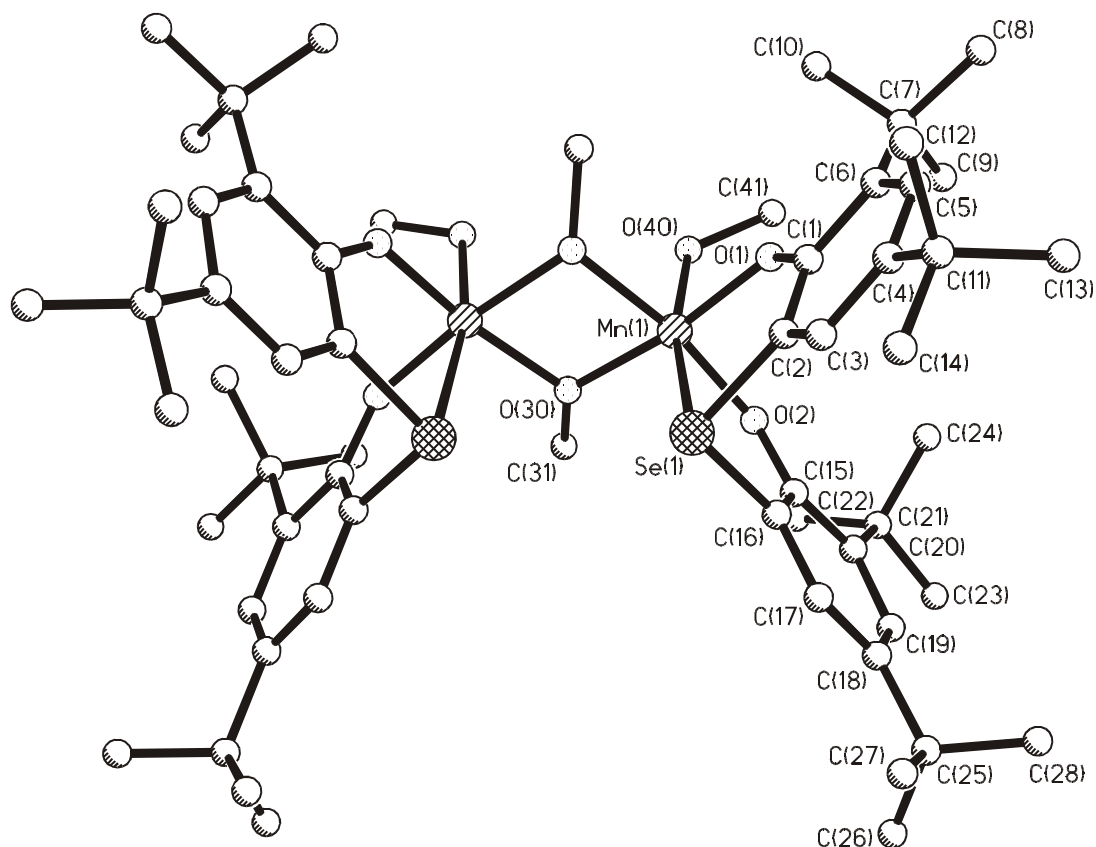


Figure 3.3.3.1 Ball and Stick diagram and atom labeling scheme for $[\text{Mn}^{\text{III}}_2\text{L}^{\text{Se}}_2(\mu\text{-OMe})_2(\text{MeOH})_2]$ (**13**).

The two Mn(III) ions (Mn-Mn = 3.038 Å) are related by the crystallographic plane of symmetry and symmetrically bridged by two methoxide ligands. The bisphenolate ligand with O,Se,O donor set, is facially coordinated with both the central Mn(III) ions. Two bridging methoxy oxygens and two phenolate oxygens from ligands form the equatorial plane of the octahedral geometry for both Mn(III) center. One selenium atom from the ligand and one oxygen atom from the methanol molecule complete the coordination sphere. Two selenium atoms from the ligands and the methanol molecules attached with two metal centers are *cis* to

each other and related by σ symmetry where the plane passes through the two oxygen atoms of the bridging methoxide ligand. Two manganese atoms and two bridging methoxy oxygens form a perfect plane, with Mn(1)-O(30)-Mn#(1) and O(30)-Mn(1)-O#(30) angles of 102.5 and 77°, respectively. Mn-Se and Mn-O(40) form the axial plane with O(40)-Mn-Se bond angle deviating from 180° makes it distorted octahedral. The axial Mn-O(40) bond distance is longer which is a direct consequence of the Jahn-Teller distortion of the coordination polyhedron along the O(40)-Mn-Se direction. This is common for a Mn(III) h.s complex having d^4 electronic configuration. This complex is comparable to the Cr(III) complexes **9** and **11** other than the orientation of the methanol molecules. Although two methanol molecules are transposed syn to each other no methanol-methanolate bridging is observed in this case.

Table 3.3.3.1 Selected bond distances (Å) and angles (deg) for **13**

| | | | |
|--------------------|-----------|---------------------|----------|
| Mn(1)-O(1) | 1.866(7) | Mn(1)-O(2) | 1.856(6) |
| Mn(1)-O(30) | 1.939(6) | Mn(1)-O(30)#1 | 1.956(6) |
| Mn(1)-O(40) | 2.257(6) | Mn(1)-Se(1) | 2.711(2) |
| C(1)-O(1) | 1.340(10) | C(15)-O(2) | 1.341(9) |
| Mn(1)-Mn(1)#1 | 3.038(3) | | |
| O(2)-Mn(1)-O(1) | 94.8(3) | O(2)-Mn(1)-O(30) | 93.6(3) |
| O(1)-Mn(1)-O(30) | 171.6(3) | O(2)-Mn(1)-O(30)#1 | 170.2(3) |
| O(1)-Mn(1)-O(30)#1 | 94.7(3) | O(30)-Mn(1)-O(30)#1 | 77.0(3) |
| O(2)-Mn(1)-O(40) | 92.1(2) | O(1)-Mn(1)-O(40) | 89.0(3) |
| O(30)-Mn(1)-O(40) | 89.9(2) | O(30)#1-Mn(1)-O(40) | 91.0(2) |
| O(2)-Mn(1)-Se(1) | 82.9(2) | O(1)-Mn(1)-Se(1) | 82.4(2) |
| O(30)-Mn(1)-Se(1) | 99.5(2) | O(30)#1-Mn(1)-Se(1) | 95.5(2) |
| O(40)-Mn(1)-Se(1) | 168.6(2) | Mn(1)-O(30)-Mn(1)#1 | 102.5(3) |

3.3.3.2 Molecular structure of [Mn^{IV}L^{Se}]₂(15)

The X-ray analysis confirms that the complex with M:L = 1:2 is formed. Figure 3.3.3.2 below shows the ORTEP diagram of the independent molecule with the atom-labeling scheme. Selected bond distances and angles are given in Table 3.3.3.2.

The complex consists of a neutral unit composed of a central pseudo-octahedral manganese ion surrounded by two tridentate ligands bound in a facial manner (*fac*-SeO₂ donor set). The complex is synthesized from its Mn(III) counterpart by chemical oxidation with FcPF₆ and the formed complex crystallizes with reduced form of Fc⁺, i.e. ferrocene present in the solution. One solvent molecule, MeCN is also present in the unit cell.

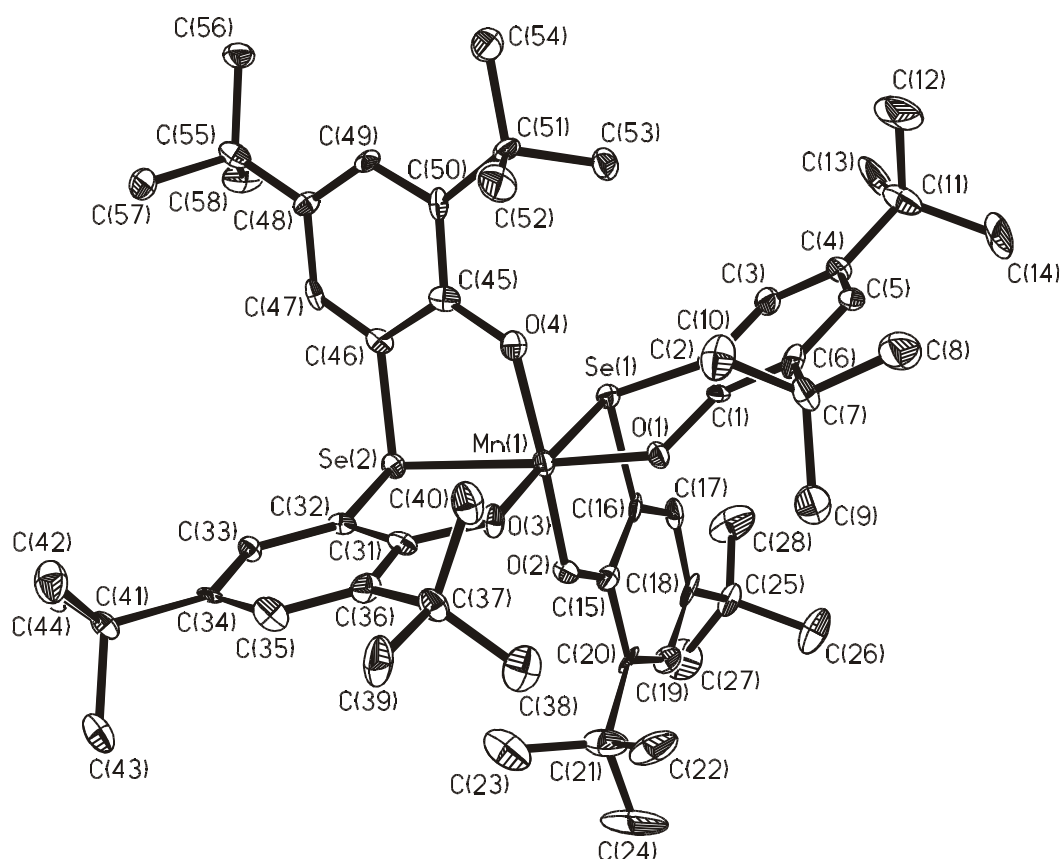


Figure 3.3.3.2 ORTEP and atom labeling scheme for $[Mn^{IV}L^{Se}_2](15)$

Table 3.3.3.2 Selected bond distances (Å) and angles (deg) for **15**

| | | | |
|-------------------|------------|------------------|------------|
| Mn(1)-O(1) | 1.848(5) | Mn(1)-O(2) | 1.866(5) |
| Mn(1)-O(3) | 1.841(5) | Mn(1)-O(4) | 1.876(5) |
| Mn(1)-Se(1) | 2.4717(14) | Mn(1)-Se(2) | 2.4848(14) |
| C(1)-O(1) | 1.343(8) | C(15)-O(2) | 1.321(9) |
| C(31)-O(3) | 1.342(8) | C(45)-O(4) | 1.332(8) |
| O(3)-Mn(1)-O(1) | 93.2(2) | O(3)-Mn(1)-O(2) | 92.0(2) |
| O(1)-Mn(1)-O(2) | 93.9(2) | O(3)-Mn(1)-O(4) | 94.0(2) |
| O(1)-Mn(1)-O(4) | 91.5(2) | O(2)-Mn(1)-O(4) | 171.7(2) |
| O(3)-Mn(1)-Se(1) | 178.1(2) | O(1)-Mn(1)-Se(1) | 86.4(2) |
| O(2)-Mn(1)-Se(1) | 86.2(2) | O(4)-Mn(1)-Se(1) | 87.9(2) |
| O(3)-Mn(1)-Se(2) | 87.2(2) | O(1)-Mn(1)-Se(2) | 177.0(2) |
| O(2)-Mn(1)-Se(2) | 89.0(2) | O(4)-Mn(1)-Se(2) | 85.6(2) |
| Se(1)-Mn(1)-Se(2) | 93.36(5) | | |

The ligands coordinate through the phenolate oxygens and selenium donor. All the phenols are deprotonated making the formal oxidation state of the central ion Mn(IV). Two phenolate oxygens and two selenium atoms from two ligands form the equatorial plane, where two same types of atoms occupy *cis*-positions with respect to each other. The remaining phenolate

oxygen atoms, mutually *trans*, complete the coordination sphere. The bond angles O(2)-Mn-O(4) [171.7(2)°], O(3)-Mn-Se [178.1(2)°], O(1)-Mn-Se(1) [177.0(2)°], O(1)-Mn-O(2) [93.9(2)°] and O(3)-Mn-O(4) [94.0(2)°] clearly indicate the system to be a distorted octahedron. All the phenyl rings attached to the phenolate oxygen atoms are planar, indicating the retention of aromaticity of the phenyl rings upon coordination. The mean Mn-O (phenolate) distance of 1.8587 Å is consistent with other Mn(IV) complexes reported in literature.¹⁴ So the system is a genuine Mn(IV) and no ambiguity remains regarding the oxidation state of the metal, where the ligand behaves like ‘innocent’ in this metal complex in the higher oxidation state. The Mn-O bond lengths are in accord with d³ Mn(IV) complex, which corroborates also with the EPR and magnetic susceptibility measurements.

3.3.3.3 Molecular structure of [Mn^{IV}L^S₂](17)

This complex is isostructural with complex **15** and hence details are not discussed here. The ORTEP diagram along with atom labeling scheme is shown in Figure 3.3.3.3, selected bond angles and bond distances are given in the Table 3.3.3.3.

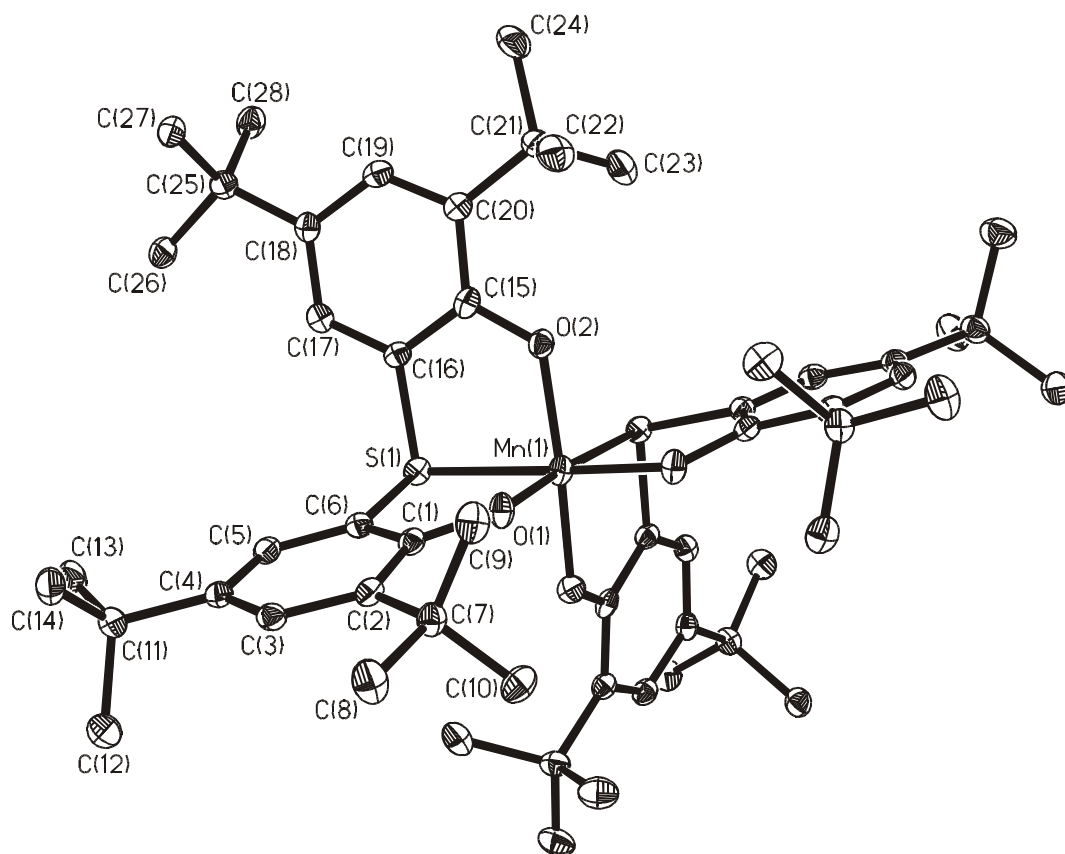


Figure 3.3.3.3 ORTEP and atom labeling scheme for [Mn^{IV}L^S₂](17).

Table 3.3.3.3 Selected bond distances (Å) and angles (deg) for 17

| | | | |
|---------------------|-----------|---------------------|------------|
| Mn(1)-O(1) | 1.840(2) | Mn(1)-O(1)#1 | 1.840(2) |
| Mn(1)-O(2) | 1.886(2) | Mn(1)-O(2)#1 | 1.886(2) |
| Mn(1)-S(1) | 2.3586(8) | Mn(1)-S(1)#1 | 2.3586(8) |
| C(1)-O(1) | 1.343(3) | C(15)-O(2) | 1.346(3) |
| O(1)#1-Mn(1)-O(1) | 90.91(11) | O(1)#1-Mn(1)-O(2) | 92.29(8) |
| O(1)-Mn(1)-O(2) | 96.57(8) | O(1)#1-Mn(1)-O(2)#1 | 96.58(8) |
| O(1)-Mn(1)-O(2)#1 | 92.29(8) | O(2)-Mn(1)-O(2)#1 | 167.36(12) |
| O(1)#1-Mn(1)-S(1)#1 | 85.92(6) | O(1)-Mn(1)-S(1)#1 | 175.96(6) |
| O(2)-Mn(1)-S(1)#1 | 86.06(6) | O(2)#1-Mn(1)-S(1)#1 | 85.60(6) |
| O(1)#1-Mn(1)-S(1) | 175.96(6) | O(1)-Mn(1)-S(1) | 85.92(6) |
| O(2)-Mn(1)-S(1) | 85.60(6) | O(2)#1-Mn(1)-S(1) | 86.06(6) |
| S(1)#1-Mn(1)-S(1) | 97.35(4) | | |

3.3.3.4 Molecular structure of $[\text{Fe}_2\text{L}^{\text{Se}}_2(\mu\text{-OMe})_2(\text{MeOH})_2]$ (18)

The crystal structure consists of discrete dinuclear molecules. The structure of the molecule and atom labeling schemes are shown in Figure 3.3.3.4, and bond parameters are given in Table 3.3.3.4.

Each molecule consists of two iron(III) centers which are related by a crystallographic inversion center. Each iron is coordinated by two *cis*-phenolate oxygen atoms and one selenium atom of the tridentate ligand, and the octahedral environment is completed by a pair of methoxo groups which asymmetrically bridge the two Fe(III) ions, and one oxygen atom of a coordinated methanol molecule. Two iron and two methoxo oxygen atoms constitute a perfect plane.

The bridging angles Fe(1)-O(30)-Fe(1)# [106.11(11)°] and Fe(1)-O(30)#-Fe(1)# and O(30)-Fe(1)-O(30)# [73.89(11)°] and O(30)-Fe(1)#-O(30)# are equal. The dimethoxo bridge is significantly asymmetric [$d(\text{Fe}(1)\text{-O}(30)) = d(\text{Fe}(1)\#\text{-O}(30)\#) = 2.010(2)\text{Å}$, $d(\text{Fe}(1)\text{-O}(30)\#) = d(\text{Fe}(1)\#\text{-O}(30)) = 1.979(2)\text{Å}$; $\Delta d = 0.031\text{Å}$].

The similar asymmetric Fe_2O_2 core has been described by Walker and Poli and Palaniandavar et al.¹⁵ The asymmetry of the Fe-O-Fe-O structural unit is also evident from the difference in the external bond angles [Fe(1)-O(30)-C(31) = 126.3(2)°; Fe(1)#-O(30)-C(31) = 127.5(2)°] at the methoxo oxygen. The bridging Fe-OMe, Fe-O(phenolate) [Fe(1)-O(1), 1.940(3)Å; Fe(1)-O(2), 1.927(2)Å] and Fe-O(40)methanol[2.070(3)Å] are in their normal range.¹⁶ Both, the angles at oxygen [106.11(11)°] and those at iron [72.89(11)°] are equal and typical for an Fe-O-Fe-O ring.¹⁷ The preference of an Fe-O-Fe-O ring for the O-Fe-O angle close to 76° leads to distortions in the remaining angles in the coordination sphere from ideal octahedral. An

increase or decrease from the ideal value of 90° occurs for the other angles O(40)-Fe(1)-O(30) [$98.29(10)^\circ$], Se(1)-Fe(1)-O(30) [$87.76(7)^\circ$], O(40)-Fe(1)-O(30)# [$91.65(11)^\circ$] and a decrease from 180° for O(2)-Fe(1)-O(30) [$165.37(11)^\circ$] and O(1)-Fe(1)-O(30)# [$166.87(10)^\circ$] angles making the coordination geometry a distorted octahedral one.

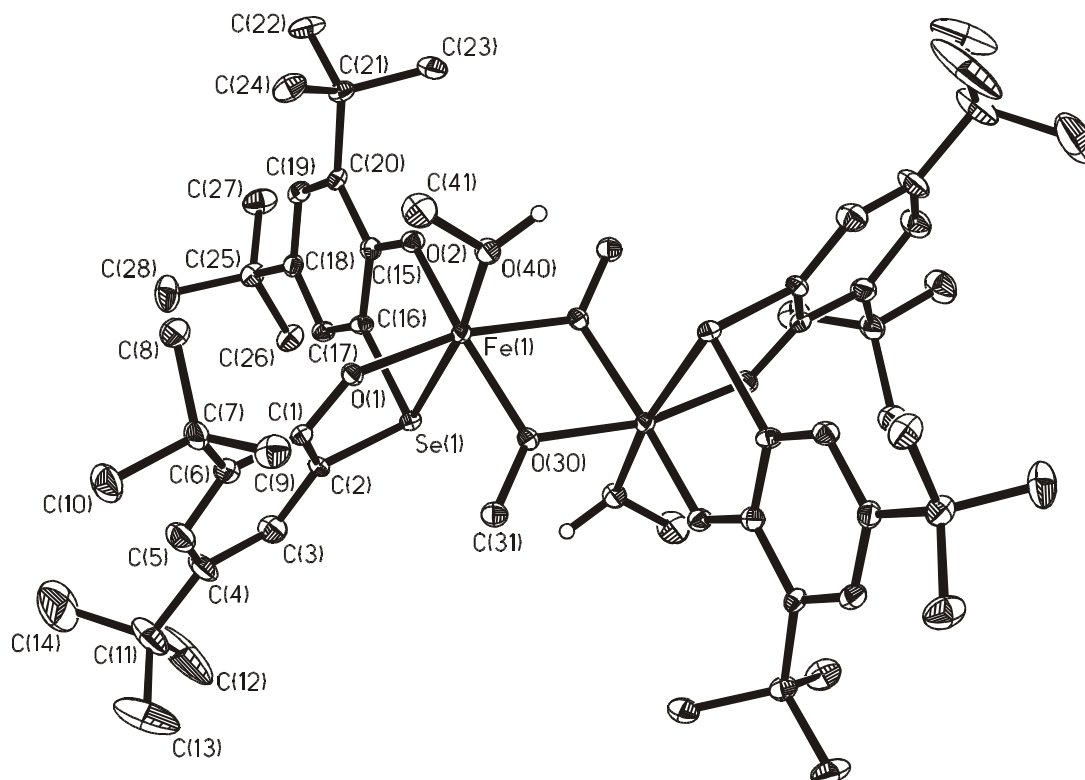


Figure 3.3.3.4 ORTEP and atom labeling scheme for $[\text{Fe}_2\text{L}^{\text{Se}}_2(\mu\text{-OMe})_2(\text{MeOH})_2]$ (**18**)

The oxygen of the methanol molecule, O(4), coordinated to Fe(1), is hydrogen-bonded to another methanol molecule. There is a hydrogen-bonding network between three other non-coordinated methanol molecules. The long Fe-O(30) bond is relatively weak because it is *trans* to the stronger and hence shorter Fe-O(phenolate) bond, which mitigates the lewis acidity of the iron center and decrease its affinity for the methanolate bridge. The asymmetry of the Fe-O-Fe-O bridge originates from the *cis* phenolate coordination of the ligand.

Table 3.3.3.4 Selected bond distances (Å) and angles (deg) for **18**

| | | | |
|--------------------|------------|---------------------|------------|
| Fe(1)-O(1) | 1.940(3) | Fe(1)-O(2) | 1.927(3) |
| Fe(1)-O(30) | 2.010(2) | Fe(1)-O(30)#1 | 1.979(2) |
| Fe(1)-O(40) | 2.070(3) | Fe(1)-Se(1) | 2.6476(8) |
| C(1)-O(1) | 1.321(4) | C(15)-O(2) | 1.333(4) |
| Fe(1)-Fe(1)# | 3.188(3) | | |
| O(2)-Fe(1)-O(1) | 96.33(11) | O(2)-Fe(1)-O(30) | 165.37(11) |
| O(1)-Fe(1)-O(30) | 93.15(10) | O(2)-Fe(1)-O(30)#1 | 95.99(11) |
| O(1)-Fe(1)-O(30)#1 | 166.87(10) | O(30)-Fe(1)-O(30)#1 | 73.89(11) |
| O(2)-Fe(1)-O(40) | 92.45(11) | O(1)-Fe(1)-O(40) | 92.36(11) |
| O(30)-Fe(1)-O(40) | 98.29(10) | O(30)#1-Fe(1)-O(40) | 91.65(11) |
| O(2)-Fe(1)-Se(1) | 82.46(8) | O(1)-Fe(1)-Se(1) | 82.59(8) |
| O(30)-Fe(1)-Se(1) | 87.76(7) | O(30)#1-Fe(1)-Se(1) | 94.54(7) |
| O(40)-Fe(1)-Se(1) | 172.35(8) | Fe(1)-O(30)-Fe(1)#1 | 106.11(11) |

3.3.3.5 Molecular structure of $\text{Bu}_4\text{N}[\text{FeL}^{\text{Se}}_2]$ (**19**)

The crystal lattice consists of discrete $[\text{Bu}_4\text{N}]^+$ and $[\text{FeL}_2^{\text{Se}}]^-$ ions. The ORTEP diagram of the anion with the atom-labeling scheme is shown in Figure 3.3.3.5. Selected bond parameters are given in Table 3.3.3.5.

The central metal ion, Fe(III) is in a distorted octahedral environment with a FeO_4Se_2 coordination sphere. Two tridentate ligands with O,Se,O donor set bind the metal in *fac*- SeO_2 manner. Two phenolates and two selenium atoms from two ligands form the equatorial plane where atoms of the same type occupy *cis*-positions. The remaining two phenolates are *trans* to each other satisfying the hexacoordinated sites. O(2)-Fe-O(4) and O(1)-Fe-Se(2) bond angles $[156.75(7)^\circ$ and $171.91(7)^\circ]$ are in accord with the distorted nature of the complex from an ideal octahedron.

The average Fe-O (phenolate) bond distance is 1.912 Å which is in the normal Fe(III)-O bond lengths- Fe-O(2) and Fe-O(4) bonds $[1.929(2)$ and $1.934(2)\text{Å}]$ are a little longer in the range of corrected values. This may arise due to the deviation from the ideal octahedral geometry. The bond lengths and angles in the cation $[\text{Bu}_4\text{N}]^+$ seems to be reasonable and are comparable with reported values.¹⁸

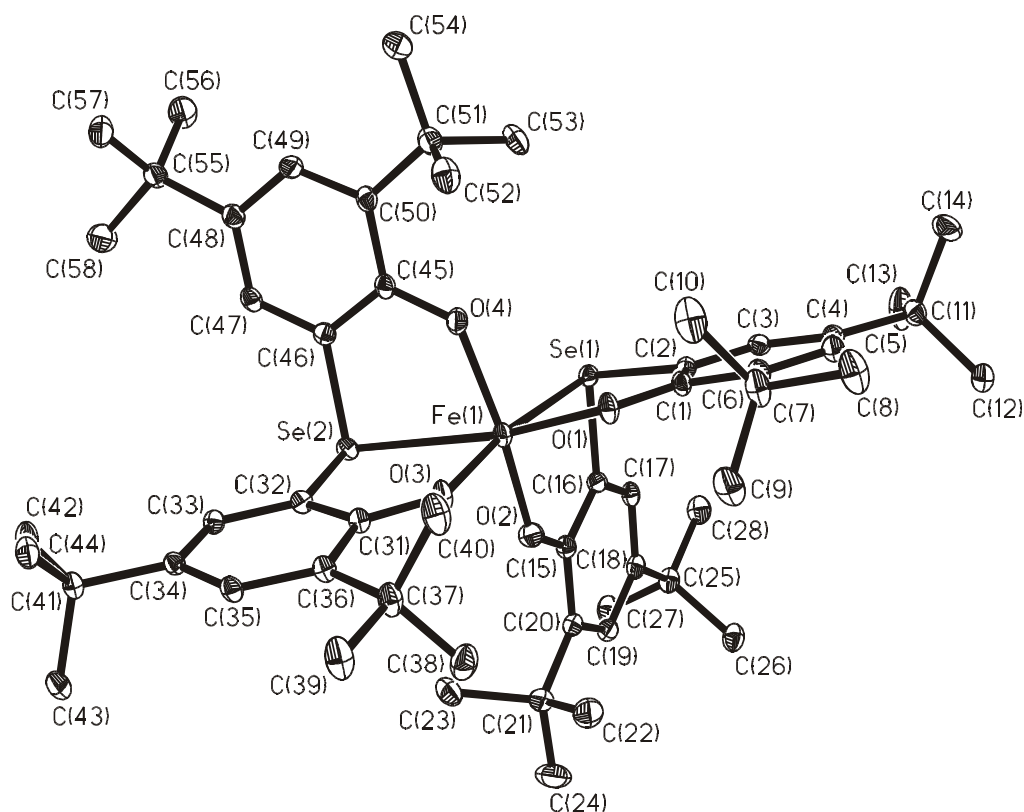


Figure 3.3.3.5 ORTEP and atom labeling scheme for $[\text{FeL}^{\text{Se}}_2]^-$ (**19**).

Table 3.3.3.5: Selected bond distances (\AA) and angles ($^\circ$) for **19**:

| | | | |
|-------------------|-----------|------------------|-----------|
| Fe(1)-O(1) | 1.892(2) | Fe(1)-O(3) | 1.893(2) |
| Fe(1)-O(2) | 1.929(2) | Fe(1)-O(4) | 1.934(2) |
| Fe(1)-Se(1) | 2.7966(5) | Fe(1)-Se(2) | 2.7797(5) |
| C(1)-O(1) | 1.330(3) | C(15)-O(2) | 1.324(3) |
| C(31)-O(3) | 1.324(3) | C(45)-O(4) | 1.321(3) |
| O(1)-Fe(1)-O(3) | 102.17(7) | O(1)-Fe(1)-O(2) | 100.77(8) |
| O(3)-Fe(1)-O(2) | 93.28(8) | O(1)-Fe(1)-O(4) | 93.82(8) |
| O(3)-Fe(1)-O(4) | 101.28(8) | O(2)-Fe(1)-O(4) | 156.75(7) |
| O(1)-Fe(1)-Se(2) | 171.91(6) | O(3)-Fe(1)-Se(2) | 79.98(5) |
| O(2)-Fe(1)-Se(2) | 86.83(5) | O(4)-Fe(1)-Se(2) | 78.09(5) |
| O(1)-Fe(1)-Se(1) | 79.69(5) | O(3)-Fe(1)-Se(1) | 170.82(6) |
| O(2)-Fe(1)-Se(1) | 77.54(5) | O(4)-Fe(1)-Se(1) | 87.49(5) |
| Se(2)-Fe(1)-Se(1) | 99.43(2) | | |

3.3.3.6 Molecular structure of $\text{Bu}_4\text{N}[\text{FeL}^{\text{Se}}\text{L}^{\text{Se}'}]^-$ (**20**)

Although the analytical and spectroscopic data unambiguously showed the presence of the mononuclear $\text{Bu}_4\text{N}[\text{FeL}^{\text{Se}}\text{L}^{\text{Se}'}]^-$ unit as the smallest unit, an X-ray analysis was undertaken to remove the doubts regarding connectivity. The structure analysis shows that the lattice consists of discrete $[\text{Bu}_4\text{N}]^+$ and $[\text{FeL}^{\text{Se}}\text{L}^{\text{Se}'}]^-$ ions. An ORTEP diagram of the anion with the atom labeling scheme is shown in Figure 3.3.3.6, with the selected bond parameters in Table 3.3.3.6.

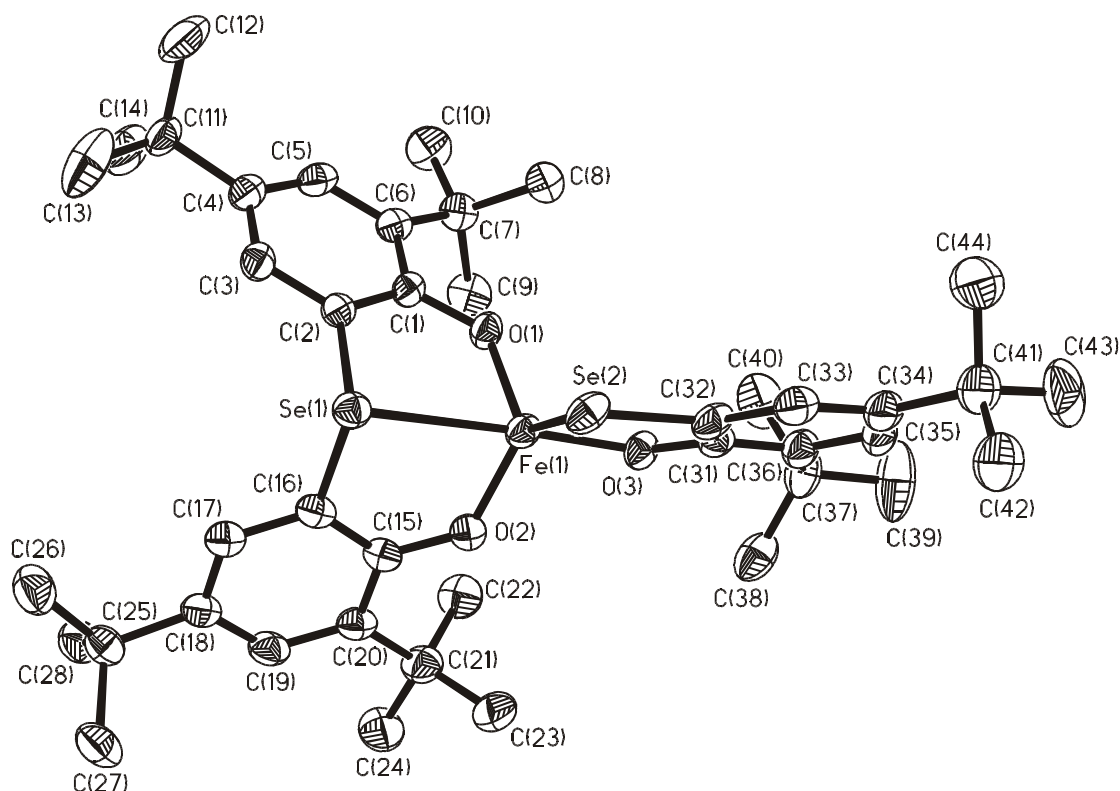


Figure 3.3.3.6 ORTEP and atom labeling scheme for $[\text{FeL}^{\text{Se}}\text{L}^{\text{Se}'}]^-$ (**20**)

Table 3.3.3.6 Selected bond distances (\AA) and angles (deg) for **20**

| | | | |
|------------------|------------|-------------------|------------|
| Fe(1)-O(1) | 1.886(3) | Fe(1)-O(3) | 1.889(3) |
| Fe(1)-O(2) | 1.867(3) | Fe(1)-Se(1) | 2.7434(9) |
| Fe(1)-Se(2) | 2.4565(9) | C(1)-O(1) | 1.339(5) |
| C(15)-O(2) | 1.337(6) | C(31)-O(3) | 1.332(5) |
| O(2)-Fe(1)-O(1) | 110.35(14) | O(2)-Fe(1)-O(3) | 101.07(14) |
| O(1)-Fe(1)-O(3) | 105.11(14) | O(2)-Fe(1)-Se(2) | 125.77(11) |
| O(1)-Fe(1)-Se(2) | 119.45(10) | O(3)-Fe(1)-Se(2) | 86.09(10) |
| O(2)-Fe(1)-Se(1) | 80.77(10) | O(1)-Fe(1)-Se(1) | 81.57(10) |
| O(3)-Fe(1)-Se(1) | 171.71(10) | Se(1)-Fe(1)-Se(2) | 86.31(3) |

The iron center is in a trigonal bipyramidal FeSe₂O₃ environment. One ligand with an O,Se,O donor set and the other with an O,Se donor set satisfies the five coordination sites. Two phenolates from tridentate ligand form the equatorial plane. The Fe-Se(1) and Fe-O(3) bonds, which are mutually in *trans* positions, form axial linkages, whereas Fe-O(1), Fe-O(2) and Fe-Se(2) are in the equatorial plane. The bond distances are significantly shorter than those for six-coordinated complex **19**. The Fe-O bond distances are consistent with d⁵ h.s. electronic configuration for Fe(III) center.

3.3.4 ELECTRONIC SPECTROSCOPY

The optical spectra for complexes **13-21** have been measured in CH₂Cl₂ in the range 300-1000 nm. The bands are of charge-transfer origin, as is clear from their high absorption coefficient values.¹⁹

Table 3.3.4.1 Optical spectral data for complexes 13-21

| Complex | λ_{\max} , nm (ϵ , M ⁻¹ cm ⁻¹) |
|-----------|---|
| 13 | 387(5940), 618(1160) |
| 14 | 372sh(5440), 461(1790) |
| 15 | 357sh(8100), 532(7550), 700sh(2580) |
| 16 | 386(5310), 444sh(3400), 600(920) |
| 17 | 349sh(9540), 522(7650), 700sh(2780) |
| 18 | 484 (3600) |
| 19 | 463(9650) |
| 20 | 341sh (10940), 504 (9650) |
| 21 | 492(7690) |

From the spectral data in Table 3.3.4.1 it is clear that the dinuclear Mn(III) complexes **13** and **16** are very similar. The peak at ~380 nm is of phenolate to Mn(III) charge-transfer origin. As it has already been discussed, these complexes are susceptible to aerial oxidation in non-coordinating solvent. In CH₂Cl₂, the color slowly changes from green to violet with formation and increase of a band around 530 nm (phenolate to Mn(IV) charge-transfer) and leaving a shoulder at the initial 380 nm range.

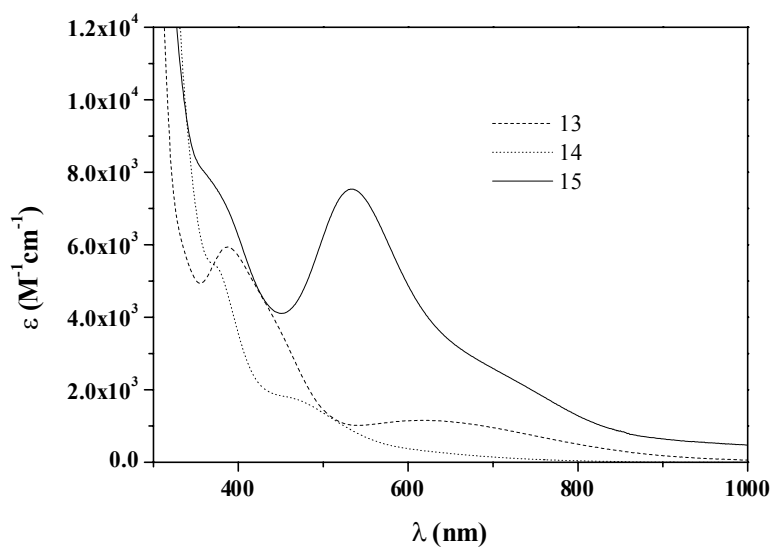


Figure 3.3.4.1 UV-vis spectra for complexes **13-15** at room temperature in CH_2Cl_2 .

The UV-vis spectra of **14** exhibit a ligand-to-metal charge transfer (LMCT) band around 461 nm and a π - π^* transition of the ligand at around 370 nm. No d-d bands are observed due to the presence of strong tail of the charge transfer band at lower energy.

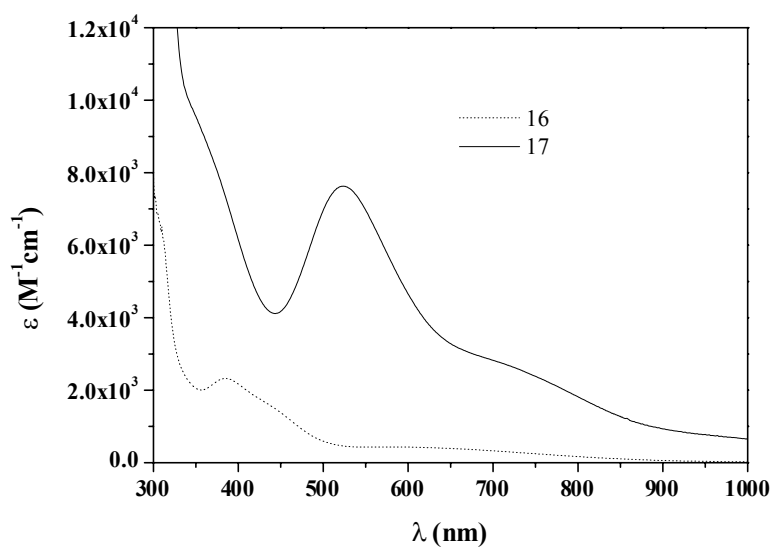


Figure 3.3.4.2 UV-vis spectra for complexes **16 and 17** at room temperature in CH_2Cl_2 .

Mn(IV) having d^3 electron configuration is expected to exhibit three absorption bands due to d-d electronic transitions (from the octahedral approximation ${}^4\text{A}_{2g} \rightarrow {}^4\text{T}_{2g}$ and ${}^4\text{A}_{2g} \rightarrow {}^4\text{T}_{1g}$). Usually they are of low intensity and are dominated by strong charge transfer tails in the

region. Based on the intensity, the band at around 530 nm can be assigned to LMCT transition for complexes **15** and **17**.

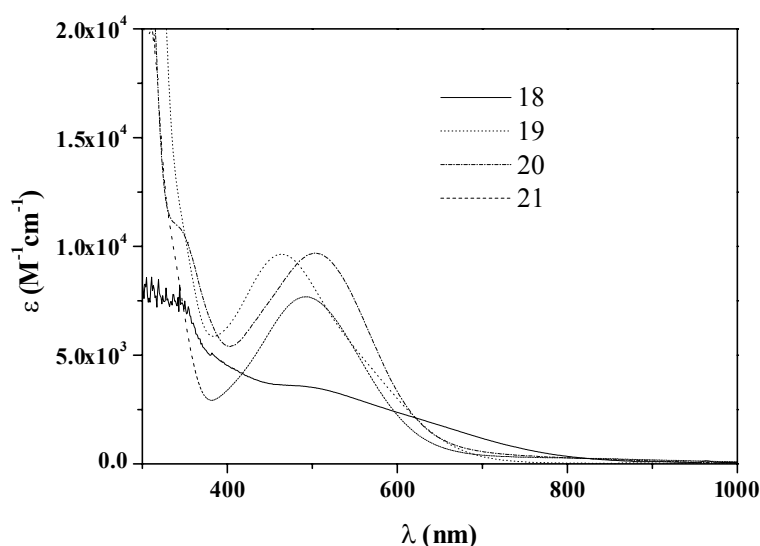


Figure 3.3.4.3 UV-vis spectra for complexes **18-21** at room temperature in CH_2Cl_2 .

As is seen from Table 3.3.4.1 and Figure 3.3.4.3, the optical spectra for complexes **18-21** are dominated by phenolate to Fe(III) charge transfer bands.

3.3.5 MAGNETISM

Magnetic measurements for polycrystalline samples of complexes **13-21** were done in the temperature range, 2 - 290 K in an applied field of 1 T.

The magnetic behaviour of **13**, **16** and **18** is typical for antiferromagnetically coupled dinuclear complexes. At 290 K the $\mu_{\text{eff}}(\chi_{\text{M}} \cdot T)$ values of $6.09 \mu_{\text{B}}$ ($4.64 \text{ cm}^3 \text{Kmol}^{-1}$) and $6.42 \mu_{\text{B}}$ ($5.16 \text{ cm}^3 \text{Kmol}^{-1}$) decrease monotonically with decreasing temperature until they reach μ_{eff} value of $0.52 \mu_{\text{B}}$ ($0.034 \text{ cm}^3 \text{Kmol}^{-1}$) and $0.99 \mu_{\text{B}}$ ($0.12 \text{ cm}^3 \text{Kmol}^{-1}$) at 2K for **13** and **16** respectively. This clearly indicates the exchange coupling between the two paramagnetic Mn(III) centers ($S_{\text{Mn}} = 2$) with a resulting $S_{\text{t}} = 0$ ground state for both complexes. Similarly, at 290K the $\mu_{\text{eff}}(\chi_{\text{M}} \cdot T)$ value of $6.78 \mu_{\text{B}}$ ($5.74 \text{ cm}^3 \text{Kmol}^{-1}$) decreases with decreasing temperature, until it reaches the value of $0.94 \mu_{\text{B}}$ ($0.112 \text{ cm}^3 \text{Kmol}^{-1}$) at 2K, indicating the exchange coupling between two Fe(III) centers ($S_{\text{Fe}} = 2.5$) with a resulting $S_{\text{t}} = 0$ ground state for **18**. Using the Heisenberg spin-Hamiltonian $\hat{H} = -2J \hat{S}_1 \cdot \hat{S}_2$ for an isotropic exchange coupling between two spins S_1 and S_2 , the experimental magnetic data were simulated using a least

square fitting computer program²⁰ with full-matrix diagonalization of exchange coupling, Zeeman splitting and axial zero-field interaction (DS_Z^2), if necessary. Solid lines represent the best fit with parameters: $J = -11.8 \text{ cm}^{-1}$, $g_{\text{Mn}} = 1.998$ for **13**, $J = -8.2 \text{ cm}^{-1}$, $g_{\text{Mn}} = 1.998$ for **16** and $J = -13.24 \text{ cm}^{-1}$, $g_{\text{Fe}} = 2.0$ for **18**. The calculated antiparallel exchange falls in the range observed for other μ -methoxo manganese(III) and iron(III) dimes.²¹

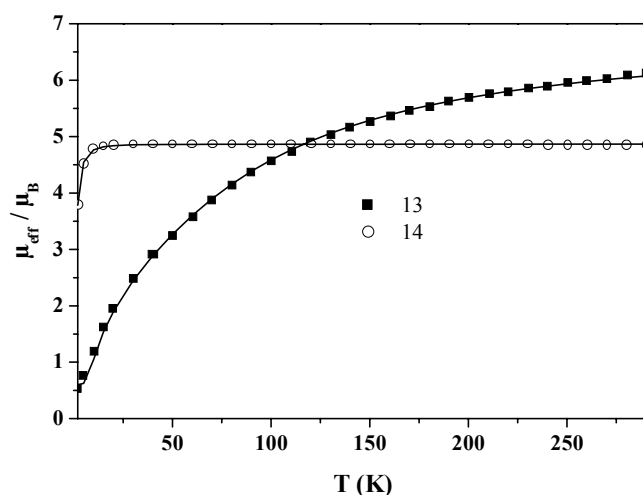


Figure 3.3.5.1 Magnetic measurements for complexes **13** and **14**.

Above $T = 10\text{K}$ complex **14** shows essentially temperature independent μ_{eff} value of $4.74 \pm 0.01 \mu_{\text{B}}$, confirming the metal ion in the d^4 h.s. Mn(III) state. Simulation of the magnetic moment yields $g_{\text{Mn}} = 1.987$ and a zero-field splitting parameter $|D| = 2.914 \text{ cm}^{-1}$, which is in the normal range for the Mn(III) ion.

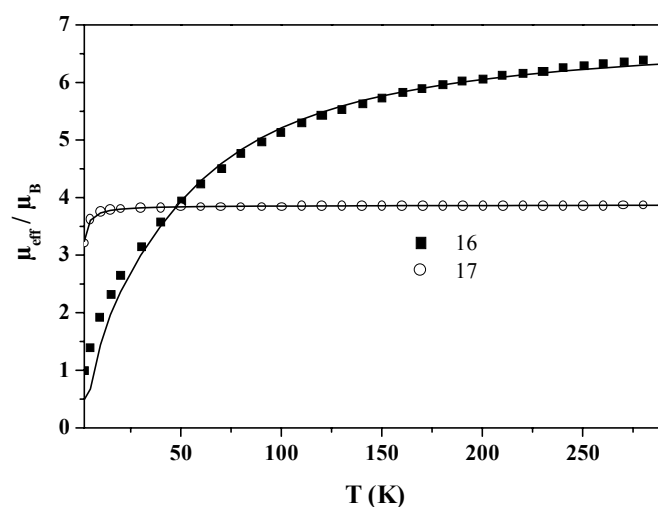


Figure 3.3.5.2 Magnetic measurements for complexes **16** and **17**.

Interesting magnetic behaviour is observed for complexes **15** and **17**, depending upon the way of synthesis. As has already been discussed, they could be synthesized by two different pathways, either by the oxidation of the Mn(III) congener with FcPF_6 or by aerial oxidation of the corresponding dimer. During chemical oxidation from the Mn(III) monomer, ferrocene cocrystallizes and therefore a higher μ_{eff} value is observed than the calculated μ_{eff} value for a d^3 ion. This can be rationalized by the observed μ_{eff} value for the batch of complex synthesized by aerial oxidation, where there is no ferrocene in the crystalline solid. The chemically oxidized complex shows above 20 K μ_{eff} value of $4.33 \pm 0.01 \mu_B$ (Figure 3.3.5.3). Simulation of the data yield $g_{\text{Mn}} = 2.268$ and 1.908 for the same Mn(IV) complex isolated by chemical oxidation (**15Fc**) and aerial oxidation (**15**), respectively. The higher μ_{eff} value for the Mn(IV) complex, synthesized chemically, can be explained by the contribution of high TIP from ferrocene present in the crystals. The room temperature magnetic moment of **17** in solid state is $3.85 \mu_B$, which is very close to the spin-only value for a d^3 system. Simulation of the magnetic data results in parameter $g_{\text{Mn}} = 1.994$ with $\text{TIP} = 28.9 \times 10^{-6} \text{ cm}^3 \text{ mol}^{-1}$ and $\theta = -0.657 \text{ K}$.

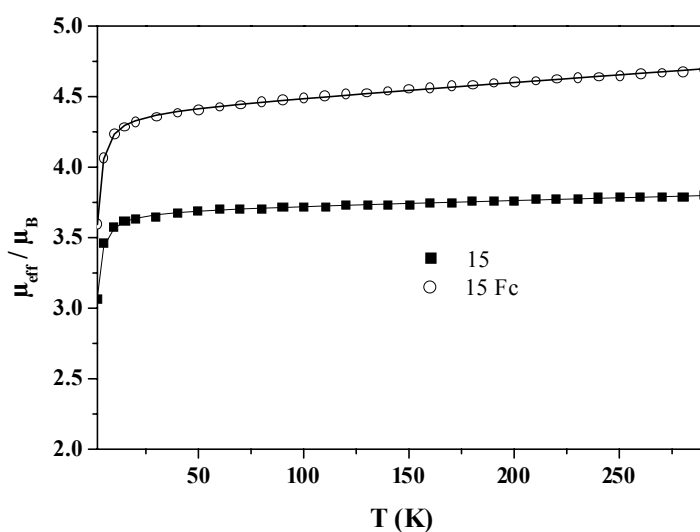


Figure 3.3.5.3 Magnetic measurements for complex **15**, isolated by different methods.

Above 10 K complexes **19**, **20** and **21** exhibit μ_{eff} values of 6.14 ± 0.03 , 5.88 ± 0.01 and $5.88 \pm 0.01 \mu_B$, respectively. This clearly shows that the complexes contain a d^5 h.s. ion, i.e., Fe(III). Simulations of the experimental magnetic moment data yield $g_{\text{Fe}} = 2.074$ ($\theta = -0.39 \text{ K}$) for **19**, $g_{\text{Fe}} = 2.0$ ($\theta = -0.96 \text{ K}$, $\text{TIP} = 256 \times 10^{-6} \text{ cm}^3 \text{ mol}^{-1}$) for **20** and $g_{\text{Fe}} = 2.0$ ($\theta = -0.96 \text{ K}$, $\text{TIP} = 216 \times 10^{-6} \text{ cm}^3 \text{ mol}^{-1}$) for **21**.

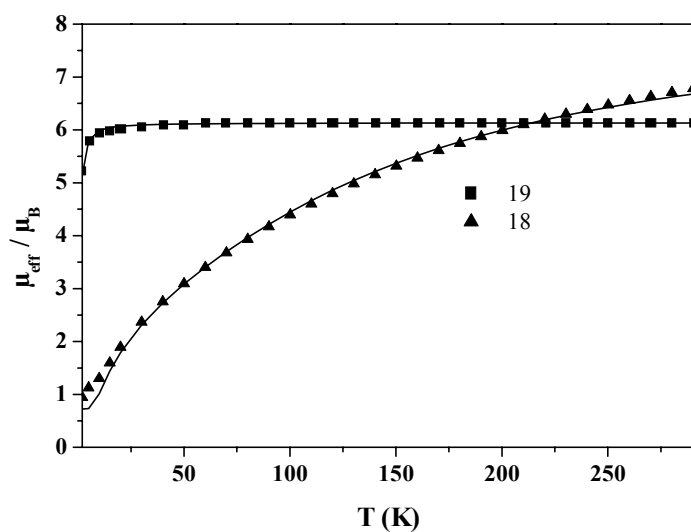


Figure 3.3.5.4 Magnetic measurements for complexes **18** and **19**.

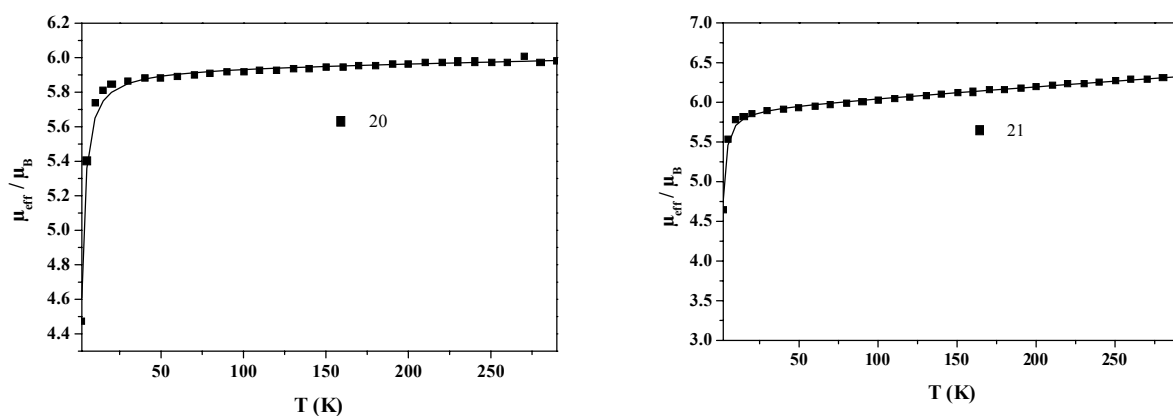


Figure 3.3.5.5 Magnetic measurements for complexes **20** (left) and **21** (right).

3.3.6 ELECTROCHEMISTRY

The electrochemical properties of the complexes **14**, **15**, **17**, **19**, **20** and **21** in CH₂Cl₂ solutions were investigated by voltammetric methods (cyclic voltammetry and square wave voltammetry). The cyclic voltammograms of **14** and **15** are identical, which show that the two species are electrochemically interconvertible.

Table 3.3.6.1 Redox potentials for complexes **17-21**(vs Fc^+/Fc)

| Complex | $E^{\text{ox}}_{1/2}$ (V) | $E^{\text{red}}_{1/2}$ (V) | Fc^+/Fc (V) |
|-----------|---------------------------|----------------------------|-----------------------------|
| 17 | 0.898* | -0.22 | 0.238 |
| 19 | 0.085, 0.501* | --- | 0.234 |
| 20 | -0.18* | --- | 0.232 |
| 21 | -0.17* | --- | 0.232 |

* CV peak potentials for irreversible processes.

Controlled potential coulometry at +0.3 V vs Fc^+/Fc (in CH_2Cl_2 solutions at -25°C) shows that the Mn^{III} complex **14** can be $1e^-$ oxidized, and the optical spectral changes (Figure 3.3.6.1) recorded during coulometry show unambiguously that the product of the oxidation is the Mn^{IV} form **15** (the final spectrum after one-electron oxidation is very similar to that of **15**). The cyclic voltammogram of the interconversion at a low scan rate (0.05 V/s) is shown in Figure 3.3.6.2. Oxidative and re-reductive peaks are seen, but the separation of the peaks is about 0.3 V, i.e., much higher than that of a simple $1e^-$ redox process (0.06 V). This high peak separation was found to depend strongly on the material of the working electrode (Pt and glassy carbon were used) and on the treatment of its surface (polishing procedure) prior to the measurements. This provides evidence that the high peak separation originates from a heterogeneous low electron exchange rate across the electrode surface rather than from the interfering homogeneous reactions.

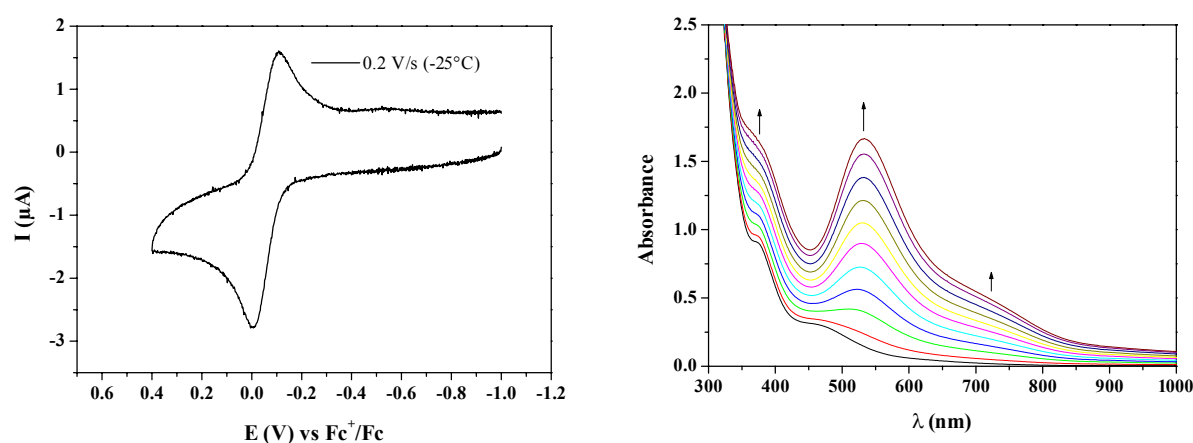


Figure 3.3.6.1 Cyclic voltammograms of **14** in CH_2Cl_2 at -25°C (left) and optical spectral change during one-electron oxidation (right).

At higher scan rates (measured up to 30 V/s) the cyclic voltammograms are more complex. When the scan is started at positive potentials and the reduction of Mn^{IV} is the *first* process, the reductive wave shows with increasing scan rate only the characteristics of slow electron transfer: peak broadening and a shift of the wave-maximum towards positive potentials. When, however, the scan is started on the cathodic side, all Mn^{IV} in the surrounding of the electrode is reduced to Mn^{III} during the equilibration time (or, alternatively; when a solution of Mn^{III} is used) and the reduction is the *second* process, which takes place only short time after the oxidation. In this case an additional wave grows with increasing scan rate, on expense of the peak for the "direct" reduction of Mn^{IV} to Mn^{III} seen at low scan rates. Clearly this extra peak must arise from a short-lived intermediate formed during the oxidation of Mn^{III} . At 30 V/s scan rate the wave for "direct" reduction is almost disappeared and the reduction takes place predominantly via the intermediate. It is noted that the oxidation appears at similar potentials as a single peak at all scan rates.

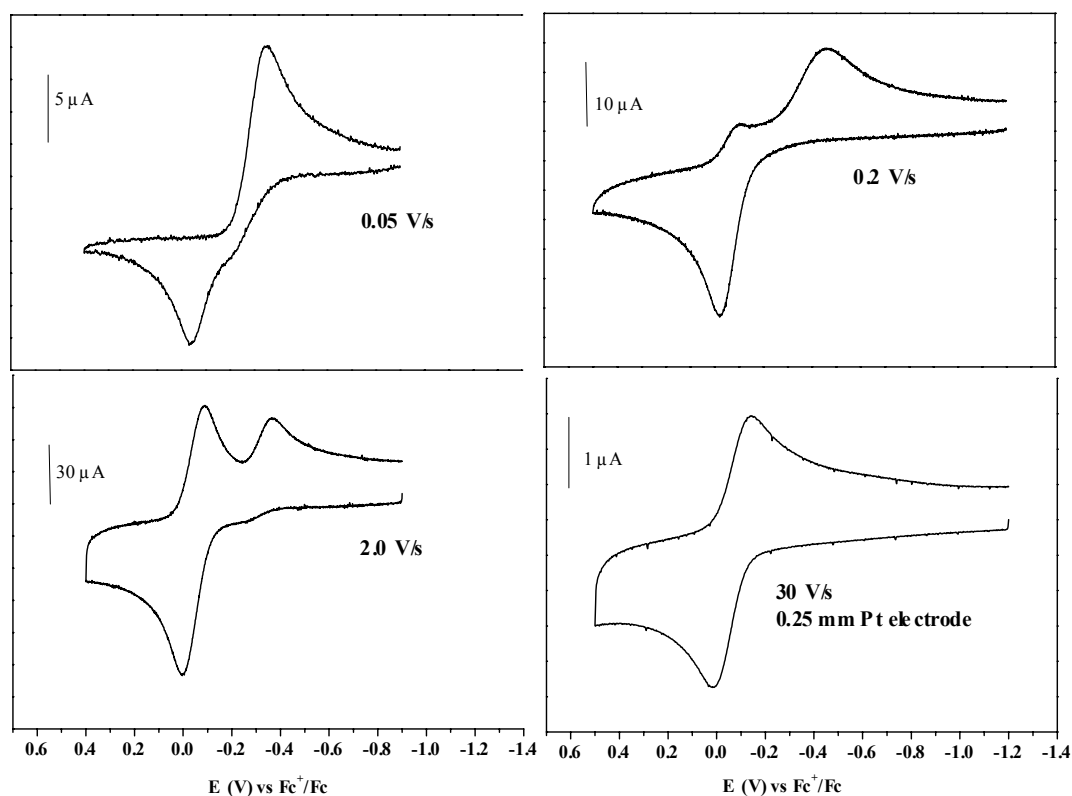
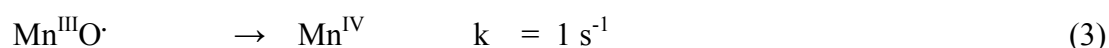
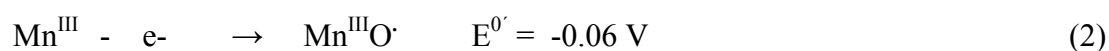
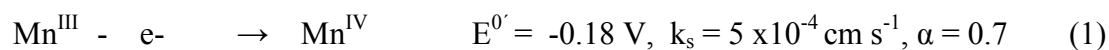


Figure 3.3.6.2 Cyclic voltammograms of **14** in CH_2Cl_2 at room temperature.

This intermediate, which becomes visible at high scan rates because the "direct" metal-centered $\text{Mn}^{\text{III}}/\text{Mn}^{\text{IV}}$ oxidation is kinetically hindered, must be formed by a ligand-centered oxidation, which generates the Mn^{III} -phenoxyl radical ($\text{Mn}^{\text{III}}\text{O}^\cdot$) species. In course of a slow scan it transforms into the thermodynamically more stable Mn^{IV} form, which is re-reduced at potentials $< 0\text{V}$. At high scan rates, when the time required for a scan is shorter than the lifetime of the phenoxyl radical, ligand-centered reduction at -0.2V takes place.



The presence of two species and their approximate redox potentials can be seen even more pronounced from square wave voltammograms measured at different frequencies given in Figure 3.3.6.3 (range 4.5 - 80 Hz).

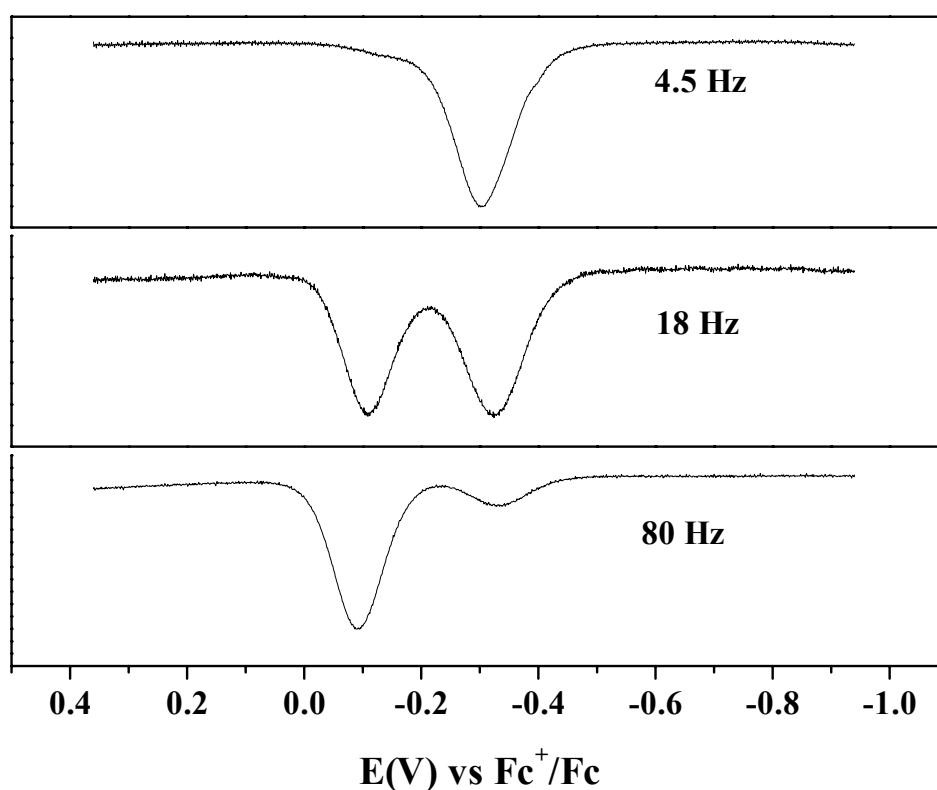


Figure 3.3.6.3 Square wave voltammograms of **14** in CH_2Cl_2 at room temperature.

By digital simulation it is possible to reproduce the cyclic voltammograms at all scan rates using only equations (1) - (3) and the single set of parameters presented in the scheme. Examples are shown in Figure 3.3.6.4. This provides further evidence that the underlying reaction scheme of equation (1) - (3) is correct. It is noted however that the range of possible rate constants of equation (3) is $0.5 - 2.0 \text{ s}^{-1}$ because the extent of transient Mn^{III} -phenoxyl radical formation (and hence the appearance of the additional reductive peak at -0.06V , the key fitting feature), is co-determined by the ratio of the contributions of the two competing reactions (1) and (2). The contribution of (1), being a heterogeneous process, depends critically on the state of the working electrode surface and could not be fully controlled.

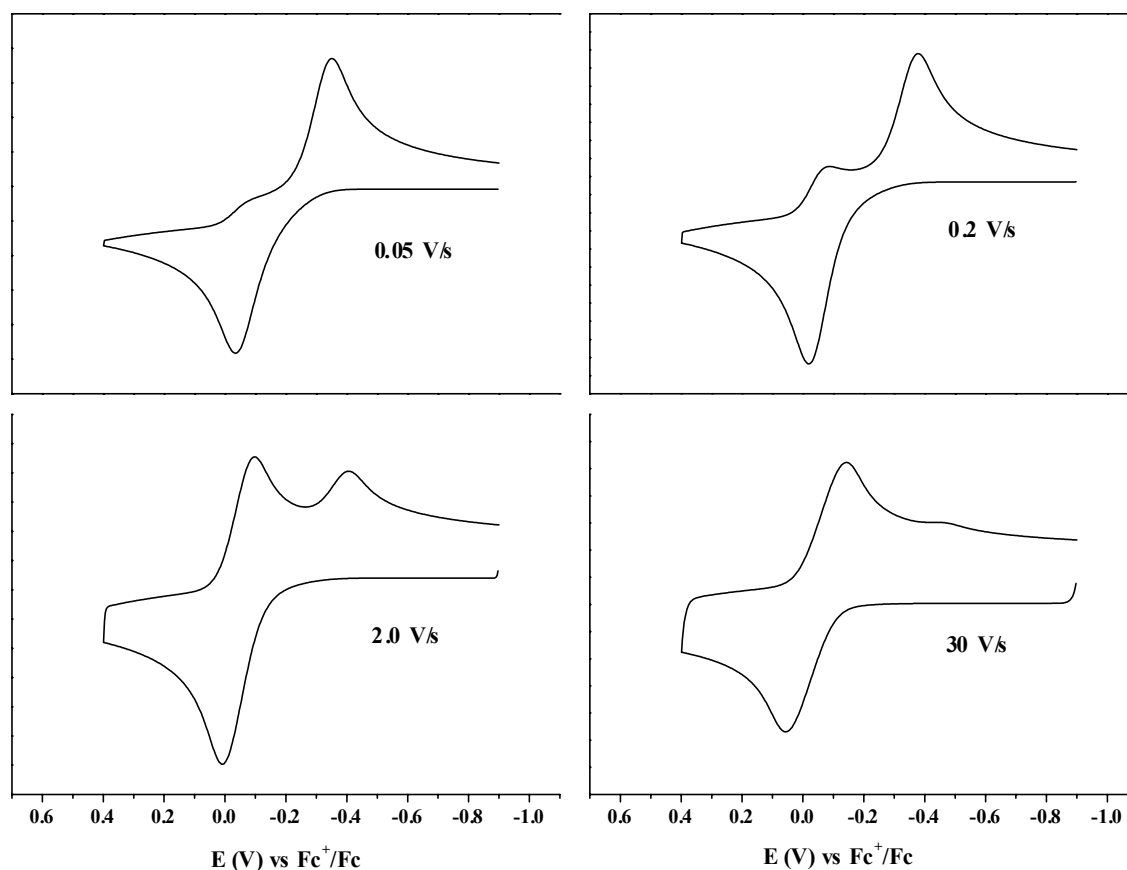


Figure 3.3.6.4 Simulations of the square wave voltammograms of 14

The difference of the redox potentials of $\text{Mn}^{\text{IV}}/\text{Mn}^{\text{III}}$ and Mn^{III} -phenoxyl radical/ Mn^{III} yield an equilibrium constant and a free energy change for the transformation of the phenoxyl radical into the Mn^{IV} species (equation (3)) of $K = 1.1 \times 10^3$ and $\Delta G^\circ = -17.4 \text{ kJ/mol}$ respectively, at 25°C .

At lower temperatures the rate constants of (1) and (3) are expected to decrease, both with the consequence that less Mn^{IV} is present when it comes to re-reduction. Therefore, at a given scan rate, the $\text{Mn}^{\text{IV}}/\text{Mn}^{\text{III}}$ wave should be more suppressed and the reversible Mn^{III} -phenoxyl radical/ Mn^{III} wave more pronounced at a lower temperature. This is, indeed, the case as seen in Figure 3.3.6.1.

The Mn(IV) complex **17** exhibits redox processes at 0.898 and -0.22 V. The latter process can be assigned as electrochemically quasireversible Mn(III)/Mn(IV) process and the former as a ligand based oxidation to the Mn(IV) phenoxyl radical. The oxidation to the phenoxyl radical is chemically irreversible in nature. The complexes **15** and **17** show very similar electrochemical behaviour.

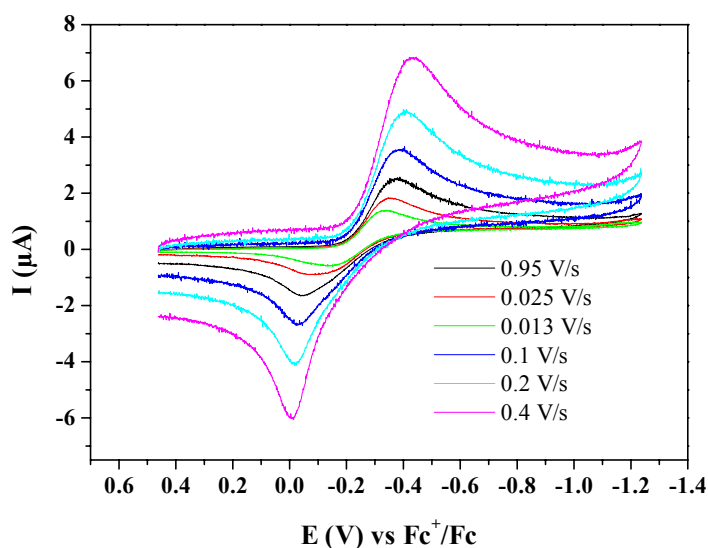


Figure 3.3.6.5 Cyclic voltammogram of **17** in CH_2Cl_2 at room temperature.

The Fe(III) complexes **19**, **20** and **21** all show ligand-centered irreversible oxidations. Complex **19** exhibits two oxidative redox-waves at 0.085 and 0.501 V vs Fc^+/Fc . The first wave is a chemically reversible and electrochemically quasireversible oxidation and the second one is irreversible. Controlled potential coulometry (-25°C) at 0.25 V vs Fc^+/Fc clearly suggests that the first wave is a one-electron oxidation of the phenolate to the phenoxyl radical. This is confirmed from the optical spectral change during the coulometry (Figure 3.3.6.6) where the peak around 400 nm increases corresponding to the radical-to-metal charge transfer band.

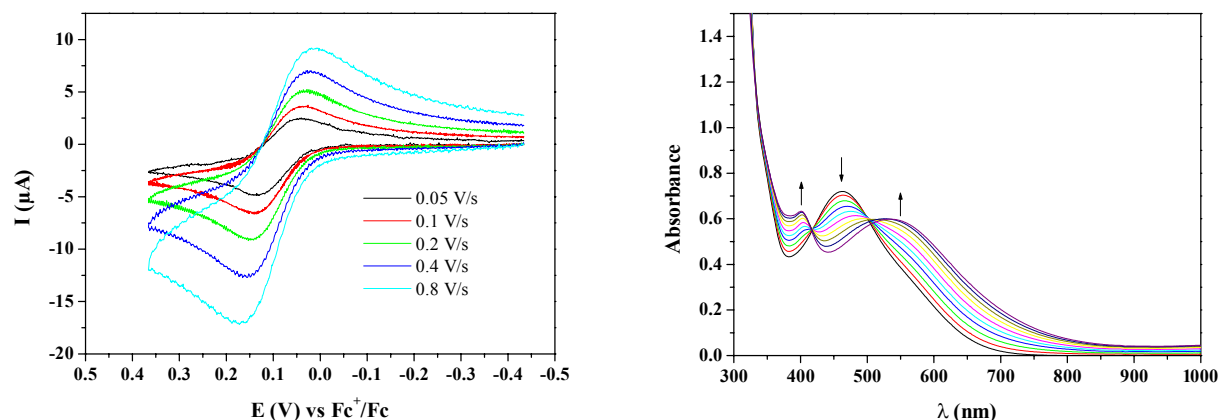


Figure 3.3.6.6 Cyclic voltammograms of **19** in CH_2Cl_2 at room temperature (left) and optical spectral change during one-electron oxidation (right)

Complexes **20** and **21** exhibit only one irreversible oxidative wave at relatively negative potentials (-0.18 V and -0.17 V vs Fc^+/Fc , respectively). This is assigned to ligand-based oxidation.

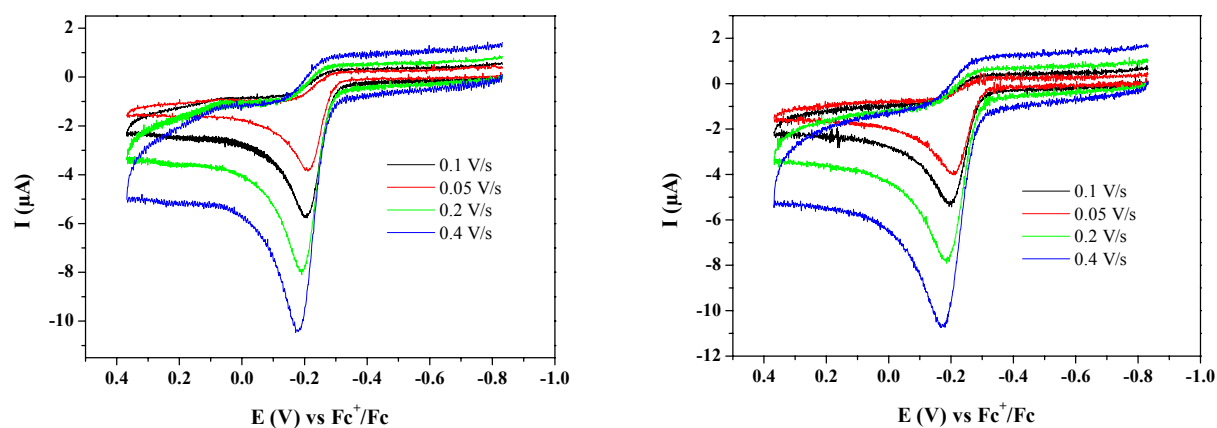
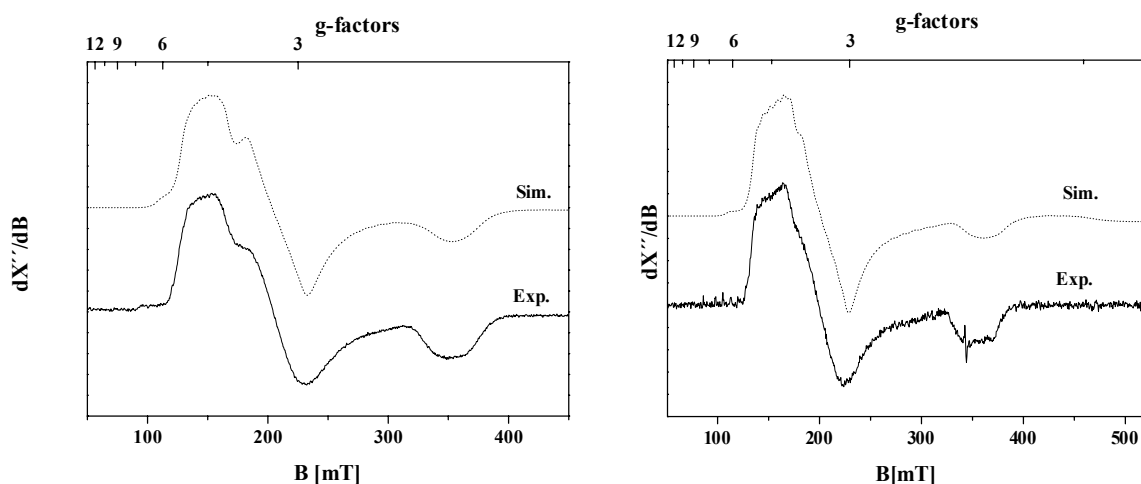


Figure 3.3.6.7 Cyclic voltammograms of **20** (left) and **21** (right) in CH_2Cl_2 at room temperature.

3.3.7 EPR SPECTROSCOPY

The EPR spectra of complexes **15** and **17** with simulations are given in Figure 3.3.7.1 to show the signals observed for Mn(IV) complexes. Mn(IV) is a d^3 system and can theoretically be compared with isoelectronic Cr(III) compounds.²²

The complexity of the EPR spectra of d^3 ions in an axial field ($E/D = 0$) is dependent upon the magnitude of the zero-field splitting parameters. The complexity can be simplified when the axial zero-field splitting parameter D takes one of two limiting forms for which D is either much larger than the applied microwave frequency ($2D \gg h\nu$) or much smaller than ($2D \ll h\nu$) ($h\nu = 0.31 \text{ cm}^{-1}$ for X-band). In the first case, two signals occur. The first is strong signal at low field and the second is a weaker $g = 2$ component, observed for catecholate^{23a} and sorbitolato^{23b} Mn(IV) complexes. In the later case, when D is small, the $g = 2$ signal dominates with weak low field signals, observed for thiohydroxamato^{14c} and thiocarbamato²⁴ Mn(IV) complexes. The EPR spectra become isotropic when $D = 0$, exhibiting a strong signal in the $g = 2$ region.



*Figure 3.3.7.1 X-band EPR spectra for complexes **15** (left) in CH_2Cl_2 at 30K and **17** (right) in CH_2Cl_2 /toluene at 20K. Experimental conditions (—): microwave frequency 9.45 GHz (**15**); 9.64 GHz (**17**), microwave power 0.1 mW (**15**); 0.2 mW (**17**), modulation amplitude 10G (**15**); 10 G (**17**). The simulations (----): $g = 2.0$, $D = 0.56 \text{ cm}^{-1}$, $E/D = 0.11$, $A = \{125, 140, 54\} \times 10^{-4} \text{ cm}^{-1}$ for **15** and $g = 2.0$, $D = 0.472 \text{ cm}^{-1}$, $E/D = 0.09$, $A = \{120, 140, 60\} \times 10^{-4} \text{ cm}^{-1}$ for **17**; Lorentzian line with frequency-dependent line width $W = 670 \text{ G}$ (**15**); $W = 550 \text{ G}$ (**17**).*

Both the complexes **15** in CH_2Cl_2 at 30K and **17** in a CH_2Cl_2 /toluene solvent mixture at 20K show dominant signals at $g \sim 3-6$ and $g \sim 2$ with weakly resolved ^{55}Mn hyperfine lines ($I = 5/2$). The EPR spectra for both complexes are $S = 3/2$ powder pattern from spin multiplets with moderately strong zero-field splitting (ZFS , $D \geq h\nu$). The signals at $g \sim 5$ and 3 can be assigned to powder resonance of the $|m_s = \pm 1/2\rangle$ Kramer Doublets (KD) for fields along the molecular

y- and x-direction, respectively. The trough at $g \sim 2$ originated from the z-resonances of $|m_s = \pm 1/2\rangle$ KD. Significant population of the $|m_s = \pm 3/2\rangle$ KD is indicated by the presence of low field hyperfine lines at $g \sim 6$, which also originated from fields in z-direction.

Simulation of the experimental spectra gives the parameters, $D = 0.472 \text{ cm}^{-1}$, $E/D = 0.09 \text{ cm}^{-1}$, $g = 2$ and $A = (120, 140, 60) \times 10^{-4} \text{ cm}^{-1}$ for **17** and $D = 0.56 \text{ cm}^{-1}$, $E/D = 0.11 \text{ cm}^{-1}$, $g = 2$ and $A = (125, 140, 54) \times 10^{-4} \text{ cm}^{-1}$ for **15**. The positive ZFS ($D > 0$) clearly indicates the ground state properties $|\pm 1/2\rangle$ resonances.

3.3.8 MÖSSBAUER SPECTROSCOPY

The zero-field Mössbauer spectrum of solid **18** at 80K is given in Figure 3.3.8.1 and is a doublet. A least-square fit of the spectrum yields isomer shift value $\delta = 0.513 \text{ mms}^{-1}$ and quadrupole splitting $\Delta E_Q = 1.912 \text{ mms}^{-1}$. The Mössbauer isomer shift supports the high-spin Fe(III) state for both the irons, although quadrupole splitting is large for high spin iron (III) and are in the range for Fe(III) complexes with μ_2 -oxo bonds.²⁵

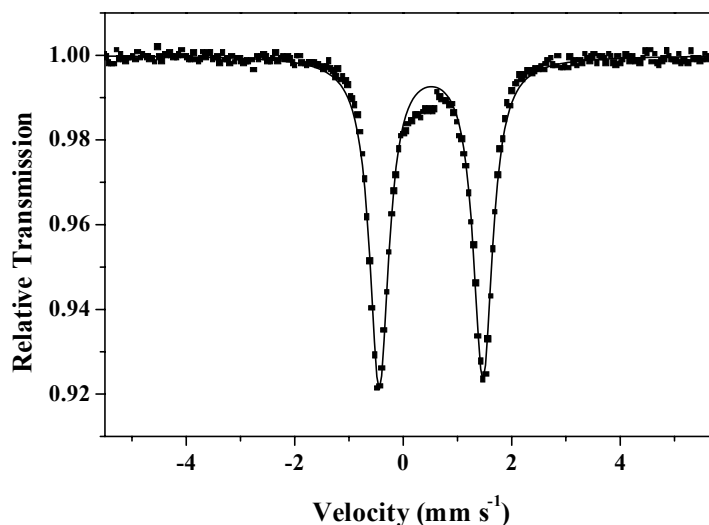


Figure 3.3.8.1 Mössbauer spectrum of **18**.

The asymmetric behaviour and isomer shift value for a typical Fe(III) complex were observed for complexes **19**, **20** and **21**.

3.3.9 REACTIVITY STUDIES WITH THE MANGANESE(III) COMPLEX AS CATALYST: OXIDATION OF ALKENES IN PRESENCE OF H₂O₂

The Mn(III) dimer **13** is very reactive in solution. In the presence of air it forms the Mn(IV) mononuclear complex **15**, whereas addition of base forms the Mn(III) mononuclear complex **14**. The aerial oxidation reaction and the formation of the Mn(IV) monomer **15** can be monitored spectrophotometrically as seen in Figure 3.3.9.1.

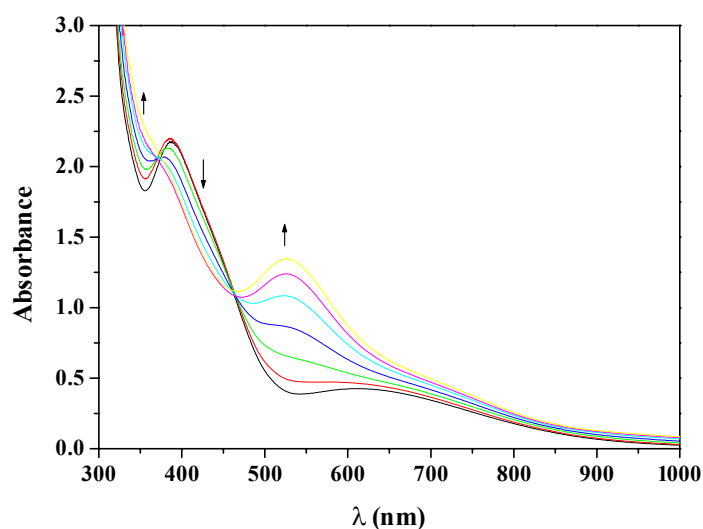
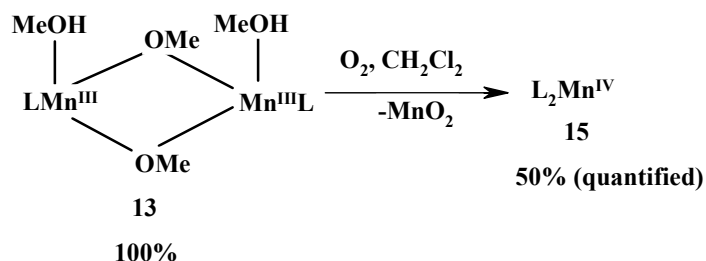


Figure 3.3.9.1 UV-vis spectral change during the aerial oxidation of **13** in CH₂Cl₂ solution at room temperature.

Formation of **15** from **13** (and also **17** from **16**) by aerial oxidation is very interesting, probably proceeding through metal-oxo or peroxo intermediate species. This is again supported by the formation of MnO₂ as one of the products during this transformation.



Scheme 3.3.9.1 Aerial oxidation of **13** to **15** (and **16** to **17**) in CH₂Cl₂ at room temperature.

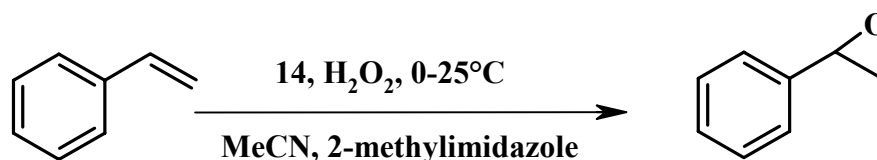
These results and observations led us to study the reactivity of the complex, i.e., the oxidation reaction (epoxidation of alkenes). Unfortunately, air was found not to be an effective oxidant,

but Mn(III)-monomer **14** is an active oxidation catalyst with dihydrogen peroxide as the oxidant.

The catalytic oxidation reactions were carried out under standard conditions: 10^{-5} mol of complex **14** was dissolved with stirring in 10 ml MeCN at 0°C. Subsequently, 10^{-2} mol of substrate, 10^{-3} mol of 2-methylimidazole and 10^{-2} mol of H₂O₂ were added ($t = 0$). After sometime, the solution became yellow and the sample was analysed and quantified using internal standards. The presence of the base is important during the oxidation process.

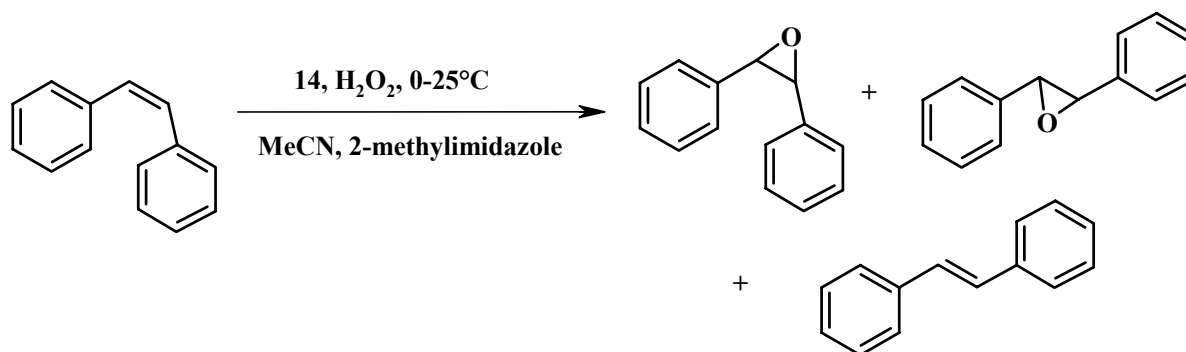
Oxidation of Styrene

The major oxidation product observed in the GC from styrene is styreneoxide. The product was quantified after 4 h of reaction using undecane as an internal standard, giving 69 turnovers. No other products were observed even after a long reaction time.



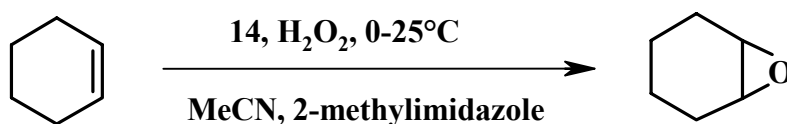
Oxidation of *cis*-Stilbene

In the oxidation reactions of *cis*-stilbene catalyzed by complex **14**, isomerization occurs, resulting in both *cis*- (8 turnovers) and *trans*-epoxides (10 turnovers). *Trans*-stilbene(18 turnovers) is also observed in the reaction mixture.



Oxidation of Cyclohexene

Oxidation of cyclohexene with the Mn-complex **14** gave epoxide as a major product, with simultaneous formation of small amounts of cyclohexenol and cyclohexenone (due to allylic oxidation). The products were quantified using undecane as an internal standard after 6 h. The oxidation of cyclohexene with **14** gave a turnover number of 42 towards the epoxide, and additionally the allylic oxidation products were formed with a turnover number of 11.



This oxidation of alkenes proceeds via peroxide or hydroperoxide mechanism, formed *in situ* during the reaction of the Mn(III) complex and H₂O₂.

3.4 POLYNUCLEAR NICKEL(II) COMPLEXES OF BISPHENOL LIGAND (Ni₄/L^S, Ni₄/L^{Se}, Ni₅/L^N, Ni₆/L^N)

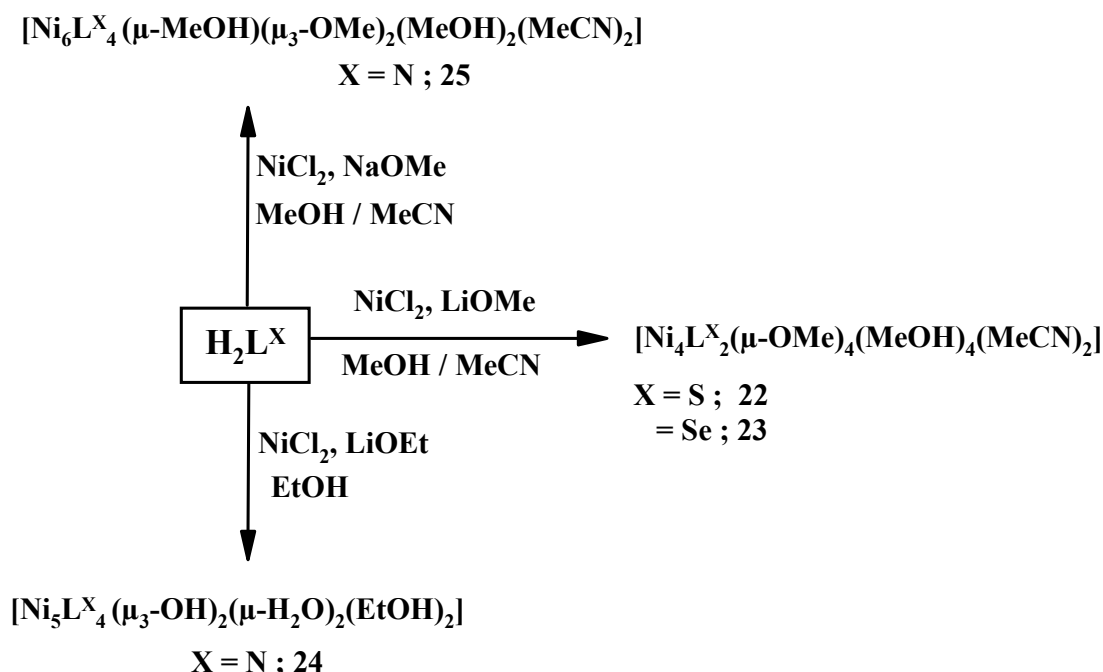
There is currently a lot of interest in "single molecular magnets" (SMMs),²⁶ that is polynuclear cages which display magnetic hysteresis effects which are of a molecular origin. These cages can exhibit quantum tunnelling of magnetization and the interest is because of the technological implications of molecules which display the characteristics of a magnetic memory.²⁷ In addition SMMs present a challenge to synthetic and structural chemists because they are difficult to prepare, often they have unpredictable structures and magnetism. It is now understood that a large spin ground state (S) and a negative axial anisotropy (D) are a prerequisite.

One approach to the latter problem is to target families of high nuclearity cages, where it may be possible to study series of cages and examine systematically how structures relate to magnetism. This part of the chapter deals with the synthesis and structural characterization of a series of polynuclear nickel complexes with heterodonor bisphenol ligand system, and their magnetic behaviour.

3.4.1 SYNTHESIS

Different polynuclear nickel complexes were synthesized according to Scheme 3.4.1.1. The ligands H₂L^S, H₂L^{Se} and H₂L^N react with NiCl₂·6H₂O in different solvent systems in the presence of base yielding a variety of polynuclear Ni(II) complexes having unique structural and magnetic properties. Sulfur and selenium-heterodonor containing ligands react with NiCl₂ in a mixed solvent of MeOH and MeCN in the presence of a methoxide base, affording the tetranuclear Ni₄O₄ cubane complexes **22** and **23**, respectively, with high yield. On the other hand, the ligand H₂L^N reacts with the same Ni(II)-salt in EtOH. Subsequent recrystallization from CH₂Cl₂ and EtOH gives the pentanuclear Ni(II) complex **24**. But when the same reaction is carried out in a dry MeOH and MeCN solvent mixture, a hexanuclear Ni(II) complex **25** is isolated. That a dry solvent is important for the hexanuclearity has been confirmed by

repeated experiments during the standardization of the reaction. All the reactions were carried out at room temperature.



Scheme 3.4.1.1 Synthetic scheme for polynuclear Ni(II) complexes.

3.4.2 INFRARED AND MASS SPECTROSCOPY

The presence of strong peaks for **22** and **23** in the region $2960\text{-}2820\text{ cm}^{-1}$ corresponds to the C-H stretching of *tert*-butyl groups and indicates the complexation of the metal ion with the ligand. A sharp O-H stretching band for the free ligand around 3400 cm^{-1} is replaced by a broad band, also indicating the complexation of the ligand losing its O-H character. Weak bands in the region $2300\text{-}2250\text{ cm}^{-1}$ correspond to the CN stretching of MeCN molecule bonded to the metal ion. Other $\nu(\text{C}=\text{C})$, $\nu(\text{C}-\text{O})$ and $\nu(\text{C}-\text{H})$ bands are also observed in the normal ranges. A sharp band at 1047 cm^{-1} for both **22** and **23** is due to the $\nu(\text{OMe})$ group of the bridging methoxide ligand.

Complexes **24** and **25** show very similar IR spectrum except for the $\nu(\text{CN})$ peak from the bonded MeCN molecule in the region $2300\text{-}2250\text{ cm}^{-1}$ for **25**. Strong peaks in the region $2990\text{-}2850\text{ cm}^{-1}$ are from the $\nu(\text{C}-\text{H})$ of the methyl groups of the ligand. Other $\nu(\text{C}=\text{C})$, $\nu(\text{C}-\text{O})$ and $\nu(\text{C}-\text{H})$ bands are also observed in the expected regions for **24** and **25**.

Mass spectrometry in both the EI and ESI modes does not provide any useful information about the composition of the polynuclear Ni(II) complexes **22-25**. Because of the polynuclear

nature of the complexes, they probably decompose at the applied temperature in EI and ESI mass spectrometry.

3.4.3 X-RAY CRYSTAL STRUCTURE

Complexes **23-25** were structurally characterized by X-ray analysis. Other analyses confirm that the Ni(II) complex of $\text{H}_2\text{L}^{\text{S}}$ **22**, is isostructural with **23**, although without a crystal structure.

3.4.3.1 Molecular structure of $[\text{Ni}_4\text{L}^{\text{Se}}(\mu\text{-OMe})_4(\text{MeOH})_4(\text{MeCN})_2]$ (**23**)

X-ray quality crystals were obtained directly from the reaction mixture of MeCN and MeOH (1:5). The unit cell contains one independent Ni_4O_4 cubic cluster. Relevant bond distances and angles are summarized in Table 3.4.3.1 and the ORTEP diagram is given in Figure 3.4.3.1.

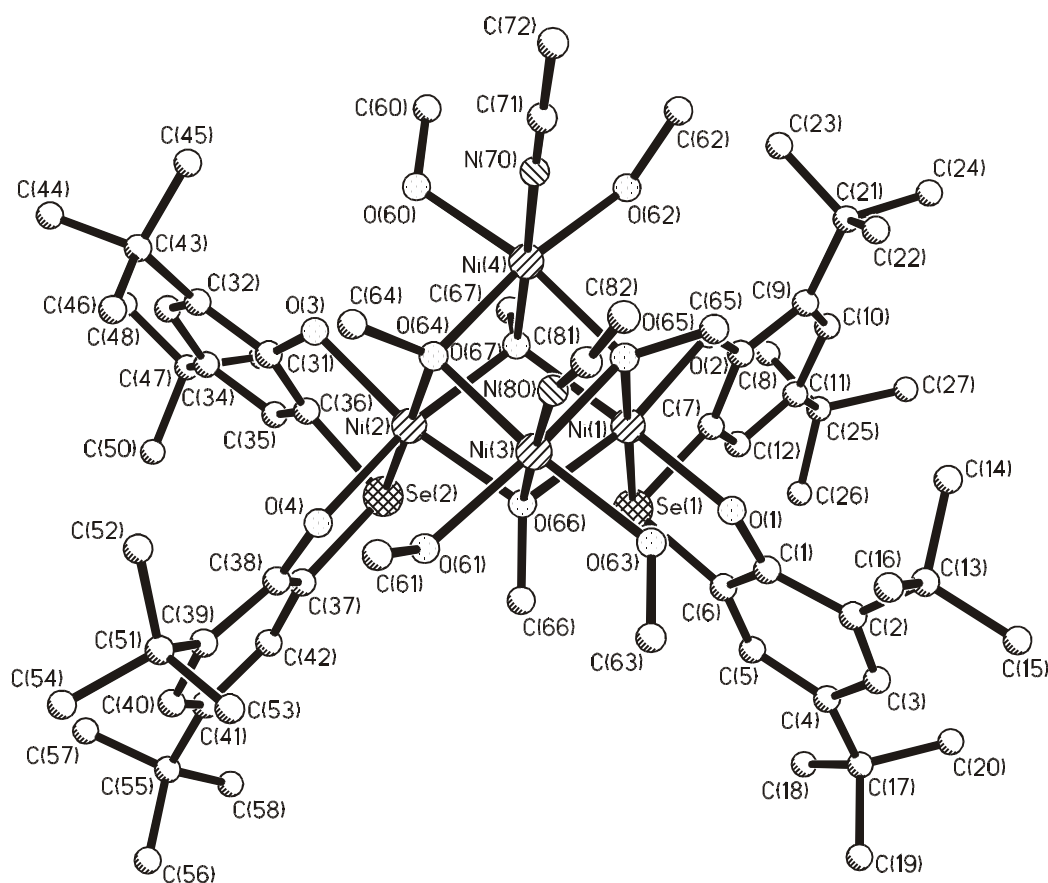


Figure 3.4.3.1 ORTEP and atom labeling scheme for complex **23**.

The structure of each cluster consists of four Ni atoms alternated with four bridging methoxide oxygen atoms at the corners of a cube. All the Ni atoms are in a distorted

octahedral environment. Ni(1) and Ni(2) are coordinated by three methoxide oxygen atoms and by a facially coordinated O,Se,O donor set from the deprotonated ligand $[L^{Se}]^{2-}$ where two phenolate oxygen atoms from the ligand and two oxygen atoms from the methoxide form the equatorial plane. Ni(1)-Se(1), Ni(1)-O(65) and Ni(2)-Se(2), Ni(2)-O(64) are *trans* to each other, forming the axial plane. Both Ni(3) and Ni(4) are coordinated by three methoxide oxygen atoms and two methanol oxygen atoms, where two methanol oxygens and two methoxy oxygens form the equatorial plane. The remaining coordination site is satisfied by one nitrogen atom from the acetonitrile molecule for both Ni atoms, which is *trans* to another oxygen atom of the methoxo group forming the axial plane.

Table 3.4.3.1 Selected bond distances (\AA) and bond angles ($^\circ$) for complex **23**

| | | | |
|-------------------|------------|-------------------|------------|
| Ni(1)-O(1) | 2.039(2) | O(1)-C(1) | 1.329(4) |
| Ni(1)-O(2) | 2.047(2) | O(2)-C(8) | 1.327(4) |
| Ni(1)-O(65) | 2.056(2) | O(3)-C(31) | 1.390(5) |
| Ni(1)-O(67) | 2.073(2) | O(4)-C(38) | 1.332(4) |
| Ni(1)-O(66) | 2.093(2) | Ni(1)-Se(1) | 2.4452(6) |
| Ni(2)-O(3) | 2.054(2) | Ni(3)-O(66) | 2.011(2) |
| Ni(2)-O(4) | 2.060(2) | Ni(3)-O(65) | 2.036(2) |
| Ni(2)-O(64) | 2.058(2) | Ni(3)-O(64) | 2.043(2) |
| Ni(2)-O(66) | 2.074(2) | Ni(3)-O(63) | 2.058(2) |
| Ni(2)-O(67) | 2.082(2) | Ni(3)-O(61) | 2.073(2) |
| Ni(2)-Se(2) | 2.4480(6) | Ni(3)-N(80) | 2.074(3) |
| Ni(4)-O(67) | 2.031(2) | Ni(4)-O(65) | 2.034(2) |
| Ni(4)-O(64) | 2.043(2) | Ni(4)-O(60) | 2.054(3) |
| Ni(4)-O(62) | 2.076(3) | Ni(4)-O(67) | 2.031(2) |
| Ni(4)-N(70) | 2.066(3) | | |
| Ni(1)-O(67)-Ni(2) | 101.45(10) | Ni(4)-O(67)-Ni(2) | 96.15(10) |
| Ni(4)-O(67)-Ni(1) | 95.93(9) | Ni(1)-O(66)-Ni(2) | 101.05(10) |
| Ni(3)-O(66)-Ni(1) | 96.09(9) | Ni(3)-O(66)-Ni(2) | 96.41(10) |
| Ni(3)-O(65)-Ni(1) | 96.48(10) | Ni(4)-O(65)-Ni(1) | 96.40(9) |
| Ni(4)-O(65)-Ni(3) | 97.44(10) | Ni(4)-O(64)-Ni(2) | 96.54(10) |
| Ni(3)-O(64)-Ni(2) | 95.94(10) | Ni(3)-O(64)-Ni(4) | 96.93(10) |
| O(1)-Ni(1)-O(2) | 96.49(10) | O(1)-Ni(1)-O(65) | 90.69(9) |
| O(2)-Ni(1)-O(65) | 95.73(9) | O(1)-Ni(1)-O(67) | 170.61(9) |
| O(2)-Ni(1)-O(67) | 90.35(9) | O(65)-Ni(1)-O(67) | 82.20(9) |
| O(1)-Ni(1)-O(66) | 94.52(9) | O(2)-Ni(1)-O(66) | 168.72(9) |
| O(65)-Ni(1)-O(66) | 81.69(9) | O(67)-Ni(1)-O(66) | 78.44(9) |
| O(1)-Ni(1)-Se(1) | 86.57(7) | O(2)-Ni(1)-Se(1) | 86.90(7) |
| O(65)-Ni(1)-Se(1) | 176.40(7) | O(67)-Ni(1)-Se(1) | 100.26(6) |
| O(66)-Ni(1)-Se(1) | 96.19(6) | | |

| | | | |
|-------------------|------------|-------------------|------------|
| O(3)-Ni(2)-O(64) | 92.07(9) | O(3)-Ni(2)-O(4) | 97.97(10) |
| O(64)-Ni(2)-O(4) | 95.42(9) | O(3)-Ni(2)-O(66) | 169.84(10) |
| O(64)-Ni(2)-O(66) | 82.10(9) | O(4)-Ni(2)-O(66) | 90.88(10) |
| O(3)-Ni(2)-O(67) | 92.34(10) | O(64)-Ni(2)-O(67) | 82.12(9) |
| O(4)-Ni(2)-O(67) | 169.48(10) | O(66)-Ni(2)-O(67) | 78.66(9) |
| O(3)-Ni(2)-Se(2) | 86.51(7) | O(64)-Ni(2)-Se(2) | 177.83(7) |
| O(4)-Ni(2)-Se(2) | 86.40(7) | O(66)-Ni(2)-Se(2) | 99.07(6) |
| O(67)-Ni(2)-Se(2) | 96.30(6) | | |
| O(66)-Ni(3)-O(65) | 84.22(9) | O(66)-Ni(3)-O(64) | 84.06(9) |
| O(65)-Ni(3)-O(64) | 82.71(10) | O(66)-Ni(3)-O(63) | 89.18(10) |
| O(65)-Ni(3)-O(63) | 88.37(10) | O(64)-Ni(3)-O(63) | 169.29(10) |
| O(66)-Ni(3)-O(61) | 88.15(10) | O(65)-Ni(3)-O(61) | 170.29(10) |
| O(64)-Ni(3)-O(61) | 90.55(10) | O(63)-Ni(3)-O(61) | 97.54(11) |
| O(66)-Ni(3)-N(80) | 177.73(11) | O(65)-Ni(3)-N(80) | 93.72(12) |
| O(64)-Ni(3)-N(80) | 96.63(12) | O(63)-Ni(3)-N(80) | 89.82(12) |
| O(61)-Ni(3)-N(80) | 93.99(12) | | |
| O(67)-Ni(4)-O(65) | 83.80(9) | O(67)-Ni(4)-O(64) | 83.75(9) |
| O(65)-Ni(4)-O(64) | 82.75(10) | O(67)-Ni(4)-O(60) | 89.06(10) |
| O(65)-Ni(4)-O(60) | 170.10(10) | O(64)-Ni(4)-O(60) | 89.69(10) |
| O(67)-Ni(4)-O(62) | 88.87(10) | O(65)-Ni(4)-O(62) | 90.73(10) |
| O(64)-Ni(4)-O(62) | 170.63(10) | O(60)-Ni(4)-O(62) | 95.99(11) |
| O(62)-Ni(4)-N(70) | 92.73(12) | O(67)-Ni(4)-N(70) | 178.40(11) |
| O(65)-Ni(4)-N(70) | 96.09(11) | O(64)-Ni(4)-N(70) | 94.65(11) |
| O(60)-Ni(4)-N(70) | 90.86(12) | | |

The average Ni-O (phenolate) bond distance is 2.045 Å, and the Ni-O(methoxide) bond distance is 2.075 Å. The bond distances differ depending upon the relevant Ni-O-Ni bond angles. The Ni-O-Ni angles in the cluster vary from 95-101°, making the [Ni₄O₄] cluster slightly distorted towards lower symmetry. This is evident from the bond angles Ni(1)-O(66)-Ni(2) and Ni(1)-O(67)-Ni(2) [101.05 and 101.45°] whereas other Ni-O-Ni bond angles are in the range of 95-96°. All phenyl rings of the ligand are planar and retain their aromaticity after complexation. The charge balance requires four nickel in +2 oxidation state, which is in accord with magnetic measurements.

3.4.3.2 Molecular structure of [Ni₅L^N₄ (μ₃-OH)₂(μ-H₂O)₂(EtOH)₂] (24)

The ORTEP diagram with atom labeling scheme is shown in Figure 3.4.3.2 and selected bond parameters in Table 3.4.3.2.

arm, the six-coordinated nickel center is coordinated by two oxygens and one nitrogen from the ligand, one μ_3 -hydroxide oxygen, one μ_2 -H₂O bridging oxygen bridged with central nickel and the other oxygen from the EtOH molecule where the ligand is bonded in meridional manner making the coordination sphere a distorted octahedral. This makes the central nickel [Ni(3)] to be in a NiO₆ coordination environment. Bridged H₂O and bonded EtOH molecules further stabilize the cluster through hydrogen-bonds. H₂O is hydrogen bonded to O(1) and O(41). Hydrogens from EtOH are also hydrogen-bonded to O(35) and O(61) in two side arms.

Table 3.4.3.2 Selected bond distances (Å) and bond angles (deg) for complex 24

| | | | |
|---------------------|------------|---------------------|------------|
| Ni(1)-O(1) | 1.999(3) | Ni(1)-O(15) | 2.047(3) |
| Ni(1)-O(300) | 2.081(3) | Ni(1)-O(100) | 2.096(3) |
| Ni(1)-N(8) | 2.083(4) | Ni(1)-O(101) | 2.159(3) |
| Ni(2)-O(35) | 1.980(3) | Ni(2)-O(100) | 2.024(3) |
| Ni(2)-O(15) | 2.031(3) | Ni(2)-N(28) | 2.100(4) |
| Ni(2)-O(21) | 2.044(3) | Ni(3)-O(200) | 2.011(3) |
| Ni(3)-O(100) | 2.009(3) | Ni(3)-O(75) | 2.097(3) |
| Ni(3)-O(21) | 2.102(3) | Ni(3)-O(201) | 2.126(3) |
| Ni(3)-O(101) | 2.128(3) | Ni(4)-O(55) | 2.059(3) |
| Ni(4)-O(41) | 1.999(3) | Ni(4)-O(400) | 2.069(4) |
| Ni(4)-N(48) | 2.087(4) | Ni(4)-O(200) | 2.085(3) |
| Ni(4)-O(201) | 2.187(3) | Ni(5)-O(61) | 1.983(3) |
| Ni(5)-O(55) | 2.046(3) | Ni(5)-O(200) | 2.030(3) |
| Ni(5)-O(75) | 2.053(3) | Ni(5)-N(68) | 2.109(4) |
| C(1)-O(1) | 1.353(6) | C(15)-O(15) | 1.348(6) |
| C(21)-O(21) | 1.346(6) | C(35)-O(35) | 1.353(6) |
| O(1)-Ni(1)-O(15) | 167.33(14) | O(1)-Ni(1)-O(300) | 97.52(13) |
| O(15)-Ni(1)-O(300) | 91.05(13) | O(1)-Ni(1)-N(8) | 92.34(15) |
| O(15)-Ni(1)-N(8) | 96.20(14) | O(300)-Ni(1)-N(8) | 95.07(14) |
| O(1)-Ni(1)-O(100) | 89.11(13) | O(15)-Ni(1)-O(100) | 81.73(12) |
| O(300)-Ni(1)-O(100) | 88.70(13) | O(100)-Ni(1)-N(8) | 175.75(14) |
| O(1)-Ni(1)-O(101) | 92.62(12) | O(15)-Ni(1)-O(101) | 77.10(12) |
| O(300)-Ni(1)-O(101) | 164.01(13) | N(8)-Ni(1)-O(101) | 96.84(14) |
| O(100)-Ni(1)-O(101) | 79.10(12) | O(35)-Ni(2)-O(15) | 89.06(13) |
| O(35)-Ni(2)-O(100) | 96.63(15) | O(35)-Ni(2)-O(21) | 172.21(14) |
| O(100)-Ni(2)-O(15) | 83.91(13) | O(15)-Ni(2)-O(21) | 89.22(13) |
| O(100)-Ni(2)-O(21) | 78.64(12) | O(100)-Ni(2)-N(28) | 112.41(14) |
| O(35)-Ni(2)-N(28) | 91.50(14) | O(21)-Ni(2)-N(28) | 92.29(14) |
| O(15)-Ni(2)-N(28) | 163.59(14) | O(200)-Ni(3)-O(75) | 77.70(13) |
| O(200)-Ni(3)-O(100) | 177.78(14) | O(200)-Ni(3)-O(21) | 103.18(13) |
| O(100)-Ni(3)-O(75) | 103.80(13) | O(75)-Ni(3)-O(21) | 117.96(13) |
| O(100)-Ni(3)-O(21) | 77.62(13) | O(100)-Ni(3)-O(201) | 96.99(13) |
| O(200)-Ni(3)-O(201) | 81.17(13) | O(21)-Ni(3)-O(201) | 159.34(13) |
| O(75)-Ni(3)-O(201) | 82.63(13) | O(100)-Ni(3)-O(101) | 81.81(13) |
| O(200)-Ni(3)-O(101) | 96.27(13) | | |

| | | | |
|---------------------|------------|--------------------|------------|
| O(75)-Ni(3)-O(101) | 161.52(13) | O(21)-Ni(3)-O(101) | 80.32(12) |
| O(201)-Ni(3)-O(101) | 79.21(13) | | |
| O(55)-Ni(4)-O(41) | 166.40(13) | O(55)-Ni(4)-O(400) | 93.35(14) |
| O(41)-Ni(4)-O(400) | 96.84(14) | O(55)-Ni(4)-N(48) | 95.41(16) |
| O(41)-Ni(4)-N(48) | 92.99(16) | O(400)-Ni(4)-N(48) | 93.11(15) |
| O(55)-Ni(4)-O(200) | 82.01(13) | O(41)-Ni(4)-O(200) | 89.15(13) |
| O(400)-Ni(4)-O(200) | 89.24(14) | O(200)-Ni(4)-N(48) | 176.61(14) |
| O(55)-Ni(4)-O(201) | 76.08(13) | O(41)-Ni(4)-O(201) | 92.13(13) |
| O(400)-Ni(4)-O(201) | 164.92(15) | N(48)-Ni(4)-O(201) | 98.52(14) |
| O(200)-Ni(4)-O(201) | 78.77(13) | | |
| O(61)-Ni(5)-O(55) | 88.17(15) | O(61)-Ni(5)-O(200) | 92.64(14) |
| O(55)-Ni(5)-O(200) | 83.69(14) | O(61)-Ni(5)-O(75) | 170.92(15) |
| O(55)-Ni(5)-O(75) | 90.77(13) | O(200)-Ni(5)-O(75) | 78.29(13) |
| O(61)-Ni(5)-N(68) | 90.97(16) | O(55)-Ni(5)-N(68) | 162.04(15) |
| O(200)-Ni(5)-N(68) | 114.27(15) | O(75)-Ni(5)-N(68) | 92.80(15) |
| Ni(1)-O(15)-Ni(2) | 96.78(13) | Ni(2)-O(21)-Ni(3) | 99.91(13) |
| Ni(4)-O(55)-Ni(5) | 95.99(14) | Ni(5)-O(75)-Ni(3) | 100.09(14) |
| Ni(3)-O(100)-Ni(2) | 103.83(14) | Ni(3)-O(100)-Ni(1) | 100.30(13) |
| Ni(2)-O(100)-Ni(1) | 95.43(13) | Ni(3)-O(200)-Ni(5) | 103.88(14) |
| Ni(3)-O(200)-Ni(4) | 100.99(15) | Ni(5)-O(200)-Ni(4) | 95.67(13) |
| Ni(3)-O(101)-Ni(1) | 94.66(13) | Ni(3)-O(201)-Ni(4) | 94.22(13) |

3.4.3.3 Molecular structure of $[\text{Ni}_6\text{L}^{\text{N}}_4(\mu\text{-MeOH})(\mu_3\text{-OMe})_2(\text{MeOH})_2(\text{MeCN})_2]$ (25)

This hexanuclear Ni(II) complex was synthesized by the same method as in pentanuclear complex, but in presence of MeCN as an additional solvent. The acetonitrile solvent used during synthesis plays an important role in stabilizing such cluster. The discrete molecule contains a Ni_6 unit in the cluster as is evidenced from the ORTEP diagram shown in Figure 3.4.3.3. Selected bond parameters are given in Table 3.4.3.3.

The Ni_6 cluster is related by a crystallographic pseudo-two-fold axis of symmetry and structurally considered to be a face-shared distorted dicubane where one of the corners of each cubane is missing. Two nickel atoms Ni(1) and Ni(1)# are five-coordinated, while the other nickel centers are six-coordinated. Five-coordinated nickel centers possess square-pyramidal geometry whereas the six-coordinated nickel centers are in a distorted octahedral environment. The ligand coordinates through the O, N, O donor atoms, making the equatorial plane along with the phenolate oxygen donor from another ligand bridging Ni(1) and Ni(3)#1, while methoxide oxygen forms a Ni-O bond perpendicular to the equatorial plane. Six-

coordinated Ni(2) is octahedrally surrounded by five oxygen atoms from a μ -OMe and a MeOH, and a nitrogen from a MeCN molecule. The four oxygens O(10), O(60), O(70) and O(1) form the equatorial plane, and Ni(2)-N(50) and Ni(2)-O(10)#1 forming the axial plane are *trans* to each other. On the other side, Ni(3) is coordinated with the ligand O, N, O donor set, one MeOH oxygen and two methoxy oxygens, satisfying the coordination sphere.

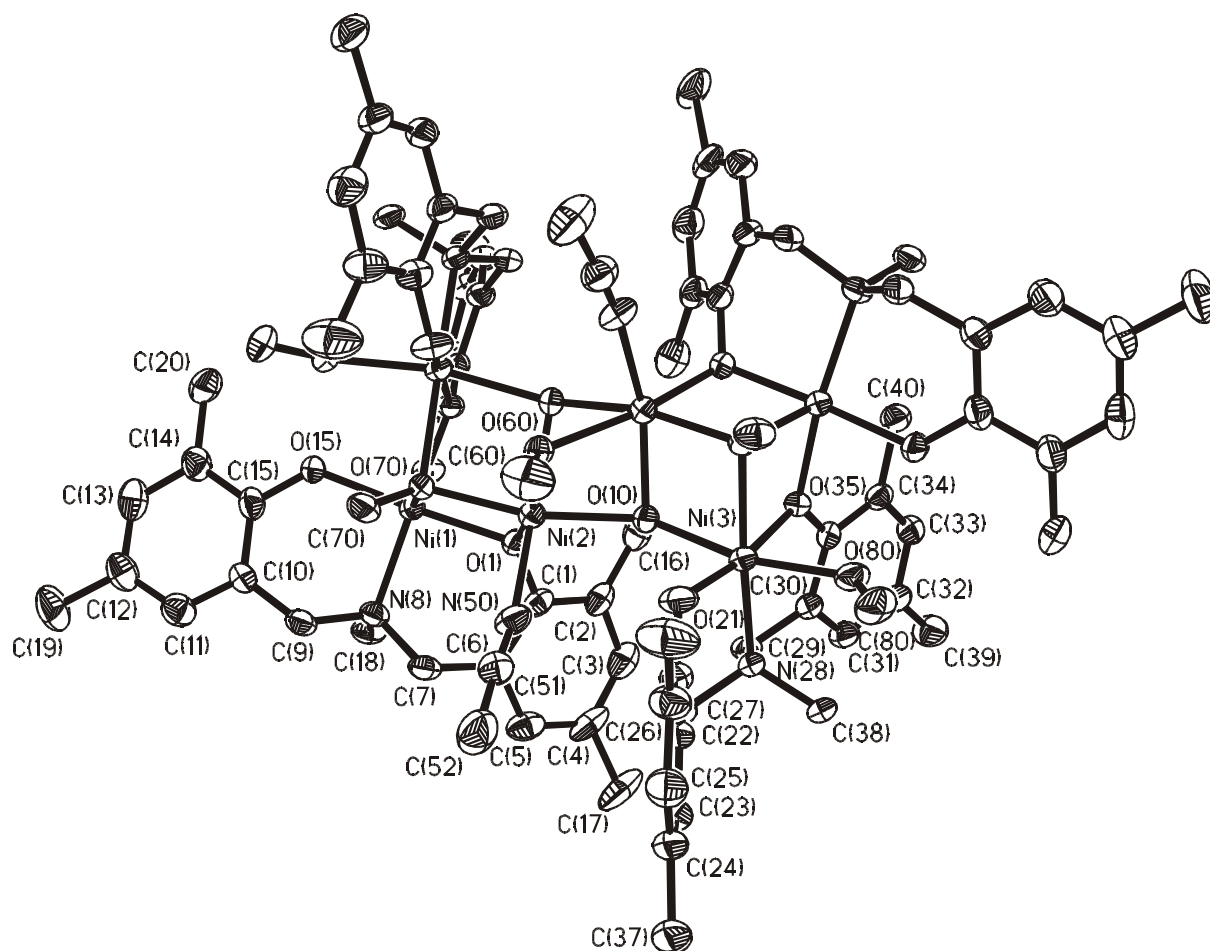


Figure 3.4.3.3 ORTEP diagram and atom labeling scheme for complex **25**.

Table 3.4.3.3 Selected bond distances (\AA) and bond angles ($^\circ$) for complex **25**

| | | | |
|---------------|----------|---------------|----------|
| Ni(1)-O(15) | 1.981(4) | Ni(1)-O(1) | 2.017(4) |
| Ni(1)-O(35)#1 | 2.030(4) | Ni(1)-O(70) | 2.031(4) |
| Ni(1)-N(8) | 2.121(5) | Ni(2)-O(10) | 2.028(4) |
| Ni(2)-O(70) | 2.031(4) | Ni(2)-O(1) | 2.054(4) |
| Ni(2)-O(10)#1 | 2.073(4) | Ni(2)-N(50) | 2.086(6) |
| Ni(2)-O(60)#1 | 2.224(9) | Ni(2)-O(60) | 2.233(8) |
| Ni(3)-O(21) | 1.989(4) | Ni(3)-O(35) | 2.038(4) |
| Ni(3)-O(80) | 2.075(5) | Ni(3)-O(10) | 2.097(4) |
| Ni(3)-N(28) | 2.101(5) | Ni(3)-O(70)#1 | 2.140(4) |

| | | | |
|---------------------|------------|---------------------|------------|
| C(1)-O(1) | 1.363(7) | C(15)-O(15) | 1.336(7) |
| C(21)-O(21) | 1.343(7) | C(35)-O(35) | 1.332(7) |
| O(15)-Ni(1)-O(1) | 177.20(16) | O(15)-Ni(1)-O(35)#1 | 88.84(15) |
| O(1)-Ni(1)-O(35)#1 | 88.39(15) | O(15)-Ni(1)-O(70) | 97.86(17) |
| O(1)-Ni(1)-O(70) | 81.38(16) | O(35)#1-Ni(1)-O(70) | 83.45(15) |
| O(15)-Ni(1)-N(8) | 90.54(18) | O(1)-Ni(1)-N(8) | 92.25(17) |
| O(35)#1-Ni(1)-N(8) | 165.41(18) | O(70)-Ni(1)-N(8) | 111.06(18) |
| O(10)-Ni(2)-O(70) | 167.39(16) | O(10)-Ni(2)-O(1) | 100.19(16) |
| O(70)-Ni(2)-O(1) | 80.50(15) | O(10)-Ni(2)-O(10)#1 | 82.67(18) |
| O(70)-Ni(2)-O(10)#1 | 84.75(15) | O(1)-Ni(2)-O(10)#1 | 96.87(17) |
| O(10)-Ni(2)-N(50) | 96.33(19) | O(70)-Ni(2)-N(50) | 95.86(19) |
| O(1)-Ni(2)-N(50) | 101.39(19) | O(10)#1-Ni(2)-N(50) | 161.6(2) |
| O(10)-Ni(2)-O(60) | 86.0(2) | O(70)-Ni(2)-O(60) | 90.3(2) |
| O(1)-Ni(2)-O(60) | 164.1(2) | O(10)#1-Ni(2)-O(60) | 69.2(2) |
| N(50)-Ni(2)-O(60) | 92.4(3) | | |
| O(21)-Ni(3)-O(35) | 171.31(16) | O(21)-Ni(3)-O(80) | 96.2(2) |
| O(35)-Ni(3)-O(80) | 87.87(18) | O(21)-Ni(3)-O(10) | 91.09(18) |
| O(35)-Ni(3)-O(10) | 83.68(16) | O(80)-Ni(3)-O(10) | 168.10(17) |
| O(21)-Ni(3)-N(28) | 94.36(18) | O(35)-Ni(3)-N(28) | 93.27(18) |
| O(80)-Ni(3)-N(28) | 90.36(18) | O(21)-Ni(3)-O(70)#1 | 91.79(16) |
| O(35)-Ni(3)-O(70)#1 | 80.60(15) | O(80)-Ni(3)-O(70)#1 | 88.86(16) |
| O(10)-Ni(3)-O(70)#1 | 81.52(15) | N(28)-Ni(3)-O(70)#1 | 173.85(18) |
| N(28)-Ni(3)-O(10) | 98.46(17) | | |
| Ni(1)-O(70)-Ni(3)#1 | 94.93(16) | Ni(2)-O(70)-Ni(3)#1 | 96.80(15) |
| Ni(2)-O(70)-Ni(1) | 99.07(17) | Ni(2)#1-O(60)-Ni(2) | 78.6(3) |
| Ni(1)#1-O(35)-Ni(3) | 98.20(17) | Ni(1)-O(1)-Ni(2) | 98.76(17) |
| Ni(2)#1-O(10)-Ni(3) | 96.85(17) | Ni(2)-O(10)-Ni(3) | 144.5(2) |
| Ni(2)-O(10)-Ni(2)#1 | 86.98(16) | | |

3.4.4 MAGNETISM

Tetranuclear Ni(II) complexes **22** and **23**

The investigation of the magnetic properties of all nickel complexes has been performed to establish the spin ground states of the clusters. The observed magnetic moments rise to a maximum of $7.54\mu_B$ (at 20 K) and $7.15\mu_B$ (at 20 K) for **22** and **23**, respectively but starts to decrease below 20 K. This maximum value may be compared with the spin-only

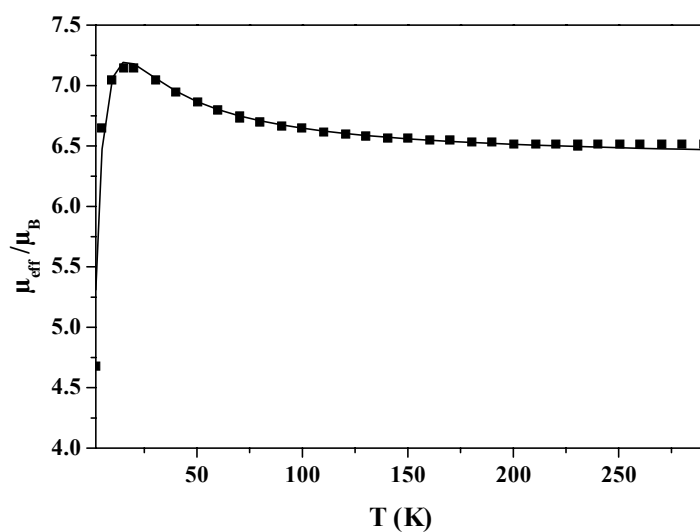


Figure 3.4.4.1a Magnetic measurements for complex **23**.

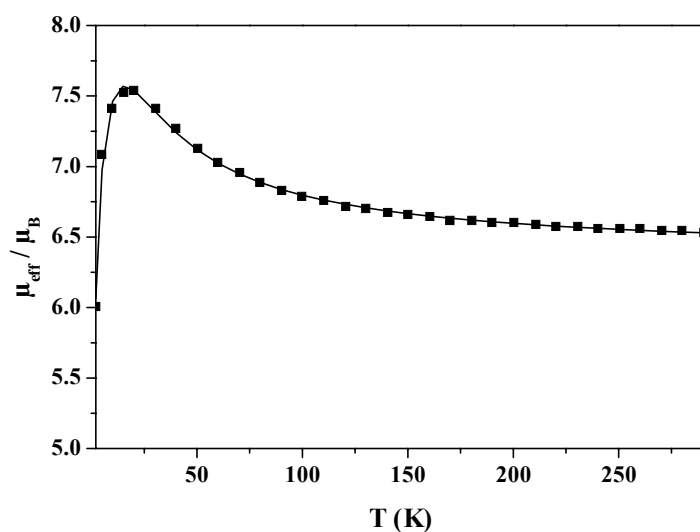


Figure 3.4.4.1b Magnetic measurements for complex **22**.

value of $8.94\mu_{\text{B}}$ calculated for an $S = 4$ ground state expected for four ferromagnetically coupled high-spin Ni(II) ions. The maximum μ_{eff} values do imply an overall ferromagnetic interaction within the cubane. The higher μ_{eff} value at 20K for **22** does indicate a stronger ferromagnetic coupling inside the cubane core than that in **23**. The deviation from T_d symmetry to a lower symmetry of the cubane core observed in the crystal structure for **23** supports the latter. Complexes **22** and **23** show two types of interactions within the cluster, but

the dominant interaction is ferromagnetic in nature, resulting in the $S = 4$ ground state as is evidenced from the μ_{eff} vs T plot in Figures 3.4.4.1a and 3.4.4.1b.

The structural and magnetochemical properties of several $[\text{Ni}_4(\text{OR})_4]$ ($R = \text{H}$, alkyl) cubanes have been reported;²⁸ in most cases the effective symmetry T_d or D_{2d} within the cubane core was used as the symmetry of the magnetic model. The magnetic behaviour of **22** and **23** contrasts with this observation because of a significant deviation towards lower symmetry. From this geometry the nature of magnetic exchange interaction was considered. The following scheme (Figure 3.4.4.2) was used to fit the magnetic data for both **22** and **23**.

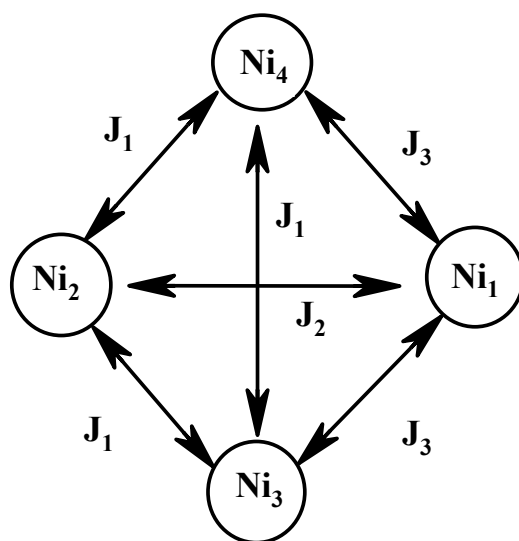


Figure 3.4.4.2 Exchange interactions in Ni_4O_4 cluster of **22** and **23**.

The experimental magnetic data have been fitted using the Heisenberg- Hamiltonian:

$$\hat{H} = -2J_1(\hat{S}_2 \cdot \hat{S}_3 + \hat{S}_3 \cdot \hat{S}_4 + \hat{S}_2 \cdot \hat{S}_4) - 2J_2 \hat{S}_1 \cdot \hat{S}_2 - 2J_3 (\hat{S}_1 \cdot \hat{S}_4 + \hat{S}_1 \cdot \hat{S}_3)$$

A very good fit can be obtained by using this model, the best set of parameters being $J_1 = +1.05 \text{ cm}^{-1}$, $J_2 = -4.1 \text{ cm}^{-1}$, $J_3 = +5.5 \text{ cm}^{-1}$ and $g = 2.25$ for **23** and $J_1 = +2.39 \text{ cm}^{-1}$, $J_2 = -5.77 \text{ cm}^{-1}$, $J_3 = +6.9 \text{ cm}^{-1}$ and $g = 2.272$ for **22**. No ZFS parameter D , TIP or PI was used to fit the magnetic data. The ground state of $S > 3$ for **22** and **23** is confirmed from the magnetization curve at 7T (Figure 3.4.4.3). Noteworthy is a downward tendency of magnetization at low temperatures presumably due to the Zeeman-splitting of the upper states.

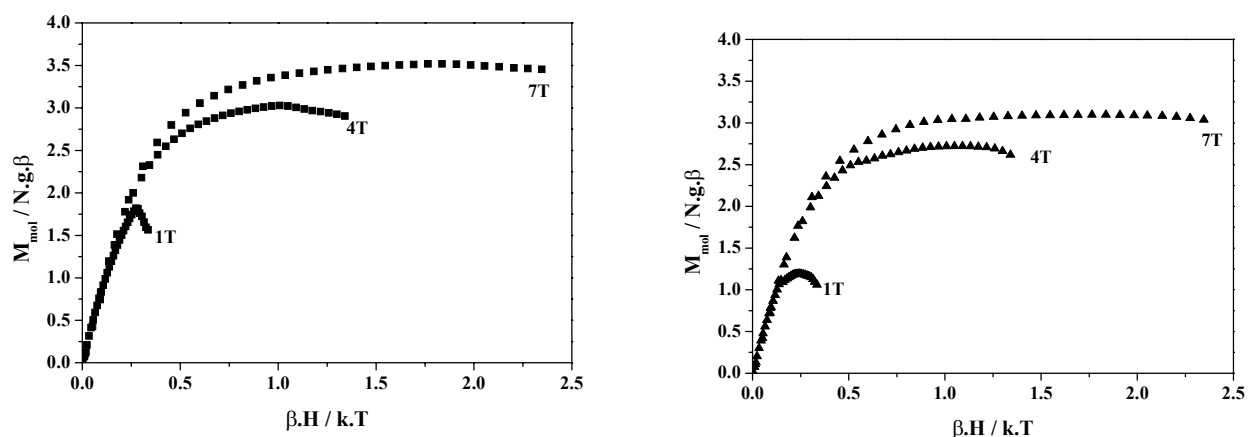


Figure 3.4.4.3 Magnetization curves for complexes **22**(left) and **23**(right)

The most important parameter described in the literature for the magnetostructural correlation of the Ni_4O_4 cubane cores is the Ni-O-Ni angle. A ferromagnetic Ni-Ni interaction is observed when the angle is very close to orthogonality. On the other hand, antiferromagnetic interactions have been observed for the Ni-O-Ni angles larger than 99° . The parameter set obtained from the fit is in accord with the magnetostructural correlation described in Table 3.4.4.1 and Figure 3.4.4.5, where the magnetic interactions (J) are represented as a function of averaged Ni-O-Ni angles for different Ni_4O_4 cubane cores described in the literature and this work. Figure 3.4.4.4 exhibits a schematic representation of the exchange interactions operative in a six-coordinated Ni(II) system.

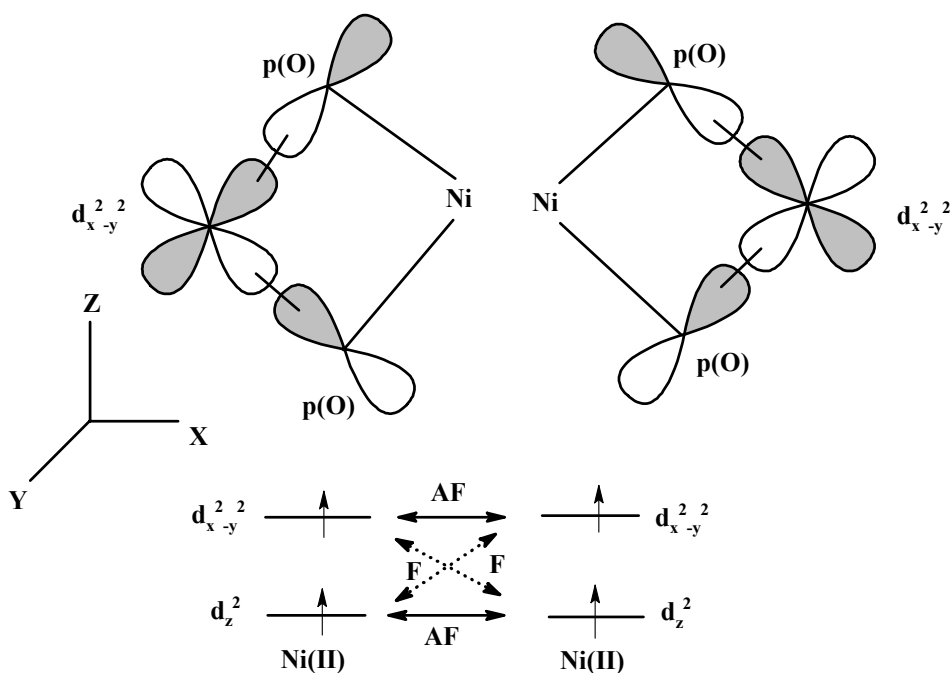


Figure 3.4.4.4 Interaction of Ni(II) ions through Ni-O-Ni.

Table 3.4.4.1 *J* as a function of the Ni-O-Ni angles for the $[Ni_4(\mu_3-OR)_4]$ cubanes

| Complex | Ni-O-Ni _{av} (deg) | <i>J</i> (cm ⁻¹) | Reference |
|---|-----------------------------|------------------------------|-----------|
| $[Ni_4(\mu_3-OMe)_4 (sal)_4(EtOH)_4]$ | 97.73 | 7.46 | 28a,b |
| $[Ni_4(\mu_3-OH)_4 (chta)_4(NO_3)_4]$ | 99.0 | -0.57 | 28c,d |
| $[Ni_4(\mu_3-OMe)_4 (TMB)_4(\mu-O_2CMe)_4]$ | 93.0 | 17.5 | 28f |
| | 100.9 | -9.1 | |
| $[Ni_4(\mu_3-OH)_4 (tzdt)_4(py)_4]$ | 95.89 | 17.5 | 28h |
| | 103.2 | -22.0 | |
| $[Ni_4(\mu_3-OMe)_4 (dbm)_4(MeOH)_4]$ | 96.7 | 2.2 | 28k |
| | 99.6 | -3.4 | |
| $[Ni_4(\mu_3-OH)_2 (pypentO)(pym)(\mu-Oac)_2(NCS)_2(OH_2)]$ | 89.9 | 15.0 | 28o |
| | 92.9 | 6.7 | |
| | 100.5 | -3.09 | |
| $[Ni_4(OMe)_2 (LH)_2(OAc)_2(MeOH)_2]$ | 95.94 | 8.0 | 28p |
| | 97.85 | 1.0 | |
| | 99.0 | -3.8 | |
| $[Ni_4(\mu_3-OMe)_4 (L^{Se})_2(MeOH)_2(MeCN)_2]$ | 96.17 | 5.50 | this work |
| | 97.17 | 1.05 | this work |
| | 101.25 | -4.1 | this work |

salH = salicylaldehyde; chta = r-1-c-3-c-5 triaminocyclohexane; TMB=2,5-dimethyl-2,5-disisocyanoheptane; dzdt = 1,3-thiazolidine-2-thione; dbmH = dibenzoylmethane; py = pyridine; pypentO = 1,5-bis[(2-pyridylmethyl)amino]-3-pentanolate: pym = 2-pyridylmethanolate.

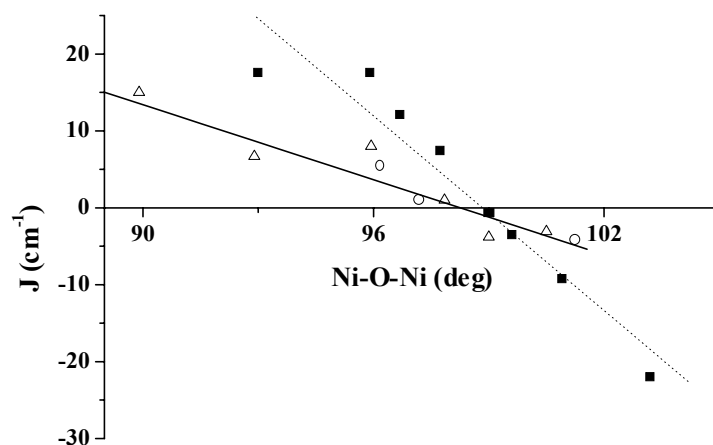


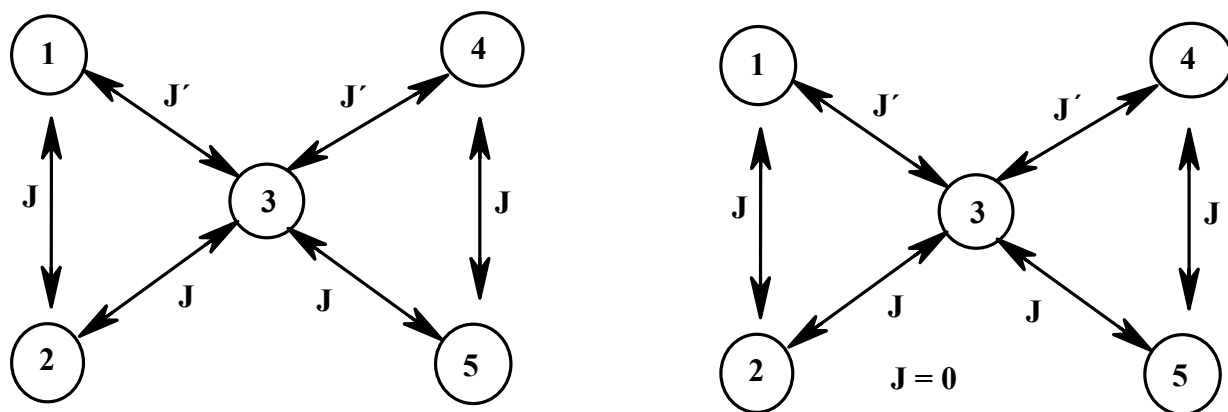
Figure 3.4.4.5 Exchange interaction for the nickel cubane core as a function of Ni-O-Ni angle (closed squares and open triangles are from the literature, and open circles are from this work. The solid line represents the best fit with the data for low symmetry cubanes and the dotted line represents the fit with the data for other reported symmetric cubanes).

A linear dependence between J and the Ni-O-Ni angle is observed and this work perfectly matches with the data for a low symmetry complex.²⁸⁰ The boundary point of Ni-O-Ni = 98.3° is seen from the correlation diagram, above which the complex shows antiferromagnetic interactions.

Pentanuclear Ni(II) complex **24**

The magnetic properties of the pentanuclear complex **24** are very interesting. A plot of μ_{eff} vs T (Figure 3.4.4.7) reveals an overall ferromagnetic coupling within the Ni₅ cluster, shows a maximum μ_{eff} value of 8.52 μ_{B} at 15 K and slightly decreases below this temperature. This maximum value is smaller than the spin-only value for the $S = 5$ state.

This maximum magnetic moment value at 15 K clearly shows that both penta- and hexa-coordinated Ni(II) present in **24** are paramagnetic with a high spin ground state. The data could not be fitted taking all six J values equal. Different Ni-O-Ni bond angles prevailing in **24** were instrumental to construct two different models were considered to fit the magnetic data for the pentanuclear complex as shown in Figure 3.4.4.6.



Model 1

Model 2

Figure 3.4.4.6 Exchange interaction models in Ni_5 cluster of **24**.

A good fit of the data obtained by considering the coupling model 1 is compared with that obtained from model 2 in Figure 3.4.4.7.

Thus using model 1 and the spin-Hamiltonian

$$\hat{H} = -2J(\hat{S}_1 \cdot \hat{S}_2 + \hat{S}_2 \cdot \hat{S}_3 + \hat{S}_4 \cdot \hat{S}_5 + \hat{S}_3 \cdot \hat{S}_5) - 2J'(\hat{S}_1 \cdot \hat{S}_3 + \hat{S}_3 \cdot \hat{S}_4)$$

the magnetic data could be fitted and the values $J' = +6.5 \text{ cm}^{-1}$, $J = -0.24 \text{ cm}^{-1}$, $g = 2.32$ were obtained. By considering $J = 0$ (fixed) in model 2, the good quality of the fit could not be reproduced and is shown in Figure 3.4.4.7 (right). Thus $J = -0.24 \text{ cm}^{-1}$ has to be considered for the fit. No Zero-field splitting parameter D , TIP or paramagnetic impurity (PI) was used to fit the magnetic data.

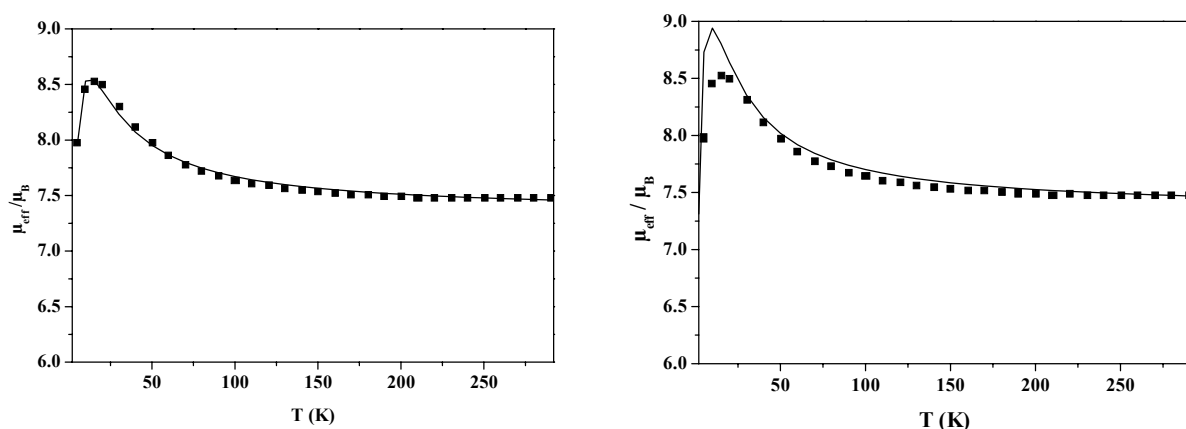


Figure 3.4.4.7 Plot of μ_{eff} vs temperature for complex **24**. The solid line was calculated using model 1 (left) and model 2 (right).

The spin ladder calculated by the evaluated J-value from the fit using model 1 shows clearly that the energy separation between the different spin states is very small, yielding a mixed ground state of $S = 5$ and $S = 4$ for the Ni_5 -cluster.

This is also observed in the magnetization measurements at 1T, 4T and 7T, as seen in Figure 3.4.4.8. The saturation behaviour observed at 7 T shows that the ground state is $S_t > 4$.

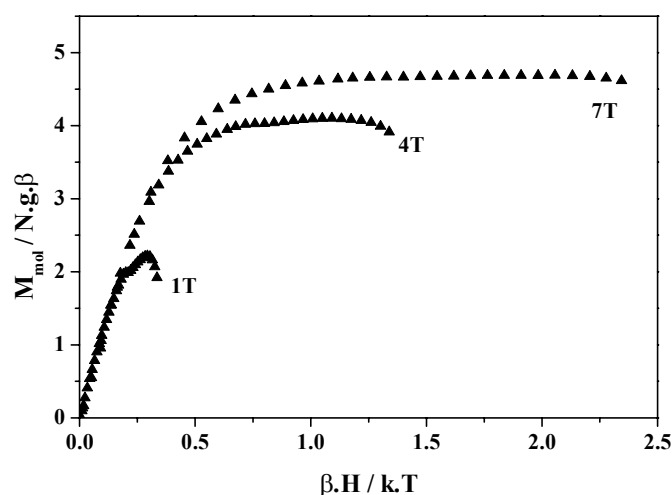


Figure 3.4.4.8 Magnetization curve for complex **24**.

Hexanuclear Ni(II) complex **25**

The plot of μ_{eff} vs T (Figure 3.4.4.10) for complex **25** reveals a dominant antiferromagnetic interaction within the cluster. There are two types of Ni(II) centers present in the cluster. But μ_{eff} value of $7.65\mu_B$ at 290K clearly shows that all Ni(II) centers are paramagnetic and coupled antiferromagnetically with $\mu_{\text{eff}} = 2.98\mu_B$ at 2K.

The following model was used to fit the experimental magnetic data:

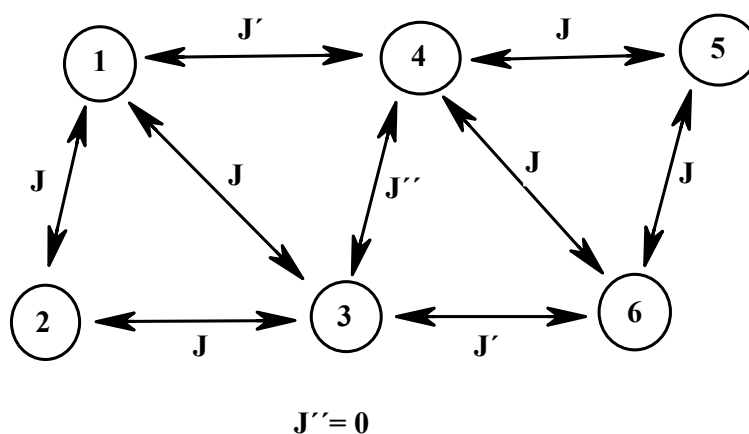


Figure 3.4.4.9 Magnetic exchange interactions in Ni_6 cluster of **25**.

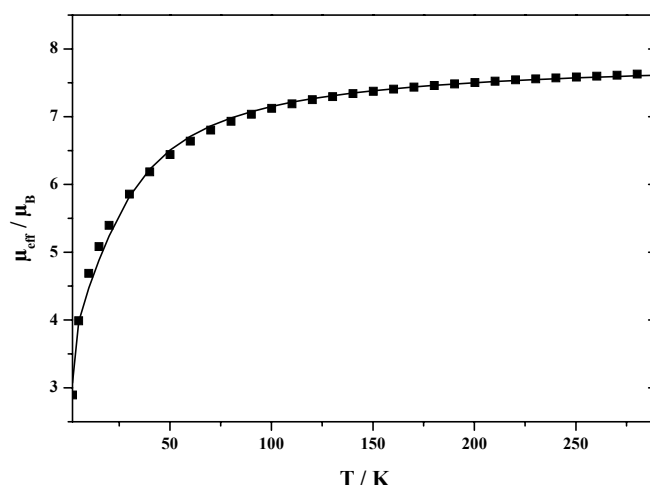


Figure 3.4.4.10 Magnetic measurements for complex **25**.

Using the spin-Hamiltonian,

$$\hat{H} = -2J(\hat{S}_1 \cdot \hat{S}_2 + \hat{S}_2 \cdot \hat{S}_3 + \hat{S}_1 \cdot \hat{S}_3 + \hat{S}_4 \cdot \hat{S}_5 + \hat{S}_5 \cdot \hat{S}_6 + \hat{S}_4 \cdot \hat{S}_6) - 2J'(\hat{S}_1 \cdot \hat{S}_4 + \hat{S}_3 \cdot \hat{S}_6)$$

the fit parameters were found to be $J = -1.79 \text{ cm}^{-1}$, $J' = -9.0 \text{ cm}^{-1}$ and $g = 2.27$.

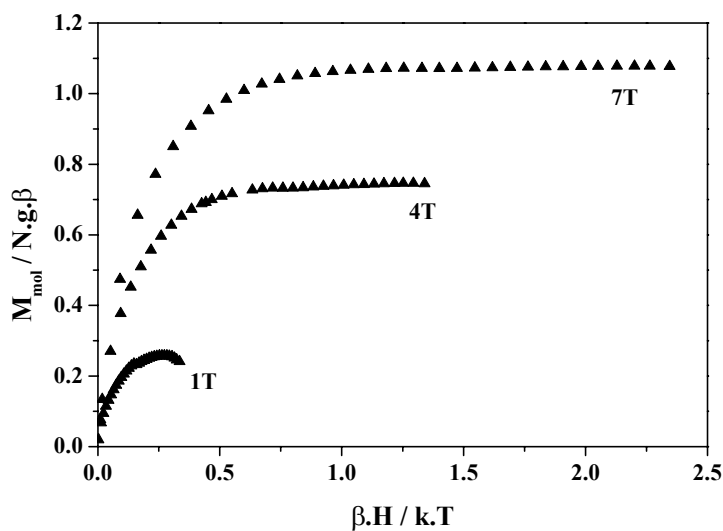


Figure 3.4.4.11 Magnetization curve for complex **25**.

The magnetization curves at 1, 4 and 7 T show (Figure 3.4.4.11) clearly that complex **25** does not possess a well-separated ground state of $S_t = 0$, as is expected for an antiferromagnetically coupled hexanuclear Ni(II) complex, but the excited state of $S_t = 1$ is energetically very close to the ground state.

References

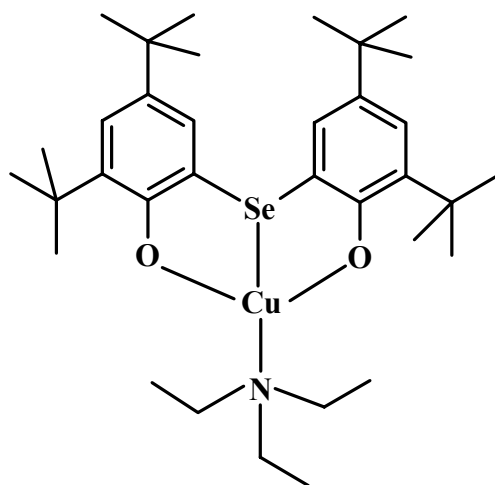
1. (a) M. J. Krische, J.-M. Lehn, *Struct. Bonding* (Berlin), **2000**, 96, 3-29 and references therein. (b) "*Hydrogen Bonding in Biological Structures*", Eds. G. A. Jeffrey, W. Sanger, Springer, Berlin, **1991**. (c) T. Steiner, *Angew. Chem.* **2002**, 114, 50.
2. F. M. Romero, R. Ziessel, M. Bonnet, Y. Pontillon, E. Ressouche, J. Schweizer, B. Delley, A. Grand, C. Paulsen, *J. Am. Chem. Soc.* **2000**, 122, 1298.
3. M. Ardon, A. Bino, *Struct. Bonding* (Berlin) **1987**, 65, 1.
4. (a) E. D. Estes, R. P. Scaringe, W. E. Hatfield, D. J. Hodgson, *Inorg. Chem.* **1976**, 15, 1179. (b) E. D. Estes, R. P. Scaringe, W. E. Hatfield, D. J. Hodgson, *Inorg. Chem.* **1977**, 16, 1605. (c) H. R. Fischer, J. Gleurup, D. J. Hodgson, E. Pedersen, *Inorg. Chem.* **1982**, 21, 3063. (d) H. R. Fischer, D. J. Hodgson, E. Pedersen, *Inorg. Chem.* **1984**, 23, 4755. (e) A. Bencini, M. D. Vaira, F. Manni, *J. Chem. Soc., Dalton Trans.* **1991**, 41. (f) M. Nakahanada, T. Fujihara, A. Fuyuhiko, S. Kaizaki, *Inorg. Chem.* **1992**, 31, 1316. (g) A. Böttcher, H. Elias, J. Gleurup, M. Neuburg, C. E. Olsen, J. Springborg, H. Weihe, M. Zehnder, *Acta Chem. Scand.* **1994**, 48, 981.
5. (a) M. Ardon, A. Bino, K. Michelsen, E. Pedersen, *J. Am. Chem. Soc.* **1987**, 109, 5855. (b) U. Bossek, K. Wieghardt, B. Nuber, J. Weiss, *Angew. Chem., Int. Ed. Engl.* **1990**, 29, 1055. (c) N. Arulsamy, J. Gleurup, D. J. Hodgson, *Inorg. Chem.* **1994**, 23, 2066.
6. K. Abdu-Dari, K. N. Raymond, D. P. Freyberg, *J. Am. Chem. Soc.* **1979**, 101, 3688.
7. J. A. Bonadies, M. L. Kirk, M. S. Lah, D. P. Kessissoglou, W. E. Hatfield, V. L. Pecoraro, *Inorg. Chem.* **1989**, 28, 2037.
8. B. G. Gafford, R. E. Marsh, W. P. Schaefer, J. H. Zhang, C. J. O'Connor, R. A. Holwerda, *Inorg. Chem.* **1990**, 29, 4652.
9. C. Reber, H. U. Güdel, M. Buiys, K. Wieghardt, P. Chaudhuri, *Inorg. Chem.* **1988**, 27, 2115.
10. J. Gleurup, D. J. Hodgson, E. Pedersen, *Acta Chem. Scand.* **1983**, A37, 161.
11. D. J. Hodgson, in "*Magneto-Structural Correlation in Exchange Coupled Systems*", Eds. R. D. Willett, D. Gatteschi, O. Kahn, D. Reidel, Dordrecht, **1985**, p. 497.
12. T. Katsuki, in *Catalytic Asymmetric Synthesis* (Ed.: I. Ojima), Wiley-VCH, Weinheim, **2000**, p. 287.
13. A. Zouni, H. T. Witt, J. Kern, P. Fromme, N. Kraub, W. Saenger, P. Orth, *Nature* **2001**, 409, 739.

14. (a) M. W. Lynch, D. N. Hendrickson, B. J. Fitzgerald, C. G. Pierpont, *J. Am. Chem. Soc.* **1984**, *106*, 2041. (b) J. H. Hartman, B. M. Foxman, S. R. Cooper, *Inorg. Chem.* **1984**, *23*, 1381. (c) S. Pal, P. Ghosh, A. Chakravorty, *Inorg. Chem.* **1985**, *24*, 3704. (d) R. O. C. Hart, S. G. Bott, J. L. Atwood, S. R. Cooper, *J. Chem. Soc., Chem. Commun.* **1992**, 895. (e) M. K. Chan, W. H. Armstrong, *Inorg. Chem.* **1989**, *28*, 3779. (f) P. S. Pavacik, J. C. Huffman, G. Christou, *J. Chem. Soc., Chem. Commun.* **1986**, 43. (g) S. K. Chandra, P. Basu, D. Ray, S. Pal, A. Chakravorty, *Inorg. Chem.* **1990**, *29*, 2423. (h) S. M. Saadeh, M. S. Lah, V. L. Pecoraro, *Inorg. Chem.* **1991**, *30*, 8. (i) M. Mikuriya, S. Shigematsu, K. Kawano, T. Tokii, H. Oshio, *Chem. Lett.* **1990**, 729. (j) B. Adam, E. Bill, E. Bothe, B. Goerdts, G. Haselhorst, K. Hildenbrand, A. Sokolowski, S. Steenken, T. Weyhermüller and K. Wieghardt, *Chem. Eur. J.* **1997**, *3*, 308.
15. (a) J. D. Walker, R. Poli, *Inorg. Chem.* **1990**, *29*, 756. (b) R. Viswanathan, M. Palaniandavar, P. Pravarakan, P. T. Muthiah, *Inorg. Chem.* **1998**, *37*, 3881.
16. (a) B. Chiari, O. Piovesana, T. Tarantelli, P. F. Zanazzi, *Inorg. Chem.* **1982**, *21*, 1396. (b) J. E. Davies, B. M. Gatehouse, *J. Chem. Soc. D* **1970**, 1166. (c) J. A. Bertrand, J. L. Breece, P. G. Eller, *Inorg. Chem.* **1974**, *13*, 927. (d) J. A. Bertrand, J. L. Breece, A. R. Kalyanaraman, G. J. Long, W. A. Baker, Jr., *J. Am. Chem. Soc.* **1970**, *92*, 5233. (e) J. A. Bertrand, J. L. Breece, P. G. Eller, *Inorg. Chem.* **1974**, *13*, 1250. (f) M. Garloch, F. E. Mabbs, *J. Chem. Soc. A* **1967**, 1598. (g) E. Fleischer, S. Hawkinson, *J. Am. Chem. Soc.* **1967**, *89*, 720.
17. J. A. Thich, C. Chih Ou, D. Powels, B. Vasiliou, D. Masteropalo, J. A. Potenza, H. J. Schugar, *J. Am. Chem. Soc.* **1976**, *98*, 145.
18. C. R. Snow and J. A. Ibers, *Inorg. Chem.* **1973**, *12*, 249.
19. A. B. P. Lever, *"Inorganic Electronic Spectroscopy"*, Elsevier, Amsterdam, **1984**.
20. F. Birkelbach, C. Krebs and V. Staemmler, unpublished computer program, Bochum, Germany, **1997**.
21. E. Fleischer, F. E. Mabbs, *J. Chem. Soc. A* **1967**, 1598.
22. (a) E. Pedersen, H. Toftlund, *Inorg. Chem.* **1974**, *13*, 1603. (b) J. C. Hemper, L. O. Morgan, W. B. Lewis, *Inorg. Chem.* **1970**, *9*, 2064. (c) L. S. Singer, *J. Chem. Phys.* **1955**, *23*, 379.
23. (a) K. D. Magers, C. G. Smith, D. T. Sawyer, *Inorg. Chem.* **1980**, *19*, 492. (b) D. T. Richens, D. T. Sawyer, *J. Am. Chem. Soc.* **1979**, *101*, 3681.
24. K. L. Brown, R. M. Dolding, P. C. Healy, J. K. Jessop, W. C. Ten, *Aust. J. Chem.* **1974**, *27*, 2075.

25. P. G. Debrunner, *"Biological Magnetic Resonance"*, Eds. L. J. Berliner, J. Reuben, Vol. 13, Plenum Press, **1993**, p. 59 and references cited therein.
26. (a) R. Sessoli, D. Gatteschi, A. Caneschi, M. A. Novak, *Nature* **1993**, 365, 141. (b) R. Sessoli, H.-L. Tsai, A. R. Schake, S. Wang, J. B. Vincent, K. Folting, D. Gatteschi, G. Christou, D. N. Hendrickson, *J. Am. Chem. Soc.* **1993**, 115, 1804.
27. (a) J. R. Friedman, M. P. Sarachick, J. Teguda, R. Ziolo, *Phys. Rev. Lett.* **1996**, 76, 3830. (b) L. Thomas, F. Liuti, R. Ballou, D. Gatteschi, R. Sessoli, B. Barbara, *Nature* **1996**, 383, 145. (c) C. Sangregorio, T. Ohm, C. Paulson, R. Sessoli, D. Gatteschi, *Phys. Rev. Lett.* **1997**, 78, 4645.
28. (a) J. E. Andrew, A. B. Blake *J. Chem. Soc. A* **1969**, 1456. (b) A. Barnes, W. E. Hatfield, *Inorg. Chem.* **1971**, 10, 2355. (c) B. Aurivillius, *Acta Chem. Scand. A*, **1977**, 31, 501. (d) P. D. W. Boyd, R. L. Martin, G. Schwarzenbach, *Aus. J. Chem.* **1988**, 41, 1449. (e) *Inorg. Chim. Acta* **1978**, 26, 113. (f) W. L. Gladfelter, M. W. Lynch, W. P. Schaefer, D. N. Hendrickson, H. B. Gray, *Inorg. Chem.* **1981**, 20, 2329. (g) K. Bizilj, S. G. Hardin, B. F. Hoskins, P. J. Oliver, E. R. T. Tiekink, G. Winter, *Aust. J. Chem.* **1986**, 39, 1035. (h) L. Ballester, E. Coronado, A. Gutiérrez, A. Monge, M. F. Perpinán, E. Pinilla, T. Rico, *Inorg. Chem.* **1992**, 31, 2053. (i) A. J. Atkins, A. J. Blake, M. Schröder, *J. Chem. Soc., Chem. Commun.* **1993**, 1662. (j) A. J. Blake, E. K. Brechin, A. Codron, R. O. Gould, C. M. Grant, S. Parsons, J. M. Rawson, R. E. P. Winpenny, *J. Chem. Soc., Chem. Commun.* **1995**, 1983. (k) M. A. Halcrow, J.-S. Sun, J. C. Huffman, G. Christou, *Inorg. Chem.* **1995**, 34, 4167. (l) M. S. E. Fallah, E. Rentschler, A. Caneschi, D. Gatteschi, *Inorg. Chim. Acta* **1996**, 247, 231. (m) A. Escuer, M. Font-Bardía, S. B. Kumar, X. Solans, R. Vicente, *Polyhedron* **1999**, 18, 909. (n) M. L. Tong, H. K. Lee, S.-L. Zheng, X.-M. Chen, *Chem. Lett.* **1999**, 1087. (o) J. M. Clemente-Juan, B. Chansou, B. Donnadieu, J.-P. Tuchagues, *Inorg. Chem.* **2000**, 39, 5515. (p) S. Mukherjee, T. Weyhermüller, E. Bothe, K. Wieghardt, P. Chaudhuri, *Eur. J. Inorg. Chem.* Submitted.

Chapter 4

SYNTHESIS, CHARACTERIZATION AND REACTIVITY STUDY OF COPPER(II) COMPLEXES OF SELENOBISPHENOL LIGAND

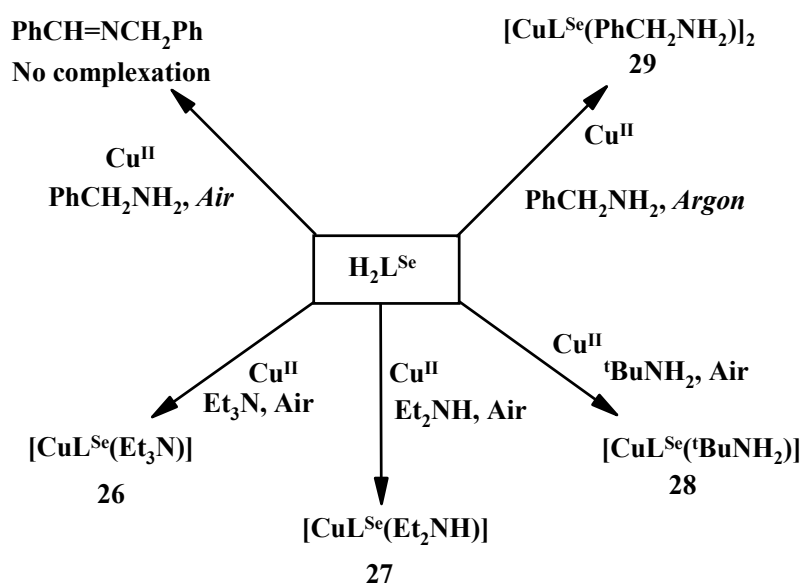


4.1 INTRODUCTION

Metal complexes of phenol-containing ligands play an important role in phenoxyl radical mediated homogeneous catalytic oxidation of organic substrates.¹ Depending upon the ligand system the radical intermediate can be detected and characterized. For stable radical systems intermediates can be isolated whereas for less stable radical systems they can either be detected by the available analytical techniques or by reacting with suitable substrates and subsequently identifying the products to postulate the mechanism of transformation. Although sometimes it is difficult to make out the active species involved directly, but transformation of the suitable substrate might give an idea about the short-lived reactive intermediate. This chapter deals with the study of Cu(II) complexes of the selenobisphenol ligand and their structural tuning by suitable donor atoms for use as homogeneous catalysts. Two such catalytic oxidation processes, amine and alcohol oxidation, are discussed using suitable substrates and catalysts. A detailed kinetic study for such oxidations is also discussed. The biological relevance of these catalytic oxidation reactions has been discussed in chapter 1 concerning the objectives of this thesis work. This result represents the first example of a functional model of the enzymes copper amine oxidases, showing that the metal-center can act as an electron pool mimicking the redox-cofactor of these metalloenzymes.

4.2 SYNTHESIS

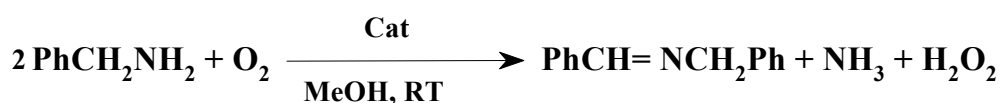
Ligand $\text{H}_2\text{L}^{\text{Se}}$ reacts with copper (+2) ion in the presence of different amines giving rise to a variety of Cu(II) complexes as shown in the Scheme 4.2.1.



Scheme 4.2.1 Synthesis of Cu(II) complexes in presence of different amines.

The ligand $\text{H}_2\text{L}^{\text{Se}}$ reacts with Cu(I) or Cu(II) salt in methanolic solvent in the presence of different amine bases of known ligating properties to form four-coordinated square-planar Cu(II) complexes, in which the fourth coordination site is occupied by the corresponding amine base. Tertiary amines (e.g., Et_3N), secondary amines (e.g., Et_2NH), and primary amines without any α -H atom (e.g., $^t\text{BuNH}_2$) do form such complexes as is evidenced by isolation of **26**, **27** and **28**, respectively.

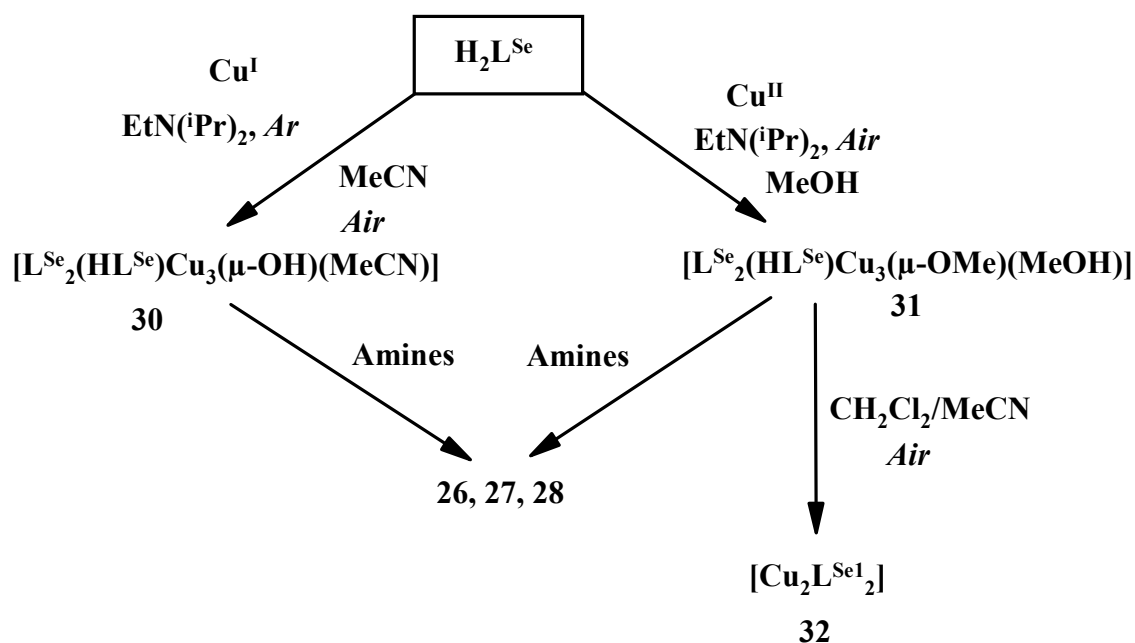
But, when the amine is a primary amine with at least one α -H atom a totally different reactivity is observed. If the reaction is carried out in the presence of benzylamine under argon a dinuclear Cu(II) complex **29** is isolated, where two benzylamine molecules disposed in *anti* positions are attached to two Cu(II) centers. When the same reaction is carried out in air no such Cu(II) complex could be isolated. Instead an organic product, benzylidenebenzylamine ($\text{PhCH}=\text{NCH}_2\text{Ph}$), is detected, which is a Schiff base condensation product of benzaldehyde and benzylamine. Benzaldehyde is formed by the aerial oxidation of benzylamine, catalyzed by a Cu(II) complex, formed *in situ* in solution. *This oxidative deamination reaction is found to be catalytic in nature.*



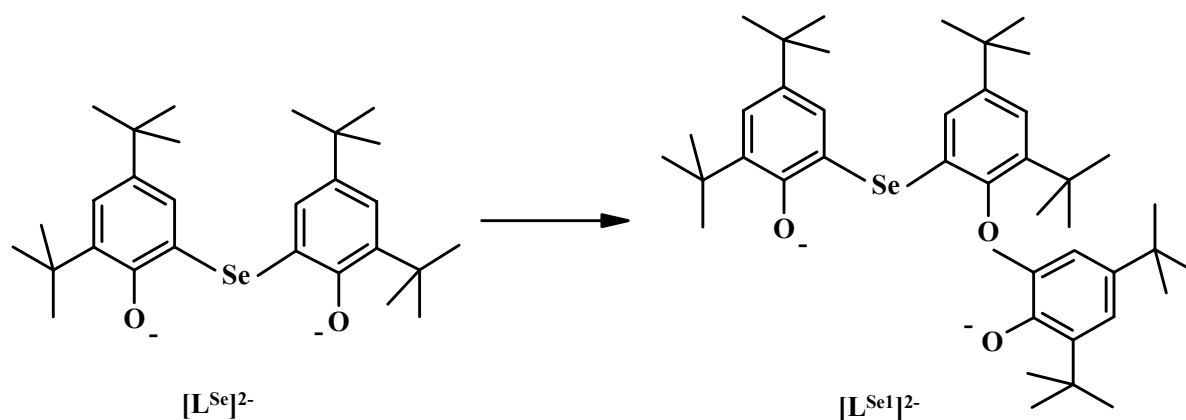
Scheme 4.2.2 Aerial oxidation of benzylamine catalyzed by Cu(II) complex.

Bulky tertiary amines, e.g., $(^i\text{Pr})_2\text{NEt}$ (weak base also) do not coordinate to copper because of steric reason where it just behaves as a base to deprotonate the ligand and trinuclear Cu(II) complexes are formed according to the Scheme 4.2.3.

Treatment of the trinuclear complexes **30**, **31** with respective amines results in the mononuclear complexes **26**, **27**, **28** whereas with benzylamine they form oxidized products under air. Interestingly, complex **31** reacts with the oxygen of air in a solvent mixture of CH_2Cl_2 and MeCN(1:1) forming a small amount of dinuclear Cu(II) complex **32** with a modified ligand(L^{Se1}) as shown in the Scheme 4.2.3 along with the trinuclear species. GC-analysis after removal of copper ion from the solution confirms the formation of the modified ligand L^{Se1} . Isolation of pure dinuclear species **32** was not possible because of the presence of trinuclear species as an impurity that remains in the mixture.

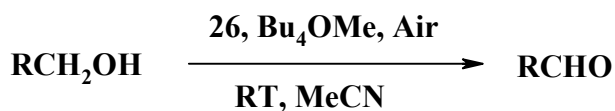


Scheme 4.2.3 Synthesis of trinuclear Cu(II) complexes and their reactivity.



Scheme 4.2.4 Ligand modified through complexation.

The mononuclear amine complex **26**, $[\text{CuL}^{\text{Se}}(\text{Et}_3\text{N})]$ in combination with base (methanolic Bu_4NOMe or BuLi) in MeCN under air reacts with primary alcohols to oxidize them catalytically to the corresponding carbonyl compounds, as shown in the Scheme 4.2.5.



Scheme 4.2.5 Aerial oxidation of primary alcohols catalyzed by Cu(II) complex **26**.

4.3 INFRARED AND MASS SPECTROSCOPY

IR and Mass spectrometry are found to be useful analytical tools for initial characterization of the complexes **26-31**. Coordination of the ligand with the metal ion is confirmed by notifying the differences between the IR spectrum of the complex and that of the free ligand. The sharp $\nu(\text{OH})$ band of free ligand is replaced by a broad band indicating the loss of phenol character of the ligand upon coordination. All the complexes show a strong band around 2900 cm^{-1} due to $\nu(\text{C-H})$ of *tert*-butyl groups, a strong proof for ligand coordination. For complexes **27**, **28** and **29**, sharp $\nu(\text{N-H})$ peaks are observed in the $3340\text{-}3260\text{ cm}^{-1}$ region, clearly suggesting the coordination of the respective amines with the metal center. Complexes **30** and **31** show $\nu(\text{OH})$ bands due to OH or HOME overlapping in the region of the broad band from coordinated phenolate. Peaks of the coordinated MeCN molecule is also observed for **30** in the region of 2320 cm^{-1} . Other C-H, C=C and C-O vibrations for all the complexes are observed in the expected region.

For the mononuclear complexes **26-28** EI-MS shows peaks of the $[\text{L}^{\text{Se}}\text{Cu}]^+$ unit. At high temperature applied for EI-MS the coordinated amines get out from the Cu-site, but peaks for respective amines are observed clearly in the fragmentation pattern. A similar case is also observed for complex **29**, where its dimeric nature is lost during the experimental condition. But the ESI (positive ion in CH_2Cl_2) mass spectrum shows clearly the $[\text{M}+\text{H}]^+ = 653$ (100%) peak confirming the composition of the complex. Other complexes are expected to show similar characteristic peaks in the ESI (positive mode) mass spectra. EI and ESI measurements for the trinuclear complexes **30** and **31** do not give any idea about their composition-this may be because of their decomposition/dissociation in the gas phase, as expected for polynuclear metal complexes.

4.4 X-RAY CRYSTAL STRUCTURE

4.4.1 Molecular structure of $[\text{CuL}^{\text{Se}}(\text{Et}_3\text{N})]$ (**26**)

X-ray crystal analysis reveals the complex to be a mononuclear Cu(II) complex with a tetracoordinate square-planar environment. The ORTEP diagram with atom labeling scheme is given in Figure 4.4.1 and the selected bond parameters are tabulated in Table 4.4.1.

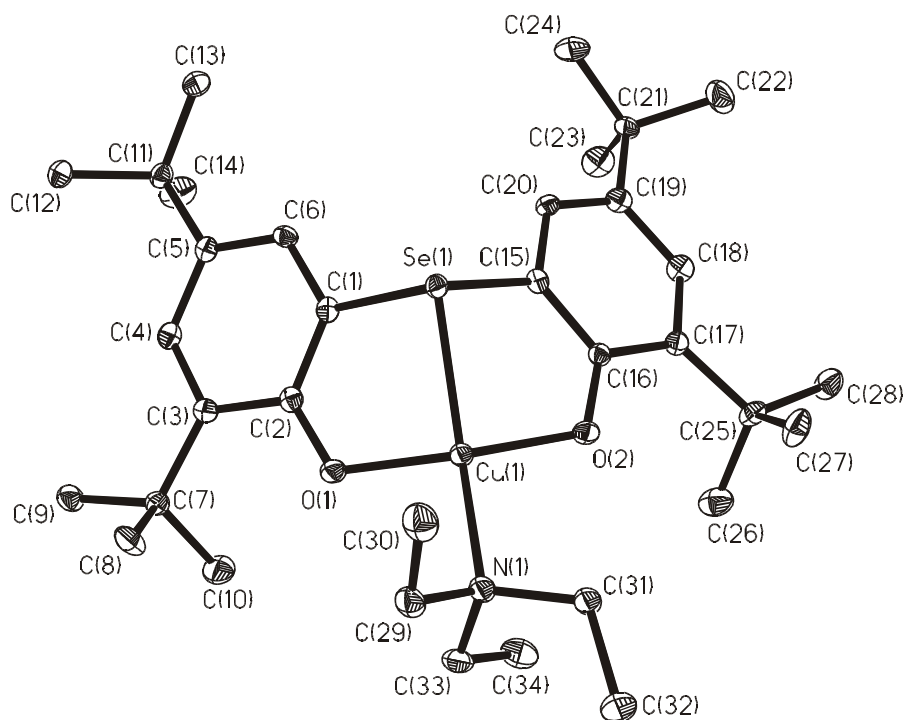


Figure 4.4.1 ORTEP and atom labeling scheme for $[\text{CuL}^{\text{Se}}(\text{Et}_3\text{N})]$ (**26**).

In the discrete molecule, the central copper ion is coordinated by the O,Se,O donor set of the ligand and by the nitrogen atom of the Et_3N molecule, forming a square planar environment. Two phenolate oxygen atoms and selenium and nitrogen atoms are bonded *trans* to each other, having an O(1)-Cu-O(2) bond angle at $150.25(8)^\circ$ and Se(1)-Cu-N(1) angle at $153.13(7)^\circ$, thus making the geometry deviated from ideal square-planar. This may arise because of the flexible ligand character of Et_3N , as is evidenced from the O(1)-Cu-Se(1) [$89.05(6)^\circ$] and O(2)-Cu-Se(1) [$89.27(6)^\circ$] angles. The phenyl rings attached to phenolate oxygens are planar and retain aromaticity after complexation. Both the phenols are deprotonated and the complex is confirmed to be a Cu(II) complex. The Cu-O(phenolate) [1.895\AA] and Cu-N [$2.052(2)\text{\AA}$] bonds are also in the normal range for Cu(II) complexes.^{1a}

4.4.2 Molecular structure of $[\text{CuL}^{\text{Se}}(\text{Et}_2\text{NH})]$ (**27**)

This complex is isostructural with complex **26** as is evidenced from the ORTEP diagram shown in Figure 4.4.2 and the bond parameters in Table 4.4.1. So details are not discussed here about the structural aspect of this complex.

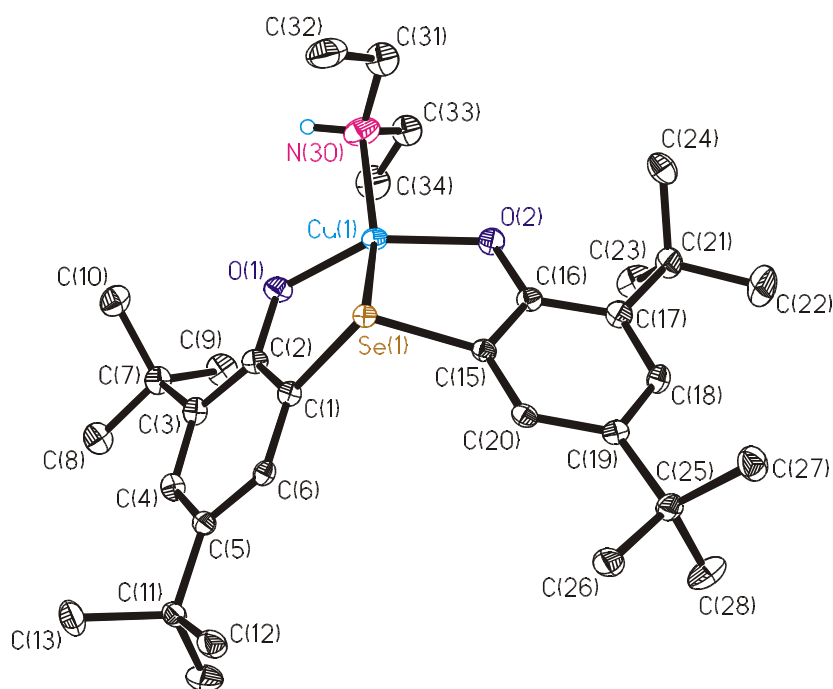


Figure 4.4.2: ORTEP and atom labeling scheme for $[\text{CuL}^{\text{Se}}(\text{Et}_2\text{NH})]$ (**27**).

Table 4.4.1 Selected bond distances (\AA) and angles (deg) for complexes **26** and **27**

| 26 | | 27 | |
|------------------|-----------|-------------------|------------|
| Cu(1)-O(1) | 1.898(2) | Cu(1)-O(1) | 1.879(2) |
| Cu(1)-O(2) | 1.889(2) | Cu(1)-O(2) | 1.885(2) |
| Cu(1)-Se(1) | 2.3922(6) | Cu(1)-Se(1) | 2.3842(5) |
| Cu(1)-N(1) | 2.052(2) | Cu(1)-N(30) | 2.029(3) |
| C(2)-O(1) | 1.330(3) | C(2)-O(1) | 1.335(4) |
| C(16)-O(2) | 1.336(3) | C(16)-O(2) | 1.335(4) |
| O(2)-Cu(1)-O(1) | 150.25(8) | O(2)-Cu(1)-O(1) | 147.82(11) |
| O(2)-Cu(1)-N(1) | 98.02(9) | O(2)-Cu(1)-N(30) | 98.41(13) |
| O(2)-Cu(1)-Se(1) | 89.05(6) | O(2)-Cu(1)-Se(1) | 90.40(7) |
| N(1)-Cu(1)-Se(1) | 153.13(7) | N(30)-Cu(1)-Se(1) | 147.00(10) |
| N(1)-Cu(1)-O(1) | 96.80(8) | N(30)-Cu(1)-O(1) | 98.15(13) |
| Se(1)-Cu(1)-O(1) | 89.27(6) | Se(1)-Cu(1)-O(1) | 90.53(7) |

4.4.3 Molecular structure of $[\text{CuL}^{\text{Se}}(\text{PhCH}_2\text{NH}_2)]_2$ (**29**)

The structure analysis of this complex shows the presence of a dinuclear unit as the smallest unit present in the crystal. The asymmetric dinuclear unit $\text{Cu}_2\text{L}^{\text{Se}}_2$ consists of one four-

coordinated and another five-coordinated copper center. The ORTEP drawing of the molecule is displayed in Figure 4.4.3, with selected bond distances and angles provided in Table 4.4.2.

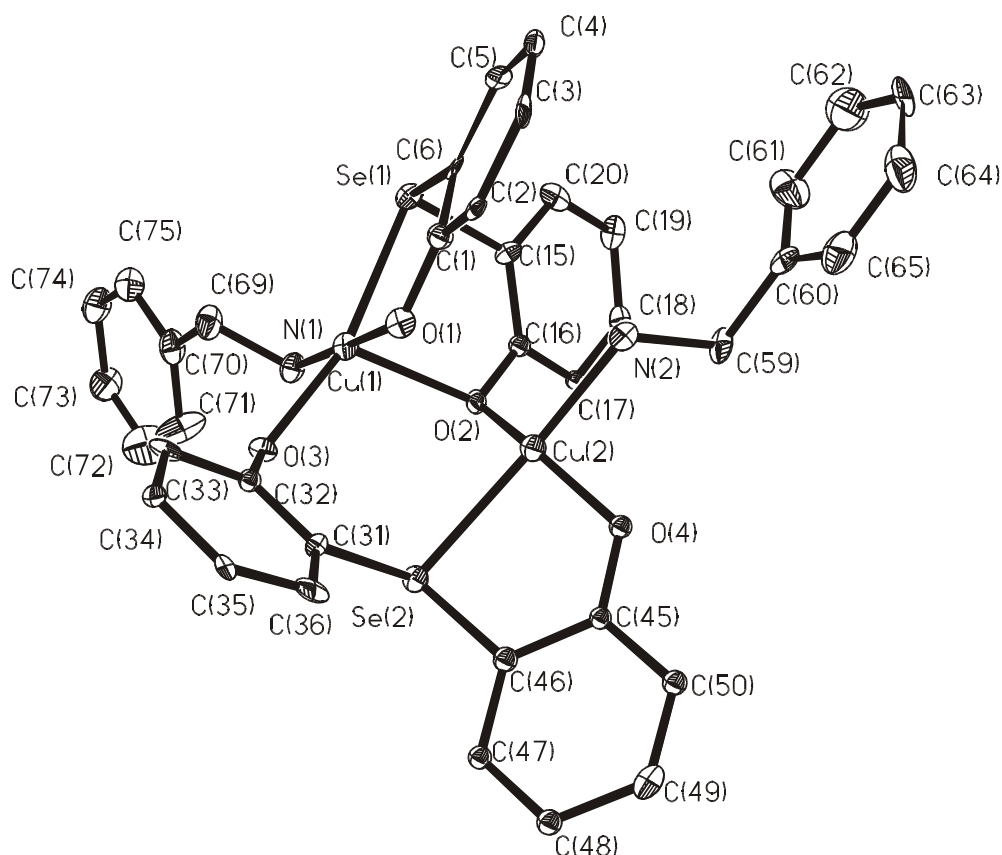


Figure 4.4.3 ORTEP and atom labeling scheme for $[\text{CuL}^{\text{Se}}(\text{PhCH}_2\text{NH}_2)]_2$ (**29**) (*tert*-butyl groups are not shown).

The copper ion Cu(2) is in a distorted square-planar environment having a CuO_2SeN coordination sphere. Ligand with the O,Se,O donor atoms coordinate with Cu(1) in *facial* manner to develop a distorted square pyramidal geometry with CuNO_4 environment. One phenolate oxygen O(2) acts as a bridging unit between Cu(1) and Cu(2) centers. Two phenolates, O(4) and bridging O(2) from two different ligands, the selenium atom and the nitrogen atom form the plane for the Cu(2) center. The Cu(2)-O(2) and Cu(2)-O(4) bonds, which are in mutually *trans* position, similar to Cu(2)-Se(2) and Cu(2)-N(2). The bond distances for the five-coordinated center Cu(1) is significantly longer than those for the four-coordinated Cu(2) center [Cu(1)-O(1) 1.946(5) Å, Cu(2)-O(4) 1.878(5) Å]. The angle O(2)-Cu(2)-O(4) at 154.8(2)° deviates significantly from linearity, as well as the angle Se(2)-Cu(2)-N(2) at 166.4(2)°. But the angle for five coordinated Cu(1), O(1)-Cu(1)-N(1) at 179.3(3)° is linear. The dimeric formulation in the solid state is confirmed by magnetic susceptibility and EPR measurements on powdered samples. In solution it also exists as a dimer, as established by solution EPR spectroscopy.

Table 4.4.2 Selected bond distances (Å) and angles (deg) for complex **29**

| | | | |
|------------------|------------|------------------|-----------|
| Cu(1)-O(1) | 1.946(5) | Cu(1)-O(3) | 1.947(5) |
| Cu(1)-N(1) | 2.024(7) | Cu(1)-O(2) | 2.220(5) |
| Cu(1)-Se(1) | 2.4503(14) | Cu(2)-O(4) | 1.878(5) |
| Cu(2)-O(2) | 1.960(5) | Cu(2)-N(2) | 2.017(6) |
| Cu(2)-Se(2) | 2.4685(14) | | |
| Cu(1)-Cu(2) | 3.122(5) | | |
| C(1)-O(1) | 1.320(10) | | |
| C(16)-O(2) | 1.346(9) | | |
| C(32)-O(3) | 1.352(9) | | |
| C(45)-O(4) | 1.333(9) | | |
| O(1)-Cu(1)-O(3) | 94.9(2) | O(1)-Cu(1)-N(1) | 179.3(3) |
| O(3)-Cu(1)-N(1) | 84.9(3) | O(1)-Cu(1)-O(2) | 93.4(2) |
| O(3)-Cu(1)-O(2) | 110.3(2) | N(1)-Cu(1)-O(2) | 87.3(2) |
| O(1)-Cu(1)-Se(1) | 87.5(2) | O(3)-Cu(1)-Se(1) | 164.8(2) |
| N(1)-Cu(1)-Se(1) | 92.6(2) | O(2)-Cu(1)-Se(1) | 84.49(14) |
| O(4)-Cu(2)-O(2) | 154.8(2) | O(4)-Cu(2)-N(2) | 88.5(2) |
| O(2)-Cu(2)-N(2) | 96.2(2) | O(4)-Cu(2)-Se(2) | 87.0(2) |
| O(2)-Cu(2)-Se(2) | 93.3(2) | N(2)-Cu(2)-Se(2) | 166.4(2) |
| Cu(1)-O(2)-Cu(2) | 96.4(2) | | |

This asymmetry in the bridging bond lengths is also noteworthy which arises due to the nature of asymmetry of the molecule as a whole.

4.4.4 Molecular structure of $[L^{Se}_2(HL^{Se})Cu_3(\mu-OH)(MeCN)]$ (**30**)

The structure of the complex consists of a trinuclear unit containing the $L^{Se}_2(HL^{Se})Cu_3$ core. The molecular geometry and the atom labeling scheme, as well as selected bond lengths and angles for this complex are presented below.

There are two types of copper bonded in the trinuclear unit, two of them, Cu(2) and Cu(3), are four-coordinated distorted square planar and the central copper Cu(1) is five-coordinated distorted square pyramidal in geometry. With the theta (θ) range for the data collection small, the structure of this complex is found to be of mediocre quality.

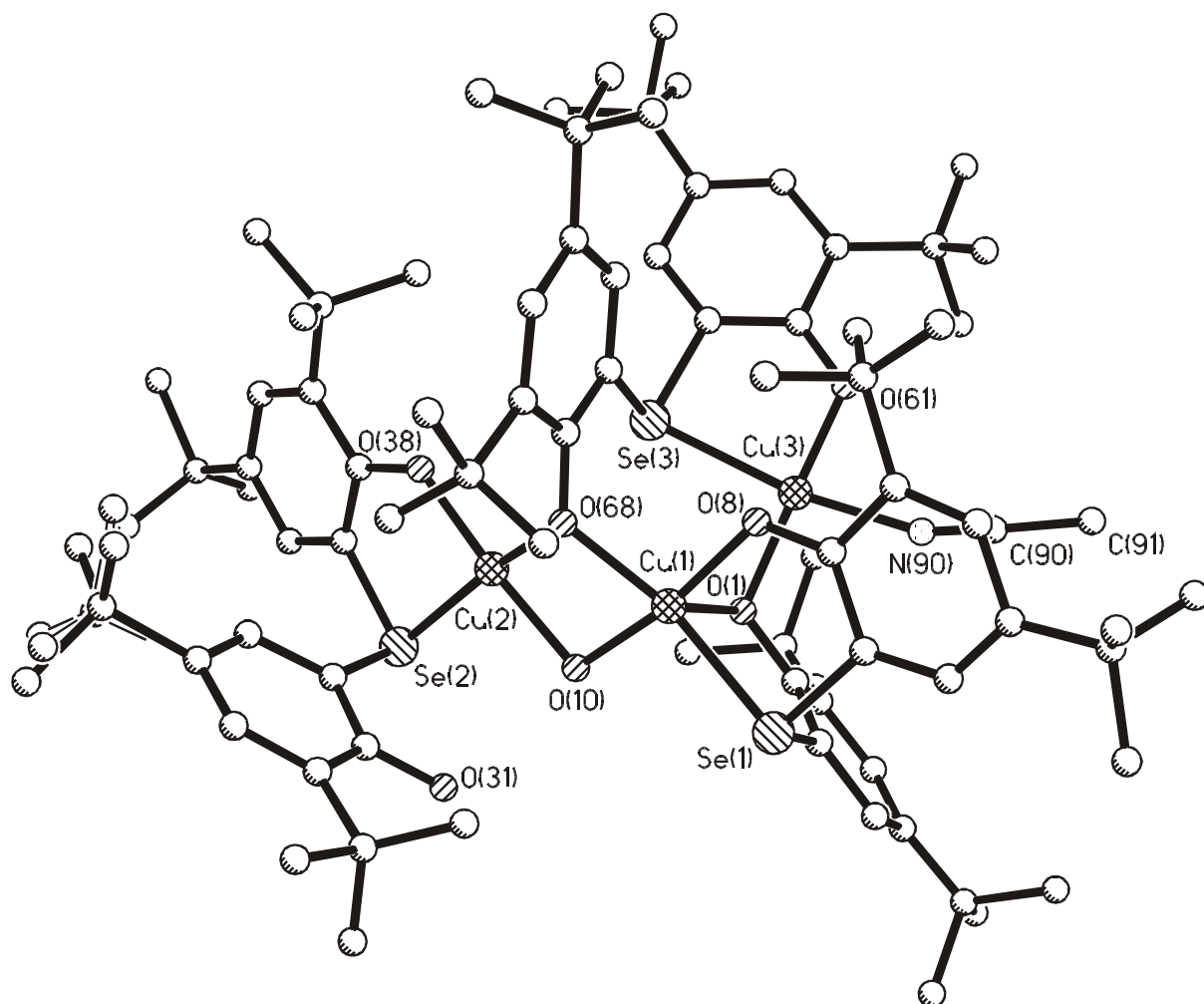


Figure 4.4.4 Ball and Stick diagram and atom labeling scheme for $[L^{Se}_2(HL^{Se})Cu_3(\mu-OH)(MeCN)]$ (**30**).

The central copper Cu(1) is facially coordinated to the ligand with O, Se, O donor atoms at distances Cu(1)-O(1) [2.248 (13) Å], Cu(1)-Se(1) [2.433(4) Å] and Cu(1)-O(8) [1.924(14)Å]. The coordination geometry is distorted square pyramidal and is completed by two oxygen atoms, O(10)[bridging OH (from water) between Cu(1) and Cu(2)] and O(68) [from phenolate bridge between Cu(1) and Cu(2)], resulting in the CuO₄Se coordination polyhedra. Phenolate oxygen O(1), Se(1) and O(68) make the equatorial plane, while O(8) and O(10) are *trans* to each other making the axial plane with an O(8)-Cu(1)-O(10) angle at 168.3(6)°.

Cu(2) is surrounded by two bridging oxygen atoms and one phenolate oxygen atom O(38) and Se(2), where O(10)-Cu(2)-O(38) and O(68)-Cu(2)-Se(2) angles are at 174.8(6) and 167.5(4)°, respectively, deviating considerably from ideal square-planar geometry. The protonated

phenolate oxygen O(31) remains non-coordinated, most probably bonded with O(10) through a hydrogen bond.

Table 4.4.3 Selected bond distances (Å) and angles (deg) for complex 30

| | | | |
|-------------------|-----------|-------------------|-----------|
| Cu(2)-O(38) | 1.863(14) | Cu(2)-O(68) | 1.936(14) |
| Cu(2)-O(10) | 1.961(13) | Cu(2)-Se(2) | 2.400(4) |
| Cu(1)-O(8) | 1.924(14) | Cu(1)-O(10) | 1.970(14) |
| Cu(1)-O(68) | 1.974(14) | Cu(1)-O(1) | 2.248(13) |
| Cu(1)-Se(1) | 2.433(4) | Cu(3)-O(61) | 1.879(13) |
| Cu(3)-O(1) | 1.961(13) | Cu(3)-N(90) | 2.00(2) |
| Cu(3)-Se(3) | 2.470(4) | Cu(1)-Cu(2) | 3.012(4) |
| Cu(2)-Cu(3) | 4.722(4) | Cu(1)-Cu(3) | 3.078(4) |
| C(1)-O(1) | 1.36(2) | C(8)-O(8) | 1.29(2) |
| C(31)-O(31) | 1.38(2) | C(38)-O(38) | 1.34(2) |
| C(61)-O(61) | 1.29(2) | C(68)-O(68) | 1.36(2) |
| O(8)-Cu(1)-O(10) | 168.3(6) | O(8)-Cu(1)-O(1) | 93.7(5) |
| O(10)-Cu(1)-O(1) | 82.7(5) | O(68)-Cu(1)-O(1) | 118.2(5) |
| O(8)-Cu(1)-Se(1) | 87.8(4) | O(10)-Cu(1)-Se(1) | 102.7(4) |
| O(68)-Cu(1)-Se(1) | 158.0(4) | O(1)-Cu(1)-Se(1) | 83.2(3) |
| O(38)-Cu(2)-O(68) | 97.5(6) | O(38)-Cu(2)-O(10) | 174.8(6) |
| O(68)-Cu(2)-O(10) | 77.9(6) | O(38)-Cu(2)-Se(2) | 88.6(4) |
| O(68)-Cu(2)-Se(2) | 167.5(4) | O(10)-Cu(2)-Se(2) | 96.5(4) |
| O(61)-Cu(3)-O(1) | 159.0(5) | O(61)-Cu(3)-N(90) | 85.4(7) |
| O(1)-Cu(3)-N(90) | 97.5(7) | O(61)-Cu(3)-Se(3) | 87.0(4) |
| O(1)-Cu(3)-Se(3) | 92.3(4) | N(90)-Cu(3)-Se(3) | 169.2(6) |
| Cu(1)-O(10)-Cu(2) | 100.0(6) | Cu(1)-O(68)-Cu(2) | 100.8(7) |
| Cu(1)-O(1)-Cu(3) | 93.7(6) | | |

Similarly Cu(3) makes a distorted square-planar geometry by bonding with two phenolate O(61) and O(1) [trans to each other with an angle at 159.0(5)°] and Se(3) and N(90)[trans to each other at 169.2(6)°]. The unique coordination environment makes the Cu₃L^{Se}₃ unit asymmetric, with three copper atoms at the corners of an isosceles triangle. Cu(1) and Cu(2) are bridged by one phenolate and one hydroxy resulting in a Cu(1)-Cu(2) bond length at 3.012(4) Å. On the other hand Cu(1) and Cu(3) are bridged through only one phenolate, whereas Cu(2) and Cu(3) are not directly linked through such bridging mode. The structural parameters are in well agreement with magnetic exchange between the paramagnetic Cu(II) centers.

4.4.5 Molecular structure of $[L^{Se}_2 (L^{Se}H)Cu_3(\mu\text{-OMe})(MeOH)]$ (**31**)

This complex consists of the triangular trinuclear neutral unit $L^{Se}_2 (HL^{Se})Cu_3$. The structure is very similar to that of **30**, and hence the detailed geometry is not discussed here. The only difference observed in this complex is the bridging unit between Cu(1) and Cu(2) being methoxo instead of hydroxo, and the fourth coordination site of Cu(3) is satisfied by one oxygen atom from the MeOH molecule instead of MeCN in **30**. The molecular geometry with the atom-labeling scheme is presented in Figure 4.4.5 and selected bond parameters are presented in Table 4.4.4.

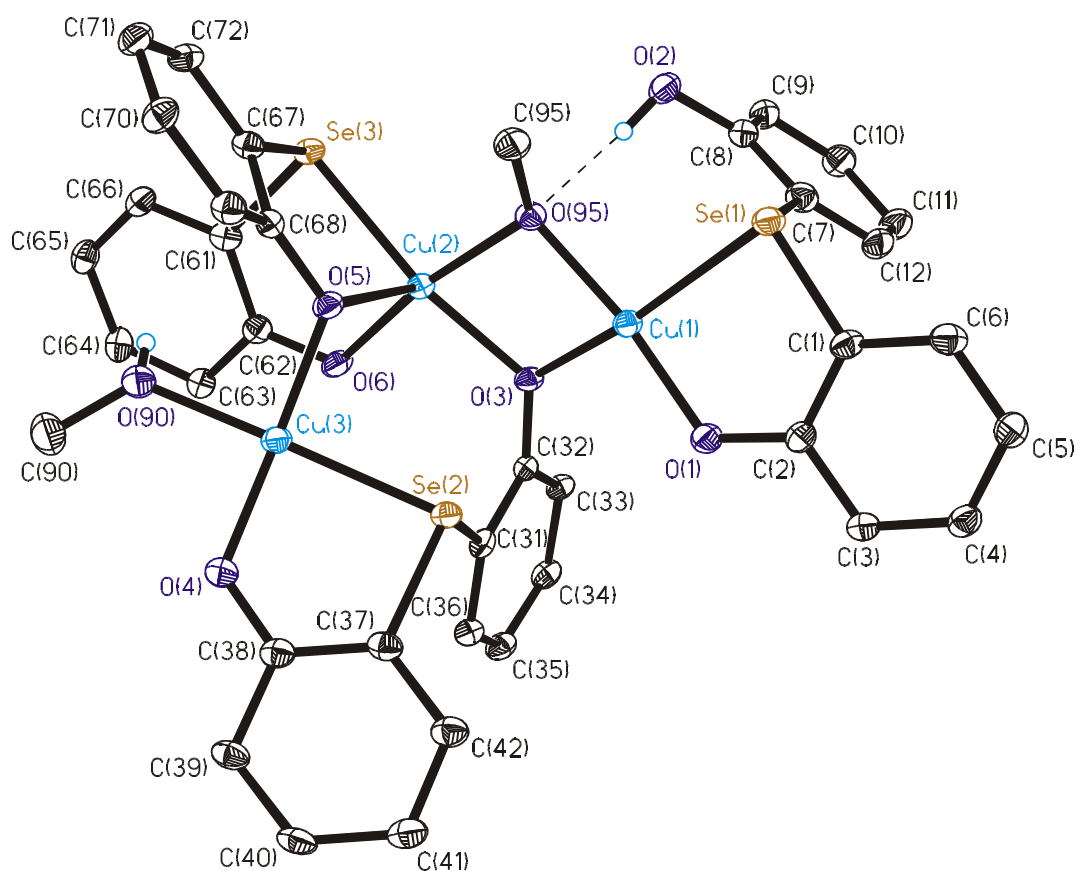


Figure 4.4.5 ORTEP and atom labeling scheme for $[L^{Se}_2 (HL^{Se})Cu_3(\mu\text{-OMe})(MeOH)]$ (**31**) (tert-butyl groups are not shown).

Table 4.4.4 Selected bond distances (\AA) and angles (deg) for complex **31**

| | | | |
|-------------|-----------|-------------|-----------|
| Cu(1)-O(1) | 1.859(2) | Cu(1)-O(95) | 1.939(2) |
| Cu(1)-O(3) | 1.942(2) | Cu(1)-Se(1) | 2.4024(5) |
| Cu(2)-O(6) | 1.895(2) | Cu(2)-O(95) | 1.969(2) |
| Cu(2)-O(3) | 1.973(2) | Cu(2)-O(5) | 2.322(2) |
| Cu(2)-Se(3) | 2.4205(5) | Cu(3)-Se(2) | 2.4356(5) |
| Cu(3)-O(4) | 1.871(2) | Cu(3)-O(5) | 1.915(2) |

| | | | |
|-------------------|-----------|-------------------|-----------|
| Cu(3)-O(90) | 2.039(2) | Cu(1)-Cu(2) | 3.0176(5) |
| C(2)-O(1) | 1.323(4) | C(8)-O(2) | 1.384(4) |
| C(32)-O(3) | 1.364(3) | C(38)-O(4) | 1.328(4) |
| C(68)-O(5) | 1.340(3) | C(62)-O(6) | 1.336(4) |
| O(1)-Cu(1)-O(95) | 172.34(9) | O(1)-Cu(1)-O(3) | 96.33(9) |
| O(95)-Cu(1)-O(3) | 78.48(8) | O(1)-Cu(1)-Se(1) | 90.05(7) |
| O(95)-Cu(1)-Se(1) | 96.51(6) | O(3)-Cu(1)-Se(1) | 162.97(6) |
| O(6)-Cu(2)-O(95) | 170.26(8) | O(6)-Cu(2)-O(3) | 93.59(8) |
| O(95)-Cu(2)-O(3) | 77.02(8) | O(6)-Cu(2)-O(5) | 93.52(9) |
| O(95)-Cu(2)-O(5) | 92.47(8) | O(3)-Cu(2)-O(5) | 112.41(8) |
| O(6)-Cu(2)-Se(3) | 89.17(6) | O(95)-Cu(2)-Se(3) | 99.32(6) |
| O(3)-Cu(2)-Se(3) | 165.78(6) | O(5)-Cu(2)-Se(3) | 81.29(5) |
| O(4)-Cu(3)-O(5) | 163.51(9) | O(4)-Cu(3)-O(90) | 91.50(9) |
| O(5)-Cu(3)-O(90) | 91.18(9) | O(4)-Cu(3)-Se(2) | 88.10(7) |
| O(5)-Cu(3)-Se(2) | 91.38(6) | O(90)-Cu(3)-Se(2) | 172.29(8) |
| Cu(1)-O(3)-Cu(2) | 100.83(9) | Cu(1)-O(95)-Cu(2) | 101.09(9) |
| Cu(2)-O(5)-Cu(3) | 99.33(8) | | |

4.4.6 Molecular structure of $[\text{L}^{\text{Se}^1}_2\text{Cu}_2]$ (**32**)

Single crystal was obtained during recrystallization of complex **31** from a solvent mixture of CH_2Cl_2 and MeCN. The dimeric unit $\text{Cu}_2\text{L}^{\text{Se}^1}_2$ consists of two modified ligand $[\text{L}^{\text{Se}^1}]^{2-}$ (formed during recrystallization from ligand L^{Se} as shown in the scheme 4.2.4.), where two phenolates act as bridging unit between two Cu(II) centers. The etheral oxygen atoms do not coordinate with metal ion. The modified ligand thus also behaves as a tridentate ligand. The Ball and Stick diagram with atom labeling scheme is shown in Figure 4.4.6, and selected bond parameters are given in the Table 4.4.5.

Both copper centers are tetracoordinated by two ligands with the O, Se, O donor set, resulting in a CuO_3Se coordination polyhedron, where both the Cu(II) are distorted square planar in geometry. The Cu(1)-O(1) distance at 1.860(4) Å and the Cu(2)-O(4) distance at 1.861(4) Å are significantly shorter than the Cu(1)-O(6) [1.962(4) Å] and Cu(2)-O(3) [1.964(4) Å]. The phenolate oxygens O(1) and O(3) from one ligand coordinated to Cu(1) are *trans* to each other making an O(1)-Cu(1)-O(3) angle at 173.5(2)°. Similarly, the O(4)-Cu(2)-O(6) angle at 172.0(2)° clearly shows the coordination geometry as a distorted square-planar. Phenolate oxygen O(1) and Se(1) are *cis* to each other. All the C(aromatic)-O(phenolate) bond distances are equal within the 3σ range C(1)-O(1) [1.320(7) Å], C(51)-O(4) [1.328(7) Å], C(64)-O(6) [1.372(7) Å] and C(14)-O(3) [1.362(7) Å]. Cu(1)-Cu(2) distance is 2.8593(11) Å.

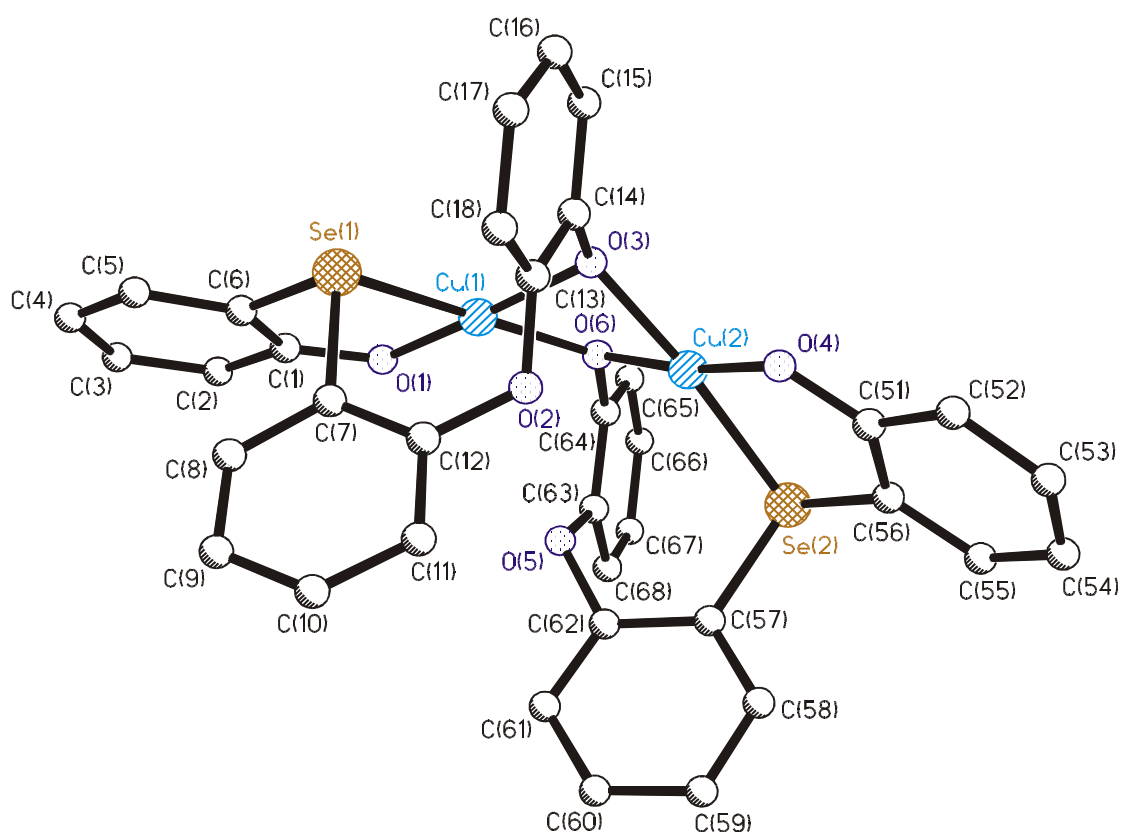


Figure 4.4.6 Ball and Stick diagram and atom labeling scheme for $[L^{Se1}_2Cu_2]$ (**32**) (tert-butyl groups are not shown).

Table 4.4.5 Selected bond distances (\AA) and angles (deg) for complex **32**

| | | | |
|------------------|------------|------------------|------------|
| Cu(1)-O(1) | 1.860(4) | Cu(1)-O(3) | 1.937(4) |
| Cu(1)-O(6) | 1.962(4) | Cu(2)-O(4) | 1.861(4) |
| Cu(2)-O(6) | 1.936(4) | Cu(2)-O(3) | 1.964(4) |
| Cu(2)-Se(2) | 2.4265(10) | Cu(1)-Se(1) | 2.4192(10) |
| Cu(1)-Cu(2) | 2.8593 | | |
| C(1)-O(1) | 1.320(7) | C(14)-O(3) | 1.362(7) |
| C(51)-O(4) | 1.328(7) | C(64)-O(6) | 1.372(7) |
| O(1)-Cu(1)-O(3) | 173.5(2) | O(1)-Cu(1)-O(6) | 99.3(2) |
| O(3)-Cu(1)-O(6) | 76.7(2) | O(1)-Cu(1)-Se(1) | 89.27(13) |
| O(3)-Cu(1)-Se(1) | 95.14(13) | O(6)-Cu(1)-Se(1) | 170.08(12) |
| O(4)-Cu(2)-O(6) | 172.0(2) | O(4)-Cu(2)-O(3) | 96.4(2) |
| O(6)-Cu(2)-O(3) | 76.7(2) | O(4)-Cu(2)-Se(2) | 88.52(13) |
| O(6)-Cu(2)-Se(2) | 98.62(12) | O(3)-Cu(2)-Se(2) | 174.11(12) |
| Cu(1)-O(3)-Cu(2) | 94.3(2) | Cu(1)-O(6)-Cu(2) | 94.4(2) |

4.5 ELECTRONIC SPECTROSCOPY

The electronic spectra of the complexes have been recorded in CH_2Cl_2 solution in the range 300-1000 nm at ambient temperature. The electronic spectra of **26**, **27** and **28** are very similar. They all display a moderately intense ($\epsilon \sim 500\text{-}600 \text{ M}^{-1} \text{ cm}^{-1}$) broad unsymmetrical d-d transition in the visible range (550-750 nm) of an unsymmetrically ligated $\text{O}_2\text{Cu}^{\text{II}}\text{SeN}$ chromophore (distorted square planar), in accord with asymmetric square planar copper(II) monomers with $(d_x^2-y^2)^1$ configuration.

Table 4.5.1 Electronic spectral data for complexes **26-31** in CH_2Cl_2

| Complex | λ_{max} , nm (ϵ , $\text{M}^{-1}\text{cm}^{-1}$) |
|-----------|--|
| 26 | 735 (585), 595sh(385) |
| 27 | 690 (474), 570sh(366) |
| 28 | 688 (388), 570sh (298), 485sh (194) |
| 29 | 483(969), 655 (898) |
| 30 | 482 (6730), 600sh (3700) |
| 31 | 467 (7200), 625sh (3880) |

On the other hand, complex **29** shows two asymmetric bands in the visible region, corresponding to d-d transitions of the asymmetric Cu(II) dimer with a relatively high intensity ($\epsilon = 1000 \text{ M}^{-1} \text{ cm}^{-1}$).

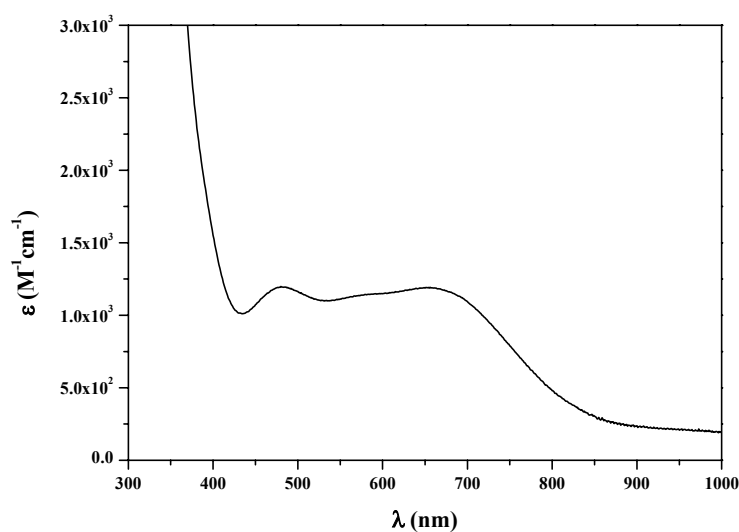


Figure 4.5.1 Electronic spectrum of complex **29** in CH_2Cl_2 .

Interestingly, trinuclear species **31** shows two bands in the visible region (630 nm and 480 nm). But, in CH₂Cl₂, with time the nature of the spectrum changes dramatically and finally shows only one band at 460 nm. This is believed to be due to a self-decomposition of the complex in CH₂Cl₂ solvent under air. Isolation of the dinuclear species **32** of the modified ligand supports this decomposition.

4.6 MAGNETISM

The observed temperature-independent magnetic moments for **26-28** (Table 4.6.1) confirm the monomeric nature of the complexes in the solid state.

Table 4.6.1 Magnetic moments for complexes 26-31 in solid state

| Complex | $\mu_{\text{eff}}/\mu_{\text{B}}$ (T) |
|-----------|---|
| 26 | 1.3 (2K), 1.73(20K), 1.78(290K) |
| 27 | 1.41(2K), 1.82(20K), 1.85(290K) |
| 28 | 1.73(2K), 1.80-1.81(20-290K) |
| 29 | 1.69(2K), 2.45(10K), 2.60(100K), 2.66(290K) |
| 30 | 1.84(2K), 2.07(100K), 2.54(290K) |
| 31 | 1.79(10K), 1.84(100K), 2.30(290K) |

Simulations of magnetic data yield, $g_{\text{Cu}} = 2.06$ ($\theta = -1.34\text{K}$) for **26**, $g_{\text{Cu}} = 2.13$ ($\theta = -0.968\text{K}$) for **27** and $g_{\text{Cu}} = 2.085$ (TIP = 150×10^{-6} emu, $\theta = -0.107\text{K}$) for **28**.

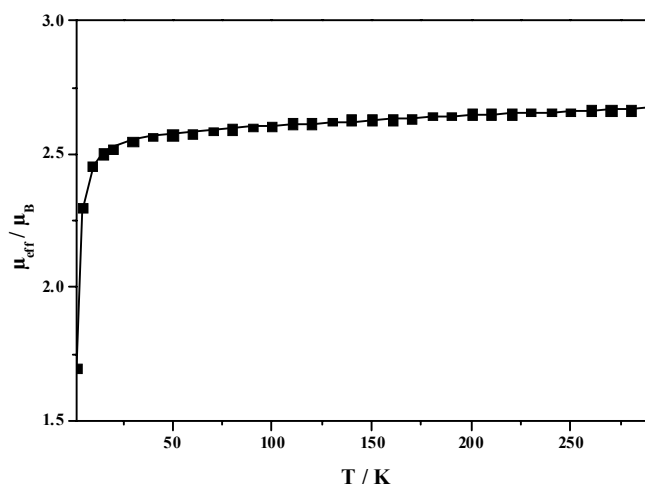


Figure 4.6.1 Magnetic measurements for complex 29.

In contrast, solid **29** displays a temperature dependent magnetic moment /dimer of $2.50 \pm 0.1 \mu_B$ in the range 290-30 K, which then drops to $1.69 \mu_B$ at 2 K. By using the Heisenberg, Dirac, van Vleck spin Hamiltonian $\hat{H} = -2J\hat{S}_1 \cdot \hat{S}_2$ ($S_1 = S_2 = 1/2$), the magnetic data have been fitted satisfactorily, taking into account exchange coupling and Zeeman splitting (full-matrix diagonalization approach). A small intramolecular antiferromagnetic exchange coupling of $J = -1.3 \text{ cm}^{-1}$ ($g = 2.103$ and $TIP = 207 \times 10^{-6} \text{ emu}$) has been established, in accord with its dimeric structure in the solid state

A number of studies have reported symmetric and asymmetric trinuclear copper complexes in order to model the structure and physical properties of the entire trinuclear metal site in multicopper oxidase.³⁻⁹ Complexes **30** and **31** can be placed in the class of asymmetric trinuclear Cu(II) complexes with $\mu\text{-OH}$ and $\mu\text{-OMe}$ bridging.

The room temperature magnetic moments of 2.54 and $2.30 \mu_B$ for complexes **30** and **31**, respectively, are considerably smaller than the expected value ($3.0 \mu_B$) for three coupled Cu(II) ions, and they decrease gradually upon cooling. This is characteristic of significant antiferromagnetic interactions between Cu(II) ions with the trinuclear complex, as shown in the Figure 4.6.3. The results indicate that there is a strong antiferromagnetic spin-exchange interaction among the nearest Cu(II) ions within each molecule.

Two different models can be considered to fit the experimental magnetic data. One model considers all the interaction having three J values different from each other. Another one uses two J values, where J_3 is not considered.

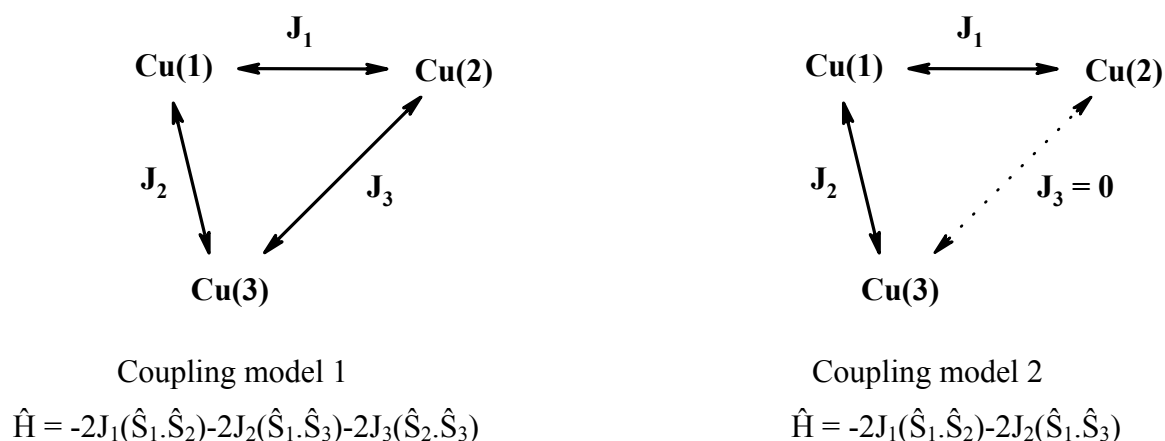


Figure 4.6.2 Schematic diagram of the exchange coupling in trinuclear complexes **30** and **31**.

Using the model 1, data for complex **30** were fitted giving $J_1 = -198 \text{ cm}^{-1}$, $J_2 = -100 \text{ cm}^{-1}$ and $J_3 = -46 \text{ cm}^{-1}$ ($g = 2.06$ and $TIP = 180 \times 10^{-6} \text{ emu}$), not very different from those obtained using model 2 ($J_1 = -181 \text{ cm}^{-1}$, $J_2 = -134 \text{ cm}^{-1}$, $g = 2.05$, $TIP = TIP = 180 \times 10^{-6} \text{ emu}$). This clearly shows that there is very little or no magnetic interaction between Cu(2) and Cu(3), in

accord with the crystal structure (absence of bridged bonding between them). So coupling model 2 is more realistic in terms of bond connectivities and exchange pathway.

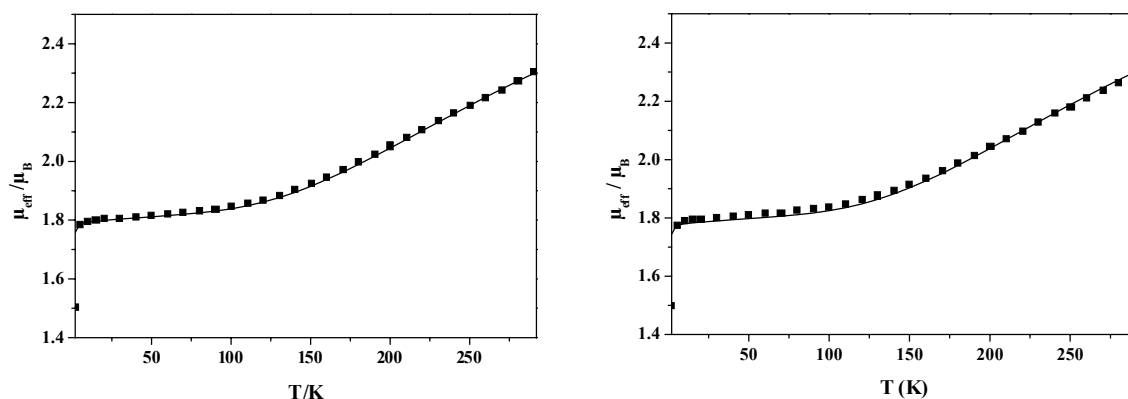


Figure 4.6.3 Plot of μ_{eff} (per Cu_3) vs temperature for complex **30**. The solid line was calculated using model 1 (left) and model 2 (right).

Similarly, using the model 2 fitting results are $J_1 = -275 \text{ cm}^{-1}$, $J_2 = -182 \text{ cm}^{-1}$ and $J_3 = 0$ ($g = 2.086$, $\text{TIP} = 180 \times 10^{-6} \text{ emu}$) for **31**.

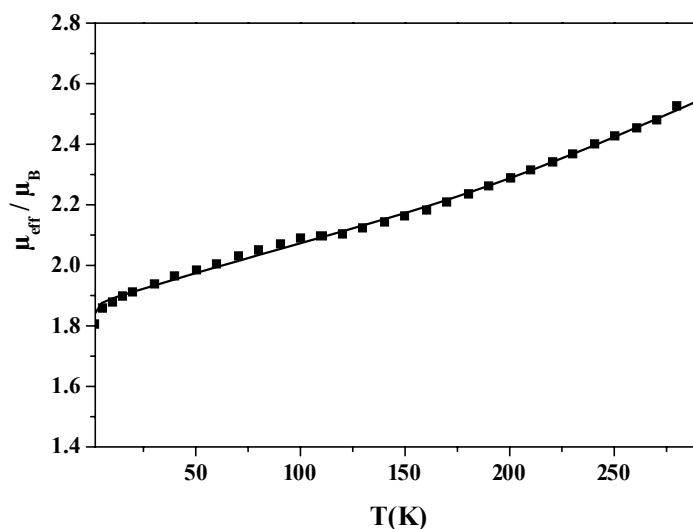


Figure 4.6.4 Plot of μ_{eff} (per Cu_3) vs temperature for complex **31**.

Both complexes thus show an $S = \frac{1}{2}$ ground state with moderate exchange coupling between neighbouring Cu(II) ions and are comparable.

4.7 EPR SPECTROSCOPY

The X-band EPR spectra of the complexes were recorded both in solution and in solid state. As an example for the series of mononuclear Cu(II) complexes **26-28**, the spectrum of **26** has been recorded in frozen CH_2Cl_2 solution at 10 K (Figure 4.7.1) which displays the typical features of a tetragonally distorted Cu(II) complex with $(d_x^2 - y^2)^1$ electronic configuration. Simulation of the spectrum yielded parameters $g_x = 2.03$, $g_y = 2.11$, $g_z = 2.23$, $A_x = 0.26 \times 10^{-4}$, $A_y = 19.18 \times 10^{-4}$ and $A_z = 136.73 \times 10^{-4} \text{ cm}^{-1}$. This proves the monomeric nature of the complex and is consistent with an $S = \frac{1}{2}$ ground state. Similar spectra are anticipated for **27** and **28**.

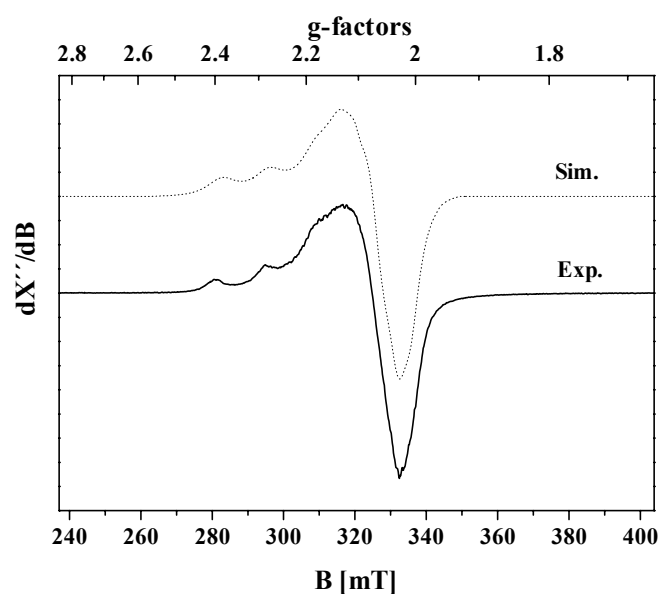


Figure 4.7.1 X-band EPR spectrum of complex **26** in CH_2Cl_2 at 9.9 K. Experimental conditions (—): microwave frequency 9.43 GHz, microwave power 6.4 μW , modulation amplitude 10 G. The simulations (----): $g = \{2.0324, 2.1089, 2.2299\}$; $A = \{0.26, 19.18, 136.73\} \times 10^{-4} \text{ cm}^{-1}$; Lorentzian line with angular-dependent line width $W = \{68, 70, 122\} \text{ G}$.

In contrast, the EPR spectrum of **29**, a dinuclear Cu(II) complex recorded as polycrystalline solid, is governed by a resonance at $g \sim 2.0$, with copper hyperfine splittings due to two Cu(II) sites ($I = 3/2$), resulting in seven resolved hyperfine lines, and, in addition, a half-field signal at $g \sim 4.0$ ($\Delta M_S = 2$). This clearly indicates the dinuclear nature of the complex with a diamagnetic ground state. In CH_2Cl_2 solution, complex **29** also displays $\Delta M_S = 1$ resonance below $g = 2$ (350-420 mT) and the characteristic half-field signal at $g \sim 4.0$ ($\Delta M_S = 2$), together with copper hyperfine splitting. This does indicate that the complex exists as dimer also in solution.

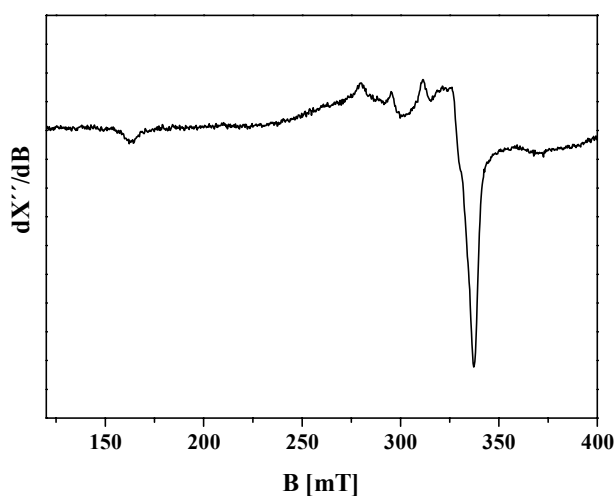


Figure 4.7.2 X-band EPR spectrum of complex **29** in CH_2Cl_2 at 10.5 K. Experimental conditions (—): microwave frequency 9.45 GHz, microwave power 1.0 μW , modulation amplitude 16 G.

The EPR spectrum for **30** in solid-state at 2.7 K shows an axial signal centered near $g = 2$, typically of a tetragonally distorted copper environment and consistent with an $S = \frac{1}{2}$ ground state. Simulation of the spectrum gives parameters $g_x = 2.05$, $g_y = 2.10$, $g_z = 2.21$, $A_{xx} = 18.6 \times 10^{-4} \text{ cm}^{-1}$, $A_{yy} = 11.4 \times 10^{-4} \text{ cm}^{-1}$ and $A_{zz} = 125.5 \times 10^{-4} \text{ cm}^{-1}$.

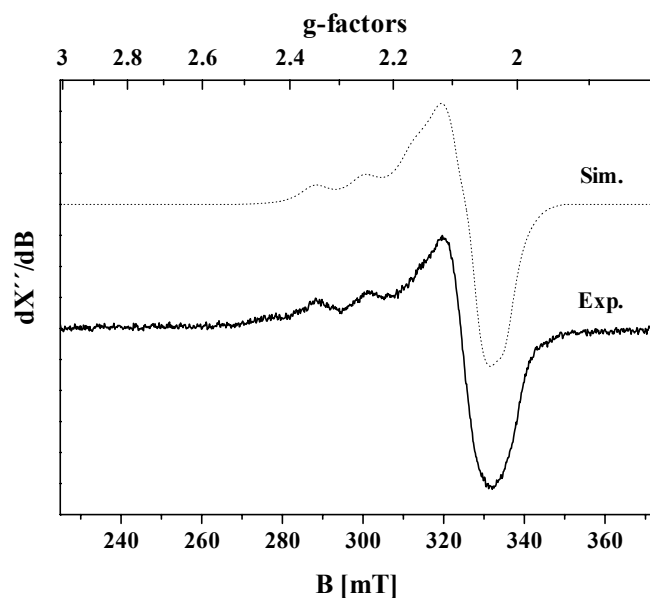


Figure 4.7.3 X-band EPR spectrum of complex **30** in solid state at 2.7 K. Experimental conditions (—): microwave frequency 9.47 GHz, microwave power 0.2 μW , modulation amplitude 12 G. The simulations (----): $g = \{2.045, 2.101, 2.21\}$; $A = \{18.6, 11.4, 125.5\} \times 10^{-4} \text{ cm}^{-1}$; Lorentzian line with angular-dependent line width $W = \{80, 67, 110\} \text{ G}$.

Similarly, in CH_2Cl_2 solution at 2.6 K, complex **30** displays features of a tetragonally distorted Cu(II) complex with clear copper hyperfine splitting. Simulation of the spectrum yields parameters, $g_x = 2.04$, $g_y = 2.09$, $g_z = 2.24$, $A_{xx} = 0.25 \times 10^{-4} \text{ cm}^{-1}$, $A_{yy} = 12.7 \times 10^{-4} \text{ cm}^{-1}$ and $A_{zz} = 140 \times 10^{-4} \text{ cm}^{-1}$, typical of a mononuclear Cu(II) complex with an $S = \frac{1}{2}$ ground state.

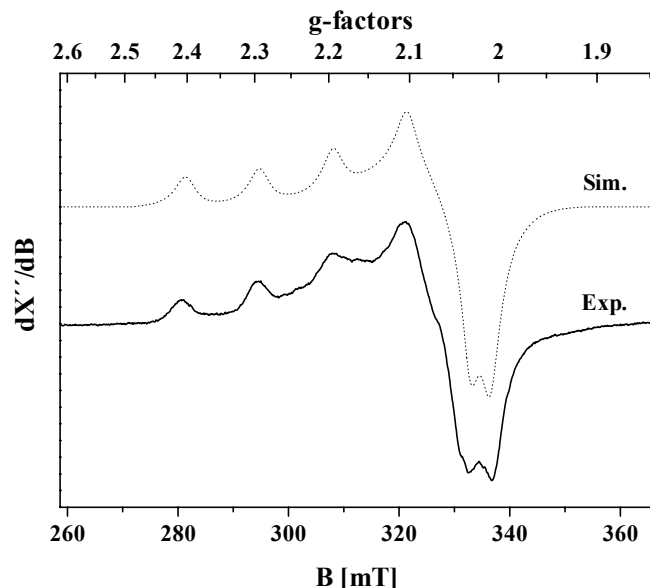


Figure 4.7.4 X-band EPR spectrum of complex **30** in CH_2Cl_2 at 2.6 K. Experimental conditions (—): microwave frequency 9.46 GHz, microwave power 3.2 μW , modulation amplitude 6 G. The simulations (----): $g = \{2.035, 2.087, 2.242\}$; $A = \{0.25, 12.7, 140\} \times 10^{-4} \text{ cm}^{-1}$; Lorentzian line with angular-dependent line width $W = \{45, 150, 53\} \text{ G}$.

4.8 REACTIVITY STUDIES

It has already been discussed in the early part of this chapter that trinuclear species **31** forms a modified ligand containing dinuclear Cu(II) complex **32** in a solvent mixture of CH_2Cl_2 and MeCN in air. Formation of a new species is also clearly seen from the time-dependent spectral change passing through an isosbestic point.

In addition to that, complex **31** in CH_2Cl_2 reacts with 2,4-di-*tert*-butylphenol to oxidize it to the coupled product, biphenol. It is believed that the dinuclear Cu(II) phenoxyl diradical produced in this system couple with free phenoxyl radical formed *in situ* to give the modified Cu(II) dimer, **32**. Formation of the diradical species is reported for the ligand system $\text{H}_2\text{L}^{\text{S}}$.^{1a} Free phenoxyl radical is formed by the self-decomposition of the complex and reaction on

ligand. Detection of biphenol also indicates the formation of phenoxyl radical *in situ* during this transformation.

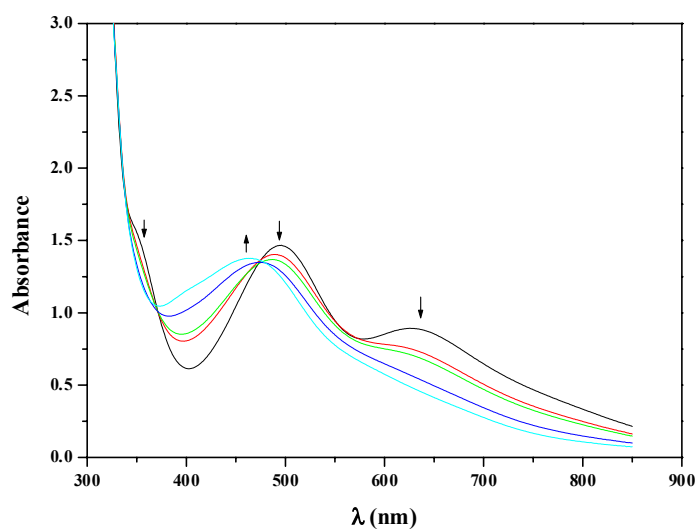
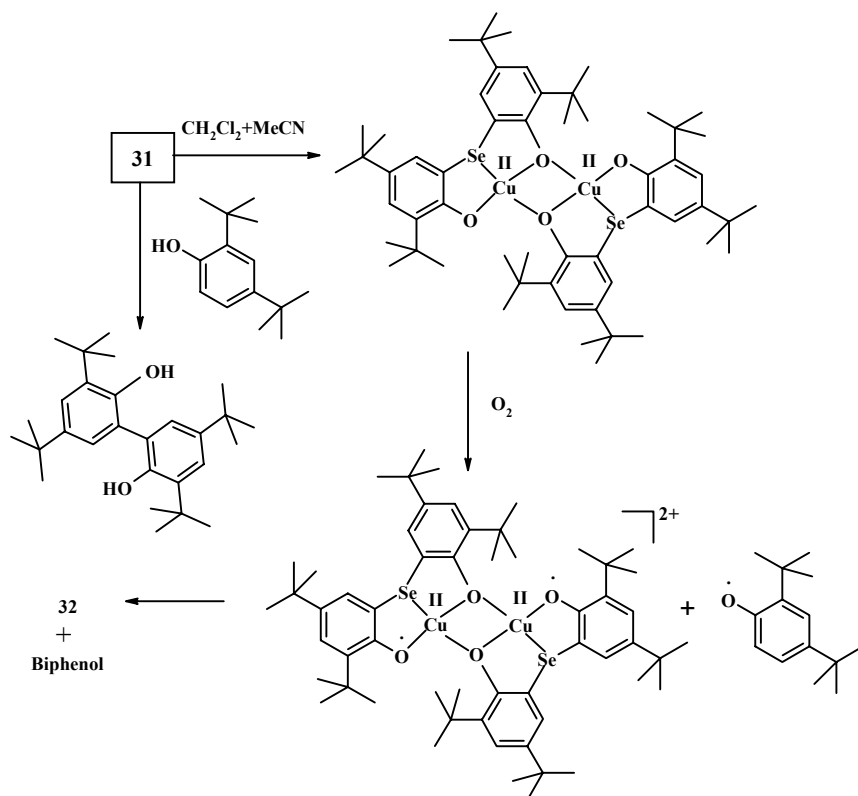


Figure 4.8.1 UV-Vis spectral change with time for complex **31** in CH_2Cl_2 .

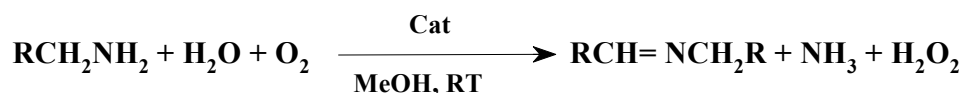
All these results clearly show that the system undergoes transformation to generate very reactive phenoxyl radical species, as is evidenced from the typical radical mediated reactions.



Scheme 4.8.1 Reactivity of trinuclear complex **31**.

4.8.1 Catalytic oxidation of primary amines

Primary amines with at least one α -H atom undergo oxidative deamination reaction in the presence of Cu(I) salt and ligand H_2L^{Se} . It has been shown in scheme 4.2.1 that Cu(II) complexes containing such amines (e.g. benzylamine) are very reactive under air. Conversion of primary amines to the corresponding carbonyl compounds or their Schiff base condensation product under such reactions conditions is catalytic in nature.



Scheme 4.8.1.1 Catalytic amine oxidation reaction.

In a standardized experimental set-up the catalyst was generated in the following fashion: To a mixture of CuCl and ligand H_2L^{Se} (1:1; 2.5 mM) in dry MeOH (50 ml) under argon atmosphere were added the corresponding primary amines (125 mM) (Benzylamine or α -methylbenzylamine or dibenzylamine or cyclohexylamine). The resulting solution was stirred at $22 \pm 1^\circ\text{C}$ for 24 h in an open vessel in the presence of air. The product were then quantitatively analysed for organic products by GC-MS using an internal standard, NH_3 was detected qualitatively. H_2O_2 was not detected in the reaction solution, may be because of decomposition by Cu(II) complex showing catalase activity. The uptake of O_2 was also measured volumetrically. The turnover number (TON) was then determined as the number of mole of product per mole of catalyst. When the substrate is benzylamine only the organic product benzylidenebenzylamine was detected, with 17 turnovers. Similar Schiff-base products were observed for dibenzylamine and cyclohexylamine. On the other hand, acetophenone was detected as the only oxidation product of α -methylbenzylamine with 10 turnovers.

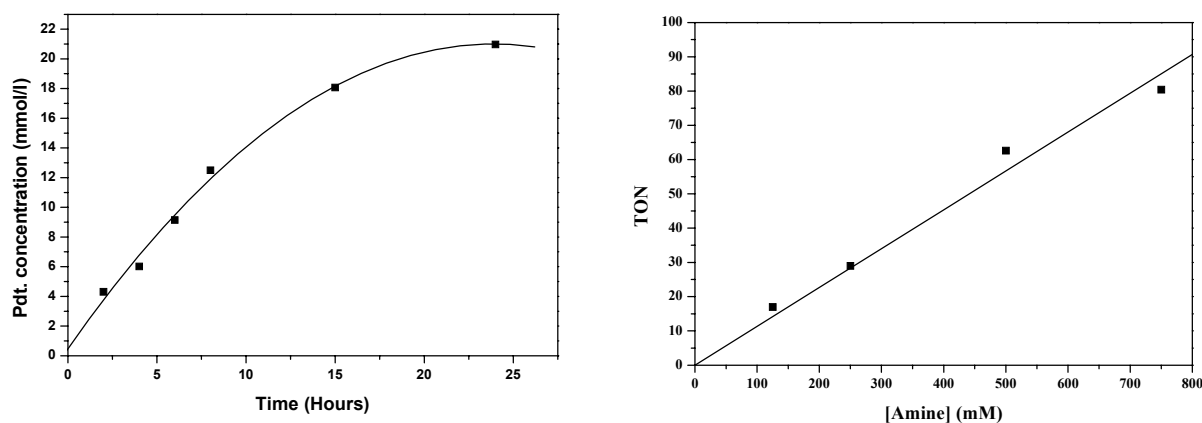
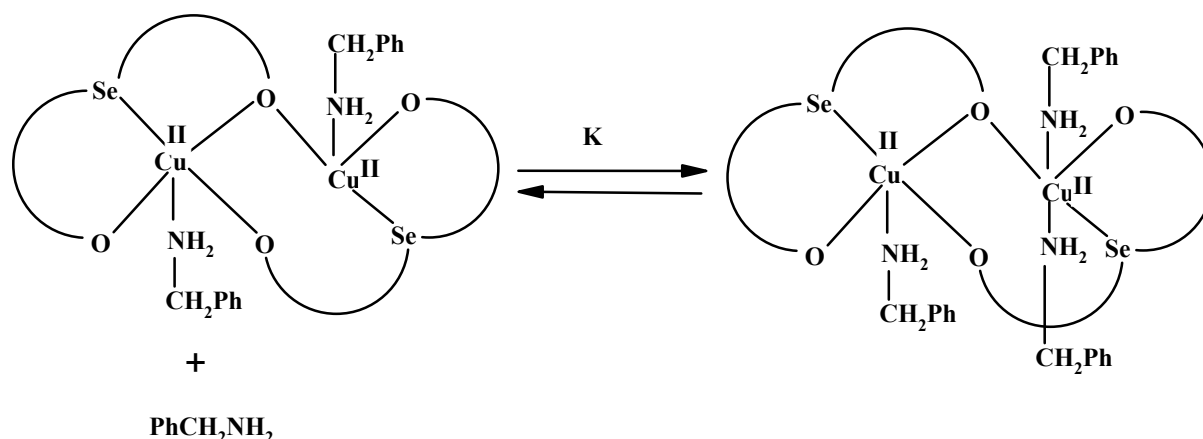


Figure 4.8.1.1 Kinetic data for amine oxidation.

The kinetics of the catalytic oxidative deamination of primary amines have been measured by variation of the total concentration of $[\text{CuCl}]$, $\text{H}_2\text{L}^{\text{Se}}$ (1.25 mM-6.25 mM) and $[\text{amine}]$ (125 mM-750mM) under 1 bar of air in MeOH. Water does not coordinate to any intermediate in the catalytic cycle, and has no influence on the rate of the reaction. From all these data a rate law was deduced:

$$\text{Rate} = k[\text{catalyst}][\text{amines}]$$

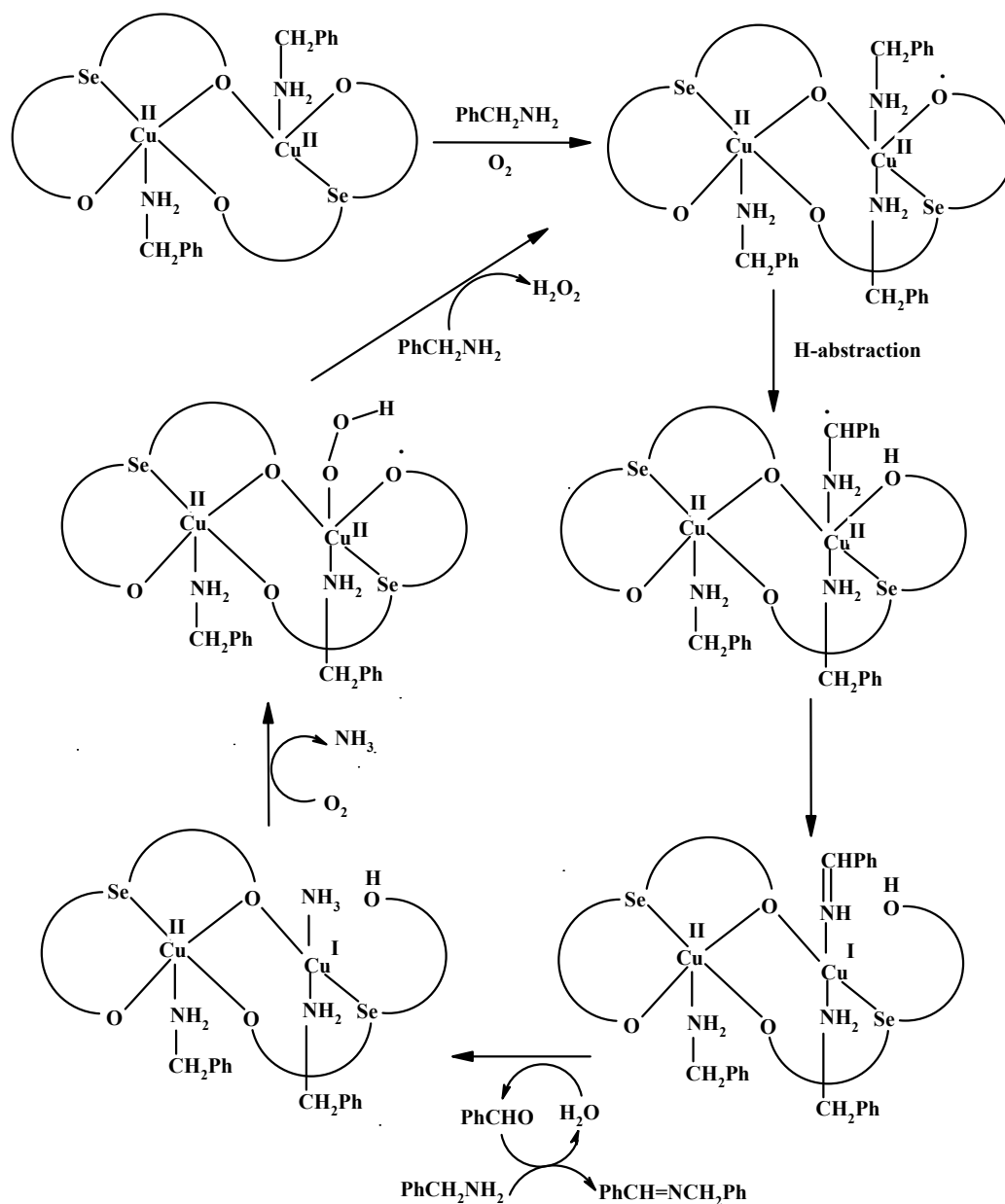
From the UV-vis and EPR spectra of the solution during benzylamine oxidation it is clear that the dinuclear Cu(II) complex, **29** is formed in the solution. It is believed that the complex does participate in the catalytic cycle after coordination to another molecule of benzylamine. The observed first order dependence on both the copper and amine concentrations implies that the four-coordinated Cu(II) center of the dimer binds a substrate amine molecule with formation of a five coordinate intermediate. Although higher amine concentrations were used, no saturation kinetics was observed. This implies that the binding constant K is small.



*Scheme 4.8.1.2 Binding of substrate amine molecule to dimer, **29**.*

By using at the α -carbon selectively deuterated benzylamine as substrate, $\text{C}_6\text{H}_5\text{CD}_2\text{NH}_2$, a kinetic isotope effect (KIE) under turnover conditions of 4 at $22 \pm 1^\circ\text{C}$ has been determined. This implies that in the above five-coordinate intermediate H atom abstraction from the α -carbon atom of the coordinated benzylamine represents the rate-determining step of the deamination reaction.

From all these results the mechanism for this oxidative deamination reaction can be proposed as follows:

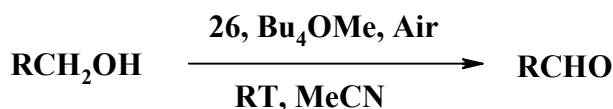


Scheme 4.8.1.3 Proposed mechanism for benzylamine oxidation.

This model thus represents the first example of a functional model for the metalloenzyme, copper amine oxidases.

4.8.2 Catalytic oxidation of primary alcohols

Mononuclear Cu(II) complex **26** in combination with base (Bu₄NOMe) in MeCN catalytically oxidizes primary alcohols to the corresponding aldehydes with moderate to high turnover numbers. This oxidation can also be performed in neat alcohol (e.g., benzyl alcohol) with base (BuLi). The only organic product observed is the aldehyde.



Scheme 4.8.2.1 Aerial oxidation of primary alcohols catalysed by Cu(II) complex, 26.

In a standardized experimental set-up the catalyst was generated in the following fashion: To a mixture of alcohol (2M) and base (40 mM Bu₄NOMe, 20% methanolic solution) in dry MeCN (10 ml) under an argon atmosphere was added the complex (2mM). The resulting green solution was then opened and stirred at 22±1°C for 24 h in an open vessel in the presence of air. The formation of aldehyde product with time was determined by taking samples at different times. For benzyl alcohol the oxidation process continues up to 10 h and then the product formation saturates. The final products were quantitatively analysed for organic products by GC-MS, using internal standard. The turnover number (TON) was then determined as the number of mole of product per mole of complex. When the substrate is benzyl alcohol the organic product benzaldehyde (100%) was detected with 95 turnovers. With substrate cinnamyl alcohol, cinnamaldehyde was detected with 27 turnovers under the same reaction conditions.

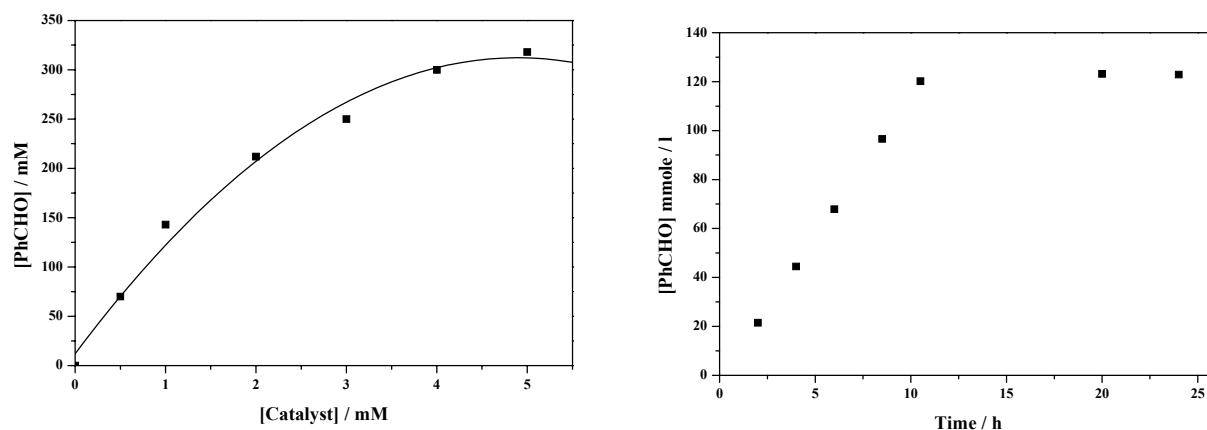


Figure 4.8.2.1 Kinetic data for alcohol oxidation.

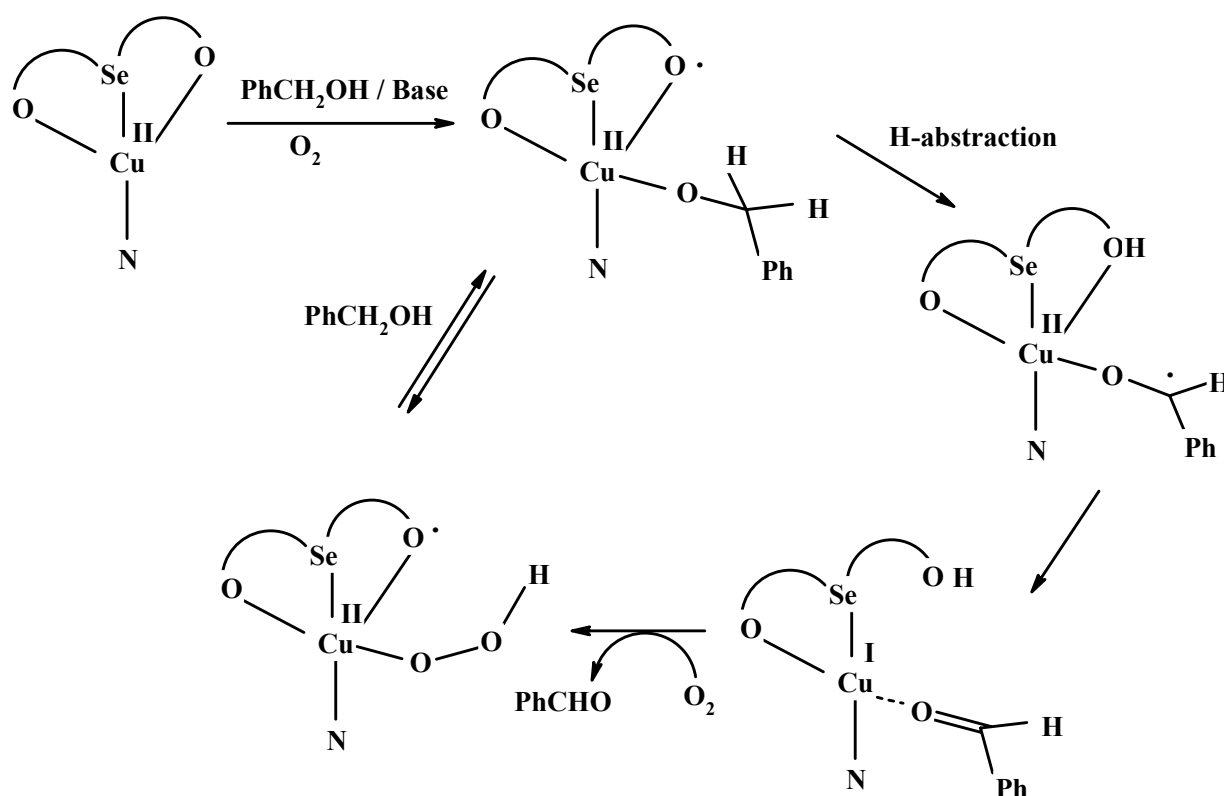
The kinetics of the catalytic alcohol oxidation has been measured by variation of total concentration of [complex] (0.5-5 mM) and [alcohols] under 1 bar of air in MeCN. From all these data a rate law was deduced:

$$\text{Rate} = k[\text{catalyst}][\text{alcohols}]$$

By using at the alpha-carbon selectively deuterated benzyl alcohol as substrate, C₆H₅CD₂OH, a kinetic isotope effect (KIE) under turnover conditions of 8.5 at 22±1°C has been

determined. This implies that H-atom abstraction from the α -carbon atom of the coordinated benzyl alcohol represents the rate-determining step of the oxidation reaction.

From all these results the mechanism for the alcohol oxidation reaction can be proposed. The mechanism is very similar to that proposed for the enzyme galactose oxidase² and a number of functional model systems.¹ It involves binding of an alcoholate ligand to the complex with formation of the phenoxyl radical species, and H-atom transfer from the alpha-carbon atom of the coordinated alcoholate ligand in the rate-determining step, with formation of a bound ketyl radical anion, which reduces in an intramolecular one-electron transfer step the Cu(II) to Cu(I) ions and formation of aldehydes. Reoxidation of the reduced catalyst with O₂ regenerates the active catalyst.



Scheme 4.8.2.2 Proposed mechanism for alcohol oxidation.

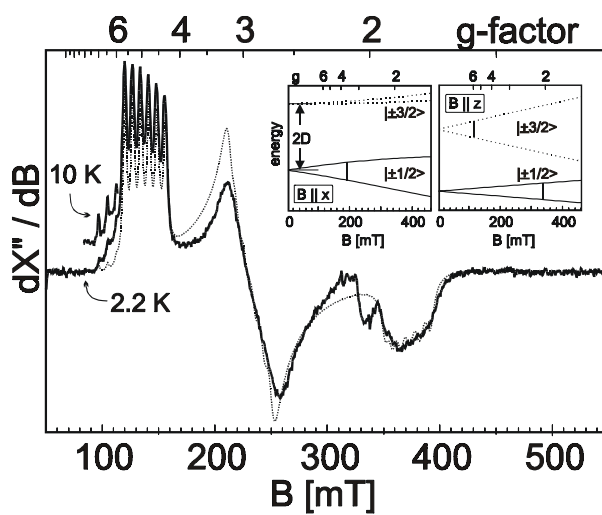
This system thus can model the functional aspect of galactose oxidase by activating small organic substrate molecules and undergoing H-atom abstraction.

References

1. (a) P. Chaudhuri, M. Hess, U. Flörke, K. Wieghardt, *Angew. Chem., Int. Ed.* **1998**, *37*, 2217. (b) P. Chaudhuri, M. Hess, T. Weyhermüller, K. Wieghardt, *Angew. Chem., Int. Ed.* **1999**, *38*, 1095. (c) P. Chaudhuri, M. Hess, J. Müller, K. Hildenbrand, E. Bill, T. Weyhermüller, K. Wieghardt, *J. Am. Chem. Soc.* **1999**, *121*, 9599. (d) Y. Wang, J. L. DuBois, B. Hedman, K. O. Hodgson, T. D. P. Stack, *Science* **1998**, *279*, 537. (e) F. Thomas, G. Gellon, I. G.-Luneau, E. S.-Aman, J.-L. Pierre, *Angew. Chem. Int. Ed.* **2002**, *41*, 3047.
2. J. W. Whittaker, in *Metal Ions in Biological Systems*, H. Siegel, A. Siegel, Eds; Marcel Dekker: New York, **1994**; Vol 30, p 315.
3. (a) R. Becket, B. F. Hoskins, *J. Chem. Soc., Dalton Trans.* **1972**, 291. (b) R. J. Butcher, C. J. O'Connor, E. Sinn, *Inorg. Chem.* **1981**, *20*, 537. (c) F. B. Huisbergen, R. W. M. Ten Hoedt, G. C. Verschoor, J. Reedijk, A. L. Spek, *J. Chem. Soc., Dalton Trans.* **1983**, 539. (d) J. P. Costes, F. Dahan, J. P. Laurent, *Inorg. Chem.* **1986**, *25*, 413. (e) Y. Angus, R. Louis, B. Metz, C. Bouden, J. P. Gisselbrecht, M. Gross, *Inorg. Chem.* **1991**, *30*, 3155. (f) P. Chaudhuri, M. Winter, B. P. C. Della Vedova, E. Bill, A. Trautwein, S. Gehring, P. Fleisschhauer, B. Nuber, J. Weiss, *Inorg. Chem.* **1991**, *30*, 2148. (g) S. Meenakumari, A. R. Chakravarty, *J. Chem. Soc., Dalton Trans.* **1992**, 2749. (h) D. Christodoulou, C. George, L. K. Keefer, *J. Chem. Soc., Chem. Commun.* **1993**, 937. (i) P. J. van Konings-bruggen, J. W. van Hal, R. A. G. de Graaf, J. G. Reedijk, *J. Chem. Soc., Dalton Trans.* **1993**, 2163.
4. K. D. Karlin, Q.-F. Gan, A. Farooq, S. Liu, J. Zubieta, *Inorg. Chem.* **1990**, *29*, 2549.
5. P. Chaudhuri, I. Karpenstein, M. Winter, C. Butzlaff, E. Bill, A. X. Trautwein, U. Flörke, H.-J. Haupt, *J. Chem. Soc., Chem. Commun.* **1992**, 321.
6. D. E. Fenton, H. Osaka, *J. Chem. Soc., Dalton Trans.* **1993**, 1349.
7. H. Adams, N. A. Bailey, M. J. S. Dwyer, D. E. Fenton, P. C. Hellier, P. D. Hempstead, J. M. Latour, *J. Chem. Soc., Dalton Trans.* **1993**, 1207.
8. S. Meenakumari, S. K. Tiwary, A. R. Chakravarty, *Inorg. Chem.* **1994**, *33*, 2085.
9. L. Spiccia, B. Graham, M. T. W. Hearn, G. Lazarev, B. Moubaraki, K. S. Murray, E. R. T. Tiekink, *J. Chem. Soc., Dalton Trans.* **1997**, 4089.

Chapter 5

TRANSITION METAL COMPLEXES OF AN AMINE BISPHENOL LIGAND WITH [O, N, O] DONOR SET



5.1 INTRODUCTION

This chapter deals with the study of a tridentate ligand containing O, N, O-donor set with an aim to scrutinize the effect of chelate ring size on the ligating properties of H_2L^N in comparison to those described in the previous chapters. The ligand H_2L^N (Methylamino-N,N-bis(2-methylene-4,6-dimethylphenol)) is depicted below.

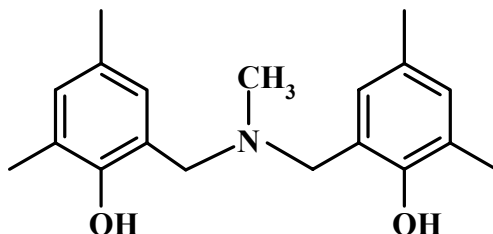
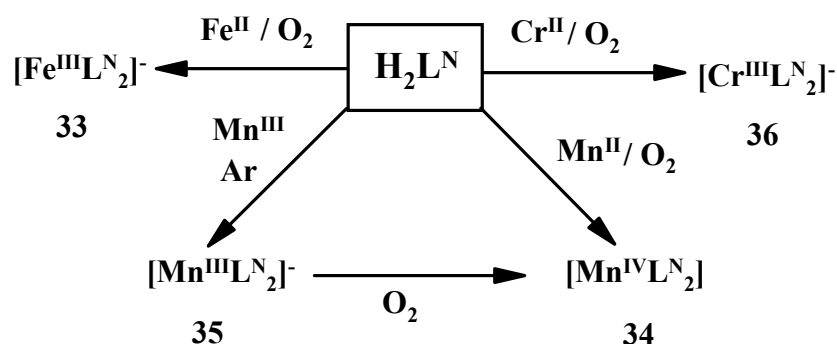


Figure 5.1.1 Structure of ligand H_2L^N .

This chapter additionally deals with two isoelectronic $[CrL^N_2]^-$ and $[MnL^N_2]$ complexes with distinctive metal-ligand covalent binding characteristics as probes for comparison of EPR-spectroscopic properties. This ligand exhibits diversified coordination properties with different transition metals. The non-oxo vanadium(IV) and polynuclear Ni(II) complexes of this ligand have already been discussed in chapters 2 and 3, respectively.

5.2 SYNTHESIS

Different transition metal complexes of H_2L^N were synthesized by the reaction of metal salts and the ligand in suitable ratio according to Scheme 5.2.1 in relatively high yield.



Scheme 5.2.1 Synthesis of complexes with ligand H_2L^N .

The mononuclear bisligand complexes $[\text{ML}^{\text{N}}_2]^{-/0}$ were easily isolated and characterized by different methods. Oxidation of the manganese center directly to the Mn(IV) species $[\text{MnL}^{\text{N}}_2]$, proceeds easily in the presence of air, indicating that the complexation by the tridentate ligand containing two phenolate oxygens effectively stabilizes an enigmatic oxidation state Mn(IV). That the mononuclear $[\text{Mn}^{\text{III}}\text{L}^{\text{N}}_2]^-$ species would be susceptible to air-oxidation is also evident from the electrochemical results.

5.3 INFRARED SPECTROSCOPY

IR spectra for complexes **33** - **36** are given in the experimental section. The peaks which convey most informations are those due to $\nu(\text{OH})$ which occur as broad peaks in the region $3200 - 3400 \text{ cm}^{-1}$. For the free ligand there is a strong peak at 3404 cm^{-1} present before complexation. This band is missing in complexes **33** - **36**, indicating that on complexation the phenol-character of the ligand has been lost. There are several peaks in the region $3000 - 2800 \text{ cm}^{-1}$ due to the methyl groups together with the other $\nu(\text{C-H})$, $\nu(\text{C}=\text{C})$ and $\nu(\text{C-O})$ vibrations found in the normal range for these types of linkages.¹

5.4 MASS SPECTROSCOPY

Mass spectrometry in the EI and ESI mode has been proved to be a very useful analytical tool for characterization of the complexes, and also provides identification of the metal centres, and, in general, the compositions are consistent with elemental analyses. Interestingly, EI-MS for **34** did not provide much useful information. On the contrary, mass spectrometry in ESI-positive mode in CH_2Cl_2 exhibits the strongest peak at m/z 649 for **34**, as expected, confirming the Mn:L ratio of 1:2, which is also consistent with the elemental analysis. In addition, a weak peak at m/z 1001 corresponding to $\text{Mn}_2\text{L}^{\text{N}}_3$ is also observed for **34**. Mass spectrometry in ESI mode in MeCN for **33**, **35**, and **36** does not leave any doubt about the compositions of **33**, **35** and **36**. Two single peaks, one at m/z 242 (in positive mode) and the other at m/z 650 or 649 or 646, (in negative mode) with the expected isotope distribution pattern, correspond to $[\text{Bu}_4\text{N}]^+$ and $[\text{FeL}^{\text{N}}_2]^-$ or $[\text{MnL}^{\text{N}}_2]^-$ or $[\text{CrL}^{\text{N}}_2]^-$ species, respectively, thus confirming the formulation $[\text{Bu}_4\text{N}][\text{ML}^{\text{N}}_2]$ with $\text{M} = \text{Fe}$ **33**, Mn **35**, Cr **36**.

5.5 ELECTRONIC SPECTROSCOPY

The optical spectra for complexes **33-36** (Figure 5.5.1) have been measured in the range 300 - 1000 nm. The bands are likely to be of charge-transfer origin, as judged by their high absorption coefficients.²

Table 5.5.1 UV-Vis spectral data for complexes 33-36 in CH₂Cl₂ solution

| Complex | λ , nm (ϵ , M ⁻¹ cm ⁻¹) |
|-----------|--|
| 33 | 447 (5356) |
| 34 | 505 (7944), 352 (10938) |
| 35 | 644 (460), 427 (4222), 980 (249) |
| 36 | 707 (11), 568 (138), 400sh (142) |

The bands at 707 nm ($\epsilon = 11 \text{ M}^{-1} \text{ cm}^{-1}$), 568 nm ($\epsilon = 138 \text{ M}^{-1} \text{ cm}^{-1}$) and 400sh ($\epsilon \sim 142 \text{ M}^{-1} \text{ cm}^{-1}$) for **36** are ascribed to the d-d transition of the chromium(III) ion. The weak absorption at 707 nm ($11 \text{ M}^{-1} \text{ cm}^{-1}$) is attributable to the spin-flip $^4\text{A}_2 \rightarrow ^2\text{E}$ transitions of a d^3 configuration in an octahedral field. Thus the ligand-field strength of the aminobisphenol ligand with 17610 cm^{-1} (568 nm) is comparable with that of H₂O.³ For the ground term A_2 for the chromium(III) ion, the "mixing in" effect of the terms with the same spin multiplicity is expressed by the formula

$$g = 2.0023 - \frac{8\lambda}{10Dq}$$

where λ is the spin-orbit coupling constant for the terms involved and $10 Dq$ is the energy separating the interacting terms. For **36**, $10 Dq = 17610 \text{ cm}^{-1}$ and $\lambda = 92 \text{ cm}^{-1}$ ⁴, yield $g = 1.98$, which is identical with the g -value obtained from the simulation of the magnetic susceptibility data and the EPR spectrum in solution. This is not uncommon for chromium(III) complexes in distorted cubic crystal fields.⁵

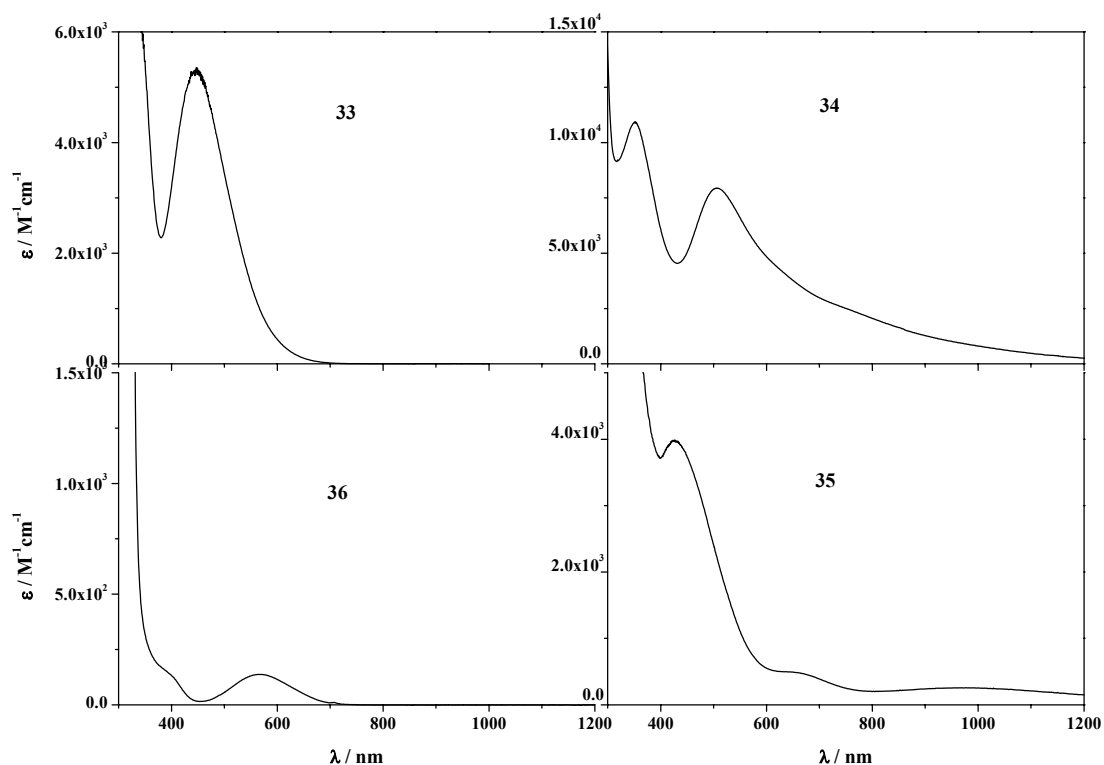


Figure 5.5.1 Optical spectra for complexes **33–36** in CH_2Cl_2 solution at room temperature.

5.6 X-RAY CRYSTAL STRUCTURE

5.6.1 Molecular structure of $[\text{Mn}^{\text{IV}}\text{L}^{\text{N}}_2]$ (**34**)

Single crystals of deep violet *mer*-trans(N,N)- $[\text{MnL}^{\text{N}}_2]\cdot\text{MeCN}$ **34** were obtained from MeCN solution by slow evaporation. As no substantial differences in bond lengths and angles are found between the two crystallographically non-equivalent molecules, only one ORTEP diagram for the structure of compound **34** is displayed in Figure 5.6.1, while selected bond lengths and angles are summarized in Table 5.6.1.

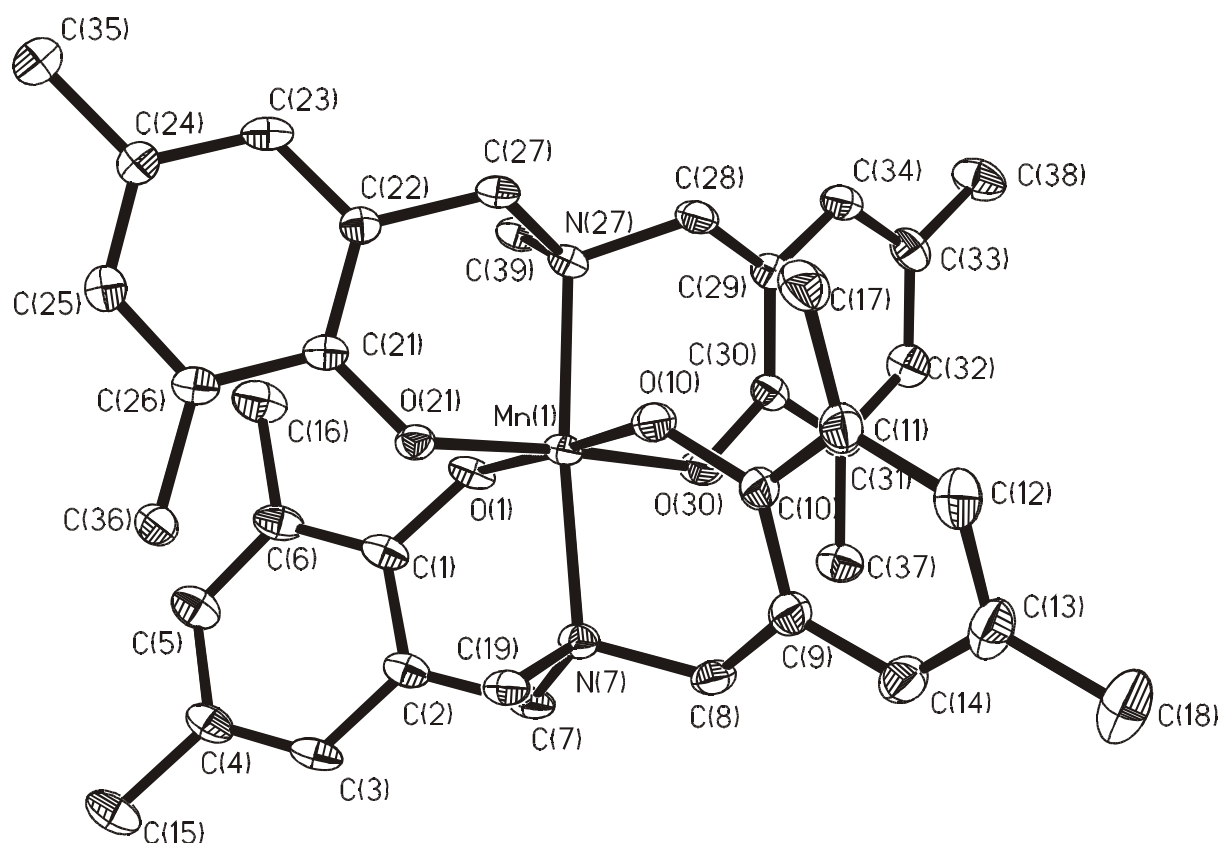


Figure 5.6.1 ORTEP and atom labeling scheme for $[Mn^{IV}L^N_2](34)$.

Table 5.6.1 Selected bond lengths (\AA) and angles (deg) for $[Mn^{IV}L^N_2](34)$

| | | | |
|-------------------|------------|-------------------|------------|
| Mn(1)-O(30) | 1.867(3) | O(21)-C(21) | 1.345(4) |
| Mn(1)-O(21) | 1.870(3) | O(30)-C(30) | 1.337(5) |
| Mn(1)-O(10) | 1.875(3) | O(10)-C(10) | 1.349(5) |
| Mn(1)-O(1) | 1.890(3) | O(1)-C(1) | 1.349(5) |
| Mn(1)-N(27) | 2.100(3) | | |
| Mn(1)-N(7) | 2.101(3) | | |
| O(30)-Mn(1)-O(21) | 176.10(11) | O(30)-Mn(1)-O(10) | 93.61(13) |
| O(21)-Mn(1)-O(10) | 86.85(11) | O(30)-Mn(1)-O(1) | 90.07(13) |
| O(21)-Mn(1)-O(1) | 89.50(12) | O(10)-Mn(1)-O(1) | 176.30(12) |
| O(30)-Mn(1)-N(27) | 90.02(12) | O(21)-Mn(1)-N(27) | 93.87(12) |
| O(10)-Mn(1)-N(27) | 88.60(12) | O(1)-Mn(1)-N(27) | 91.06(12) |
| O(30)-Mn(1)-N(7) | 85.87(12) | O(21)-Mn(1)-N(7) | 90.29(12) |
| O(10)-Mn(1)-N(7) | 87.16(12) | O(1)-Mn(1)-N(7) | 93.45(12) |
| N(27)-Mn(1)-N(7) | 173.89(13) | | |
| Mn(2)-O(41) | 1.869(3) | O(41)-C(41) | 1.354(5) |
| Mn(2)-O(61) | 1.875(3) | O(50)-C(50) | 1.341(5) |
| Mn(2)-O(50) | 1.874(3) | O(61)-C(61) | 1.345(5) |
| Mn(2)-O(70) | 1.894(3) | O(70)-C(70) | 1.343(5) |
| Mn(2)-N(67) | 2.098(3) | | |
| Mn(2)-N(47) | 2.101(3) | | |

| | | | |
|-------------------|------------|-------------------|------------|
| O(41)-Mn(2)-O(61) | 90.56(12) | O(41)-Mn(2)-O(50) | 176.85(12) |
| O(61)-Mn(2)-O(50) | 86.30(12) | O(41)-Mn(2)-O(70) | 90.59(12) |
| O(61)-Mn(2)-O(70) | 177.87(12) | O(50)-Mn(2)-O(70) | 92.55(12) |
| O(41)-Mn(2)-N(67) | 91.45(13) | O(61)-Mn(2)-N(67) | 92.53(12) |
| O(50)-Mn(2)-N(67) | 88.83(12) | O(70)-Mn(2)-N(67) | 89.23(13) |
| O(41)-Mn(2)-N(47) | 93.00(13) | O(61)-Mn(2)-N(47) | 90.93(13) |
| O(50)-Mn(2)-N(47) | 86.92(12) | O(70)-Mn(2)-N(47) | 87.22(13) |
| O(67)-Mn(2)-N(47) | 174.33(13) | | |

The overall geometry around the manganese ion Mn(1) is best described as a distorted meridional octahedron with two *trans* positioned nitrogens N(7) and N(27) of the amine bisphenolate ligand L^N . The doubly deprotonated ligand, $[O^{\wedge}N^{\wedge}O]^{2-}$ is bound in a meridional manner, the facial mode being sterically unavailable. All the phenyl rings attached to the phenolate oxygen atoms are found to be planar, indicating that upon coordination the aromaticity of the phenyl ring is retained. The small distortion from octahedral geometry is mainly caused by the acute bite angles between the phenolate O atom and the N atom of the $[ONO]^{2-}$ ligand: N(7)-Mn(1)-O(10) 87.16(12), N(7)-Mn(1)-O(30) 85.87(12) $^{\circ}$. The O(30)-Mn(1)-O(21) and O(10)-Mn(1)-O(1) angles are 176.10(10) and 176.30(12) $^{\circ}$, respectively, while the corresponding N(27)-Mn(1)-N(7) angle at 173.89(13) $^{\circ}$ deviates slightly from linearity. All the C-O bond lengths found in compound **34** are unremarkable, average 1.345(5) Å. The planarity of the MnO_4 fragment is exceedingly good; the maximum deviation from the mean plane is 0.0277 (molecule 1) and 0.0163 (molecule 2) Å (Mn). The average Mn-O and Mn-N distances of 1.877(3) and 2.100(3) Å fall in the range reported for the structurally characterized mononuclear manganese(IV) complexes but significantly shorter than the isostructural Mn(III) congener (**35**) found in the complex $[MnL^N_2]^{-}[(tacn)_2Mn_2(\mu-OAc)_3]^{+}$.^{6f}

5.6.2 Molecular structure of $[Mn^{III}L^N_2]^{-}$ unit (**35**)

As the structural parameters for $[Mn^{III}L^N_2]^{-}$ are obtained from the structural characterization of $[(tacn)_2Mn_2(\mu-OAc)_3][MnL^N_2]$, the x-ray structure determination of **35** was not performed. The ORTEP diagram of the anionic unit is shown in Figure 5.6.2 and the selected bond parameters are listed in Table 5.6.2.

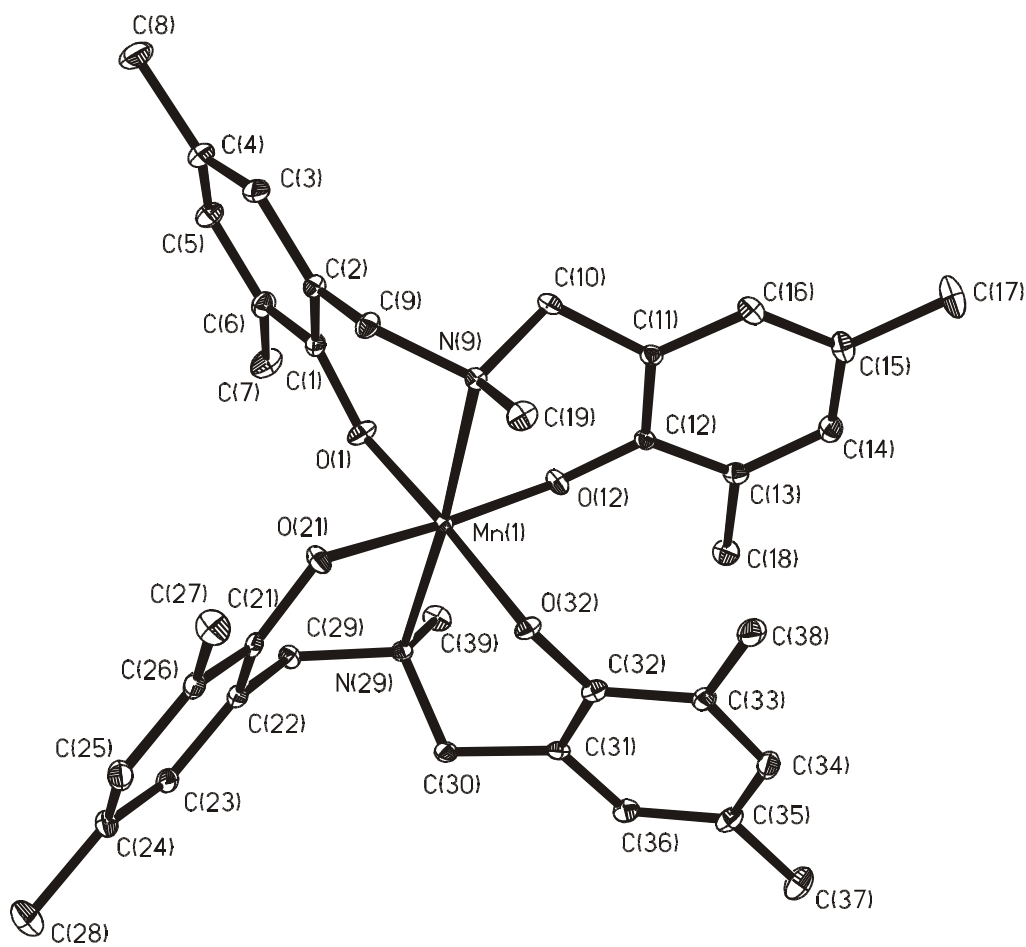


Figure 5.6.2 ORTEP and atom labeling scheme for $[Mn^{III}L^N_2]^-$ (**35**).

Table 5.6.2 Selected bond lengths (\AA) and angles (deg) for $[Mn^{III}L^N_2]^-$ (**35**)

| | | | |
|-------------------|-----------|-------------------|------------|
| Mn(1)-O(12) | 1.913(2) | O(1)-C(1) | 1.318(4) |
| Mn(1)-O(1) | 1.919(2) | O(12)-C(12) | 1.326(3) |
| Mn(1)-O(32) | 1.920(2) | O(32)-C(32) | 1.340(4) |
| Mn(1)-O(21) | 1.926(2) | O(21)-C(21) | 1.328(4) |
| Mn(1)-N(9) | 2.317(2) | | |
| Mn(1)-N(29) | 2.322(3) | | |
| O(12)-Mn(1)-O(1) | 87.52(10) | O(12)-Mn(1)-O(32) | 92.35(9) |
| O(1)-Mn(1)-O(32) | 175.80(9) | O(12)-Mn(1)-O(21) | 176.50(10) |
| O(1)-Mn(1)-O(21) | 89.96(10) | O(32)-Mn(1)-O(21) | 90.33(10) |
| O(12)-Mn(1)-N(9) | 89.34(9) | O(1)-Mn(1)-N(9) | 87.64(9) |
| O(32)-Mn(1)-N(9) | 96.56(9) | O(21)-Mn(1)-N(9) | 88.13(9) |
| O(12)-Mn(1)-N(29) | 92.24(9) | O(1)-Mn(1)-N(29) | 88.14(9) |
| O(32)-Mn(1)-N(29) | 87.66(9) | O(21)-Mn(1)-N(29) | 90.10(9) |
| N(29)-Mn(1)-N(9) | 175.43(9) | | |

Structurally this unit is different from the neutral Mn(IV) complex, **34**. The manganese ion is in a facial octahedral environment with two trans positioned nitrogens N(9) and N(29) of the ligand. N(9)-Mn(1)-N(29) angle at 175.43(9)° deviates slightly from linearity making a small distortion from octahedral geometry. That complex **35** shows average Mn-O and Mn-N distances of 1.920(2) Å and 2.320(2) Å with Jahn-Teller elongation along N-Mn-N direction confirms the oxidation state of manganese to be high-spin d^4 Mn(III). By comparing that complex with those of a d^3 Mn(IV) complex it is clearly evident that shortening of bonds occurs with higher oxidation state which corroborates also with the EPR measurements.

5.6.3 Molecular structure of $\text{Bu}_4\text{N}[\text{Cr}^{\text{III}}\text{L}^{\text{N}}_2]$ (**36**)

The lattice consists of discrete $[\text{Bu}_4\text{N}]^+$ and $[\text{Cr}^{\text{III}}\text{L}^{\text{N}}_2]^-$ ions. A Ball and Stick drawing of the anion in **36** with atom labeling scheme is shown in Figure 5.6.3. Selected bond parameters are listed in Table 5.6.3.

Each ligand acts as a meridional ONO donor. The angles within the coordination sphere, CrN_2O_4 are very close to an ideal octahedron. The ranges of *cis* and *trans* angles at the chromium center Cr(1) are 87.3(3) - 93.4(3) and 175.9(3) - 177.7(3)°, respectively. The CrO_4 fragment is within experimental error, planar deviation being 0.0105 Å; the planarity of N(8)O(15)N(28)O(1) and of N(8)O(21)N(28)O(35) is also good: the maximum deviation from the mean plane is 0.0086 and 0.0128 Å (Cr1). The salicylaldimine fragment, e.g., O(35)C(35)C(30)C(29)N(28) chelate ring, is folded along the O(35)N(28) line - the fold angle being 89.7°.

Complex **36**, being one of the structurally characterized numerous bis(homoleptic) chromium(III) complexes,⁷ does not warrant any special discussion. As expected the average distances Cr-O = 1.948(20) Å and Cr-N = 2.132(20) Å are significantly longer than the corresponding bond lengths in complex **34** containing the isoelectronic but +IV charged manganese center. The bond lengths and angles in the cation $[\text{Bu}_4\text{N}]^+$ of **36** seem reasonable and are comparable with the reported values.⁸

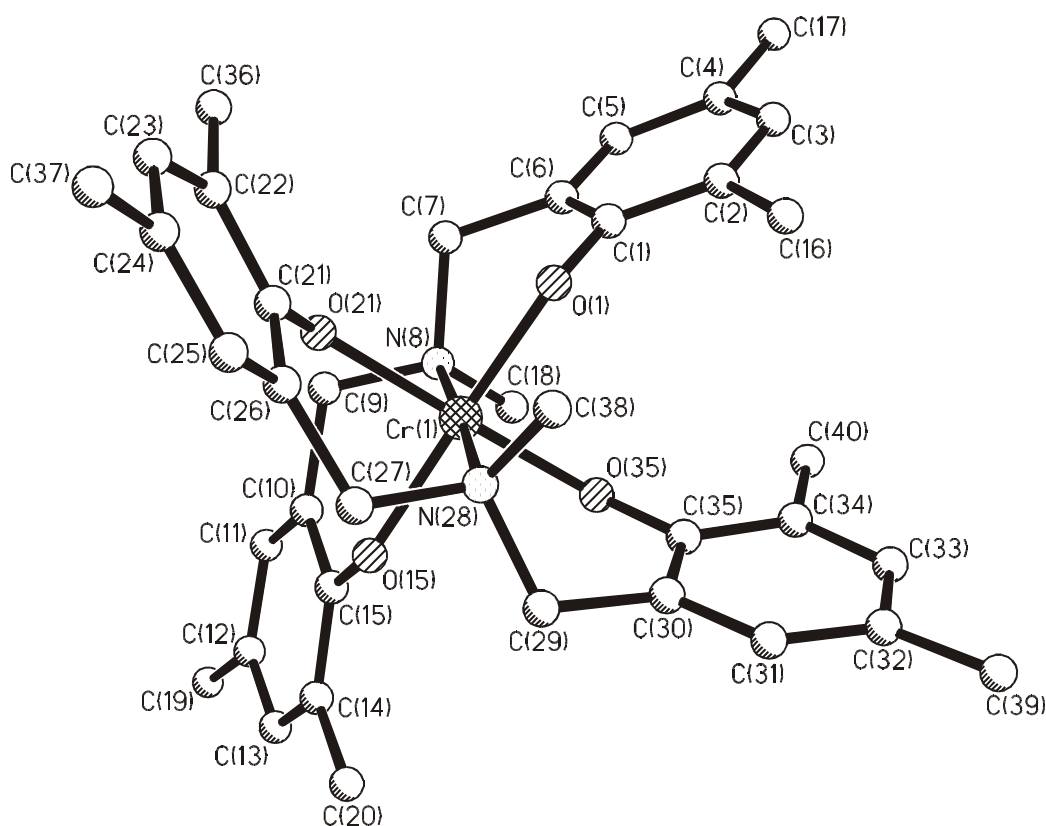


Figure 5.6.3 Ball and Stick diagram and atom labeling scheme for $[\text{Cr}^{\text{III}}\text{L}_2]^-$ (**36**).

Table 5.6.3 Selected bond distances (\AA) and angles (deg) for $[\text{Bu}_4\text{N}][\text{Cr}^{\text{III}}\text{L}_2]$ (**36**)

| | | | |
|-------------------|----------|-------------------|-----------|
| Cr(1)-O(35) | 1.928(5) | C(1)-O(1) | 1.336(11) |
| Cr(1)-O(1) | 1.943(5) | C(21)-O(21) | 1.316(12) |
| Cr(1)-O(21) | 1.958(6) | C(35)-O(35) | 1.347(10) |
| Cr(1)-O(15) | 1.961(6) | | |
| Cr(1)-N(8) | 2.113(9) | | |
| Cr(1)-N(28) | 2.151(8) | | |
| O(35)-Cr(1)-O(1) | 89.3(2) | O(35)-Cr(1)-O(21) | 177.0(3) |
| O(1)-Cr(1)-O(21) | 90.0(2) | O(35)-Cr(1)-O(15) | 90.8(3) |
| O(1)-Cr(1)-O(15) | 175.9(3) | O(21)-Cr(1)-O(15) | 90.1(2) |
| O(35)-Cr(1)-N(8) | 89.1(3) | O(1)-Cr(1)-N(8) | 93.4(3) |
| O(21)-Cr(1)-N(8) | 88.0(3) | O(15)-Cr(1)-N(8) | 90.6(3) |
| O(35)-Cr(1)-N(28) | 91.8(3) | O(1)-Cr(1)-N(28) | 88.7(3) |
| O(21)-Cr(1)-N(28) | 91.1(3) | O(15)-Cr(1)-N(28) | 87.3(3) |
| N(8)-Cr(1)-N(28) | 177.7(3) | | |

5.7 ELECTROCHEMISTRY

The electrochemical properties of complexes **33**, **34**, **35** and **36** in CH_2Cl_2 solutions were investigated by voltametric methods (Cyclic Voltammetry, CV, and square wave voltammetry, SQW). The cyclic voltammograms of **34** and **35** are identical, which shows that the two species are electrochemically interconvertible. Linear sweep experiments in stirred solution reveal that the interconversion takes place at -0.645 V, where **35** is oxidized and **34** is reduced, i.e. the redox wave at that potential is manganese-centered.

From Figure 5.7.1 and Table 5.7.1 it is seen that the anionic complexes **33** and **36** exhibit redox processes at moderately negative potentials (at -0.205 V and -0.375 V vs. Fc^+/Fc), which are oxidations according to linear sweep experiments in stirred solutions. The redox potentials of **33** and **36** are similar, irrespective of the nature of the central metal ion. Therefore we assign these oxidations to be ligand-based, i.e. oxidation of phenolate to phenoxyl radical.

*Table 5.7.1 Redox potentials in V vs. Fc^+/Fc at the respective total charges of complexes **33** - **36**, observed in CV and SQW experiments in CH_2Cl_2 solutions*

| Complex/ | 3+ / 2+ | 2+ / 1+ | + / 0 | 0 / 1- | 0 / 1- | 1- / 2- |
|---------------|----------|---------|---------|----------|----------|----------|
| Charge | lig.ox. | lig.ox. | lig.ox. | lig.ox. | met.cen. | met.cen. |
| 33 | --- | --- | --- | - 0.205* | --- | - 2.108 |
| 34, 35 | + 0.930* | + 0.647 | + 0.447 | --- | - 0.645 | --- |
| 36 | + 0.804 | + 0.619 | + 0.321 | - 0.375 | --- | --- |

* CV peak potentials for irreversible processes.

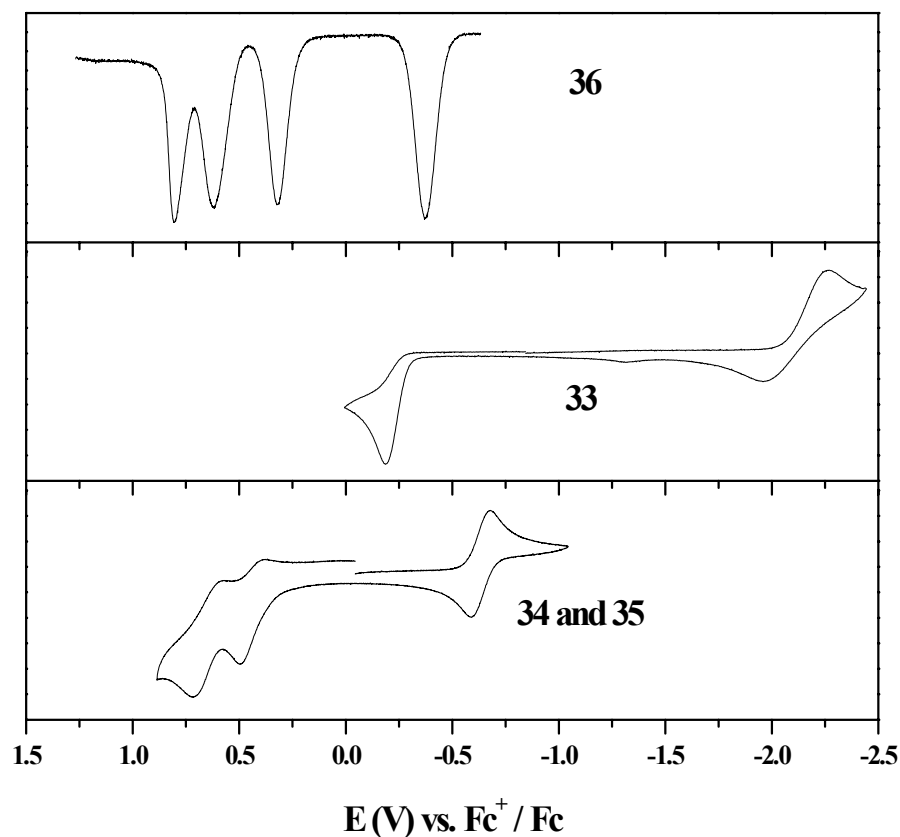


Figure 5.7.1 Cyclic and square wave voltammograms (CV, SQW) of complexes **33-36** in CH_2Cl_2 solution containing $\sim 10^{-3}$ M substance and 0.1 M Bu_4NPF_6 [scan rate: 0.2 V s^{-1} (CV), 30 Hz (SQW)]. Working electrode, 2 mm glassy carbon, counter electrode Pt, reference electrode Ag/AgNO_3 and referenced vs. Fc^+/Fc added as internal standard after each set of experiments.

In Figure 5.7.1 the (metal-centered) reductive waves of the Fe^{III} complex at potentials < -1 V are displayed. They are reversible, but broad and with peak potential separations strongly depending on the scan rate in a way, which is characteristic for slow heterogeneous electron transfer kinetics. It is evident from Figure 5.7.1 that the oxidation and first reduction of the monoanionic Fe^{III} complex **33** is shifted against each other to a similar extent (1.0 V). Complexes **34** and **35** are neutral at potentials > -0.645 V, and they show an oxidation at exactly the same potential (+0.447 V), which is therefore also assigned to the phenoxyl radical formation. The same applies to the oxidation of the neutral form of **36** (i.e. its second oxidation), which has a similar redox potential (+0.321 V).

Likewise, the second oxidation of the manganese complex **34** and the third oxidation of the chromium complex **36**, which both originate from monocations, are again very similar (+0.727 V and +0.797 V) and are, therefore, thought to be due to phenoxyl radical formation. Hence it appears that all oxidations (with exception of the 0/- redox process of **35**, where oxidation of manganese is easier than that of the phenolate) represent ligand-centered phenoxyl radical formations from phenolates. The corresponding redox potentials are practically solely determined by the total charge of the complexes and are almost independent of the nature of the central metal ion (Table 5.7.1).

With increasing potentials more oxidations occur, most readily detected with **36** where a fourth oxidation was found, which is sufficiently reversible on the time scale of the voltammetric experiments to allow a redox potential determination. Table 5.7.1 lists the redox potentials, including two peak potentials of irreversible oxidation waves.

5.8 MAGNETISM

Magnetic susceptibility data for polycrystalline samples of complexes **33** - **36** were collected in the temperature range 2 - 290 K in an applied magnetic field of 1 T. We start our discussion with the magnetic properties of the mononuclear complexes $[\text{Bu}_4\text{N}][\text{Fe}^{\text{III}}\text{L}^{\text{N}}_2]$ **33**, $[\text{Bu}_4\text{N}][\text{Mn}^{\text{III}}\text{L}^{\text{N}}_2]$ **35**, $[\text{Mn}^{\text{IV}}\text{L}^{\text{N}}_2]$ **34** and $[\text{Bu}_4\text{N}][\text{Cr}^{\text{III}}\text{L}^{\text{N}}_2]$ **36**. Above $T \approx 10$ K complexes **33**, **35**, **34** and **36** (Figure 5.8.1) exhibit essentially temperature independent μ_{eff} values of 5.91 ± 0.01 , 4.83 ± 0.01 , 3.80 ± 0.02 and 3.87 ± 0.02 μ_{B} , respectively. Thus magnetic measurements of **33** and **35** show unambiguously that **33** and **35** contain a d^5 h.s. ion, i.e. Fe(III) and a d^4 h.s. ion, i.e. Mn(III), respectively.

Simulations of the experimental magnetic moment data yield $g_{\text{Fe}} = 2.00$ for **33** and $g_{\text{Mn}} = 1.975$ for **35**. There are three unpaired electrons on Mn(IV) in **34** and Cr(III) in **36** and the "spin-only" ($g = 2.00$) magnetic moment is $3.87 \mu_{\text{B}}$. The experimental μ_{eff} values clearly indicate that we are dealing with genuine Mn(IV) **34** and Cr(III) **36** species, in complete agreement with X-ray and EPR results. Simulations of the experimental magnetic moment data yield $g_{\text{Mn}} = 1.97$, $\text{TIP} = 50 \times 10^{-6} \text{ cm}^3 \text{ mol}^{-1}$ for **34** and $g_{\text{Cr}} = 1.98$, $\text{TIP} = 116 \times 10^{-6} \text{ cm}^3 \text{ mol}^{-1}$ for **36**. Simulated TIP (Temperature Independent Paramagnetism) for **36** is in well agreement with the calculated TIP of $118.6 \times 10^{-6} \text{ cm}^3 \text{ mol}^{-1}$ according to equation:

$$\text{TIP} = 8N\beta^2/10Dq \quad [\beta = 0.261 \text{ cm}^{-1}]$$

by using 10 Dq-value of 17610 cm^{-1} evaluated from the optical absorption spectrum.

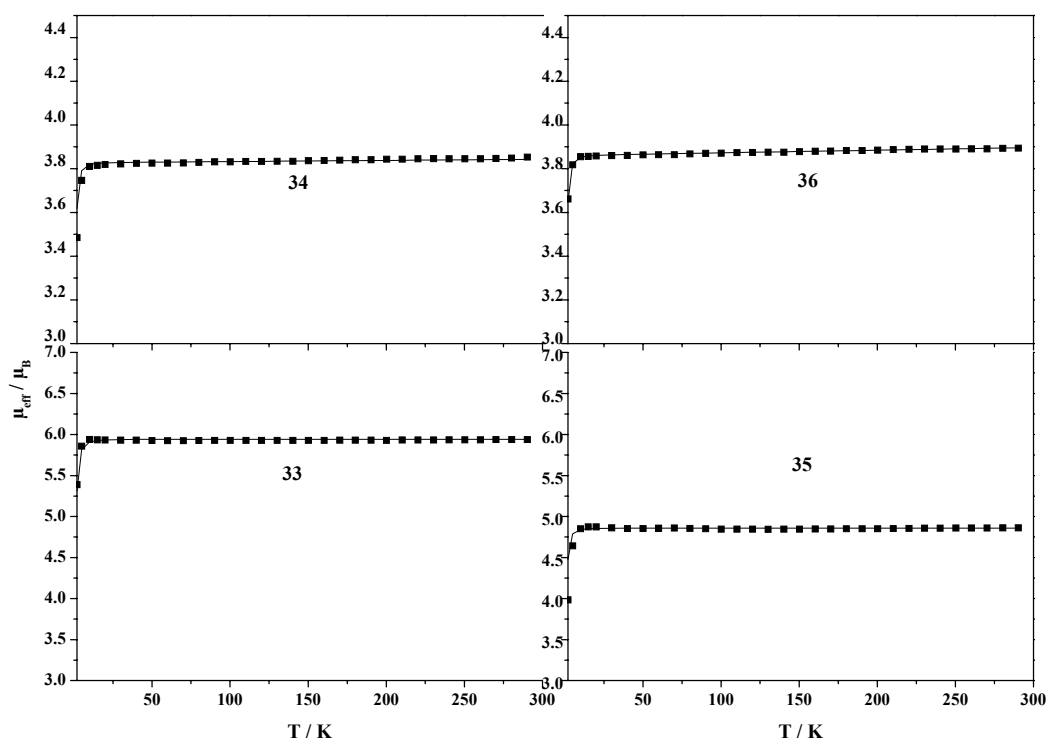


Figure 5.8.1 Magnetic measurements for complexes **33-36**.

5.9 EPR SPECTROSCOPY

X-band EPR spectra of the Mn(IV) and Cr(III) compounds **34** and **36** could be obtained from frozen solutions of the materials. Figure 5.9.1 presents the low-temperature derivative spectra of **34** in CH₂Cl₂-toluene (1:2), and of **36** in CH₂Cl₂-toluene (1:2) and in MeCN. Both compounds show dominant signals at $g \approx 3-6$ and $g \approx 2$. The appearance of the spectra depends partly on the nature of the solvent used. Whereas the Mn(IV) complex in CH₂Cl₂-toluene shows well resolved sextets of the characteristic ⁵⁵Mn hyperfine lines ($I = 5/2$), the Cr(III) spectrum appears to be fairly broad in different solvents. The EPR spectra of both complexes are $S = 3/2$ powder pattern from spin multiplets with moderately strong zero-field splitting (ZFS, $D \geq h\nu$) close to the limit of energetically well isolated Kramers doublets (KD).^{9,10} In a first interpretation the distinct g_{\perp} signals at $g \approx 5$ and $g \approx 3$ which are best observed for **34**, can be assigned to the powder resonances of the $|m_s = \pm 1/2\rangle$ KD for fields along the molecular y- and x-direction, respectively. The trough at $g \approx 2$ originates from the z-resonances of $|m_s = \pm 1/2\rangle$ as indicated in the inset in Figure 5.9.1. The splitting of the g_{\perp}

signals around $g_{\perp} = 4$ reflects a deviation from axial ZFS according to a rhombicity parameter $E/D \approx 0.1-0.2$. Significant population of the $|m_s = \pm 3/2\rangle$ KD is indicated by the presence of distinct low-field hyperfine lines seen at $g \approx 6$, which also originate from fields in z-direction. Their weak intensity results from the wide field range of the respective powder absorption spectrum that extends to resonance fields above 0.6 T ($g_x, g_y \approx 1$, hardly measurable in the field-swept derivative spectrum because of excessive line widths). The temperature dependence of the intensity ratio of the resolved lines at $g_z \approx 6$ ($|\pm 3/2\rangle$) and $g_y \approx 5$ ($|\pm 1/2\rangle$), which was recorded in the range 1.8 K - 12 K, shows clear ground state properties of $|\pm 1/2\rangle$ resonances (not depicted) according to revealed positive ZFS ($D > 0$).

The basic interpretation of the spectrum **34** could be further substantiated by spin-Hamiltonian simulations based on the following equation:

$$H = D [S_z^2 - S(S+1)/3 + (E/D)(S_x^2 - S_y^2)] + \mu_B \mathbf{B} \cdot \mathbf{g} \cdot \mathbf{S} + \mathbf{S} \cdot \mathbf{A} \cdot \mathbf{I}$$

The result is shown as thin dotted line in Figure 5.9.1 (left) and the parameters obtained from the fit are $D = 1.6(\pm 0.4) \text{ cm}^{-1}$, $E/D = 0.172(\pm 0.01)$, $g = 1.99$ and $A = (67, 67, 74) \times 10^{-4} \text{ cm}^{-1}$. The resolved features of the experimental spectra are well reproduced in the simulation, whereas the overall intensity distribution is partly deviating due to the presence of broad shoulders, which were found to be somewhat preparation-dependent. We assume that some contributions of the experimental spectrum are considerably broadened by g-strain and distributions of ZFS parameters. A more detailed discussion of this feature is given below for the spectra of **36**. Particularly the $g_z \approx 6$ signals from $|\pm 3/2\rangle$ appear to be enhanced relatively to the $g_{\perp} = 3-6$ signals from $|\pm 1/2\rangle$ which, however, reflects more an effective attenuation of the $|\pm 1/2\rangle$ derivative lines. A selective broadening of the $|\pm 1/2\rangle$ derivative lines is plausible from a consideration of the corresponding rhombogram⁹ for $S = 3/2$ which shows that the $g_{x,y}$ ($|\pm 1/2\rangle$) resonances of the lower KD are much more E/D-dependent than the $g_z(|\pm 1/2\rangle)$ resonances of the upper KD. In the simulations the amplitude of the $g = 6$ contribution cannot be explained by any positive or negative D value without such a broadening. Nevertheless, the presence of g_z ($|\pm 3/2\rangle$) signals in the simulated spectra and their temperature dependence provides an estimate for the upper limit of the D parameter. Furthermore, a lower limit is derived from the resonance position of the g_z ($|\pm 1/2\rangle$) signals since low D values lead to level mixing within the spin quartet with the consequence of up-field shift of the trough at $g \approx 2$, which is not observed in experiment.

The spectra of compound **36** obtained in different solvents deviate considerably from what is expected for typical $S = 3/2$ spectra with large ZFS (Figure 5.9.1, right). This is partly due to lower D values compared to **34**, which induces level mixing of KD's and inter-doublet

transitions at higher fields. The major ‘distortion’, however, results from a distribution of E/D as could be shown by corresponding simulations (thin dotted lines). The theoretical spectra are superpositions of a series of powder spectra with different E/D values, which are sampled from a Gaussian distribution with half-width (E/D). Similar behavior was previously described for other $S = 3/2$ spectra measured from an $[4\text{Fe-4S}]^{1+}$ cluster with $S = 3/2$ ground state¹¹ or for mixed-metal cubane cluster of the type $[3\text{FeV-4S}]^{2+}$.¹² There it was argued that the origin of the variations in the rhombicity might be found in modulations of the molecule conformations induced by micro-heterogeneity of the environment. Although, the spectra of **36** recorded in MeCN and CH_2Cl_2 -toluene show significantly different appearances, they virtually have identical spin-Hamiltonian parameters, which differ mainly in the widths of their E/D-distributions. Thus, we trust that the average spin-Hamiltonian parameters for **36** $D = 0.5(\pm 0.4) \text{ cm}^{-1}$, $E/D = 0.23(\pm 0.01)$, $g = 1.98$ are of general validity.

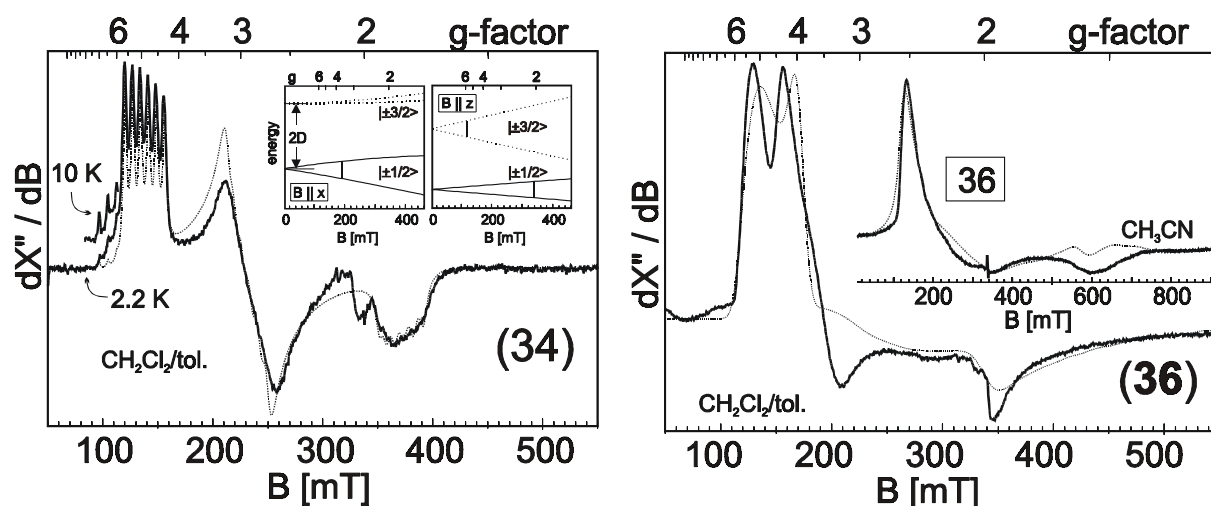


Figure 5.9.1 X- band EPR spectra of **34** in CH_2Cl_2 -toluene (1:2) and of **36** in CH_2Cl_2 -toluene (1:2) and in MeCN (right inset). The simulation (thin dotted line) and energies (left inset) of the magnetic sublevels of the $S = 3/2$ manifold as a function of the field applied in x- and z- directions.

The g values and ZFS parameters of **34** and **36** are nicely in the range found for other Cr(III) compounds,¹³ Mn(IV) compounds¹⁴ or other transition metal complexes with $3d(t_{2g})^3$ configuration and spin $S = 3/2$ like V(II)¹⁵ or even Fe(V).¹⁶ As mentioned above, the g value of these systems depends on spin-orbit interaction with excited spin triplet terms due to $t_{2g} \rightarrow e_g$ excitations which in octahedral symmetry are $10 D_q$ above the $^4B_{1g}$ ground state. It was pointed out earlier¹⁷ that the major contribution to the ZFS parameter D in distorted

octahedral symmetry comes from excited 2E_g and ${}^2B_{2g}$ doublet states rather than triplets.⁹ The doublet states result from spin-pairing in the t_{2g} orbital subset and, thus, are much lower in energy than $10D_q$. As a result D is sensitive to the strength of the equatorial ligands with the consequence that stronger π -interaction leads to *larger* D values. This is exactly the trend that is observed for **34** and **36**. The Mn(IV) compound, with its higher ionic charge and shortened metal-ligand bonds, subjected to the stronger covalency and, hence, stronger π -interaction, shows a significantly large ZFS than the Cr(III) compound **36**. From the stronger σ -interactions and larger $10D_q$ splitting the opposite trend in D would be predicted if D would owe its origin predominantly to the excited quartet states. To the best of our knowledge complexes **34** and **36** represent the first example of a series $3d^3$ complexes with Cr(III) and Mn(IV) in the same ligand system which allows such a direct comparison.

5.10 SOLUTION STUDY

Although the crystallographically characterized complex was found to be meridional in nature, complex **5** VL^N_2 is separated as a mixture of two isomers (*fac*- and *mer*-) from the reaction solution. The isolation of two isomers depends upon the work-up procedure of the reaction solution. If the reaction solution is concentrated after 25 h and the solid is analyzed by the LC, 100% *mer*-isomer is seen. On keeping the filtrate for another 25 h, the solid isolated is also 100% *mer*-isomer. This filtrate, on keeping for another 25 h yields a mixture of *mer*- and *fac*- isomer in 73:27 ratio as analyzed by the LC. On the other hand, LC-analyses of the acetonitrile reaction solution indicate no change of the percentage of *mer*-isomer (>99%) with time. On the basis of these observations, following conclusions can be made:

1. There is no equilibrium in solution between the two isomeric forms.
2. A very small amount of *fac*-isomer is formed initially, which eventually shows increased percentage in the LC after isolation of the major *mer*-isomer in two consecutive batches.
3. The difference of the solubility products of two isomers is small.
4. When the concentration of *mer* : *fac* attains the 73 : 27, two isomers are separated from the solution at the same time.

The solid isolated from the reaction solution after 75 h also exists in two isomeric forms in CH_2Cl_2 solution as has been pointed out in **chapter 2**. When the complex is dissolved in CH_2Cl_2 at room temperature followed by immediate LC analysis, both *fac*- and *mer*- isomers are seen. If this time be considered as the initial time ($t = 0$), and the LC analyses are

performed as a function of time, the change of the relative isomer percentage can be monitored.

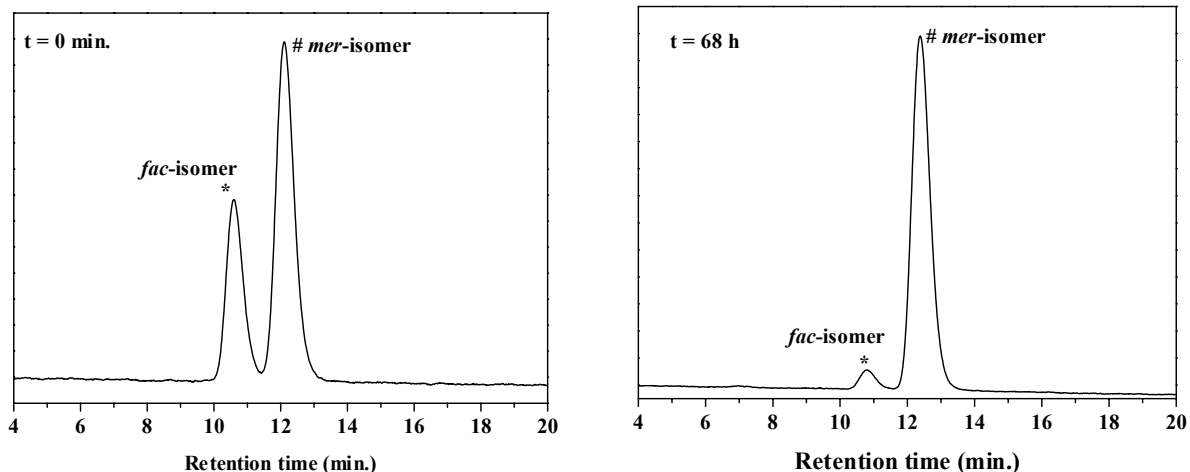


Figure 5.10.1 LC-spectra of complex 5 at $t = 0$ (left) and $t = 68$ h (right).

With time the percentage of the *fac*-isomer decreases whereas that of the *mer*-isomer increases. After keeping the solution for 90 h, and the LC analyses at certain time intervals gives the idea about this change (100% *mer*-isomer is obtained after 90 h). The *fac*-isomer transforms completely to the *mer*-isomer in solution. The LC-MS, clearly indicating the two isomers present in the solution at initial or intermediate time, confirms the presence of only *mer*-form after ca. 90 h.

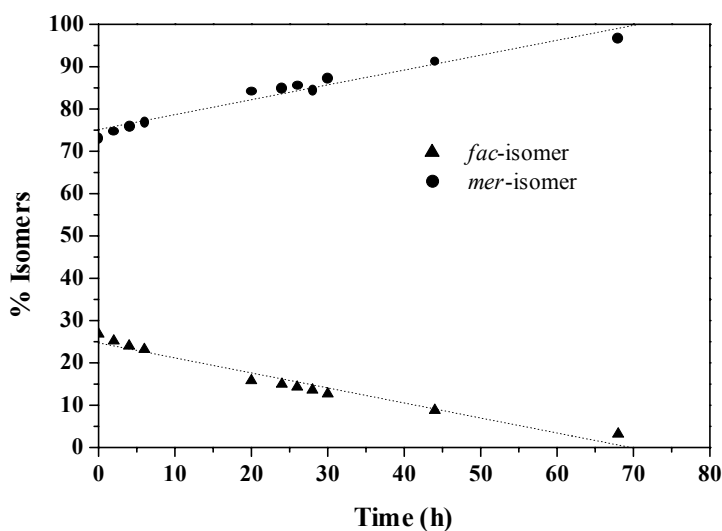


Figure 5.10.2 Change of the isomer-percentage with time for complex 5 in CH_2Cl_2 solution. The percentages are obtained from the LC-analysis.

This change can also be observed in the solution-EPR spectra at low temperature. At the very beginning, the spectrum shows a mixture of two isomers, whereas at $t = 90$ h, only one isomer is seen. The spectrum obtained at $t = 0$ can be simulated by considering two isomers in the ratio obtained from the LC-analysis (*fac*: *mer* = 27:73). On the other hand, the EPR spectrum of the same solution after 90 h shows only one isomer in 100% and can be simulated perfectly as seen in the Figure 5.10.3.

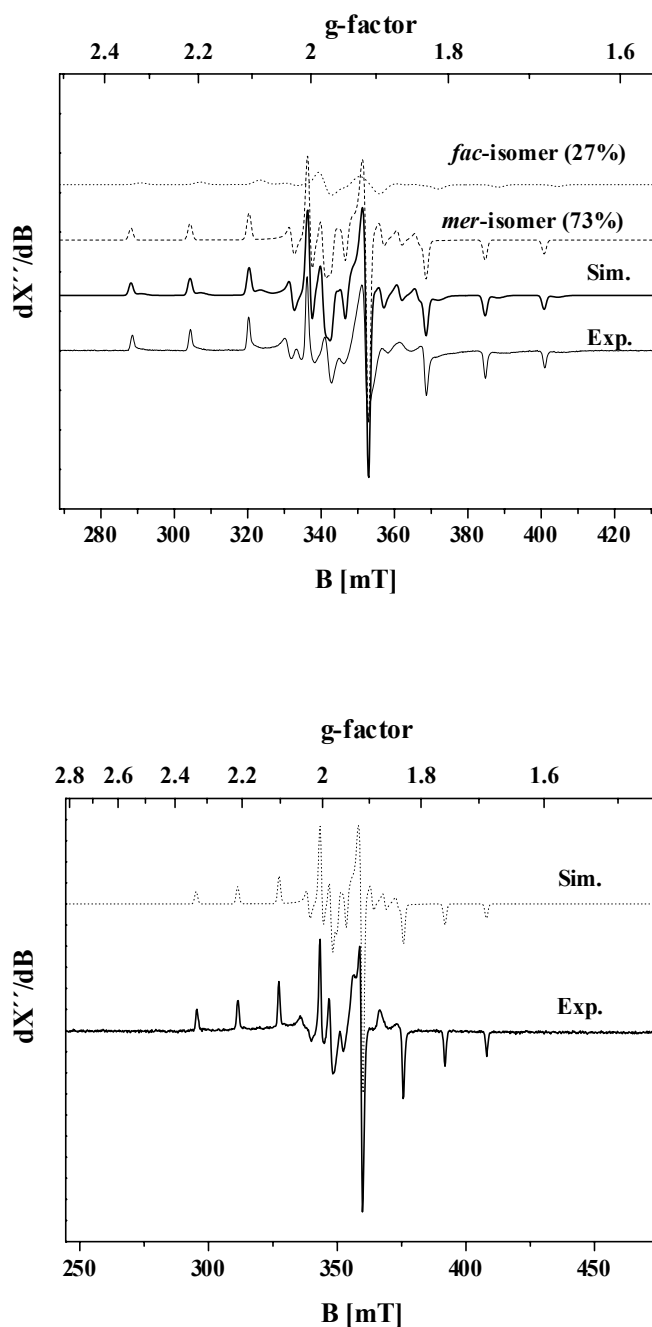
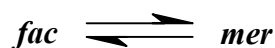


Figure 5.10.3 EPR spectra of complex **5** at $t = 0$ (top), $T = 9.9$ K and at $t = 90$ h in $\text{CH}_2\text{Cl}_2 + \text{toluene}$ (below), $T = 33.8$ K. Experimental conditions (—): microwave frequency 9.44 GHz (top); 9.64 GHz (below), microwave power 0.01 μW (top); 0.2 μW (below), modulation amplitude 5 G (top); 5 G (below). The simulations for spectrum at the top (---): $g = \{1.93, 1.96, 1.94\}$, $A = \{44, 14, 147\} \times 10^{-4} \text{ cm}^{-1}$ (*fac*-isomer); $g = \{1.932, 1.966, 1.958\}$, $A = \{44, 14, 147\} \times 10^{-4} \text{ cm}^{-1}$ (*mer* isomer); Gaussian line with frequency-dependent line width $W_f = 80$ G (*fac*) and 30 G (*mer*).

On the other hand, complex **34**, the Mn(IV) complex, shows solution-behaviour in which the nature of change is opposite. When complex **34** is dissolved in methanol and the LC-analysis

is performed, only one isomer is found (100%). This is the *mer*-isomer as confirmed from the solid-state crystal structure analysis. But with time the percentage of the *mer*-isomer decreases and a second isomer (*fac*-) increases (Figure 5.10.4). After 80 min there is no more any change and the percentage of two isomers becomes constant with a *fac*: *mer* ratio of 1:4. At this stage two isomers equilibrate in solution with the K_{eq} value found to be 4.



$$K_{eq} = [mer]/[fac] = 4$$

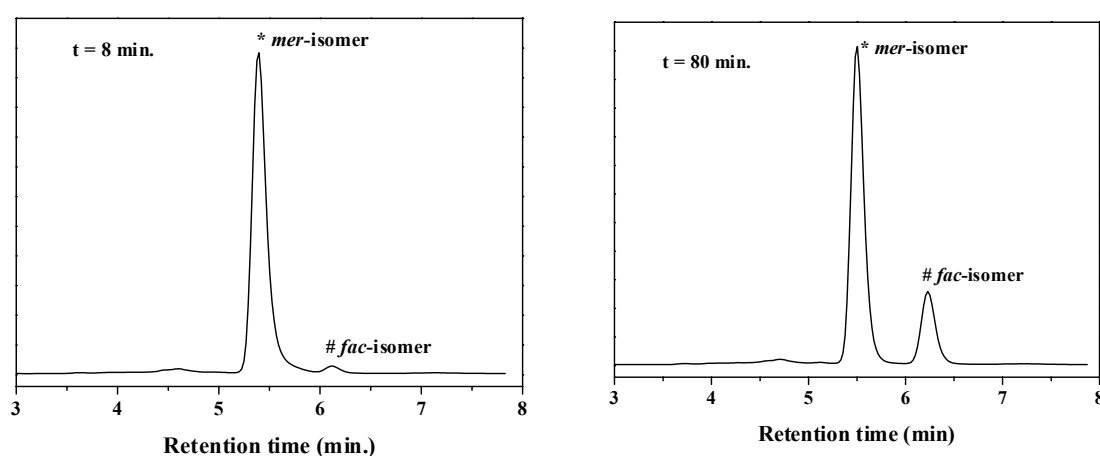


Figure 5.10.4 LC-spectra of complex **34** at $t = 8$ min (left) and $t = 80$ min (right).

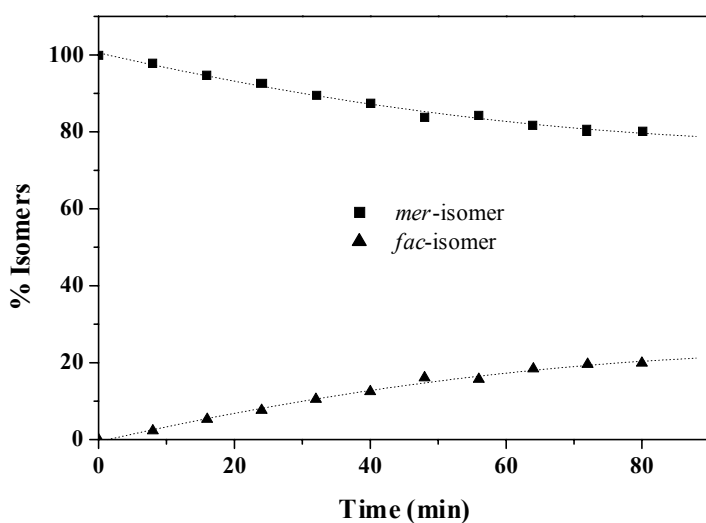


Figure 5.10.5 Change of the isomer-percentage with time for complex **34** in CH_2Cl_2 solution. The percentage of isomers is obtained from the LC-analysis.

The isomerization processes for the isostructural **5** and **34** can be rationalized on the basis of the effective ionic radii for V(IV) and Mn(IV). V(IV), with larger ionic radius (0.58Å) than that of Mn(IV) (0.53Å)¹⁸, is prone to change the coordination mode of the ligand from facial to meridional because of the steric availability in the meridional form.

This line of argument is in accord with the observation that the Mn(III) complex **35**, whose structure determination in the solid state shows the presence of only facial form, remains facial also in solution. Mn(III) has the largest ionic radius of 0.65Å amongst these three ions and thus stabilizes the more sterically demanding facial form.

References

1. M. Hesse, H. Meier, B. Zeeh, ''*Spektroskopische Methode in der Organischen Chemie*'', Georg Thieme Verlag, Stuttgart, 1995.
2. A. B. P. Lever, ''*Inorganic Electronic Spectroscopy*'', Elsevier, Amsterdam, **1984**.
3. C. K. Jorgenson, *Acta Chem. Scand.* **1957**, 8, 1686.
4. J. S. Griffith, ''*The Theory of Transition-metal Ions*'', Cambridge University Press, Cambridge, **1971**.
5. (a) B. R. McGarvey, ''*Transition Metal Chemistry*'', Ed. R. L. Carlin, Vol. 3, Marcel Dekker, Inc. New York, **1968**. (b) L. S. Forster, ''*Transition Metal Chemistry*'', Ed. R. L. Carlin, Vol. 5, Marcel Dekker, Inc. New York, **1969**.
6. (a) M. W. Lynch, D. N. Hendrickson, B. J. Fitzgerald, C. G. Pierpont, *J. Am. Chem. Soc.* **1984**, 106, 2041. (b) J. H. Hartman, B. M. Foxman, S. R. Cooper, *Inorg. Chem.* **1984**, 23, 1381. (c) S. K. Chandra, P. Basu, D. Ray, S. Pal, A. Chakravorty, *Inorg. Chem.* **1990**, 29, 2423 and references therein. (d) M. Mikuriya, S. Shigematsu, K. Kawano, T. Tokii, H. Oshio, *Chem. Lett.* **1990**, 729. (e) B. Adam, E. Bill, E. Bothe, B. Goerdts, G. Haselhorst, K. Hildenbrand, A. Sokolowski, S. Steenzen, T. Weyhermüller, K. Wieghardt, *Chem. Eur. J.* **1997**, 3, 308. (f) P. Chaudhuri, *unpublished result*.
7. (a) S. M. Couchman, J. C. Jeffery, P. Thornton, M. D. Ward, *J. Chem. Soc., Dalton Trans.* **1968**, 1163. (b) F. E. Hahn, T. J. McMurtry, A. Hugi and K. N. Raymond, *J. Am. Chem. Soc.* **1990**, 112, 1854.
8. C. R. Snow, J. A. Ibers, *Inorg. Chem.* **1973**, 12, 249.
9. F. E. Mabbs, D. Collison, ''*Electron Paramagnetic Resonance of d Transition Metal Compounds*'', Elsevier, Amsterdam **1992**.
10. J. R. Pilbrow, ''*Transition Ion Electron Paramagnetic Resonance*'', Clarendon Press, Oxford **1990**.
11. M. Hans, W. Buckel, and E. Bill, *Eur. J. Biochem.* **2000**, 267, 7082.
12. C. Hauser, E. Bill, and R. Holm, *Inorg. Chem.* in press.
13. (a) L. S. Singer, *J. Chem. Phys.* **1955**, 23, 379. (b) B. R. McGarvey, *J. Chem. Phys.* **1964**, 41, 3743. (c) E. Pedersen, H. Toftlund, *Inorg. Chem.* **1974**, 13, 1603. (d) D. A. Sommerville, R. D. Jones, B. M. Hoffmann, F. Basolo, *J. Am. Chem. Soc.* **1977**, 99, 8195. (e) D. E. Bolster, P. Gülich, W. E. Hatfield, S. Kremer, E. W. Müller, K. Wieghardt, *Inorg. Chem.* **1982**, 22, 1725. (f) N. Shaham, H. Cohen, D. Meyerstein, E. Bill, *J. Chem. Soc., Dalton Trans.* **2000**, 3082. (g) D. Burdinski, E. Bill, F. Birkelbach, K. Wieghardt, P. Chaudhuri, *Inorg. Chem.* **2001**, 40, 1160.

14. (a) M. J. Camenzind, F. J. Hollander, C. L. Hill, *Inorg. Chem.* **1983**, 22, 3776. (b) C. Duboc-Toia, H. Hummel, E. Bill, A.-L. Barra, G. Chouteau, K. Wieghardt, *Angew. Chem.* **2000**, 39, 2888.
15. C. J. H. Jacobsen, E. Pedersen, J. Villadsen, H. Weihe, *Inorg. Chem.* **1993**, 32, 1216.
16. (a) K. Meyer, E. Bill, B. Mienert, T. Weyhermüller, K. Wieghardt, *J. Am. Chem. Soc.* **1999**, 121, 4859. (b) C. A. Grapperhaus, B. Mienert, E. Bill, T. Weyhermüller, K. Wieghardt, *Inorg. Chem.* **2001**, 40, 4191.
17. L. L. Lohr, W. N. Lipscomb, *J. Chem. Phys.* **1963**, 38, 1607.
18. R.D. Shannon, *Acta Cryst.* **1976**, A32, 751.

Chapter 6

CONCLUSIONS AND PERSPECTIVES

CONCLUSIONS

The bisphenol ligands, in general, provide very rich coordination chemistry with first-row transition metal ions. They are good π -donor ligands and stabilize higher oxidation state of central metal ions resulting in highly covalent M-O bonds. Electronic, magnetochemical, electrochemical and structural properties of the complexes can be tuned by putting different heterodonor and ring substituents. Ring substituents and chelate ring size affect electronic and structural parameters, whereas electronegativity of the heterodonor atoms affects mainly electronic properties. The formation of the phenoxyl radicals depends upon the strong M-O covalent bond and the low electronegativity of heterodonor atoms. The present study gives a general idea about this relationship. Formation of the complexes with different heterodonor bisphenol ligands depends not only on the nature of the ligands but also on the metal ions. The main outcomes of this study are listed below:

Chapter 2

Six new **non-oxo vanadium(IV) complexes** were synthesized by using tridentate bisphenol ligands.

- They were synthesized by a general method. π -Donation from the ligand stabilizes the + 4 oxidation state. High intensity bands attributed to ligand-to-metal charge transfer processes dominate the UV-vis spectra of the complexes.
- S, Se, P and PO heterodonor containing bisphenol ligands bind to vanadium ion in the facial manner, whereas N-containing ligands coordinate in meridionally. The formation of six-membered rings favours such coordination for N-containing ligands. The vanadium-phenolate bond distances are in accord with the oxidation state of + 4.
- The magnetic moments for complexes at room temperature are typical of a d^1 system with spin-orbit coupling and g-anisotropy.
- In the cyclic voltammetry of these complexes containing S, Se, P, PO heterodonor ligands show two reversible redox peaks assignable to a one-electron oxidation to V(V) and the other to a one-electron reduction to V(III) are observed. The V(IV) complex of the N-containing ligand exhibits a reversible reductive wave to V(III) but two oxidative waves, one reversible one electron oxidation to V(V) and other one is ligand-based irreversible oxidation to the phenoxyl radical. The vanadium complex of H_2L^{N1} shows similar redox behaviour, but the reduction to V(III) is irreversible, whereas two oxidations are fully reversible. The formation of the phenoxyl radical

after second electrochemical oxidation was confirmed by the isotropic signal at $g \sim 2$ in the EPR measurement. The highly electronic +I effect of *tert*-butyl groups on the ligand eases the formation of the phenoxyl radical species in compared to that of the methyl substitution. This clearly shows the electronic effect on the redox potentials tuned by the remote substituent.

- EPR-spectra of frozen solution of the complexes in a variety of solvents or solvent mixtures show well-defined eight-line vanadium ($I = 7/2$) hyperfine typical of V(IV) with a d^1 electronic configuration. The V(IV) complex of the P-containing ligand exhibits superhyperfine due to phosphorus ($I = 1/2$). Each of the eight lines again split into three lines. This is the first of this kind of superhyperfine splitting observed in a vanadium complex. EPR spectroscopy has been proved to constitute a vital role in correlating structural and electronic (covalency) properties of the complexes.
- The vanadium (IV) complex of the P-containing ligand is very unstable in solution under air. It is oxidized to vanadyl (V) complex, with simultaneous oxidation of P(III) to P(V). Other complexes are relatively stable in non-coordinating dry solvents.
- The study of this series of vanadium complexes of bisphenol ligands gave an in-depth idea of interaction of phenolate with vanadium ion, which is relevant to the vanadium enzymes containing tyrosine residue.

Chapter 3

During the study of the **coordination properties of bisphenolate ligands with transition metal complexes**, the ligands H_2L^S , H_2L^{S-S} , H_2L^{Se} , H_2L^{Se-Se} and H_2L^N were examined. They show a variety of bonding possibilities with different first-row transition metal ions.

* Four μ -dimethoxo dichromium(III) complexes were synthesized and characterized. Two of them are having the novel hydrogen bonded $CH_3O---H---OCH_3^-$ bridging unit.

- These hydrogen bonded complexes were synthesized from the non-hydrogen bonded starting complexes by treatment of the latter with a base. An acid-base dependent equilibrium has been established between the two forms.
- These hydrogen bonded complexes exhibit the weakest coupling observed for dichromium(III) centers in bis-alkoxo/bis-phenoxo-bridged compounds reported.
- These four complexes represent the first example of coordination compounds in tuning the spin coupling interactions by hydrogen bonds.

* The bisphenol ligands show unique chelating ability with manganese and iron giving rise to a diverse set of complexes.

- The ligands $\text{H}_2\text{L}^{\text{S}}$ and $\text{H}_2\text{L}^{\text{Se}}$ form μ -dimethoxo dimanganese(III) complexes. They are very air sensitive in non-coordinating solvents and transformed to Mn(IV) mononuclear complexes. Four phenolate donor oxygen stabilize Mn(IV) unit. This transformation could be inhibited in the presence of a base where the Mn(III) monomer is formed.
- The Mn(III) monomer of the ligand $\text{H}_2\text{L}^{\text{Se}}$ can be oxidized chemically to the Mn(IV) monomer using FcPF_6 .
- UV-vis spectra of the Mn(III) dimer and the Mn(IV) monomer are dominated by highly intense CT bands but d-d bands are also observed for the Mn(III) monomer of the Se-containing bisphenol ligand.
- EPR spectra of Mn(IV) monomers of S- and Se-containing bisphenol ligands are typical of $S = 3/2$ axial spectra with rhombic distortion having intense signal at $g \sim 4$ and weak signal at $g \sim 2$.
- The Mn(III) monomer of $\text{H}_2\text{L}^{\text{Se}}$ is a good catalyst in oxidizing alkenes to the corresponding alkene oxides in the presence of H_2O_2 as oxidant with moderate turnovers.
- Two five-coordinate Fe(III) complexes were discussed. Fe(II) reduces the S-S and Se-Se bonds of the corresponding ligands during the formation of the complexes.
- All iron complexes discussed here are in oxidation state of + 3, as confirmed by the magnetic and Mössbauer measurements.

* Unlike vanadium, chromium, manganese and iron, nickel reacts differently with these bisphenol ligands. No mono or dinuclear complexes were isolated. Instead, its tendency to form polynuclear Ni(II) complexes gave diverse spin ground states depending upon the nuclearity and structural parameters.

- Four polynuclear Ni(II) complexes were synthesized. The ligands $\text{H}_2\text{L}^{\text{S}}$ and $\text{H}_2\text{L}^{\text{Se}}$ form tetranuclear cubane $[\text{Ni}_4(\text{OMe})_4]$ cores, whereas the ligand $\text{H}_2\text{L}^{\text{N}}$ forms penta- or hexanuclear Ni(II) complexes depending upon the reaction conditions. The $\text{Ni}_4/\text{H}_2\text{L}^{\text{Se}}$, $\text{Ni}_5/\text{H}_2\text{L}^{\text{N}}$ and $\text{Ni}_6/\text{H}_2\text{L}^{\text{N}}$ were structurally characterized. The Ni(II) complex of $\text{H}_2\text{L}^{\text{S}}$ is isostructural with the $\text{Ni}_4/\text{H}_2\text{L}^{\text{Se}}$.

- Tetranuclear Ni(II) complexes exhibit an $S = 4$ spin ground state but for the pentanuclear complex the ground state is not well-defined. The hexanuclear complex exhibits not well-separated mixed $S = 0$ and 1 ground state.
- The cubane core of the tetranuclear complex is distorted towards lower symmetry. The pentanuclear complex, geometrically, is a corner-shared distorted dicubane and the hexanuclear complex is a face-shared dicubane where one of the corners of each cubane is missing.
- A good magnetostructural correlation between exchange coupling and Ni-O-Ni angles for the cubane core is observed and the data obtained from $\text{Ni}_4/\text{H}_2\text{L}^{\text{Se}}$ are in good agreement with the other low symmetry cubane structures reported in the literature.
- Polynuclear Ni(II) complexes exhibit interesting high spin ground states.

Chapter 4

The Coordination chemistry of selenium heterodonor containing bisphenol ligand with copper has been discussed in chapter 4. The formation of phenoxyl radicals *in situ* during the synthesis of the complexes in presence of air has been proved by studying the reactivity of the Cu(II) complexes with organic substrates.

- The reactivity of the ligand with copper salts in presence of different coordinating amines has been studied. Tertiary, secondary and primary amines without any α -hydrogen atom form mononuclear Cu(II) complexes. But primary amines with at least one α -hydrogen atom undergo oxidative deamination reaction under air. The oxidative deamination reaction is the first example of functional model study of copper enzymes, Amine Oxidases.
- The mononuclear complex in basic medium under air oxidizes primary alcohols to the corresponding aldehydes, mimicking the functional aspect of galactose oxidase.
- Coordinating properties with copper has been explored by synthesizing and characterizing a variety of Cu(II) complexes. Trinuclear Cu(II) complexes can be placed in the class of asymmetric trinuclear Cu(II) complexes as structural models for multicopper oxidase.
- Abstraction of H-atoms from alcohol and amine substrates clearly establishes the involvement of radicals in these oxidation processes.

The amine bisphenol ligand, H_2L^N with O, N, O donor set exhibits diversified coordination properties to prove the metal-ligand covalent bonding properties.

- Bis(homoleptic) complexes like $[Cr^{III}L_2]^-$, $[Mn^{III}L_2]^-$, $[Mn^{IV}L_2]$ and $[Fe^{III}L_2]^-$ have been isolated and thoroughly studied. It has been unambiguously shown that electrochemical oxidations are ligand-centered, i.e. formation of the phenoxyl radicals from the coordinated phenolates (except for the manganese(III) compound, where the first oxidation occurs at metal center generating Mn(IV) species). This oxidation occurs at such a low potential (-0.645 V vs. Fc^+/Fc) that the $[Mn^{III}L_2]^-$ ion is air-sensitive, thus making isolation in the presence of air of the enigmatic Mn(IV) species viable.
- Emphasis has been given in this work to structural and electronic effects arising from the incorporation of a $-CH_2$ group between the phenolic ring and the amine group in the ligand H_2L^N , methylamino-N,N-bis(2-methylene-4,6-dimethylphenol), in comparison to the corresponding ligand without the CH_2 groups, viz. the ligand N,N-bis(2-hydroxy-3,5-di-*tert*-butylphenyl)amine with the same donor atoms. For the systems studied, addition of an organic non-ligating component ($-CH_2$ group) leads to an increase not only in the number of ring member (six-membered chelate), but also makes the resulting complexes stable towards radical formation. The potential for using a ligand yielding six-membered chelate rings to generate phenoxyl radicals from coordinated phenolates, in comparison to a ligand with identical donor atoms but resulting in five-membered chelate rings, was evaluated.
- The Cr(III) and Mn(IV) complexes of this ligand represent the first example of $3d^3$ complexes of Cr(III) and Mn(IV) in the same ligand system which allows their distinctive metal-ligand covalent binding characteristics as probes for comparison of EPR spectroscopic properties.
- Mn(IV) and V(IV) complexes of ligand H_2L^N show two geometrical isomers (*fac*- and *mer*-) in solution, detected and confirmed by LC-MS and EPR spectroscopy.

PERSPECTIVES:

In order to put forward the possible future developments related to coordination chemistry of the bisphenol ligands, some ideas and perspectives are presented here.

- The correlation between structural and spectroscopic properties of non-oxo vanadium(IV) complexes, to explain the electronic state quantitatively, needs to be explored. This requires further spectroscopic investigations, e.g., Magnetic Circular Dichroism (MCD) and EPR spectroscopy. To explain the g-values obtained from the EPR measurements, corresponding d-d transition energies are necessary, which are not found from the optical spectra of the complexes due to the overlapping strong charge-transfer transitions. MCD spectroscopy might give further insight in getting d-d transition energies. Theoretical calculations might also be helpful in explaining the 'unusually' low g-values.
- Tuning of exchange coupling through hydrogen bonds in the dichromium(III) complexes of the bisphenol ligands can be further explained by synthesizing different alkoxo- bridged hydrogen-bonded chromium(III) dimers with an aim to achieve ferromagnetic coupling.
- The catalytic activity of manganese and iron complexes can be explored by studying the catalytic reactions with a variety of other substrates.
- Other high nuclearity nickel complexes having high spin ground state can be synthesized, which are very interesting from the magnetochemical point of view, by varying the reaction conditions and substitution on ligands.
- That the dithio- and diseleno-bisphenol ligands are cleaved homolytically in the presence of metal ions to form new ligands has been explained in this work. The coordination chemistry of these new ligands formed *in situ* will be very interesting to compare with the other 'non-innocent' ligands being studied at present in the laboratory.
- Further attention could be focussed on the coordination chemistry of second- and third row transition metal ions with these bisphenol ligands having a variety of heterodonor atoms and ring substituents.

These ideas are feasible and can contribute a lot to the field of coordination chemistry.

Chapter 7

EQUIPMENT AND EXPERIMENTAL WORK

7.1 METHODS AND EQUIPMENTS

All the analyses were performed at the Max-Planck-Institut für Strahlenchemie, Mülheim an der Ruhr, unless otherwise mentioned. Commercial grade chemicals were used for the synthetic purposes and solvents were distilled and dried before use.

Infrared Spectroscopy

Infrared spectra were measured from 4000 to 400 cm^{-1} as KBr pellets at room temperature on a 'Perkin-Elmer FT-IR-Spectrophotometer 2000'.

NMR Spectroscopy

^1H - and ^{13}C - NMR spectra were measured using a 'Bruker ARX 250, DRX 400 or DRX 500'. The spectra were referenced to TMS, using the ^{13}C or residual proton signals of the deuterated solvents as internal standards. VOCl_3 was used as reference in ^{51}V NMR spectra.

Mass Spectroscopy

Mass spectra in the Electron Impact mode (EI; 70 eV) were recorded on a Finnigan MAT 8200 mass spectrometer. Only characteristic fragments are given with intensities. The spectra were normalised against the most intense peak having intensity 100. Electron Spray Ionization (ESI) mass spectra were recorded either on a Finnigan Mat 95 instrument or a Hewlett-Packard HP 5989 mass spectrometer. ESI- and EI- spectra were measured by the group of Dr. W. Schrader at the Max-Planck-Institut für Kohlenforschung, Mülheim an der Ruhr.

Elemental Analysis

The determination of the C, H, N and metal content of the compounds was performed by the 'Mikroanalytischen Labor H. Kolbe', Mülheim an der Ruhr, Germany.

UV-vis Spectroscopy

UV-Vis spectra were recorded on a 'Perkin-Elmer UV-vis Spectrophotometer Lambda 19' or on a Hewlett-Packard HP 8452A diode array spectrophotometer in the range 200-1200 nm. The samples were dissolved in CH_2Cl_2 or MeCN and measured at room temperature. For UV-vis spectro-electrochemical investigations the HP 8452A diode array spectrophotometer was used, by employing a coulometry cuvet and Bu_4NPF_6 as supporting electrolyte.

Electrochemistry

Cyclic voltammetry, square wave voltammetry and linear sweep voltammetry experiments were performed using an 'EG&G Potentiostat / Galvanostat 273A'. A standard three-electrode-cell was employed with a glass-carbon working electrode, a platinum-wire auxiliary electrode and Ag/AgCl (saturated LiCl in EtOH) reference electrode. Measurements were made under an inert atmosphere at room temperature. The potential of the reference electrode was determined using Fc^+/Fc as the internal standard.

Magnetic Susceptibility Measurements

The measurements of the temperature or field dependent magnetization of the sample were performed in the range 2 to 295 K at 1, 2, 4 or 7 T on a '*Quantum Design SQUID-Magnetometer MPMS*'. The samples were encapsulated in gelatin capsules and the response functions were measured four times for each given temperature, yielding a total of 32 measured points. The resulting volume magnetization from the samples had its diamagnetic contribution compensated and was recalculated as volume susceptibility. Diamagnetic contributions were estimated for each compound by using Pascal's constants. The experimental results were fitted with the programme JULIUS calculating through full-matrix diagonalization of the Spin-Hamiltonian. The following Hamiltonian-operators were used:

$$\mathcal{H}_{\text{ZE}} = \mu_{\text{B}} \sum g_i \hat{S}_i \cdot \mathbf{B}$$

$$\mathcal{H}_{\text{HDVV}} = -2 \sum J_{ij} \hat{S}_i \cdot \hat{S}_j$$

$$\mathcal{H}_{\text{ZFS}} = \sum D_i [\hat{S}_{iz}^2 - \{S_i(S_i+1)/3\}] + E_i/D_i (\hat{S}_{ix}^2 - \hat{S}_{iy}^2)$$

Indexes i,j indicate individual spins. For the magnetic measurement the calculated g values obtained during simulation is the isotropic.

EPR Spectroscopy

First derivative X-Band EPR spectra of powdered or frozen solution samples were measured with a '*Bruker ESP 300 Spectrometer*' coupled to an '*Oxford Instruments ESR 910-Cryostat*'. Spin-Hamiltonian simulations of the EPR spectra were performed with a program which was developed from the $S = 5/2$ routines of Gaffney and Silverstone and which specifically makes use of the resonance search procedure based on a Newton-Raphson algorithm as described therein.

⁵⁷Fe-Mössbauer Spectroscopy

⁵⁷Fe-Mössbauer spectra were measured with an *Oxford Instruments* Mössbauer spectrometer in the constant acceleration mode. ⁵⁷Co/Rh was used as the radiation source. The minimum experimental linewidths were 0.24 mm/s. The temperature of the sample was controlled by an ‘*Oxford Instruments* Variox Cryostat’. Isomer shifts were determined relative to α -iron at 300K. The measurements were carried out at 80K with solid samples containing the isotope ⁵⁷Fe.

Crystallography

X-ray diffraction data were collected on an ‘*Enraf-Nonius* CAD4 Diffractometer’ or on a ‘*Siemens* Smart System’. Graphite-monochromatized Mo-K α with $\lambda = 0.71073$ Å was employed. Data were collected by the 2θ - ω scan method ($3 \leq 2\theta \leq 50^\circ$). The data were corrected for absorption and Lorentz polarization effects.

The structures were solved by direct methods and subsequent Fourier-difference techniques, and refined anisotropically by full-matrix least-squares on F^2 with the program SHELXTL PLUS. Hydrogen atoms were included at calculated positions with $U < 0.08$ Å² in the last cycle of refinement.

GC / GC-MS Analysis

GC of the organic products were performed either on HP 5890 II or HP 6890 instruments using RTX-1701 15 m S-41 or RTX-5 Amine 13.5 m S-63 columns respectively. GC-MS was performed using the above columns coupled with a HP 5973 mass spectrometer with mass selective detector.

LC / LC-MS Analysis

LC of the complexes were performed on HPLC instrumentation using a Gilson M305 pump, and the Diode-Array-Detector (DAD) SPDM 10 AV (Shimadzu corporation). MeOH 0.8 ml/min was used as eluent through a Nucleodur- 5 μ -(100Å)-C18 column. LC-MS was performed using the above column with a mass spectrometer having mass selective detector.

7.2 SYNTHESIS

7.2.1 LIGANDS

Synthesis of 2,2'-Selenobis(4,6-di-*tert*-butyl phenol) $\text{H}_2\text{L}^{\text{Se}}$

A suspension of 2,4-di-*tert*-butylphenol (61.89 g, 0.3 mole) and SeO_2 (11.1 g, 0.1 mole) in 55 ml conc. HCl was heated at 80°C with constant stirring for 2 h. The mixture was then cooled and extracted with CHCl_3 (3 x 100ml), washed with brine solution (2 x 50ml) and then with water (100 ml), dried over Na_2SO_4 and concentrated *in vacuo*. The crude brown product was then recrystallized from heptane/MeOH to obtain a pure white compound.

Yield: 18.5 g (25%)

MP: 141°C

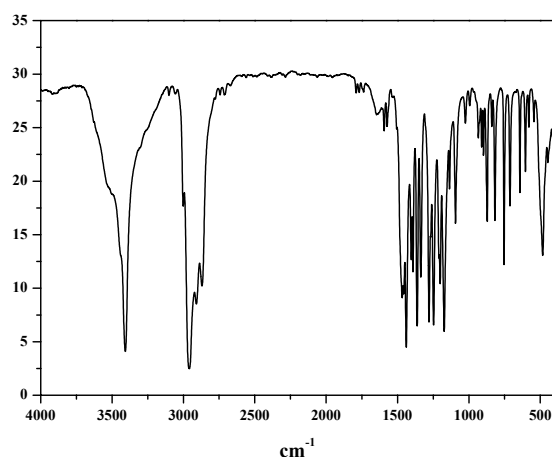
Molecular weight: 489.6 g/mol

$\text{C}_{28}\text{H}_{42}\text{SeO}_2$

Elemental analysis:

| | %C | %H |
|------------|-------|------|
| Calculated | 68.69 | 8.65 |
| Found | 68.7 | 8.7 |

IR-Spectrum:



$^1\text{H-NMR}$ (CDCl_3):

δ 1.20 (s, 18H), 1.38 (s, 18H), 6.25 (s, OH, 2H), 7.24 (m, 4H).

$^{13}\text{C NMR}$ (CDCl_3):

δ 29.5 (s, *tert*-butyl), 31.6 (s, *tert*-butyl), 34.3 (s, *tert*-butyl), 35.2 (s, *tert*-butyl), 117.0 (s), 125.4 (s), 129.6 (s), 135.7(s), 143.3 (s), 151.6 (s).

MS (EI): The desired molecular ion (490) was observed in the ratio calculated for the naturally abundant isotope mixture of Se-74, 76, 77, 78, 80 and 82.

Synthesis of 2,2'-Thiobis(4,6-di-*tert*-butyl phenol) H₂L^S

To a solution of 2, 4-di-*tert*-butylphenol (103.1 g, 0.5 mole) and anhydrous ZnCl₂ (0.51 g, 7.5 mmol) in 130 ml of petroleum ether at 0°C was added dropwise over 1 h duration a solution of SCl₂ (25.7 g, 0.25 mole) in 50 ml petroleum ether. The reaction mixture was stirred for 15 h at room temperature with a slow argon sweep to remove evolved HCl gas. The solvent was removed *in vacuo* and the residue was crystallized from MeCN to give a white solid.

Yield: 66 g (60%)

MP: 101°C

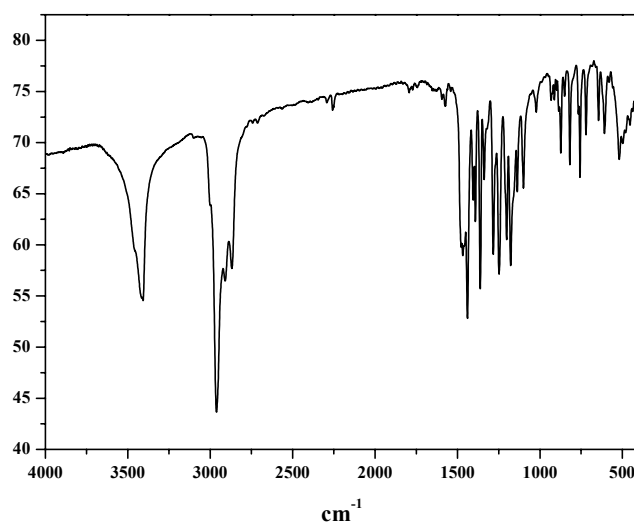
Molecular weight: 442.7 g/mol

C₂₈H₄₂SO₂

Elemental analysis:

| | %C | %H | %S |
|------------|-------|------|------|
| Calculated | 75.97 | 9.56 | 7.24 |
| Found | 75.8 | 9.7 | 7.3 |

IR-Spectrum:



¹H-NMR (CDCl₃):

δ 1.21 (s, 18H), 1.41 (s, 18H), 6.49 (s, OH, 2H), 7.24 (m, 4H).

¹³C NMR (CDCl₃):

δ 29.5 (s, *tert*-butyl), 31.3 (s, *tert*-butyl), 34.3 (s, *tert*-butyl), 35.2 (s, *tert*-butyl), 119.0 (s), 125.1 (s), 127.7 (s), 135.9(s), 143.0 (s), 151.7 (s).

MS (EI): $m/z = 442$.

Synthesis of 2,2'-Phenylphosphinebis(4,6-di-*tert*-butyl phenol) H_2L^P

To a solution of 2-bromo-4,6-di-*tert*-butylphenol (4.2 g, 14.7 mmol) in absolute Et_2O (25 ml) at $-60^\circ C$ was added dropwise within half an hour a 1.6 M solution of *n*-butyllithium (18.4 ml, 29.4 mmol) in hexane. The resulting pale yellow solution was stirred for 8 h, during which time it warmed to room temperature. After it was cooled again to $-50^\circ C$, $PhPCl_2$ (1 ml, 7.37 mmol) dissolved in 10 ml of ether was added dropwise for 90 mins. The reaction mixture was stirred overnight at $10^\circ C$ and for 2 h at room temperature and then the suspension of $LiCl$ was removed by filtration under argon. The solution was extracted as fast as possible with a vigorously oxygen-free 0.1 M solution of NaH_2PO_4 (2 x 20 ml) followed by water. The ether phase was dried over anhydrous Na_2SO_4 and then concentrated to a white solid.

Yield: 1.53 g (40%)

MP: $111^\circ C$

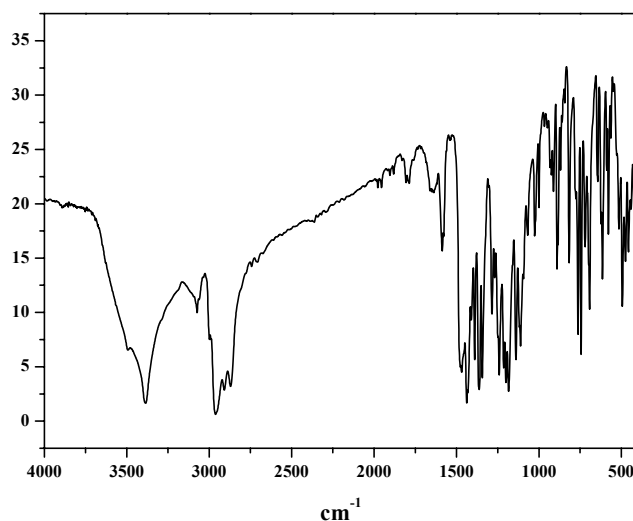
Molecular weight: 518.7 g/mol

$C_{34}H_{47}PO_2$

Elemental analysis:

| | %C | %H | %P |
|------------|-------|------|------|
| Calculated | 78.73 | 9.13 | 5.97 |
| Found | 78.6 | 9.1 | 6.0 |

IR-Spectrum:



$^1\text{H-NMR}$ (CDCl_3):

δ 1.16 (s, 18H), 1.42 (s, 18H), 6.90 (s, 2H), 6.28 (s, 2H, OH), 7.36-7.24 (m, 7H).

$^{13}\text{C NMR}$ (CDCl_3):

δ 29.7 (s, *tert*-butyl), 31.4 (s, *tert*-butyl), 34.4 (s, *tert*-butyl), 35.1 (s, *tert*-butyl), 118.3 (s), 126.4 (s), 128.6, 128.9, 132.9, 132.6 (s), 135.7(s), 142.7 (s), 155.4, 155.7 (s).

$^{31}\text{P-NMR}$ (CDCl_3):

δ – 49.9 (s, 1P).

MS (EI) : m/z = 518 [M^+ , 100%].

Synthesis of 2,2'-Phenylphosphineoxidebis(4,6-di-*tert*-butyl phenol) $\text{H}_2\text{L}^{\text{PO}}$

Method 1

100 ml of *n*-butyllithium (159 mmol 1.6 M *n*-hexane solution) were added dropwise to a solution of 2-bromo-4,6-di-*tert*-butylphenol (22.7 g, 79.5 mmol) in 200 ml Et_2O and stirred overnight at room temperature. The resulting yellow solution cooled to 0°C was treated dropwise with dichlorophenylphosphineoxide (5.5 ml) dissolved in 50 ml of Et_2O . The reaction mixture was stirred overnight at room temperature and the suspension of lithium halide was removed by filtration. The ether phase was washed with 30 ml of 1 M NaH_2PO_4 and 200 ml of water, followed by 200 ml of 1M NaH_2PO_4 . The organic layer was dried over anhydrous Na_2SO_4 and then solvent was removed *in vacuo* to yield white solid.

Yield: 10.0 g (48%)

MP: 195°C

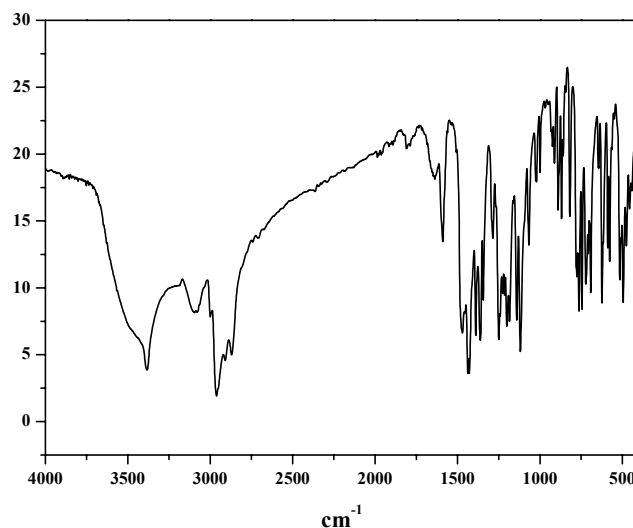
Molecular weight: 534.7 g/mol

$\text{C}_{34}\text{H}_{47}\text{PO}_3$

Elemental analysis:

| | %C | %H | %P |
|------------|-------|------|------|
| Calculated | 76.40 | 8.90 | 5.80 |
| Found | 76.6 | 8.8 | 5.7 |

Infrared spectrum:



¹H-NMR (CDCl₃):

δ 6.85 (dd, 2H), 7.61-7.44 (m, 7H), 10.62 (s, 2H, OH)

¹³C NMR (CDCl₃):

δ 29.5 (s, *tert*-butyl), 31.3 (s, *tert*-butyl), 34.2 (s, *tert*-butyl), 35.4 (s, *tert*-butyl), 109.2 (s), 110.2, 126.0 (s), 128.6, 129.3, 132.9, 131.9 (s), 132.7(s), 138.2 (s), 140.6, 160.5 (s).

³¹P-NMR (CDCl₃): δ +52.6 (s, 1P).

MS (EI): m/z = 534 [M⁺, 100%] and 519 ([H₂L^{PO}-O]⁺, 28%).

Method 2

A solution of ligand H₂L^P (50 mg, 0.096 mmol) in Et₂O was treated with a solution of H₂O₂-ether (1:10). Preparative TLC (hexane-ethylacetate 30:1 eluent) was used to obtain 49 mg (95%) of the desired product.

Synthesis of Methylamino-N, N-bis(2-methylene-4,6-dimethylphenol) H₂L^N

To a solution of 2,4-dimethylphenol (48 ml, 0.4 mol) in 130 ml MeOH was added aqueous formaldehyde (37%, 32 ml, 0.39 mol) and MeNH₂ (40%, 17.2 ml, 0.22 mol) with stirring. The solution was stirred for 20 h at 25°C and refluxed for 3 h. The two-layer system was left in a freezer for 2 d by which time the oil at the bottom solidified. The mother liquor was decanted off and the solid washed with a mixture of ⁱPrOH-MeOH (1:1, 100 ml) and air-dried.

Yield: 47.7 g (81%)

MP: 120°C

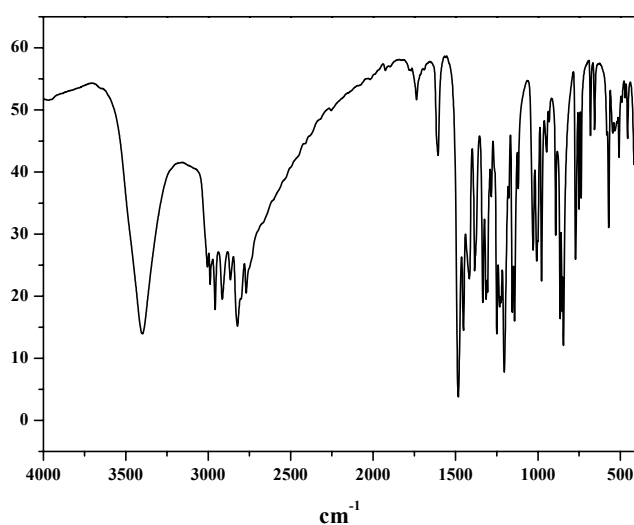
Molecular weight: 299.41 g/mol

C₁₉H₂₅NO₂

Elemental analysis:

| | %C | %H | %N |
|------------|-------|------|------|
| Calculated | 76.22 | 8.42 | 4.68 |
| Found | 76.4 | 8.3 | 4.8 |

Infrared spectrum:



¹H-NMR (CDCl₃):

δ 2.21 (s, 12H, aryl-CH₃), 2.25 (s, 3H, NCH₃), 6.72 (s, 4H, NCH₂), 6.72 (s, 2H, aryl), 6.87 (m, 2H, aryl).

MS (EI): m/z = 299 [M⁺, 60%] and 165 [M-C₉H₁₀O, 100%], 134 [M-C₁₀H₁₄ON, 89%].

Synthesis of Methylamino-N, N-bis(2-methylene-4,6-di-*tert*-butylphenol) H₂L^{N1}

This ligand was synthesized by the same procedure described for ligand H₂L^N using 2,4-di-*tert*-butylphenol instead of 2,4-dimethylphenol with high yield.

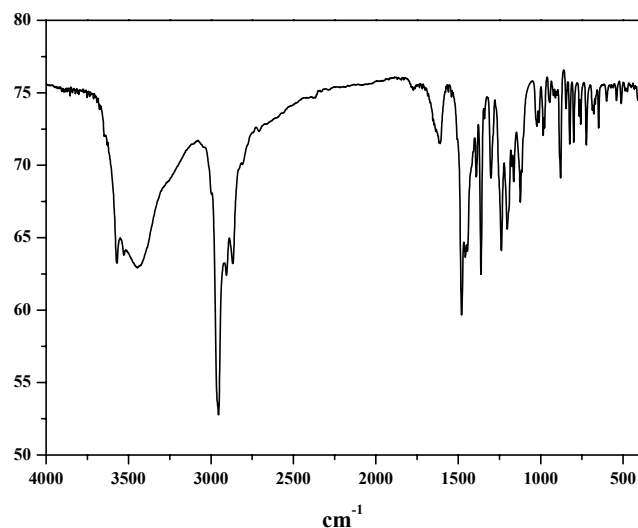
Molecular weight: 467.74 g/mol

C₃₁H₄₉NO₂

Elemental analysis:

| | %C | %H | %N |
|------------|-------|-------|------|
| Calculated | 79.61 | 10.56 | 2.99 |
| Found | 80.2 | 10.3 | 2.8 |

Infrared spectrum:



¹H-NMR (CDCl₃):

δ 1.27 (s, 18H, *tert*-butyl), 1.39 (s, 18H, *tert*-butyl), 2.21 (s, 3H, NCH₃), 3.63 (s, 4H, -CH₂-), 6.99-7.00 (d, 2H, aryl), 7.19-7.20 (d, 2H, aryl).

MS (EI): m/z = 467 [M⁺, 100%].

Synthesis of 2,2'-Diselenobis(4,6-di-*tert*-butyl phenol) H₂L^{Se-Se}

A suspension of 2,4-di-*tert*-butylphenol (6.18 g, 0.03 mol) and SeO₂ (3.33 g, 0.03 mol) in 10 ml conc. HCl was heated at 120°C with constant stirring for 4 h. The mixture was then cooled and extracted with CHCl₃ (3 x 20ml), washed with brine solution (2 x 10ml) and then with water (20 ml), dried over Na₂SO₄ and concentrated *in vacuo*. The crude brown product was then washed thoroughly with methanol to remove the monoselenide impurity giving yellow compound.

Yield: 6.0 g (70%)

MP: 108°C

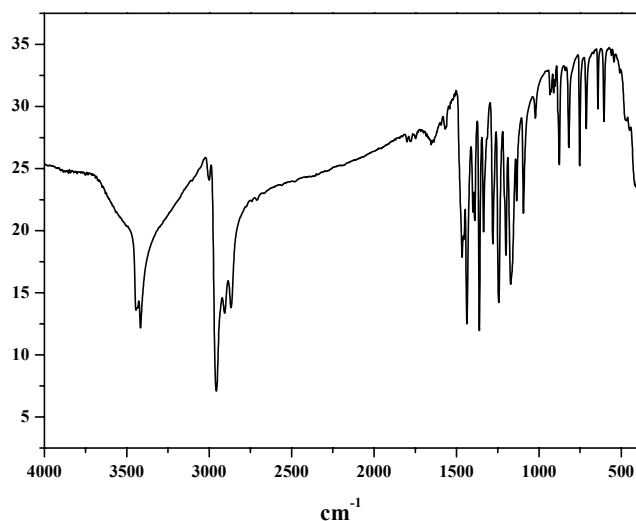
Molecular weight: 568.56 g/mol

C₂₈H₄₂Se₂O₂

Elemental analysis:

| | %C | %H |
|------------|-------|------|
| Calculated | 59.15 | 7.45 |
| Found | 58.9 | 7.6 |

IR-Spectrum:



¹H-NMR (CDCl₃):

δ 1.17-1.24 (s, 9H), 1.32-1.35 (s, 9H), 1.49 (s, 18H), 6.28 (s, OH, 2H), 7.19 (m, 4H).

MS (EI): The desired molecular ion (568) was observed in the ratio calculated for the naturally abundant isotope mixture of Se-74, 76, 77, 78, 80 and 82.

Synthesis of 2,2'-Dithiobis(4,6-di-*tert*-butyl phenol) H₂L^{S-S}

To a solution of 2,4-di-*tert*-butylphenol (15.8 g, 76.7 mmol) in 30 ml of toluene was added over a period of 2 h a solution of S₂Cl₂ (3.42 ml, 43.3 mmol) in 20 ml of toluene at room temperature. The reaction mixture was stirred at 80°C for an additional 90 mins. The solvent was evaporated and the viscous, orange-brown crude product was dissolved in hot EtOH. After cooling and recrystallization from MeOH yields light yellow compound.

Yield: 5.8 g (32%)

MP: 140°C

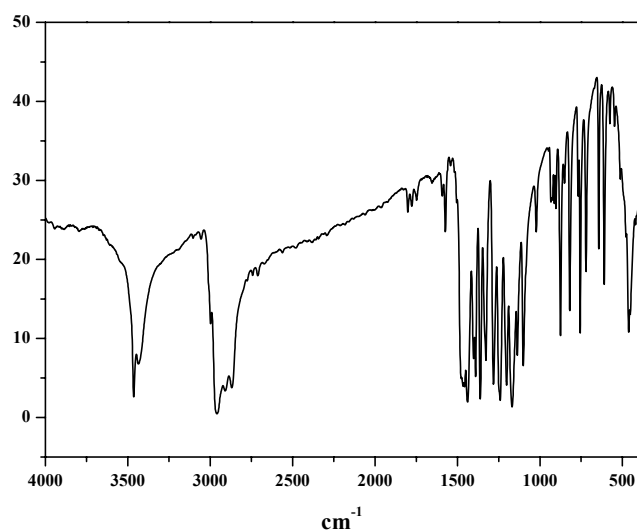
Molecular weight: 474.76 g/mol

C₂₈H₄₂S₂O₂

Elemental analysis:

| | %C | %H | %S |
|------------|-------|------|-------|
| Calculated | 70.84 | 8.92 | 13.51 |
| Found | 70.9 | 8.7 | 12.9 |

IR-Spectrum:



¹H-NMR (CDCl₃):

δ 1.28 (s, 18H), 1.41 (s, 18H), 6.52 (s, OH, 2H), 7.40-7.47 (m, 4H).

MS (EI):

$m/z = 474$ [M^+ , 44 %].

7.2.2 COMPLEXES

General method of synthesis for V(IV) complexes

In a degassed MeCN solution (40 ml) of ligand (1 mmol) was dissolved V(THF)₃Cl₃ (0.5 mmol, 0.186 g). To that violet solution 0.5 ml Et₃N was added and the resulting solution was refluxed under argon for 0.5 h. After cooling to room temperature the solution was opened to air and stirred for 5 min. The solution was then kept under a slow sweep of argon to yield crystalline solids.

The complex VL^S₂ (1)

Yield: 0.38 g (82%)

Molecular weight: 932.31 g/ mol

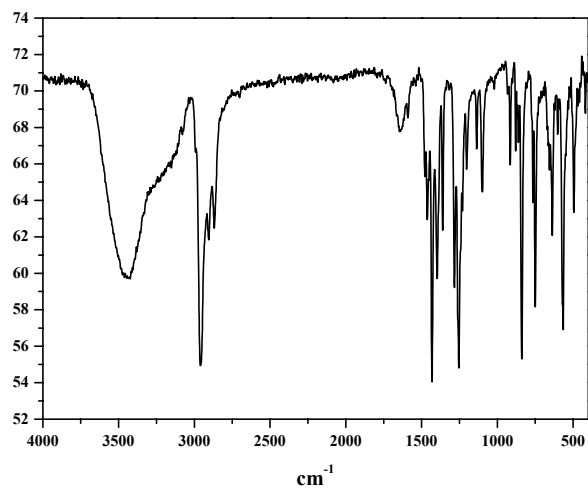


MS (EI): $m/z = 931$ [M^+ , 100%]

Elemental analysis:

| | %C | %H | %S | %V |
|------------|-------|------|------|------|
| Calculated | 72.15 | 8.65 | 6.88 | 5.46 |
| Found | 71.5 | 8.7 | 7.6 | 6.1 |

Infrared spectrum:



The complex VL^{Se}₂ (2)

Yield: 0.46 g (90%)

Molecular weight: 1026.11 g/ mol

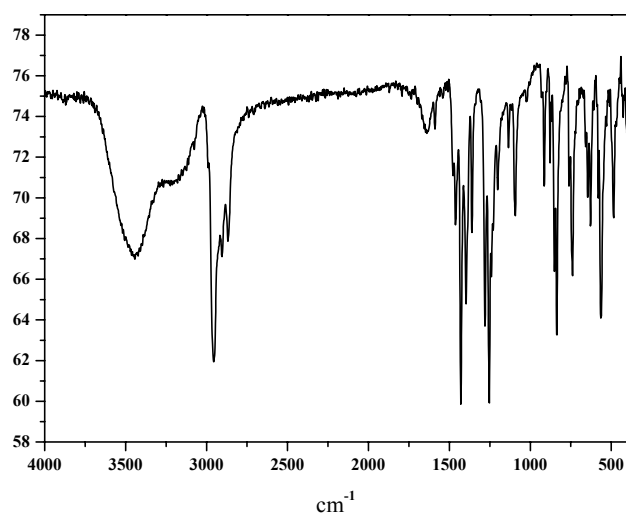
C₅₆H₈₀Se₂O₄V

MS (EI): m/z = 1027 [M⁺, 100%]

Elemental analysis:

| | %C | %H | %V |
|------------|-------|------|------|
| Calculated | 65.55 | 7.86 | 4.96 |
| Found | 65.3 | 8.0 | 5.2 |

Infrared spectrum:



The complex VL^P₂ (3)

Yield: 0.37 g (68%)

Molecular weight: 1084.35 g/ mol

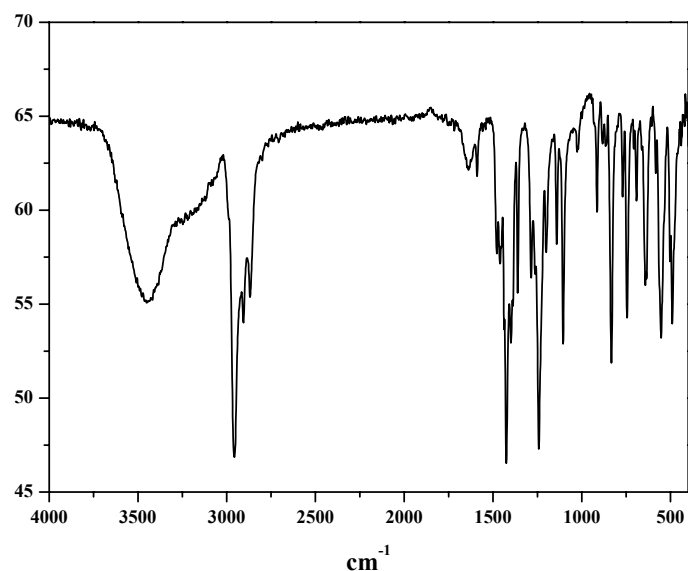


MS (EI): $m/z = 1083 [\text{M}^+, 100\%]$

Elemental analysis:

| | %C | %H | %P | %V |
|------------|-------|------|------|------|
| Calculated | 75.32 | 8.37 | 5.71 | 4.70 |
| Found | 74.5 | 8.5 | 4.6 | 4.8 |

Infrared spectrum:

**The complex VL^{PO}₂ (4)**

Yield: 0.25 g (45%)

Molecular weight: 1116.35 g/ mol

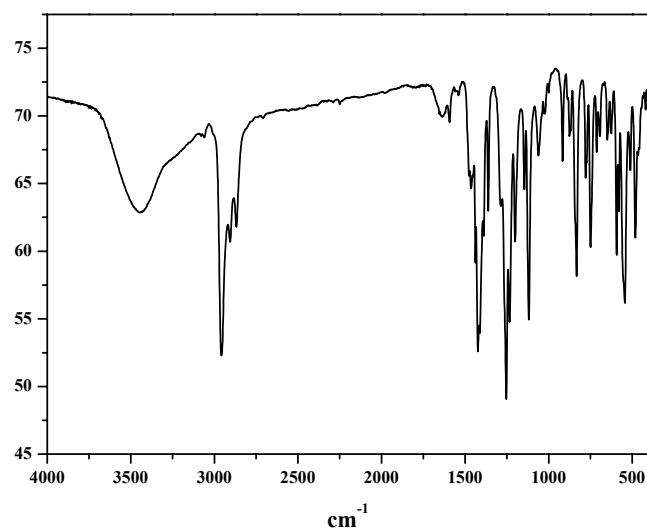


MS (EI): $m/z = 1115 [\text{M}^+, 100\%]$

Elemental analysis:

| | %C | %H | %P | %V |
|------------|-------|------|------|------|
| Calculated | 73.16 | 8.13 | 5.55 | 4.56 |
| Found | 72.7 | 7.7 | 5.9 | 4.6 |

Infrared spectrum:



The complex $\text{VL}^{\text{N}}_2 \cdot 2/3 \text{ MeCN}$ (5)

Yield: 0.23 g (68%)

Molecular weight: 673.1 g/ mol

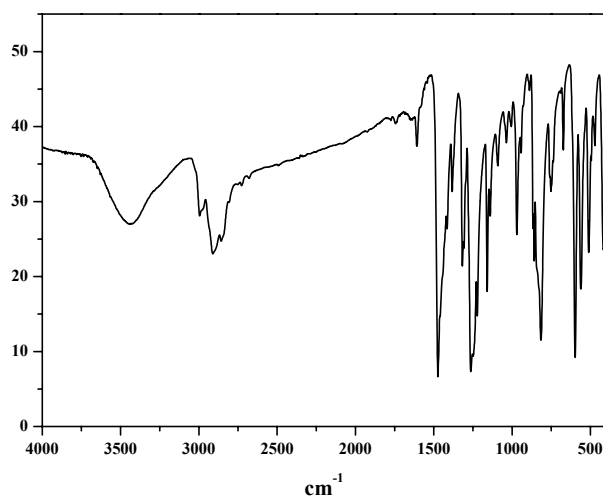
$\text{C}_{38}\text{H}_{46}\text{N}_2\text{O}_4\text{V} \cdot 2/3 \text{ MeCN}$

MS (EI): $m/z = 645 [\text{M}^+, 42\%], 377 [100\%]$

Elemental analysis:

| | %C | %H | %N | % V |
|------------|-------|------|------|------|
| Calculated | 70.19 | 7.19 | 5.55 | 7.57 |
| Found | 69.9 | 7.1 | 5.5 | 8.7 |

Infrared spectrum:



The complex VL^{N1}₂ (6)

Yield: 0.26 g (53%)

Molecular weight: 982.38 g/ mol

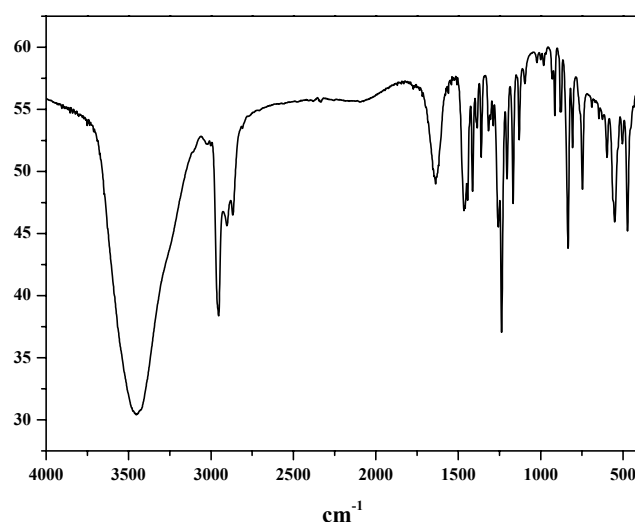
C₆₂H₉₄N₂O₄V

MS (ESI positive ion, CH₂Cl₂): m/z = 981 [M⁺, 100%]

Elemental analysis:

| | %C | %H | %N | %V |
|------------|-------|------|------|------|
| Calculated | 75.80 | 9.64 | 2.85 | 5.19 |
| Found | 75.6 | 9.5 | 2.8 | 5.3 |

Infrared spectrum:



Another method of synthesis for VL^S₂ (1) and VL^{Se}₂ (2)

To a degassed MeCN (50 ml) solution of ligand (1 mmol), VOSO₄ or VO(acac)₂ (0.5 mmol) was added. The resulting green solution was treated with 0.5 ml Et₃N and refluxed under argon for ½ h to produce a brownish violet solution. After cooling to room temperature the solution was kept under a slow sweep of argon where a brown microcrystalline compound isolated in 50-55% yield depending upon the salt used.

The complex [VO(L^{PO})(HL^{PO})] (7)

Method 1

To a degassed hot MeCN solution (25 ml) of ligand (0.5 mmol, 0.27 g) was added VO(OⁱPr)₃ (0.25 mmol, 0.06 ml). The colorless solution immediately turned blue-violet. After cooling to room temperature, a crystalline violet complex resulted within 1 h, which was separated by

filtration, washed with MeCN and dried. Single crystals were grown from a solvent mixture of CH₂Cl₂ and MeCN (1:1).

Yield: 0.21 g (74%)

Molecular weight: 1133.36 g/ mol

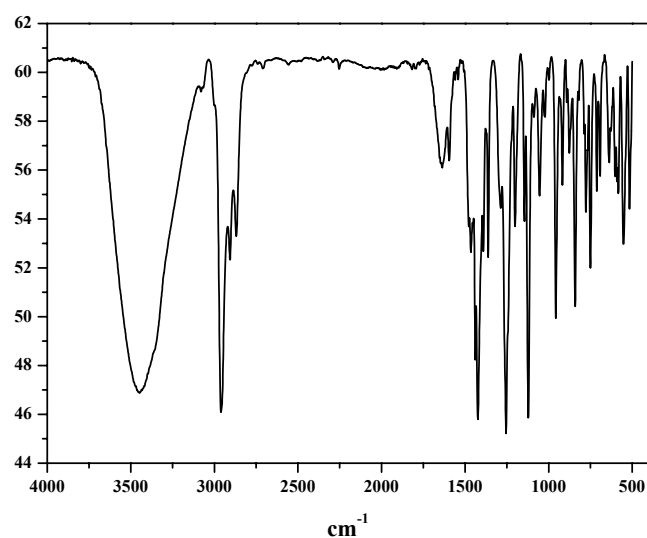
C₆₈H₉₁P₂O₇V

MS (EI): m/z = 1133 [M⁺, 56%], 534 [H₂L^{PO}, 100%]

Elemental analysis:

| | %C | %H | %V |
|------------|-------|------|------|
| Calculated | 72.05 | 8.10 | 4.50 |
| Found | 71.3 | 8.2 | 3.9 |

Infrared spectrum:



Method 2

Complex VL^P₂ was dissolved in CH₂Cl₂ and MeCN was layered over that. This solution, after keeping in air for 2 d, yielded a violet crystalline solid.

The complex [(VO)₂(L^{Se})₂(μ-OH)₂] (8)

To a degassed hot MeCN solution (25 ml) of ligand (1 mmol, 0.49 g) was added VO(OⁱPr)₃ (1 mmol, 0.24 ml). The colorless solution immediately turned blue-violet. After cooling to room temperature, a crystalline violet complex resulted within 1 h, which was separated by filtration, washed with MeCN and dried. Single crystals were grown from a solvent mixture of CH₂Cl₂ and MeCN (1:1).

Yield: 0.30 g (52%)

Molecular weight: 1143.07 g/ mol

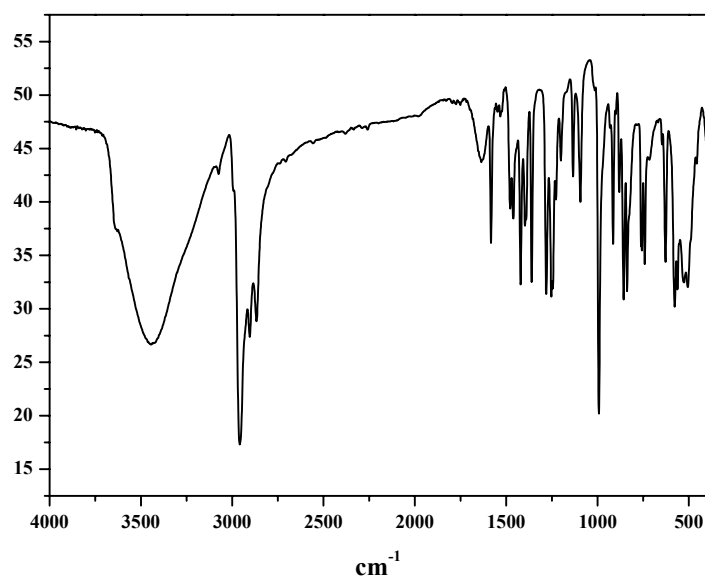


MS (EI): $m/z = 1027$ [decomposition product at high temperature, VL^{Se}_2]

Elemental analysis:

| | %C | %H | %V |
|------------|-------|------|------|
| Calculated | 58.84 | 7.23 | 8.91 |
| Found | 58.3 | 7.0 | 8.7 |

Infrared spectrum:



The complex $[\text{CrL}^{\text{Se}}(\mu\text{-OMe})(\text{MeOH})]_2$ (9)

The ligand (0.5 mmol, 0.245 g) was dissolved in dry MeOH (20 ml) and to that 2.5 ml Bu_4NOMe (20% methanolic solution) was added and stirred under argon. To that yellow solution, CrCl_2 (0.065 g, 0.5 mmol) was added and the resulting light green solution was refluxed under argon for 1 h and another 1 h under air. The solution was then filtered hot to remove any insoluble impurities and on cooling to room temperature green microcrystalline solid isolated. X-ray quality crystals were grown from a solvent mixture of CH_2Cl_2 and MeOH (1:1).

Yield: 0.13 g (43%)

Molecular weight: 1205.31 g/ mol

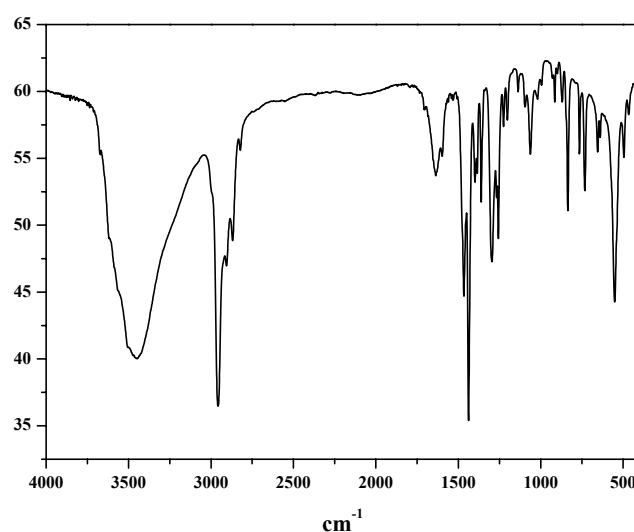


MS (EI): 1140 [M-2MeOH] and decomposition products at high temperature.

Elemental analysis:

| | %C | %H | %Cr |
|------------|-------|------|------|
| Calculated | 59.79 | 7.86 | 8.63 |
| Found | 59.3 | 8.2 | 8.2 |

Infrared spectrum:



The complex $\text{Bu}_4\text{N}[\text{Cr}_2\text{L}_2^{\text{Se}}(\mu\text{-OMe})_2(\text{OMe})(\text{MeOH})]$ (10)

The ligand (0.5 mmol 0.245 g) was dissolved in MeOH (25 ml) and to that NaOMe (0.11 g, 1 mmol) was added and stirred under argon. To that yellow solution CrCl_2 (0.065 g, 0.5 mmol) was added and the light green solution was refluxed under argon for 2 h and then 3 h under air. After cooling to room temperature Bu_4NPF_6 (0.19 g, 0.5 mmol) was added and solution was kept for slow evaporation of solvent. After 3 d green plate-like crystals were isolated.

Yield: 0.27 g (72%)

Molecular weight: 1446.77 g/mol

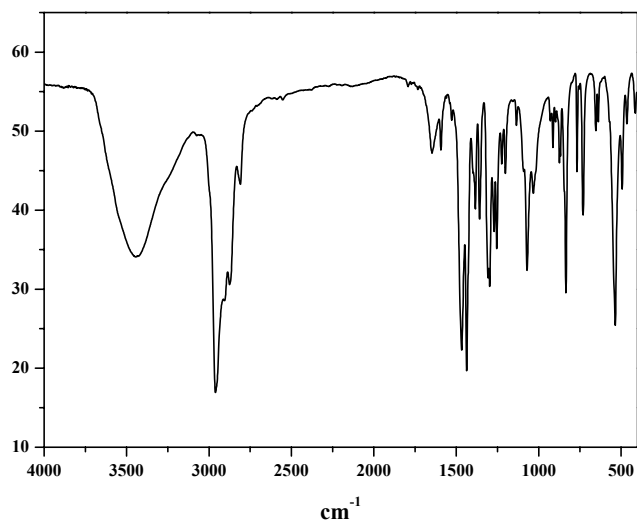


MS (ESI in CH_2Cl_2): m/z 242.3 (positive, Bu_4N^+), m/z 1171.9 (negative, M-MeOH)

Elemental analysis:

| | %C | %H | %N | %Cr |
|------------|-------|------|------|------|
| Calculated | 61.01 | 9.28 | 0.89 | 6.60 |
| Found | 61.1 | 8.7 | 0.9 | 6.3 |

Infrared spectrum:



The complex $[\text{CrL}^{\text{S}}(\mu\text{-OMe})(\text{MeOH})]_2$ (11)

The ligand (1 mmol, 0.44 g) was dissolved in dry MeOH and MeCN mixture (20 ml) and to that 2.5 ml Bu_4NOMe (20% methanolic solution) was added and stirred under argon. To that yellow solution CrCl_2 (0.13 g, 1 mmol) was added and the light green solution was refluxed under argon for 1 h, and another 1 h under air. The solution was then filtered hot to remove any insoluble impurities and on cooling to room temperature a green microcrystalline solid was isolated.

Yield: 0.22 g (40%)

Molecular weight: 1111.51 g/ mol

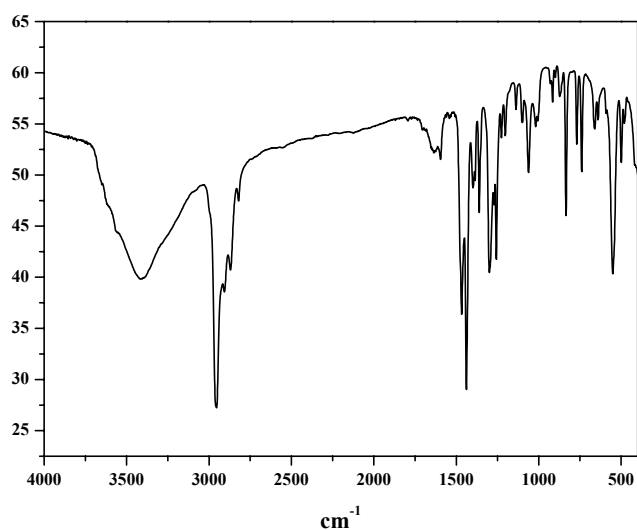


MS (EI): 1047 $[\text{M}-2\text{MeOH}]$ and decomposition products at high temperature.

Elemental analysis:

| | %C | %H | %Cr |
|------------|-------|------|------|
| Calculated | 64.07 | 8.64 | 9.06 |
| Found | 62.6 | 8.5 | 9.2 |

Infrared spectrum:



The complex $\text{Bu}_4\text{N}[\text{Cr}_2\text{L}^{\text{S}}_2(\mu\text{-OMe})_2(\text{OMe})(\text{MeOH})]$ (12)

50 mg (0.045 mmol) of complex **1** was dissolved in 5 ml CH_2Cl_2 . To that 0.5 ml Bu_4NOMe (20% methanolic solution) was added where the colour changed to deep green. To this solution was added 5 ml MeOH and 2 ml MeCN to make a layer and then allowed to diffuse and for slow evaporation. Within 2 d a deep green crystalline complex isolated.

Yield: 47 mg (78%)

Molecular weight: 1351.00 g/ mol

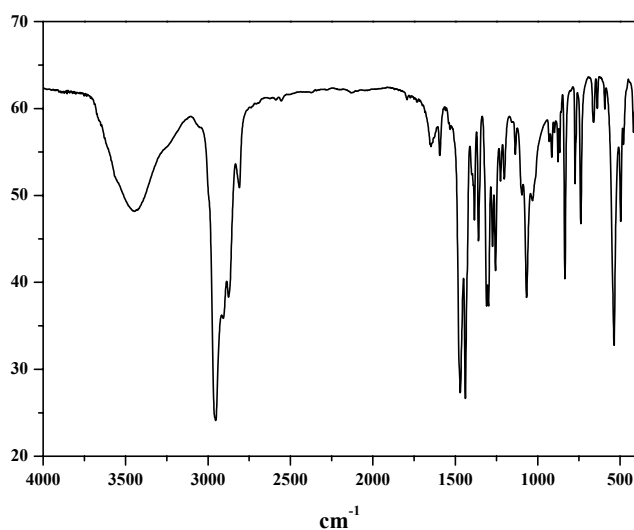
$\text{C}_{76}\text{H}_{129}\text{S}_2\text{O}_8\text{NCr}_2$

MS (ESI in MeCN): m/z 242.3 (positive, Bu_4N^+), m/z 1077.5 (negative, M-MeOH)

Elemental analysis:

| | %C | %H | %N | %Cr |
|------------|-------|------|------|------|
| Calculated | 66.76 | 9.69 | 1.01 | 7.51 |
| Found | 66.3 | 10.1 | 1.0 | 7.5 |

Infrared spectrum:



The complex $[\text{MnL}^{\text{Se}}(\mu\text{-OMe})(\text{MeOH})]_2$ (13)

The ligand (0.49 g, 1 mmol) was dissolved in dry MeOH (25 ml). To that NaOMe (0.1 g, 2 mmol) was added and stirred under argon for 5 min. To that yellow solution MnCl_2 (0.19 g, 1 mmol) was added and the resulting brown solution was refluxed under argon for 0.5 h. After cooling the solution was opened to air and stirred for another 15 min. A green microcrystalline compound was isolated, which was filtered and dried. X-ray quality crystals were grown from a solvent mixture of CH_2Cl_2 and MeOH (1:1).

Yield: 0.52 g (86%)

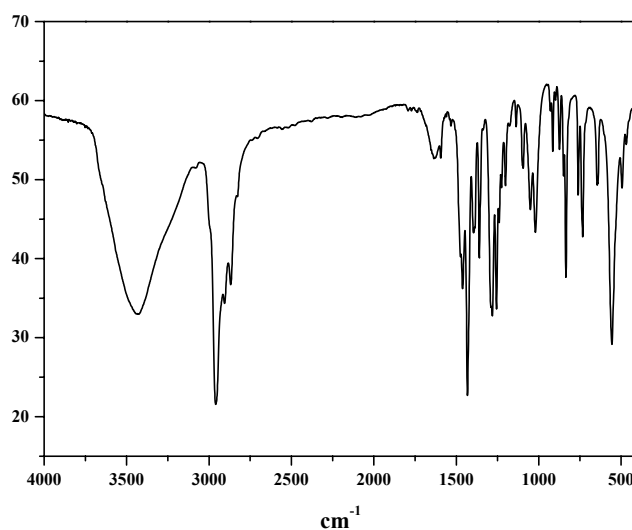
Molecular weight: 1211.20 g/ mol

$\text{C}_{60}\text{H}_{94}\text{Se}_2\text{O}_8\text{Mn}_2$

Elemental analysis:

| | %C | %H | %Mn |
|------------|-------|------|------|
| Calculated | 59.50 | 7.82 | 9.07 |
| Found | 58.0 | 8.2 | 8.7 |

Infrared spectrum:



The complex $\text{Bu}_4\text{N}[\text{MnL}^{\text{Se}}_2] \cdot \text{MeCN}$ (14)

1 mmol of ligand (0.49 g) was dissolved in 40 ml MeCN. To that Bu_4NOMe (20% methanolic solution, 1.5 ml) was added and the resulting solution was stirred for 5 min under argon. To the resulting orange solution $\text{Mn}(\text{OAc})_3$ (0.13 g, 0.5 mmol) was added and the solution was stirred under argon for 1 h at room temperature. The deep red solution was then filtered to remove any insoluble impurities and the filtrate was kept under a slow sweep of argon. Within 2 d needle like crystals were isolated.

Yield: 0.38 g (58 %)

Molecular weight: 1313.63 g/ mol

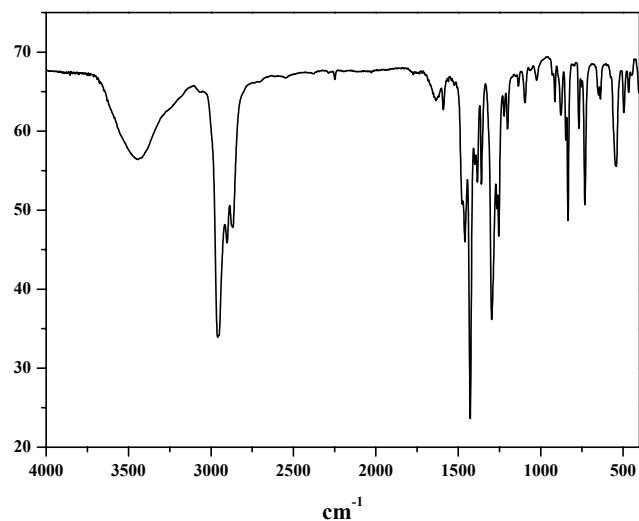
$\text{C}_{72}\text{H}_{116}\text{Se}_2\text{O}_4\text{MnN} \cdot \text{MeCN}$

MS (ESI in CH_2Cl_2): m/z 242.3 (positive, Bu_4N^+), m/z 1031 (negative, M^-)

Elemental analysis:

| | %C | %H | %N | %Mn |
|------------|-------|------|------|------|
| Calculated | 67.66 | 9.13 | 2.13 | 4.18 |
| Found | 66.2 | 8.9 | 2.7 | 4.1 |

Infrared spectrum:



The complex $[\text{MnL}^{\text{Se}}_2] \cdot \text{Fc} \cdot \text{MeCN}$ (15 Fc)

The Mn(III) monomer **14** (65 mg, 0.05 mmol) was dissolved in MeCN (10 ml). To that 25 mg FcPF₆ (0.075 mmol) was added and the solution was stirred under argon at –20°C for 2 h. The resulting deep violet solution was then filtered to remove any insoluble impurities. The solution was then concentrated to half of its original volume and kept in the refrigerator. Within 3 h needle-like crystals resulted which were filtered and dried.

Yield: 32 mg (50%)

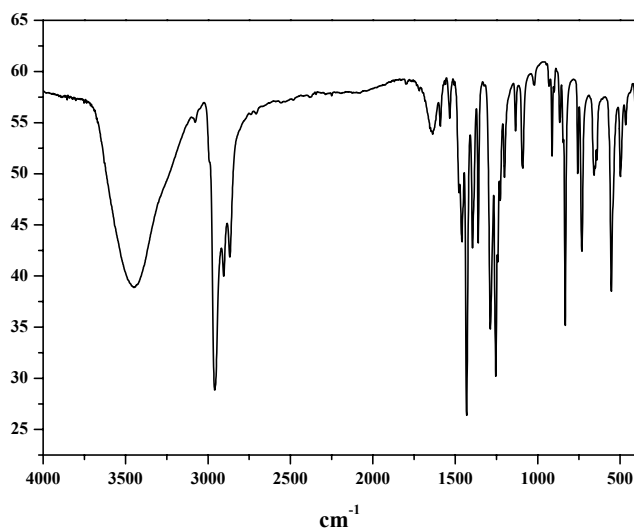
Molecular weight: 1257.14 g/ mol



Elemental analysis:

| | %C | %H | %Mn |
|------------|-------|------|------|
| Calculated | 64.97 | 7.46 | 4.37 |
| Found | 64.8 | 7.9 | 4.9 |

Infrared spectrum:



Another method of synthesis for 15:

The Mn(III) dimer **13** was dissolved in CH₂Cl₂ and kept in air for 10 h, whereupon the colour of the solution changed from deep green to deep violet. The solution was then concentrated to half of its volume and kept for 1 h. A brown solid precipitated (MnO₂), which was filtered. The violet filtrate was then concentrated, MeCN was added and then kept in the refrigerator. Overnight keeping resulted in the brown crystalline complex.

Molecular weight: 1031.11 g/ mol

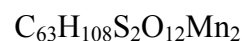


The complex [MnL^S(μ-OMe)(MeOH)]₂ · 3 MeOH (16**)**

The ligand (0.44 g, 1 mmol) was dissolved in dry MeOH (30 ml). To that Bu₄OMe (2.5 ml) was added and stirred under argon for 5 min. To that yellow solution MnCl₂ (0.125 g, 1 mmol) was added and the resulting brown solution was refluxed under argon for 0.5 h. After cooling, the solution was opened to air and stirred for another 15 min. A green microcrystalline compound was isolated which was filtered and dried. X-ray quality crystals were grown from a solvent mixture of CH₂Cl₂ and MeOH (1:1).

Yield: 0.48 g (78%)

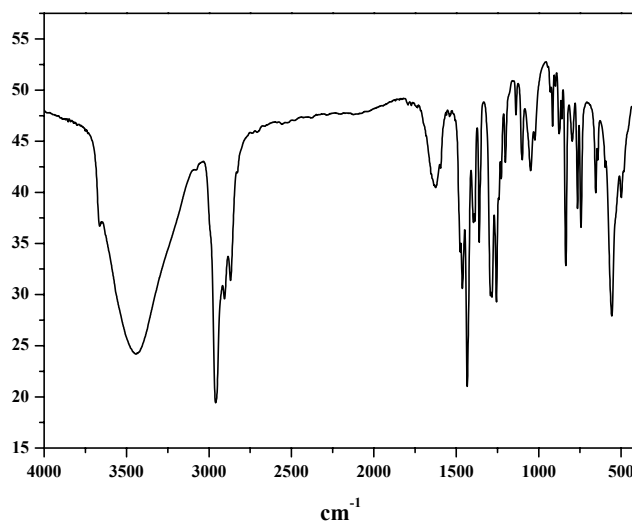
Molecular weight: 1231.54 g/ mol



Elemental analysis:

| | %C | %H | %Mn |
|------------|-------|------|------|
| Calculated | 61.44 | 8.84 | 8.92 |
| Found | 62.3 | 8.4 | 8.9 |

Infrared spectrum:



The complex $[\text{MnL}^{\text{S}}_2]$ (17)

The Mn(III) dimer **16** (0.15 g, 0.134 mmol) was dissolved in CH_2Cl_2 (15 ml) and kept under air for 10 h, whereupon the colour of the solution changed from deep green to deep violet. The solution was then concentrated to half of its volume and kept for 1 h. A brown solid precipitated (MnO_2), which was filtered. The violet filtrate was concentrated to 2 ml and 2 ml MeCN was added and the solution was kept in the refrigerator. Overnight keeping resulted in a brown crystalline complex.

Yield: 0.11 g (88 %)

Molecular weight: 936.31 g/mol

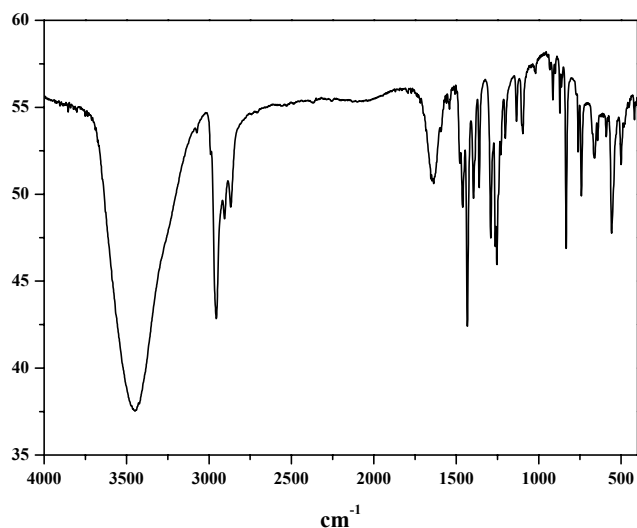


MS (EI): m/z 935 (100%)

Elemental analysis:

| | %C | %H | %S | %Mn |
|------------|-------|------|------|------|
| Calculated | 71.84 | 8.61 | 6.85 | 5.87 |
| Found | 73.1 | 8.7 | 6.8 | 5.8 |

Infrared spectrum:



The complex $[\text{FeL}^{\text{Se}}(\mu\text{-OMe})(\text{MeOH})_2] \cdot 7 \text{ MeOH}$ (18)

The ligand (0.49 g, 1 mmol) was dissolved in dry MeOH (40 ml). To that Bu_4NOMe (2.5ml 20% methanolic solution) was added and stirred under argon for 5 min. To that yellow solution FeCl_2 (0.13 g, 1 mmol) was added and the resulting brown solution was refluxed under argon for 0.5 h. After cooling, the solution was opened to air and stirred for another 15 min. A deep brown microcrystalline compound was isolated, which was filtered and air-dried. X-ray quality crystals were grown from a solvent mixture of CH_2Cl_2 and MeOH (1:1).

Yield: 0.35 g (49 %)

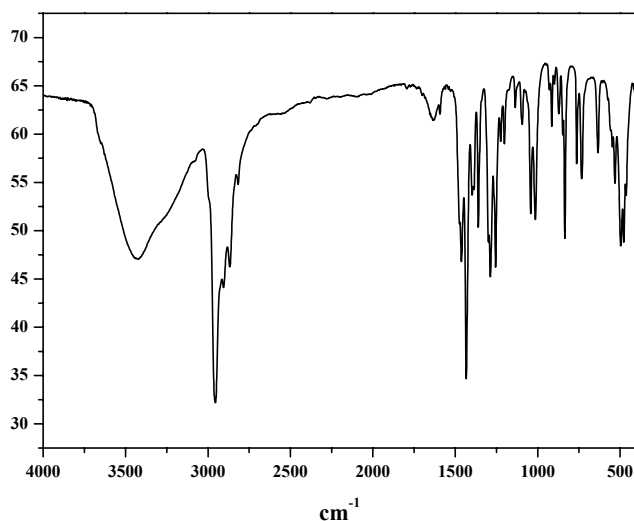
Molecular weight: 1437.31 g/ mol

$\text{C}_{60}\text{H}_{94}\text{Se}_2\text{O}_8\text{Fe} \cdot 7 \text{ MeOH}$

Elemental analysis:

| | %C | %H | %Fe |
|------------|-------|------|------|
| Calculated | 55.99 | 8.56 | 7.77 |
| Found | 57.6 | 7.2 | 8.3 |

Infrared spectrum:



The complex $\text{Bu}_4\text{N}[\text{Fe L}^{\text{Se}}_2]$ (19)

The ligand (0.49 g, 1 mmol) was dissolved in dry MeOH (30 ml). To that Bu_4NOH (3 ml 1M methanolic solution) was added and stirred under argon for 5 min. To that yellow solution FeCl_2 (0.065 g, 0.5 mmol) was added and the resulting red solution was refluxed under argon for 0.5 h. After cooling, the solution was opened to air and stirred for another 15 min. The solution was then filtered to remove any insoluble impurities and the filtrate was kept under a slow sweep of argon. Deep red crystals were isolated within 2 d.

Yield: 0.55 g (86 %)

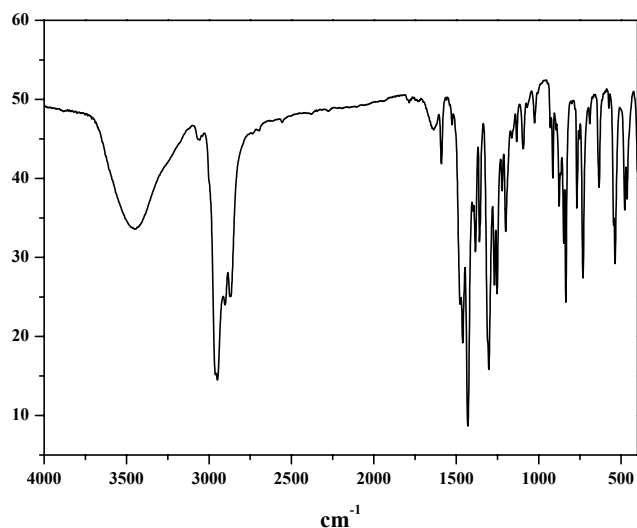
Molecular weight: 1273.48 g/ mol $\text{C}_{72}\text{H}_{116}\text{Se}_2\text{O}_4\text{FeN}$

MS (ESI in CH_2Cl_2): m/z 242.3 (positive, Bu_4N^+), m/z 1032 (negative, M^-)

Elemental analysis:

| | %C | %H | %N | %Fe |
|------------|-------|------|-----|------|
| Calculated | 67.91 | 9.18 | 1.1 | 4.39 |
| Found | 67.2 | 9.4 | 1.2 | 4.8 |

Infrared spectrum:



The complex $\text{Bu}_4\text{N}[\text{FeL}^{\text{Se}}\text{L}^{\text{Se}}]$ (20)

0.5 mmol (0.245 g) of ligand $\text{H}_2\text{L}^{\text{Se}}$ and 0.5 mmol (0.285 g) of ligand $\text{H}_2\text{L}^{\text{Se-Se}}$ were dissolved in dry MeOH (25 ml) under argon. To that light yellow solution Bu_4NOMe (2 ml 20% methanolic solution) was added which turned the solution to deep yellow. After stirring the solution for 15 min under argon, FeCl_2 (0.13 g, 1 mmol) was added and the solution turned immediately to pink red. Within 1 h a deep red crystalline complex was isolated.

Yield: 0.29 g (55 %)

Molecular weight: 1069.17 g/ mol

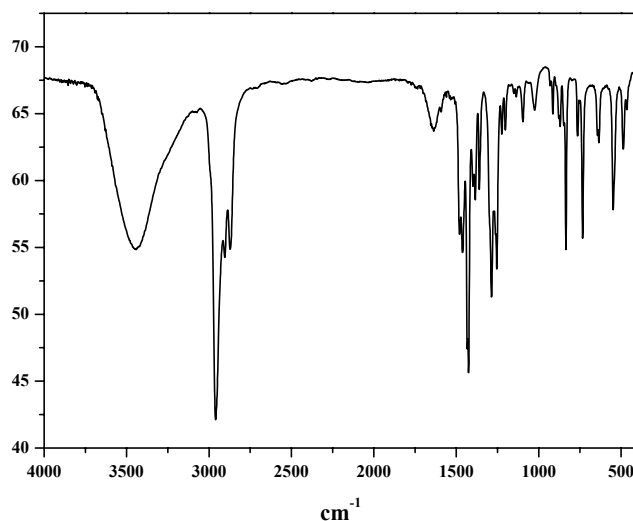
$\text{C}_{58}\text{H}_{96}\text{Se}_2\text{O}_3\text{FeN}$

MS (ESI in CH_2Cl_2): m/z 242.3 (positive, Bu_4N^+), m/z 827 (negative, M^-)

Elemental analysis:

| | %C | %H | %Fe |
|------------|-------|------|------|
| Calculated | 65.16 | 9.05 | 5.22 |
| Found | 63.0 | 8.7 | 6.4 |

Infrared spectrum:



The complex $\text{Bu}_4\text{N}[\text{FeL}^{\text{S}'}\text{L}^{\text{S}}]$ (21)

0.5 mmol (0.22 g) of ligand $\text{H}_2\text{L}^{\text{S}}$ and 0.5 mmol (0.24 g) of ligand $\text{H}_2\text{L}^{\text{S-S}}$ were dissolved in dry MeOH (25 ml) under argon. To that light yellow solution Bu_4NOMe (2ml 20% methanolic solution) was added which turned the solution to deep yellow. After stirring the solution for 15 min under argon, FeCl_2 (0.13 g, 1 mmol) was added and the solution turned immediately to pink red. Within 1 h a deep red crystalline complex was isolated.

Yield: 0.41 g (84 %)

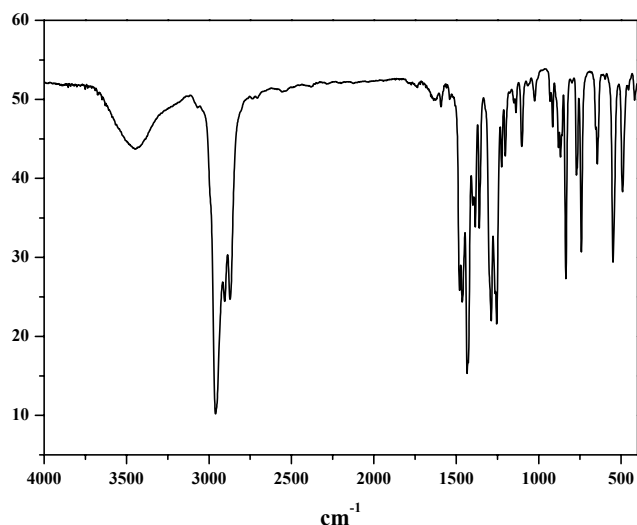
Molecular weight: 975.37 g/ mol $\text{C}_{58}\text{H}_{96}\text{S}_2\text{O}_3\text{FeN}$

MS (ESI in CH_2Cl_2): m/z 242.3 (positive, Bu_4N^+), m/z 732 (negative, M^-)

Elemental analysis:

| | %C | %H | %N | %S | %Fe |
|------------|-------|------|------|------|------|
| Calculated | 71.42 | 9.92 | 1.44 | 6.57 | 5.73 |
| Found | 70.9 | 9.8 | 1.4 | 6.6 | 5.8 |

Infrared spectrum:



The complex $[\text{Ni}_4\text{L}^{\text{S}}_2(\mu\text{-OMe})_4(\text{MeOH})_4(\text{MeCN})_2]$ (22)

1 mmol of ligand (0.44 g) was dissolved in a 12.5 ml MeOH and 2.5 ml MeCN mixture. To that LiOMe (2 ml 1 M methanolic solution, 2 mmol) was added and the solution was stirred for 5 min. $\text{NiCl}_2 \cdot 6\text{H}_2\text{O}$ (0.24 g, 1 mmol) was added to that yellow solution and the resulting green solution was stirred for 5 min and then kept for slow evaporation of solvent under air undisturbed. A green crystalline compound separated overnight.

Yield: 0.42 g (58 %).

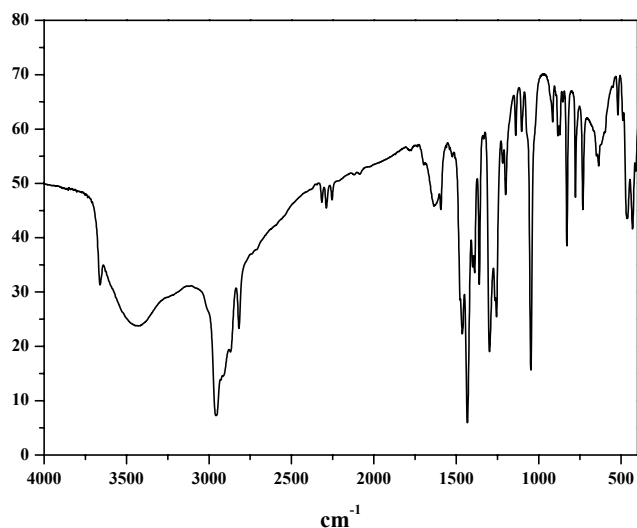
Molecular weight: 1450.54 g/ mol



Elemental analysis:

| | %C | %H | %N | %S | %Ni |
|------------|-------|------|------|------|-------|
| Calculated | 56.31 | 7.92 | 1.93 | 4.42 | 16.18 |
| Found | 55.7 | 7.9 | 2.0 | 4.3 | 15.7 |

Infrared spectrum:



The complex $[\text{Ni}_4\text{L}^{\text{Se}}_2(\mu\text{-OMe})_4(\text{MeOH})_4(\text{MeCN})_2](23)$

1 mmol of ligand (0.49 g) was dissolved in a 12.5 ml MeOH and 2.5 ml MeCN mixture. To that LiOMe (2 ml 1 M methanolic solution, 2 mmol) was added and the solution was stirred for 5 min. $\text{NiCl}_2 \cdot 6\text{H}_2\text{O}$ (0.24 g, 1 mmol) was added to that yellow solution and the resulting green solution was stirred for 5 min and then kept for slow evaporation of solvent under air undisturbed. A green crystalline compound separated overnight.

Yield: 0.34 g (44 %)

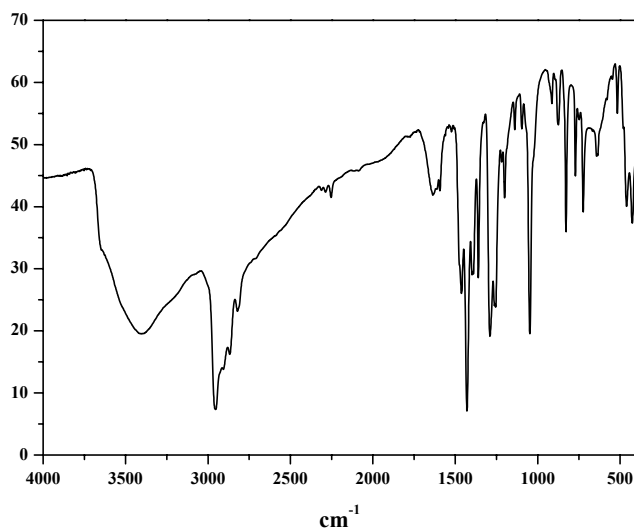
Molecular weight: 1544.34 g/mol



Elemental analysis:

| | %C | %H | %Ni |
|------------|-------|------|-------|
| Calculated | 52.89 | 7.44 | 15.20 |
| Found | 49.6 | 7.3 | 14.9 |

Infrared spectrum:



The complex $[\text{Ni}_5\text{L}^{\text{N}}_4(\mu_3\text{-OH})_2(\mu\text{-H}_2\text{O})_2(\text{EtOH})_2] \cdot 0.75 \text{CH}_2\text{Cl}_2$ (24)

1 mmol of ligand (0.30 g) was dissolved in 15 ml EtOH. To that LiOEt (2 ml 1 M methanolic solution, 2 mmol) was added and the solution was stirred for 5 min. $\text{NiCl}_2 \cdot 6\text{H}_2\text{O}$ (0.24 g, 1 mmol) was added to that yellow solution and the resulting light green solution was stirred under air. The yellowish green microcrystalline compound that separated was filtered and dried. X-ray quality crystals were grown from a solvent mixture (1:2) of CH_2Cl_2 and EtOH.

Yield: 0.32 g (75 %)

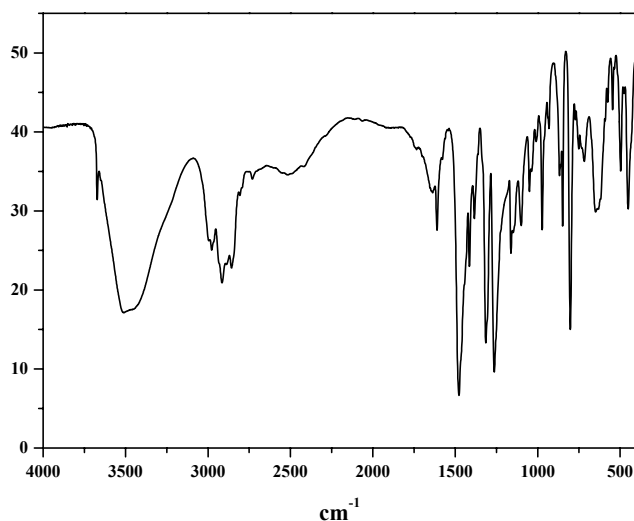
Molecular weight: 1708.96g/ mol

$\text{C}_{80}\text{H}_{110}\text{O}_{14}\text{Ni}_5\text{N}_4 \cdot 0.75 \text{CH}_2\text{Cl}_2$

Elemental analysis:

| | %C | %H | %N | %Ni |
|------------|-------|------|------|-------|
| Calculated | 56.75 | 6.58 | 3.28 | 17.17 |
| Found | 56.9 | 6.7 | 3.2 | 17.4 |

Infrared spectrum:



The complex $[\text{Ni}_6\text{L}^{\text{N}}_4(\mu\text{-MeOH})(\mu_3\text{-OMe})_2(\text{MeOH})_2(\text{MeCN})_2]$ (25)

0.5 mmol (0.15 g) of ligand was treated with NaOMe (2 ml, 0.5 M methanolic solution) in a solvent mixture of MeCN (3 ml) and MeOH (15 ml). To that $\text{NiCl}_2 \cdot 6\text{H}_2\text{O}$ (0.12 g, 0.5 mmol) was added and the light green solution was kept at room temperature. A green crystalline complex was isolated overnight.

Yield: 0.11 g (49 %)

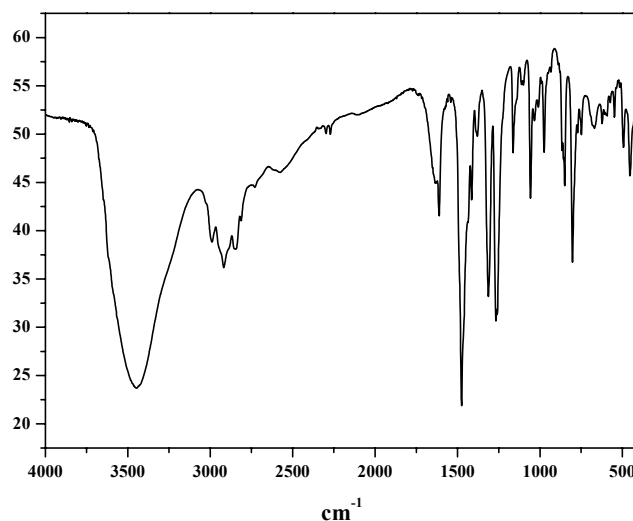
Molecular weight: 1816.04 g/ mol



Elemental analysis:

| | %C | %H | %N | %Ni |
|------------|-------|------|------|-------|
| Calculated | 56.22 | 6.55 | 4.63 | 19.39 |
| Found | 53.3 | 6.3 | 3.9 | 19.2 |

Infrared spectrum:



General method of synthesis for complexes 26-28

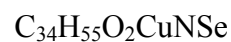
1 mmol of ligand (0.49 g) was dissolved in dry MeOH (50 ml). To that solution CuCl (0.1 g, 1 mmol) was added under argon. After addition of 0.5 ml of the respective amine the solution was refluxed under argon for 30 min. After cooling to room temperature it was opened to air. The color changed to deep green or blue immediately and within 1 h greenish microcrystalline solid separated, which was filtered and dried. Recrystallization was done from a solvent mixture of CH₂Cl₂ and MeOH(1:1).

The reaction can also be performed with CuCl₂ (1 mmol) in MeOH under air at room temperature to give the mononuclear complexes in high yield.

The complex [CuL^{Se}(Et₃N)] (26)

Yield: 0.33 g (51 %)

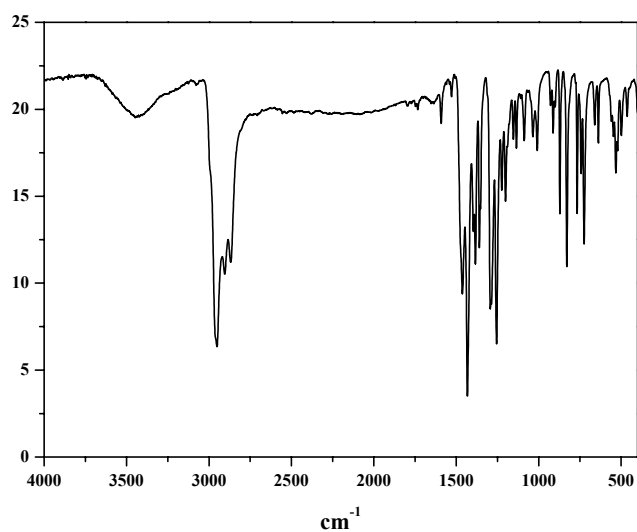
Molecular weight: 652.32 g/ mol



Elemental analysis:

| | %C | %H | %N | %Cu |
|------------|------|-----|------|------|
| Calculated | 62.6 | 8.5 | 2.15 | 9.74 |
| Found | 61.2 | 8.4 | 2.1 | 9.4 |

Infrared spectrum:



The complex [CuL^{Se}(Et₂NH)] (27)

Yield: 0.51 g (82 %)

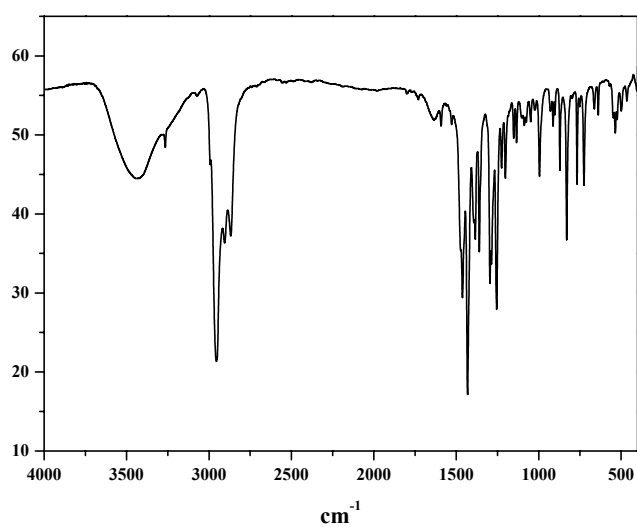
Molecular weight: 624.27 g/ mol

C₃₂H₅₁O₂CuNSe

Elemental analysis:

| | %C | %H | %N | %Cu |
|------------|-------|------|------|-------|
| Calculated | 61.57 | 8.23 | 2.24 | 10.18 |
| Found | 61.2 | 8.1 | 1.9 | 10.5 |

Infrared spectrum:



The complex $[\text{CuL}^{\text{Se}}(\text{tBuNH}_2)]$ (28)

Yield: 0.4 g (64%)

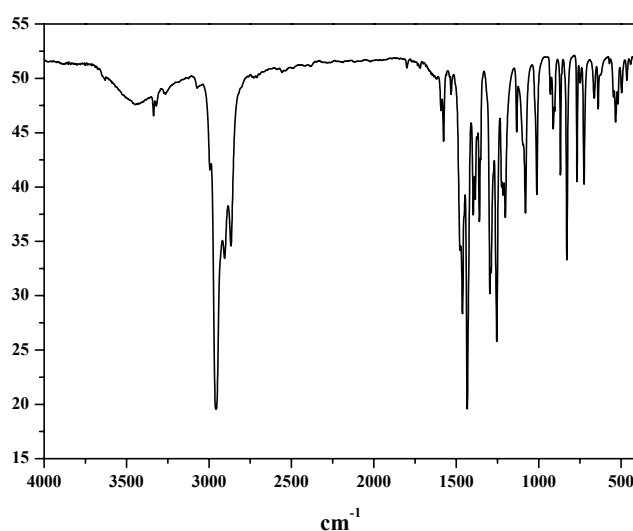
Molecular weight: 624.27 g/ mol

$\text{C}_{32}\text{H}_{51}\text{O}_2\text{CuNSe}$

Elemental analysis:

| | %C | %H | %N | %Cu |
|------------|-------|------|------|-------|
| Calculated | 61.57 | 8.23 | 2.24 | 10.18 |
| Found | 60.9 | 8.1 | 2.3 | 10.1 |

Infrared spectrum:

**The complex $[\text{CuL}^{\text{Se}}(\text{PhCH}_2\text{NH}_2)]_2 \cdot \text{H}_2\text{O}$ (29)**

1 mmol of $\text{Cu}(\text{ClO}_4)_2 \cdot 6 \text{H}_2\text{O}$ (0.37 g) was dissolved in dry MeOH (10 ml). To that a CH_2Cl_2 (10 ml) solution of 1 mmol ligand (0.49 g) and 1 ml of PhCH_2NH_2 , was added dropwise to make a layer. It was then allowed to diffuse and kept under a slow sweep of argon at room temperature. After one day deep brown crystals were separated.

Yield: 0.26 g (39 %)

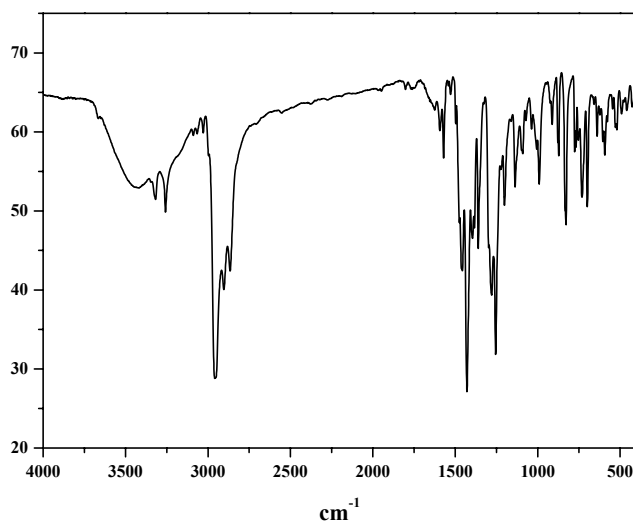
Molecular weight: 1334.59 g/ mol

$\text{C}_{70}\text{H}_{98}\text{O}_4\text{Cu}_2\text{N}_2\text{Se}_2 \cdot \text{H}_2\text{O}$

Elemental analysis:

| | %C | %H | %N | %Cu |
|------------|-------|------|------|------|
| Calculated | 63.00 | 7.55 | 2.10 | 9.52 |
| Found | 63.6 | 7.5 | 2.2 | 10.1 |

Infrared spectrum:



The complex $[L^{Se}_2(HL^{Se})Cu_3(\mu-OH)(MeCN)] \cdot MeCN$ (30)

The ligand (0.49 g, 1 mmol) was dissolved in deaerated MeCN (30 ml) and deprotonated with (*i*Pr)₂NEt (0.34 ml, 2 mmol). To that light yellow solution solid $[Cu(MeCN)_4]ClO_4$ (0.33 g, 1 mmol) was added and the solution was refluxed under argon for ½ h. After cooling to room temperature solution was opened to air whereupon the color changed to deep brown. Upon stirring for 2 h in air at room temperature a brown microcrystalline solid separated, was filtered and air-dried. X-ray quality crystals were grown from a solvent mixture of CH₂Cl₂ and MeCN(1:1).

Yield: 0.33 g (56 %)

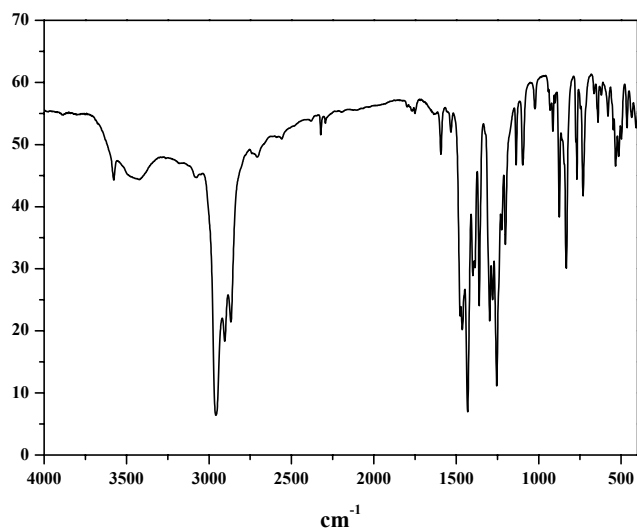
Molecular weight: 1753.42 g/ mol

$C_{86}H_{125}O_7Cu_3NSe_3 \cdot MeCN$

Elemental analysis:

| | %C | %H | %N | %Cu |
|------------|-------|------|------|-------|
| Calculated | 60.32 | 7.36 | 0.82 | 11.13 |
| Found | 60.4 | 7.5 | 0.8 | 11.2 |

Infrared spectrum:



The complex $[L^{Se}_2(HL^{Se})Cu_3(\mu-O Me)(MeOH)] \cdot CH_2Cl_2$ (31)

The ligand (0.49 g, 1 mmol) was dissolved in dry MeOH (30 ml) and deprotonated with (*i*Pr)₂NEt (0.34 ml, 2 mmol). To that light yellow solution CuCl₂ (0.17 g, 1 mmol) was added and the resulting brown solution was stirred at room temperature in air for ½ h. A brown microcrystalline solid separated, which was filtered and air-dried. X-ray quality crystals were grown from a solvent mixture of CH₂Cl₂ and MeOH (1:1).

Yield: 0.48 g (80%)

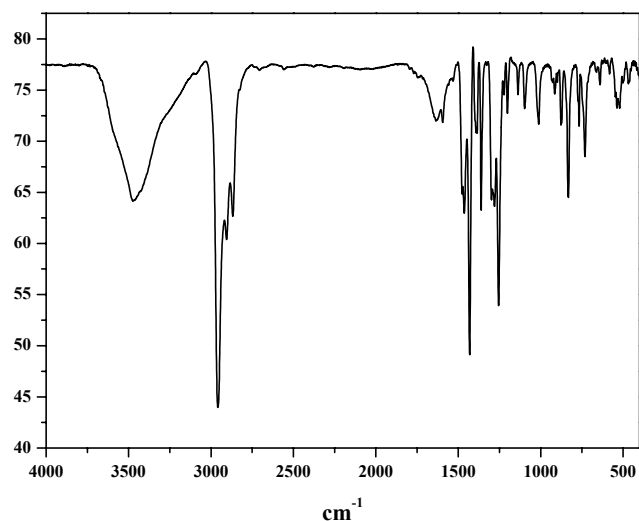
Molecular weight: 1802.31 g/ mol



Elemental analysis:

| | %C | %H | %Cu |
|------------|-------|------|-------|
| Calculated | 57.98 | 7.27 | 10.58 |
| Found | 57.6 | 7.3 | 10.7 |

Infrared spectrum:



The complex $\text{Bu}_4\text{N}[\text{Fe L}^{\text{N}}_2] \cdot 2\text{MeOH}$ (33)

To an argon-scrubbed solution of ligand (0.3 g, 1 mmol) and Bu_4NOH (2 ml) in MeOH (30 ml) was added FeCl_2 (65 mg, 0.5 mmol) whereupon the solution became red colored. The solution was refluxed under argon for 0.5 h and then for an additional 0.5 h in the presence of air, cooled to room temperature and filtered to remove any solid particles. The mother liquor was concentrated by passing a slow stream of argon. After 2 d a deep red crystalline complex was isolated by filtration and air-drying.

Yield: 0.33 g (69 %)

Molecular weight: 957.19 g / mol

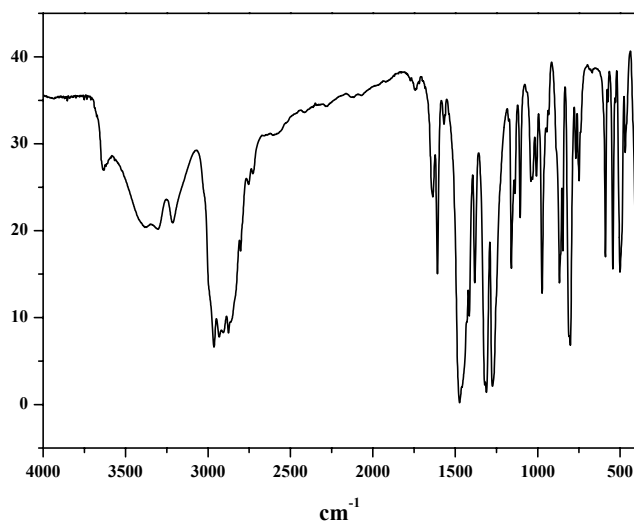
$\text{C}_{56}\text{H}_{90}\text{N}_3\text{O}_6\text{Fe}$

MS (ESI, MeCN): $m/z = 650$ [negative ion], 242 [positive ion]

Elemental analysis:

| | %C | %H | %N | %Fe |
|------------|-------|------|------|------|
| Calculated | 70.27 | 9.48 | 4.39 | 5.83 |
| Found | 70.1 | 9.2 | 4.5 | 5.9 |

Infrared spectrum:



The complex [MnL^N₂] (34)

A solution of the ligand (0.3 g, 1 mmol) in MeOH (20 ml) was treated with NaOMe (0.11 g, 2 mmol), followed by solid ‘Mn(III)-acetate’ (0.13 g, 0.5 mmol). The resulting brown solution was stirred in air for 1 h, during which the color of the solution changed to deep violet. The solution was then filtered to remove any insoluble solid and kept at room temperature in air for slow evaporation of solvent. After 2 d a violet crystalline solid was isolated by filtration. X-ray quality crystals were grown from MeCN solution by slow sweep of argon.

Yield: 0.23 g (71 %)

Molecular weight: 649.73 g / mol

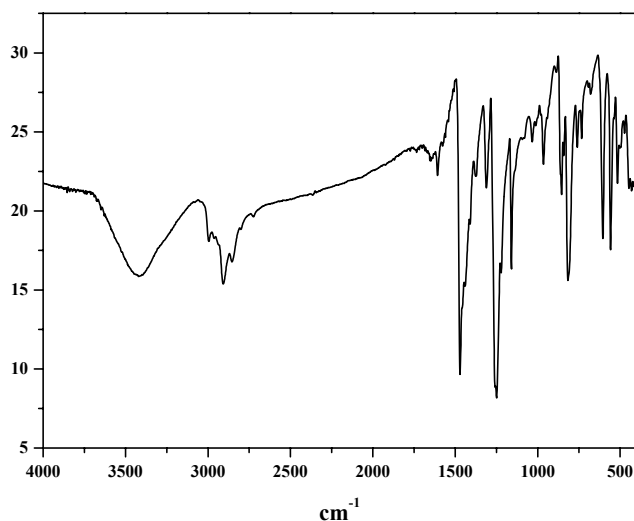
C₃₈H₄₆N₂O₄Mn

MS (ESI, CH₂Cl₂): m/z = 649 [positive ion]

Elemental analysis:

| | %C | %H | %N | %Mn |
|------------|-------|------|------|------|
| Calculated | 70.25 | 7.14 | 4.23 | 8.14 |
| Found | 68.8 | 7.1 | 4.2 | 8.5 |

Infrared spectrum:



The complex $\text{Bu}_4\text{N}[\text{MnL}^{\text{N}}_2]$ (35)

All the operations were performed under argon. ‘Manganic acetate’ (0.134 g, 0.5 mmol) was added to a solution of ligand (0.3 g, 1 mmol) and Bu_4NOH (2 ml of 1M methanolic solution) in degassed MeCN (25 ml), whereupon the solution turned to reddish brown. The resulting solution was stirred under argon for 0.5 h and kept under a sweep of argon. After 3 d a brown crystalline solid was isolated by filtration.

Yield: 0.23 g (52 %)

Molecular weight: 892.20 g / mol

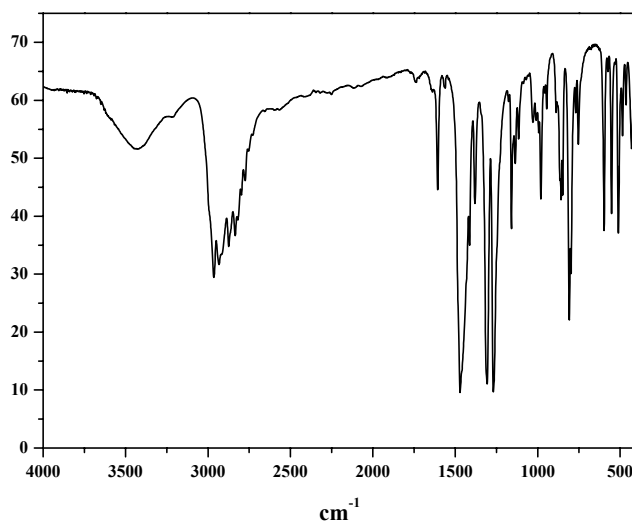
$\text{C}_{54}\text{H}_{82}\text{N}_3\text{O}_4\text{Mn}$

MS (ESI, MeCN): $m/z = 649$ [negative ion], 242 [positive ion]

Elemental analysis:

| | %C | %H | %N | %Mn |
|------------|-------|------|------|------|
| Calculated | 72.70 | 9.26 | 4.71 | 6.16 |
| Found | 71.7 | 8.9 | 4.9 | 6.5 |

Infrared spectrum:



The complex $\text{Bu}_4\text{N}[\text{CrL}^{\text{N}}_2]$ (36)

To a degassed solution of ligand (0.3 g, 1 mmol) in MeCN (15 ml) Bu_4NOMe (2.5 ml 20% methanolic solution) was added under argon. Solid anhydrous CrCl_2 (0.06 g, 0.5 mmol) was added to the above solution, whereupon a change in color from green to purple blue was observed. The colored solution was refluxed under argon for 1 h and then under air for an additional hour. The cooled solution was filtered to remove any solid particles and the mother liquor was concentrated by a slow sweep of argon. Purple-blue X-ray quality crystals were isolated by filtration after 2 d.

Yield: 0.25 g (56 %)

Molecular weight: 889.26 g / mol

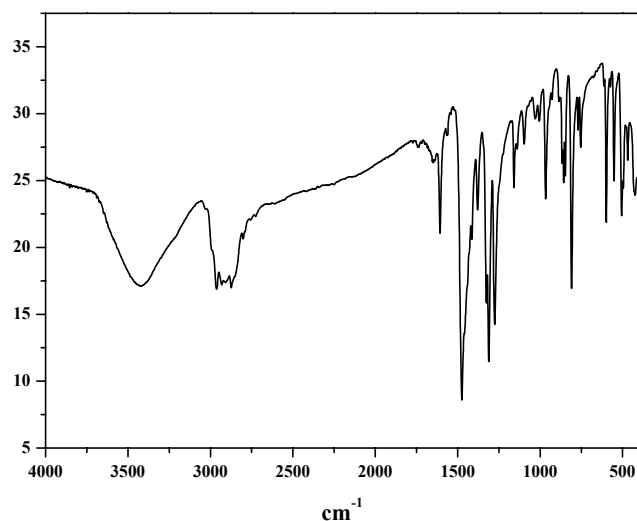
$\text{C}_{54}\text{H}_{82}\text{N}_3\text{O}_4\text{Cr}$

MS (ESI, MeCN): $m/z = 646$ [negative ion], 242 [positive ion]

Elemental analysis:

| | %C | %H | %N | %Cr |
|------------|-------|------|------|------|
| Calculated | 72.94 | 9.29 | 4.73 | 5.85 |
| Found | 71.9 | 8.7 | 5.1 | 5.5 |

Infrared spectrum:



7.3 REACTIVITY STUDIES

General method for catalytic oxidation of primary alcohols

Catalytic oxidation reactions were performed in dry MeCN at ambient temperature. Alcohol was taken in the solvent and treated with base (Bu_4NOMe 20% methanolic solution) under argon. To that solution the Cu(II) complex was added, opened to ($t = 0$) and stirred in air at room temperature for 10 h. After that the sample was taken, passed through a short silica column, washed with CH_2Cl_2 and products were detected and quantified with respect to an internal standard by GC.

General method for catalytic oxidation of primary amines

Catalytic amine oxidation reactions were performed in dry MeOH at ambient temperature. The ligand was dissolved in solvent and to that CuCl was added under argon. To the resulting yellow solution primary amine was added and the solution was refluxed under argon for 15 min. After cooling to room temperature the solution was opened ($t = 0$) and stirred in air at room temperature for 24 h. After that the sample was taken, passed through a short neutral alumina column, washed with CH_2Cl_2 and products were detected and quantified with respect to an internal standard by GC.

General method for catalytic oxidation of alkenes

Catalytic oxidation reactions were performed in dry MeCN. Alkene was taken in the solvent and treated with the complex **14** and a base, 2-methyl-imidazole at 0°C. To that solution H₂O₂ was added (t = 0) and stirred in a closed vessel. The solution changed its color slowly to yellow and a brown solid separated during when the solution attained room temperature. The solution was then analyzed by GC and products were quantified with respect to an internal standard.

Appendices

- 1) Crystallographic data**
- 2) Magnetochemical data**
- 3) Curriculum Vitae**

1) Crystallographic data

Crystal data and structure refinement for Ligand H₂L^{Se}

| H ₂ L ^{Se} | |
|------------------------------------|--|
| Empirical formula | C ₂₈ H ₄₂ SeO ₂ |
| Formula weight | 489.6 |
| Temperature | 100(2) K |
| Wavelength (MoK α) | 0.71073 Å |
| Crystal system | Orthorhombic |
| Space group | Pccn No. 56 |
| Unit cell dimensions | a = 10.641(2) Å, b = 24.267(5) Å, c = 10.424(2) Å, $\alpha = 90^\circ$ $\beta = 90^\circ$ $\gamma = 90^\circ$ |
| Volume (Å ³), Z | 2691.7(9), 4 |
| Density (calc.) Mg/m ³ | 1.208 |
| Absorption coeff | 1.415 mm ⁻¹ |
| F(000) | 1040 |
| Crystal size (mm) | 0.58 x 0.10 x 0.10 |
| θ range for data collect. | 1.68 to 23.16 deg |
| Index range | -10 \leq h \leq 11, -17 \leq k \leq 26, -10 \leq l \leq 11 |
| Reflections collected | 9436 |
| Independent reflect. | 1918 |
| Absorption correction | SADABS |
| Data/restraints/param. | 1918 / 0 / 151 |
| Goodness-of-fit on F ² | 0.953 |
| Final R indices [I $>2\sigma$ (I)] | R1=0.0474, wR2=0.1167 |
| R indices (all data) | R1=0.0651, wR2=0.1213 |

Crystal data and structure refinement for 1, 2 and 5

| | 1 | 2 | 5 |
|--|--|---|--|
| Empirical formula | C ₅₆ H ₈₀ VS ₂ O ₄ | C ₅₆ H ₈₀ VSe ₂ O ₄ | C ₃₈ H ₄₆ VN ₂ O ₄ *2/3 MeCN |
| Formula weight | 932.31 | 1026.11 | 673.08 |
| Temperature | 100(2) K | 100(2) K | 100(2) K |
| Wavelength (MoK α) | 0.71073 Å | 0.71073 Å | 0.71073 Å |
| Crystal system | Orthorhombic | Orthorhombic | Monoclinic |
| Space group | Pccn | Pccn (No. 56) | P2 ₁ /c |
| Unit cell dimensions | a = 19.6860(12) Å, b = 15.4480(12) Å, c = 18.1887(12) Å, $\alpha = 90^\circ$ $\beta = 90^\circ$ $\gamma = 90^\circ$ | a=19.4267(11) Å, b=15.3404(9) Å, c=18.8858(11) Å, $\alpha=90^\circ$ $\beta=90^\circ$ $\gamma=90^\circ$ | a=22.5319(12) Å, b=16.1089(9) Å, c=14.5134(9) Å, $\alpha=90^\circ$ $\beta=97.90(1)^\circ$ $\gamma=90^\circ$ |
| Volume (Å ³), Z | 5529.2(7), 4 | 5628.2(6), 4 | 5217.8(5), 6 |
| Density (calc.) Mg/m ³ | 1.120 | 1.211 | 1.285 |
| Absorption coeff | 0.296 mm ⁻¹ | 1.510 mm ⁻¹ | 0.329 mm ⁻¹ |
| F(000) | 2012 | 2156 | 2146 |
| Crystal size (mm) | 0.67 x 0.14 x 0.10 | 0.32 x 0.10 x 0.08 | 0.15 x 0.15 x 0.04 |
| θ range for data collect. | 2.24 to 33.00 deg | 1.69 to 24.00 deg | 4.44 to 26.00 deg |
| Index range | -30 $\leq h \leq$ 30, -23 $\leq k \leq$ 22, -27 $\leq l \leq$ 14 | -18 $\leq h \leq$ 23, -18 $\leq k \leq$ 14, -22 $\leq l \leq$ 20 | -29 $\leq h \leq$ 29, -20 $\leq k \leq$ 20, -18 $\leq l \leq$ 18 |
| Reflections collected | 40108 | 21751 | 33024 |
| Independent reflect. | 10392 [R(int)=0.1129] | 4426 | 10170 [R(int)=0.0970] |
| Absorption correction | MulScanAbs, Platon Program Suite 1999 | SADABS | Gaussian, face-in- dexed |
| Data/restraints/param. | 10340 / 0 / 285 | 4412 / 0 / 285 | 10137 / 0 / 638 |
| Goodness-of-fit on F ² | 1.024 | 1.024 | 1.019 |
| Final R indices [I \geq 2 σ (I)] | R1=0.0506, wR2=0.1207 | R1=0.0570, wR2=0.1003 | R1=0.0691, wR2=0.1616 |
| R indices (all data) | R1=0.0826, wR2=0.1483 | R=0.1107, wR2=0.1155 | R1=0.1014, wR2=0.1798 |

Crystal data and structure refinement for 7 and 8

| | 7 | 8 |
|-----------------------------------|---|--|
| Empirical formula | C ₆₈ H ₉₁ VP ₂ O ₇ *CH ₂ Cl ₂ *MeCN | C ₆₄ H ₉₄ V ₂ Se ₂ O ₈ N ₄ |
| Formula weight | 1259.27 | 1307.23 |
| Temperature | 100(2) K | 100(2) K |
| Wavelength (MoK α) | 0.71073 Å | 0.71073 Å |
| Crystal system | Triclinic | Monoclinic |
| Space group | p-1 | P2 ₁ /n |
| Unit cell dimensions | a=14.5723(9) Å, b=15.9764(12) Å, c=18.0224(14) Å, α =83.66(2) $^\circ$ β =73.39(2) $^\circ$ γ =65.61(2) $^\circ$ | a=17.625(2) Å, b=9.6819(9) Å, c=20.108(2) Å, α =90 $^\circ$ β =95.31(1) $^\circ$ γ =90 $^\circ$ |
| Volume (Å ³), Z | 3661.8(5), 2 | 3416.6(6), 2 |
| Density (calc.) Mg/m ³ | 1.142 | 1.271 |
| Absorption coeff | 1.300 mm ⁻¹ | 1.390 mm ⁻¹ |
| F(000) | 1344 | 1368 |
| Crystal size (mm) | 0.7 x 0.6 x 0.6 | 0.23 x 0.20 x 0.10 |
| θ range for data collect. | 2.25 to 33.18 deg | 1.61 to 25.00 deg |
| Index range | -20 $\leq h \leq$ 22, -24 $\leq k \leq$ 18, -24 $\leq l \leq$ 27 | -25 $\leq h \leq$ 27, -14 $\leq k \leq$ 7, -30 $\leq l \leq$ 30 |
| Reflections collected | 39123 | 25476 |
| Independent reflect. | 23692 | 5953 |
| | [R(int)=0.0234] | [R(int)=0.1006] |
| Absorption correction | SADABS | SADABS |
| Data/restraints/param. | 23670 / 10 / 759 | 5942 / 0 / 367 |
| Goodness-of-fit on F ² | 1.084 | 1.026 |
| Final R indices | R1=0.0744, [I>2 σ (I)] wR2=0.2341 | R1=0.0496, wR2=0.1120 |
| R indices (all data) | R=0.1134, wR2=0.2571 | R1=0.0915, wR2=0.1287 |

Crystal data and structure refinement for 9, 10 and 11

| | 9 | 10 | 11 |
|---------------------------------------|--|---|---|
| Empirical formula | C ₆₈ H ₁₂₆ Cr ₂ Se ₂ O ₁₆ | C _{76.5} H ₁₃₁ Cr ₂ NO _{8.5} Se ₂ | C ₆₈ H ₁₂₆ Cr ₂ S ₂ O ₁₆ |
| Formula weight | 1461.61 | 1462.74 | 1367.81 |
| Temperature | 100(2) K | 100(2) K | 100(2) K |
| Wavelength (MoK α) | 0.71073 Å | 0.71073 Å | 0.71073 Å |
| Crystal system | Triclinic | Monoclinic | Triclinic |
| Space group | p-1 | P2(1)/m | p-1 |
| Unit cell dimensions | a = 11.3263(9) Å, b = 13.1581(9) Å, c = 13.6913(9) Å, α = 82.59(1) $^\circ$ β = 86.84(1) $^\circ$ γ = 87.98(1) $^\circ$ | a=10.2757(8) Å, b=29.351(3) Å, c=13.910(10) Å, α =90 $^\circ$ β =108.88(1) $^\circ$ γ =90 $^\circ$ | a=11.3458(9) Å, b=12.9930(10) Å, c=13.5770(10) Å, α =82.99(1) $^\circ$ β =86.35(1) $^\circ$ γ =87.86(1) $^\circ$ |
| Volume (Å ³), Z | 2019.5(2), 1 | 3970(3), 2 | 1981.6(6), 1 |
| Density (calc.) Mg/m ³ | 1.202 | 1.224 | 1.146 |
| Absorption coeff | 1.226 mm ⁻¹ | 1.241 mm ⁻¹ | 0.384 mm ⁻¹ |
| F(000) | 778 | 1562 | 742 |
| Crystal size (mm) | 0.52 x 0.41 x 0.24 | 0.18 x 0.14 x 0.05 | 0.30 x 0.15 x 0.15 |
| θ range for data collect. | 2.02 to 33.00 deg | 2.95 to 26.00 deg | 4.55 to 29.00 deg |
| Index range | -16 \leq h \leq 16, -13 \leq k \leq 20, -19 \leq l \leq 20 | -15 \leq h \leq 13, -43 \leq k \leq 35, -19 \leq l \leq 20 | -15 \leq h \leq 17, -18 \leq k \leq 19, -14 \leq l \leq 20 |
| Reflections collected | 21940 | 27423 | 18367 |
| Independent reflect. | 13113 [R(int)=0.0254] | 7907 [R(int)=0.0866] | 10362 [R(int)=0.0381] |
| Absorption correction | SADABS | Gaussian, face indexed | Not corrected |
| Data/restraints/param. | 13099 / 0 / 409 | 7825/ 18 / 472 | 10271 / 0 / 408 |
| Goodness-of-fit on F ² | 0.974 | 1.052 | 1.029 |
| Final R indices [I>2 σ (I)] | R1=0.0481, wR2=0.1150 | R1=0.0594, wR2=0.1285 | R1=0.0683, wR2=0.1730 |
| R indices (all data) | R1=0.0776, wR2=0.1247 | R=0.1041, wR2=0.1915 | R1=0.0999, wR2=0.1986 |

Crystal data and structure refinement for 13, 15 and 17

| | 13 | 15 | 17 |
|--|---|---|--|
| Empirical formula | C ₆₀ H ₉₄ Mn ₂ Se ₂ O ₈ * 0.5 MeOH* 0.5 H ₂ O | C ₅₆ H ₈₀ MnO ₄ Se ₂ * Fc * MeCN | C ₅₆ H ₈₀ MnS ₂ O ₄ |
| Formula weight | 1236.18 | 1257.14 | 936.26 |
| Temperature | 100(2) K | 100(2) K | 100(2) K |
| Wavelength (MoK α) | 0.71073 Å | 0.71073 Å | 0.71073 Å |
| Crystal system | Monoclinic | Monoclinic | Orthorhombic |
| Space group | P2/n, No 13 | P2(1)/n | Pccn, No. 56 |
| Unit cell dimensions | a = 15.798(2) Å, b = 11.2908(12) Å, c = 18.644(2) Å, $\alpha = 90^\circ$ $\beta = 102.75(2)^\circ$ $\gamma = 90^\circ$ | a=24.410(3) Å, b=15.052(2) Å, c=18.558(2) Å, $\alpha=90^\circ$ $\beta=107.21(2)^\circ$ $\gamma=90^\circ$ | a=19.6760(12) Å, b=15.4393(8) Å, c=17.8833(8) Å, $\alpha=90^\circ$ $\beta=90^\circ$ $\gamma=90^\circ$ |
| Volume (Å ³), Z | 3243.6(6), 2 | 6513.3(14), 4 | 5432.7(5), 4 |
| Density (calc.) Mg/m ³ | 1.266 | 1.282 | 1.145 |
| Absorption coeff | 1.561 mm ⁻¹ | 1.580 mm ⁻¹ | 0.361 mm ⁻¹ |
| F(000) | 1300 | 2636 | 2020 |
| Crystal size (mm) | 0.12 x 0.12 x 0.05 | 0.15 x 0.14 x 0.12 | 0.28 x 0.05 x 0.04 |
| θ range for data collect. | 1.80 to 22.50 deg | 1.61 to 22.50 deg | 2.83 to 25.00 deg |
| Index range | -20 \leq h \leq 17, -12 \leq k \leq 14, -21 \leq l \leq 23 | -27 \leq h \leq 24, -13 \leq k \leq 16, -19 \leq l \leq 20 | -25 \leq h \leq 24, -20 \leq k \leq 20, -16 \leq l \leq 23 |
| Reflections collected | 19414 | 40492 | 39935 |
| Independent reflect. | 4239 | 8486 | 4781 [R(int)=0.1128] |
| Absorption correction | Not corrected | Not corrected | Gaussian face-indexed |
| Data/restraints/param. | 4202 / 67 / 330 | 8453/ 0 / 695 | 4745/ 0 / 285 |
| Goodness-of-fit on F ² | 1.050 | 0.904 | 1.027 |
| Final R indices [I \geq 2 σ (I)] | R1=0.0740, wR2=0.1737 | R1=0.0554, wR2=0.1154 | R1=0.0522, wR2=0.0866 |
| R indices (all data) | R1=0.1157, wR2=0.2044 | R1=0.1306, wR2=0.1450 | R1=0.0947, wR2=0.1016 |

Crystal data and structure refinement for 18, 19 and 20

| | 18 | 19 | 20 |
|--|---|--|---|
| Empirical formula | C ₆₀ H ₉₄ Fe ₂ Se ₂ O ₈ * 7 MeOH | C ₇₂ H ₁₁₆ FeNO ₄ Se ₂ | C ₅₈ H ₉₆ FeNSe ₂ O ₃ *2/3 H ₂ O |
| Formula weight | 1437.31 | 1273.48 | 1081.14 |
| Temperature | 100(2) K | 100(2) K | 100(2) K |
| Wavelength (MoK α) | 0.71073 Å | 0.71073 Å | 0.71073 Å |
| Crystal system | Triclinic | Monoclinic | Trigonal |
| Space group | p-1 | P2(1)/n | R-3 |
| Unit cell dimensions | a = 11.3876(8) Å, b = 13.16808(10) Å, c = 13.7062(12) Å, α = 83.28(2) $^\circ$ β = 86.92(2) $^\circ$ γ = 88.08(2) $^\circ$ | a=16.1348(12) Å, b=23.824(3) Å, c=19.000(2) Å, α =90 $^\circ$ β =94.23(2) $^\circ$ γ =90 $^\circ$ | a=27.014(2) Å, b=27.014(2) Å, c=51.115(4) Å, α =90 $^\circ$ β =90 $^\circ$ γ =120 $^\circ$ |
| Volume (Å ³), Z | 2037.4(3), 1 | 7283.6(13), 4 | 32304(4), 18 |
| Density (calc.) Mg/m ³ | 1.171 | 1.161 | 1.000 |
| Absorption coeff | 1.302 mm ⁻¹ | 1.250 mm ⁻¹ | 1.258 mm ⁻¹ |
| F(000) | 764 | 2724 | 10362 |
| Crystal size (mm) | 0.36 x 0.30 x 0.24 | Not measured | 0.12 x 0.10 x 0.06 |
| θ range for data collect. | 1.79 to 27.50 deg | 3.20 to 30.00 deg | 1.51 to 23.50 deg |
| Index range | -8 \leq h \leq 17, -20 \leq k \leq 20, -16 \leq l \leq 21 | -22 \leq h \leq 19, -36 \leq k \leq 15, -12 \leq l \leq 29 | -21 \leq h \leq 38, -38 \leq k \leq 25, -71 \leq l \leq 72 |
| Reflections collected | 17597 | 24780 | 28979 |
| Independent reflect. | 8766 [R(int)=0.0423] | 17789 [R(int)=0.0532] | 10461 [R(int)=0.0656] |
| Absorption correction | Gaussian facer-indexed | Not corrected | Gaussian face-indexed |
| Data/restraints/param. | 8761 / 0 / 422 | 17638/ 0 / 749 | 10366/ 2 / 591 |
| Goodness-of-fit on F ² | 0.992 | 1.011 | 1.019 |
| Final R indices [I \geq 2 σ (I)] | R1=0.0550, wR2=0.1442 | R1=0.0449, wR2=0.0953 | R1=0.0560, wR2=0.1164 |
| R indices (all data) | R1=0.0848, wR2=0.1570 | R1=0.0733, wR2=0.1102 | R1=0.1005, wR2=0.1595 |

Crystal data and structure refinement for 23, 24 and 25

| | 23 | 24 | 25 |
|---------------------------------------|---|--|--|
| Empirical formula | C ₆₈ H ₁₁₄ Ni ₄ Se ₂ N ₂ O ₁₂ *3.5 MeCN* 0.5 MeOH | C ₈₀ H ₁₁₀ Ni ₅ N ₄ O ₁₄ *0.75 CH ₂ Cl ₂ | C ₈₅ H ₁₁₈ Ni ₆ N ₆ O ₁₅ |
| Formula weight | 1704.08 | 1708.96 | 1816.11 |
| Temperature | 100(2) K | 100(2) K | 100(2) K |
| Wavelength (MoK α) | 0.71073 Å | 0.71073 Å | 0.71073 Å |
| Crystal system | Triclinic | Monoclinic | Monoclinic |
| Space group | p-1 | P2(1)/c | C2/c |
| Unit cell dimensions | a = 15.4538(6) Å, b = 16.6106(8) Å, c = 18.2370(10) Å, α = 90.31(1) $^\circ$ β = 108.99(1) $^\circ$ γ = 105.71(1) $^\circ$ | a=20.6988(8) Å, b=25.7220(8) Å, c=17.8131(6) Å, α =90 $^\circ$ β =111.65(1) $^\circ$ γ =90 $^\circ$ | a=20.6998(12) Å, b=15.0379(9) Å, c=28.599(2) Å, α =90 $^\circ$ β =110.98(1) $^\circ$ γ =90 $^\circ$ |
| Volume (Å ³), Z | 4238.7(4), 2 | 8814.9(5), 4 | 8312.2(9), 4 |
| Density (calc.) Mg/m ³ | 1.335 | 1.288 | 1.451 |
| Absorption coeff | 1.791 mm ⁻¹ | 1.153 mm ⁻¹ | 1.399 mm ⁻¹ |
| F(000) | 1796 | 3606 | 3832 |
| Crystal size (mm) | 0.26 x 0.25 x 0.11 | 0.19 x 0.14 x 0.13 | 0.07 x 0.04 x 0.04 |
| θ range for data collect. | 4.09 to 28.50 deg | 2.92 to 23.00 deg | 2.11 to 24.00 deg |
| Index range | -23<= h <=23, -25<= k <=25, -28<= l <=28 | -22<= h <=20, -28<= k <=28, -19<= l <=19 | -23<= h <=23, -17<= k <=17, -32<= l <=32 |
| Reflections collected | 96465 | 62882 | 20329 |
| Independent reflect. | 21433 [R(int)=0.0802] | 12227 [R(int)=0.0938] | 6529 [R(int)=0.0694] |
| Absorption correction | Gaussian, face-indexed | Gaussian, Face-indexed | Not corrected |
| Data/restraints/param. | 21321 / 150 / 873 | 12227/ 36 / 1030 | 6529/ 0 / 519 |
| Goodness-of-fit on F ² | 1.031 | 1.056 | 1.016 |
| Final R indices [I>2 σ (I)] | R1=0.0538, wR2=0.1277 | R1=0.0509, wR2=0.1287 | R1=0.0587, wR2=0.1193 |
| R indices (all data) | R1=0.0851, wR2=0.1441 | R1=0.0710, wR2=0.1416 | R1=0.1069, wR2=0.1402 |

Crystal data and structure refinement for 26, 27 and 29

| | 26 | 27 | 29 |
|-----------------------------------|---|---|---|
| Empirical formula | C ₃₄ H ₅₅ CuSeNO ₂ | C ₃₂ H ₅₁ CuNO ₂ Se | C ₇₀ H ₁₀₀ Cu ₂ N ₂ Se ₂ O ₅ |
| Formula weight | 652.32 | 624.27 | 1334.59 |
| Temperature | 100(2) K | 100(2) K | 100(2) K |
| Wavelength (MoK α) | 0.71073 Å | 0.71073 Å | 0.71073 Å |
| Crystal system | Monoclinic | Monoclinic | Triclinic |
| Space group | P2(1)/n | P2(1)/n | p-1 |
| Unit cell dimensions | a = 14.1711(10) Å, b = 12.5356(9) Å, c = 39.248(3) Å, $\alpha = 90^\circ$ $\beta = 94.96(2)^\circ$ $\gamma = 90^\circ$ | a=9.6208(12) Å, b=12.399(2) Å, c=27.000(3) Å, $\alpha=90^\circ$ $\beta=95.35(2)^\circ$ $\gamma=90^\circ$ | a=13.831(1) Å, b=14.797(2) Å, c=18.613(2) Å, $\alpha=95.22(1)^\circ$ $\beta=90.96(1)^\circ$ $\gamma=113.85(1)^\circ$ |
| Volume (Å ³), Z | 6946.0(9), 8 | 3206.8(7), 4 | 3463.5(6), 2 |
| Density (calc.) Mg/m ³ | 1.248 | 1.293 | 1.280 |
| Absorption coeff | 1.705 mm ⁻¹ | 1.843 mm ⁻¹ | 1.712 mm ⁻¹ |
| F(000) | 2760 | 1316 | 1400 |
| Crystal size (mm) | 0.23 x 0.20 x 0.08 | 0.43 x 0.34 x 0.05 | 0.25 x 0.19 x 0.14 |
| θ range for data collect. | 1.71 to 30.00 deg | 2.23 to 30.00 deg | 1.61 to 22.50 deg |
| Index range | -21 $\leq h \leq$ 20, -10 $\leq k \leq$ 18, -54 $\leq l \leq$ 59 | -10 $\leq h \leq$ 14, -18 $\leq k \leq$ 18, -41 $\leq l \leq$ 40 | -16 $\leq h \leq$ 16, -17 $\leq k \leq$ 13, -19 $\leq l \leq$ 22 |
| Reflections collected | 66185 | 25278 | 12614 |
| Independent reflect. | 19434 | 9193 [R(int)=0.0540] | 8923 [R(int)=0.0710] |
| Absorption correction | SADABS | MulAbs, Platon 99 program suite | SADABS |
| Data/restraints/param. | 19317 / 0 / 703 | 9188/ 0 / 344 | 8905/ 0 / 650 |
| Goodness-of-fit on F ² | 0.997 | 1.128 | 0.891 |
| Final R indices | R1=0.0490, [I>2 σ (I)] wR2=0.0891 | R1=0.0503, wR2=0.1298 | R1=0.0643, wR2=0.1199 |
| R indices (all data) | R1=0.1015, wR2=0.1044 | R1=0.0610, wR2=0.1339 | R1=0.1477, wR2=0.1423 |

Crystal data and structure refinement for 30, 31 and 32

| | 30 | 31 | 32 |
|---------------------------------------|---|---|---|
| Empirical formula | C ₈₆ H ₁₂₅ Cu ₃ Se ₃ NO ₇ * MeCN | C ₈₇ H ₁₃₀ Cu ₃ Cl ₂ O ₈ Se ₃ | C ₈₄ H ₁₂₀ Cu ₂ Se ₂ O ₆ *2.5 CH ₂ Cl ₂ |
| Formula weight | 1753.42 | 1802.31 | 1723.11 |
| Temperature | 100(2) K | 100(2) K | 100(2) K |
| Wavelength (MoK α) | 0.71073 Å | 0.71073 Å | 0.71073 Å |
| Crystal system | Triclinic | Triclinic | Monoclinic |
| Space group | p-1 | p-1 | C2/c |
| Unit cell dimensions | a = 15.263(4) Å, b = 17.498(5) Å, c = 18.419(6) Å, α = 76.04(2) $^\circ$ β = 69.81(2) $^\circ$ γ = 88.14(2) $^\circ$ | a=14.0807(8) Å, b=14.7358(8) Å, c=22.7829(12) Å, α =77.247(2) $^\circ$ β =80.203(2) $^\circ$ γ =80.814(2) $^\circ$ | a=18.466(2) Å, b=21.457(3) Å, c=44.773(5) Å, α =90 $^\circ$ β =100.57(2) $^\circ$ γ =90 $^\circ$ |
| Volume (Å ³), Z | 4474(2), 2 | 4506.6(4), 2 | 17439(4), 8 |
| Density (calc.) Mg/m ³ | 1.302 | 1.328 | 1.313 |
| Absorption coeff | 1.977 mm ⁻¹ | 2.022 mm ⁻¹ | 1.525 mm ⁻¹ |
| F(000) | 1830 | 1878 | 7224 |
| Crystal size (mm) | 0.18 x 0.18 x 0.10 | 0.38 x 0.20 x 0.18 | 0.20 x 0.14 x 0.08 |
| θ range for data collect. | 1.48 to 19.00 deg | 1.85 to 30.00 deg | 1.62 to 25.00 deg |
| Index range | -16 \leq h \leq 16, -19 \leq k \leq 19, -20 \leq l \leq 13 | -12 \leq h \leq 21, -14 \leq k \leq 23, -31 \leq l \leq 35 | -25 \leq h \leq 28, -21 \leq k \leq 32, -49 \leq l \leq 68 |
| Reflections collected | 11483 | 43624 | 67266 |
| Independent reflect. | 7191 [R(int)=0.1483] | 23878 [R(int)=0.0383] | 15324 |
| Absorption correction | Not corrected | SADABS | SADABS |
| Data/restraints/param. | 7104 / 31 / 461 | 23819/ 25 / 994 | 15249/ 6 / 912 |
| Goodness-of-fit on F ² | 0.925 | 0.961 | 1.036 |
| Final R indices [I>2 σ (I)] | R1=0.0883, wR2=0.1783 | R1=0.0466, wR2=0.1027 | R1=0.0751, wR2=0.1379 |
| R indices (all data) | R1=0.2267, wR2=0.2404 | R1=0.0809, wR2=0.1149 | R1=0.1300, wR2=0.1580 |

Crystal data and structure refinement for 34, 35 and 36

| | 34 | [MnL^N₂]⁻ unit of 35 in [(tacn)₂Mn₂(μ-OAc)₃]⁺ | 36 |
|-----------------------------------|---|--|--|
| Empirical formula | C ₃₈ H ₄₆ MnN ₂ O ₄ * MeCN | C ₆₂ H ₉₇ Mn ₃ N ₈ O ₁₀ | C ₅₄ H ₈₂ CrN ₃ O ₄ |
| Formula weight | 690.76 | 1279.30 | 889.26 |
| Temperature | 100(2) K | 100(2) K | 100(2) K |
| Wavelength (MoKα) | 0.71073 Å | 0.71073 Å | 0.71073 Å |
| Crystal system | Orthorhombic | Monoclinic | Hexagonal |
| Space group | Pbcn | P2(1)/n | P6 ₃ |
| Unit cell dimensions | a=15.206(1) Å, b=16.368(1) Å, c=57.152(3) Å, α=90° β=90° γ=90° | a=16.3023(6) Å, b=21.7165(9) Å, c=18.1744(6) Å, α=90° β=93.90(1)° γ=90° | a=21.498(2) Å, b=21.498(2) Å, c=19.364(2) Å, α=90° β=90° γ=120° |
| Volume (Å ³), Z | 14225(2), 16 | 6419.4(4), 4 | 7750.4(13), 6 |
| Density (calc.) Mg/m ³ | 1.290 | 1.324 | 1.143 |
| Absorption coeff. | 0.416 mm ⁻¹ | 0.643 mm ⁻¹ | 0.266 mm ⁻¹ |
| F(000) | 5872 | 2720 | 2898 |
| Crystal size (mm) | 0.49 x 0.34 x 0.29 | 0.27 x 0.16 x 0.14 | 0.20 x 0.20 x 0.06 |
| θ range for data collect. | 1.43 to 25.00 deg | 2.43 to 30.00 deg | 3.58 to 22.50 deg |
| Index range | -8<=h<=23, -25<=k<=23, -87<=l<=79 | -22<=h<=25, -32<=k<=33, -25<=l<=28 | -22<=h<=30, -30<=k<=30, -26<=l<=25 |
| Reflections collected | 108082 | 83533 | 43767 |
| Independent reflect. | 12519 | 18699 | 6710 |
| | [R(int)=0.1048] | [R(int)=0.1217] | [R(int)=0.0743] |
| Absorption correction | Face Indexed | Not Indexed | Gaussian, face-in-dexed |
| Data/restraints/param. | 12471 / 0 / 867 | 18644 / 0 / 748 | 6686 / 1 / 559 |
| Goodness-of-fit on F ² | 1.036 | 1.024 | 1.171 |
| Final R indices | R1=0.0631, wR2=0.1602 | R1=0.0745, wR2=0.1675 | R1=0.1036, wR2=0.2726 |
| [I>2σ(I)] | | | |
| R indices (all data) | R=0.0937, wR2=0.1790 | R=0.1069, wR2=0.1851 | R1=0.1163, wR2=0.2992 |
| Absol. structure parameter | ---- | ---- | 0.08(5) |

Crystal data for 3, 4 and 12

| | 3 | 4 | 12 |
|---------------------------------------|---|--|--|
| Empirical formula | C ₆₈ H ₉₀ P ₂ VO ₄ | C ₆₈ H ₉₀ P ₂ O ₆ V | C ₇₆ H ₁₂₉ Cr ₂ S ₂ O ₈ N. 2MeCN |
| Formula weight | 1084.35 | 1462.74 | 1435.03 |
| Temperature | 100(2) K | 100(2) K | 100(2) K |
| Wavelength (MoK α) | 0.71073 Å | 0.71073 Å | 0.71073 Å |
| Crystal system | Monoclinic | triclinic | Orthorhombic |
| Space group | C2/c | P-1 | Cmca |
| Unit cell dimensions | a = 20.282(6) Å, b = 18.965(6) Å, c = 36.913(11) Å, $\alpha = 90^\circ$ $\beta = 99.57(4)^\circ$ $\gamma = 90^\circ$ | a=13.572(2) Å, b=14.402(2) Å, c=17.967(3) Å, $\alpha=78.10(1)^\circ$ $\beta=77.25(1)^\circ$ $\gamma=86.72(1)^\circ$ | a=22.610(2) Å, b=29.393(3) Å, c=26.450(3) Å, $\alpha=90^\circ$ $\beta=104.863(3)^\circ$ $\gamma=90^\circ$ |
| Volume (Å ³), Z | 14000.92, 8 | 3351.44, 2 | 17578(6), 8 |
| Crystal size (mm) | | | 0.13 x 0.13 x 0.11 |
| Final R indices [I>2 σ (I)] | R1=0.1197 | R1=0.1552 | R1=0.152 |

2) Magnetochemical data

Complex VL^S₂ (1)

MW = 932.31 g/mol, $\chi_{\text{dia}} = -631.60 \times 10^{-6} \text{ cm}^3 \text{ mol}^{-1}$
m = 26.23 mg, H = 1.000 T

| No | T(K) | $\chi \cdot T_{\text{exp.}}$ | $\chi \cdot T_{\text{calc.}}$ | μ_{exp} | $\mu_{\text{calc.}}$ |
|----|--------|------------------------------|-------------------------------|--------------------|----------------------|
| 1 | 2.003 | 0.26201 | 0.34803 | 1.45372 | 1.67544 |
| 2 | 4.998 | 0.35277 | 0.35867 | 1.68681 | 1.70085 |
| 3 | 10.003 | 0.35898 | 0.36067 | 1.70159 | 1.70558 |
| 4 | 15 | 0.35983 | 0.36141 | 1.70359 | 1.70733 |
| 5 | 20.002 | 0.36158 | 0.36196 | 1.70773 | 1.70863 |
| 6 | 30.001 | 0.36486 | 0.36293 | 1.71546 | 1.71092 |
| 7 | 40 | 0.36759 | 0.36385 | 1.72187 | 1.7131 |
| 8 | 50.007 | 0.36996 | 0.36477 | 1.72741 | 1.71525 |
| 9 | 60.02 | 0.37156 | 0.36567 | 1.73115 | 1.71738 |
| 10 | 70.052 | 0.37289 | 0.36658 | 1.73423 | 1.71951 |
| 11 | 80.074 | 0.37429 | 0.36749 | 1.7375 | 1.72163 |
| 12 | 90.054 | 0.37539 | 0.36839 | 1.74003 | 1.72373 |
| 13 | 100.11 | 0.37572 | 0.36929 | 1.74081 | 1.72585 |
| 14 | 110.13 | 0.37561 | 0.3702 | 1.74056 | 1.72796 |
| 15 | 120.15 | 0.37486 | 0.3711 | 1.73882 | 1.73006 |
| 16 | 130.17 | 0.37385 | 0.372 | 1.73647 | 1.73216 |
| 17 | 140.18 | 0.37278 | 0.3729 | 1.73398 | 1.73426 |
| 18 | 150.13 | 0.37135 | 0.3738 | 1.73066 | 1.73634 |
| 19 | 160.21 | 0.37133 | 0.3747 | 1.7306 | 1.73845 |
| 20 | 170.21 | 0.37082 | 0.3756 | 1.72942 | 1.74054 |
| 21 | 180.22 | 0.37105 | 0.3765 | 1.72996 | 1.74262 |
| 22 | 190.23 | 0.37186 | 0.37741 | 1.73183 | 1.74471 |
| 23 | 200.25 | 0.37236 | 0.37831 | 1.73301 | 1.74679 |
| 24 | 210.15 | 0.37417 | 0.3792 | 1.73722 | 1.74885 |
| 25 | 220.24 | 0.37692 | 0.38011 | 1.74358 | 1.75094 |
| 26 | 230.24 | 0.37433 | 0.38101 | 1.73759 | 1.75301 |
| 27 | 240.28 | 0.38069 | 0.38191 | 1.75228 | 1.75509 |
| 28 | 250.26 | 0.38327 | 0.38281 | 1.75821 | 1.75715 |
| 29 | 260.27 | 0.38376 | 0.38371 | 1.75933 | 1.75922 |
| 30 | 270.26 | 0.38575 | 0.38461 | 1.76388 | 1.76128 |
| 31 | 280.25 | 0.38287 | 0.38551 | 1.75729 | 1.76334 |
| 32 | 290.15 | 0.39061 | 0.3864 | 1.77497 | 1.76537 |

Complex VL^{Se}₂ (2)

MW = 1026.11 g/mol, $\chi_{\text{dia}} = -647.60 \times 10^{-6} \text{ cm}^3 \text{ mol}^{-1}$
 m = 35.72 mg, H = 1.000 T

| No | T(K) | $\chi \cdot T_{\text{exp.}}$ | $\chi \cdot T_{\text{calc.}}$ | μ_{exp} | $\mu_{\text{calc.}}$ |
|----|--------|------------------------------|-------------------------------|--------------------|----------------------|
| 1 | 2.001 | 0.19371 | 0.34289 | 1.24995 | 1.663 |
| 2 | 5 | 0.33818 | 0.35324 | 1.65155 | 1.68793 |
| 3 | 10.004 | 0.35143 | 0.35519 | 1.68359 | 1.69258 |
| 4 | 15 | 0.35139 | 0.35592 | 1.6835 | 1.69432 |
| 5 | 20.002 | 0.35237 | 0.35647 | 1.68585 | 1.69562 |
| 6 | 30.002 | 0.35389 | 0.35744 | 1.68947 | 1.69793 |
| 7 | 39.999 | 0.35523 | 0.35836 | 1.69267 | 1.70012 |
| 8 | 50.007 | 0.35689 | 0.35928 | 1.69662 | 1.70229 |
| 9 | 60.033 | 0.35778 | 0.36018 | 1.69874 | 1.70444 |
| 10 | 70.055 | 0.3589 | 0.36109 | 1.70141 | 1.70658 |
| 11 | 80.069 | 0.36057 | 0.36199 | 1.70536 | 1.70871 |
| 12 | 90.093 | 0.36188 | 0.3629 | 1.70844 | 1.71084 |
| 13 | 100.08 | 0.36318 | 0.3638 | 1.7115 | 1.71296 |
| 14 | 110.13 | 0.36427 | 0.3647 | 1.71407 | 1.71509 |
| 15 | 120.14 | 0.36569 | 0.36561 | 1.71743 | 1.71721 |
| 16 | 130.16 | 0.3666 | 0.36651 | 1.71955 | 1.71933 |
| 17 | 140.18 | 0.3677 | 0.36741 | 1.72212 | 1.72145 |
| 18 | 150.19 | 0.36863 | 0.36831 | 1.72431 | 1.72355 |
| 19 | 160.2 | 0.36961 | 0.36921 | 1.7266 | 1.72566 |
| 20 | 170.21 | 0.37042 | 0.37011 | 1.72849 | 1.72777 |
| 21 | 180.22 | 0.37141 | 0.37101 | 1.7308 | 1.72987 |
| 22 | 190.23 | 0.37232 | 0.37192 | 1.73292 | 1.73197 |
| 23 | 200.24 | 0.37308 | 0.37282 | 1.73468 | 1.73407 |
| 24 | 210.02 | 0.37397 | 0.3737 | 1.73674 | 1.73611 |
| 25 | 220.24 | 0.37453 | 0.37462 | 1.73804 | 1.73825 |
| 26 | 230.24 | 0.37576 | 0.37552 | 1.74089 | 1.74034 |
| 27 | 240.25 | 0.37715 | 0.37642 | 1.74412 | 1.74242 |
| 28 | 250.25 | 0.37899 | 0.37732 | 1.74837 | 1.7445 |
| 29 | 260.27 | 0.38138 | 0.37822 | 1.75388 | 1.74659 |
| 30 | 270.25 | 0.37776 | 0.37912 | 1.74553 | 1.74866 |
| 31 | 280.26 | 0.3832 | 0.38002 | 1.75806 | 1.75074 |
| 32 | 289.99 | 0.38527 | 0.38089 | 1.76279 | 1.75275 |

Complex VL^P₂ (3)

MW = 1084.35 g/mol, $\chi_{\text{dia}} = -758.39 \times 10^{-6} \text{ cm}^3 \text{ mol}^{-1}$
 m = 36.89 mg, H = 1.000 T

| No | T(K) | $\chi \cdot T_{\text{exp.}}$ | $\chi \cdot T_{\text{calc.}}$ | μ_{exp} | $\mu_{\text{calc.}}$ |
|----|--------|------------------------------|-------------------------------|--------------------|----------------------|
| 1 | 2.004 | 0.31204 | 0.35138 | 1.58643 | 1.68348 |
| 2 | 5.003 | 0.35012 | 0.36207 | 1.68046 | 1.70888 |
| 3 | 10.003 | 0.35608 | 0.36384 | 1.69469 | 1.71307 |
| 4 | 15 | 0.35624 | 0.36434 | 1.69509 | 1.71424 |
| 5 | 20.002 | 0.35736 | 0.36464 | 1.69775 | 1.71495 |
| 6 | 30 | 0.35911 | 0.36512 | 1.70188 | 1.71606 |
| 7 | 40.002 | 0.36065 | 0.36554 | 1.70554 | 1.71706 |
| 8 | 50.009 | 0.36227 | 0.36595 | 1.70936 | 1.71803 |
| 9 | 60.034 | 0.35674 | 0.36636 | 1.69627 | 1.71899 |
| 10 | 70.052 | 0.36817 | 0.36677 | 1.72323 | 1.71994 |
| 11 | 80.074 | 0.36657 | 0.36717 | 1.71947 | 1.72088 |
| 12 | 90.09 | 0.36805 | 0.36757 | 1.72294 | 1.72182 |
| 13 | 100.12 | 0.36956 | 0.36797 | 1.72648 | 1.72277 |
| 14 | 110.09 | 0.3707 | 0.36837 | 1.72914 | 1.7237 |
| 15 | 120.15 | 0.37209 | 0.36878 | 1.73238 | 1.72464 |
| 16 | 130.17 | 0.37319 | 0.36918 | 1.73494 | 1.72558 |
| 17 | 140.18 | 0.37406 | 0.36958 | 1.73695 | 1.72652 |
| 18 | 150.19 | 0.37508 | 0.36998 | 1.73933 | 1.72746 |
| 19 | 160.21 | 0.37552 | 0.37038 | 1.74034 | 1.72839 |
| 20 | 170.14 | 0.37606 | 0.37078 | 1.74159 | 1.72932 |
| 21 | 180.22 | 0.37554 | 0.37118 | 1.74038 | 1.73026 |
| 22 | 190.23 | 0.3743 | 0.37158 | 1.7375 | 1.73119 |
| 23 | 200.23 | 0.37349 | 0.37198 | 1.73564 | 1.73213 |
| 24 | 210.24 | 0.37188 | 0.37238 | 1.73189 | 1.73306 |
| 25 | 220.16 | 0.37087 | 0.37278 | 1.72953 | 1.73398 |
| 26 | 230.25 | 0.37055 | 0.37318 | 1.72878 | 1.73492 |
| 27 | 240.25 | 0.37137 | 0.37358 | 1.7307 | 1.73585 |
| 28 | 250.27 | 0.37098 | 0.37398 | 1.72978 | 1.73678 |
| 29 | 260.27 | 0.37 | 0.37438 | 1.72751 | 1.73771 |
| 30 | 270.25 | 0.37829 | 0.37478 | 1.74675 | 1.73863 |
| 31 | 280.15 | 0.37617 | 0.37518 | 1.74186 | 1.73955 |
| 32 | 290.24 | 0.38155 | 0.37558 | 1.75426 | 1.74049 |

Complex VL^{PO}₂ (4)

MW = 1116.35 g/mol, $\chi_{\text{dia}} = -786.60 \times 10^{-6} \text{ cm}^3 \text{ mol}^{-1}$
m = 25.16 mg , H = 1.000 T

| No | T(K) | $\chi \cdot T_{\text{exp.}}$ | $\chi \cdot T_{\text{calc.}}$ | μ_{exp} | $\mu_{\text{calc.}}$ |
|----|--------|------------------------------|-------------------------------|--------------------|----------------------|
| 1 | 1.999 | 0.20753 | 0.34098 | 1.29377 | 1.65838 |
| 2 | 5 | 0.32219 | 0.35099 | 1.61204 | 1.68254 |
| 3 | 10.003 | 0.33644 | 0.35247 | 1.64731 | 1.6861 |
| 4 | 15 | 0.33764 | 0.35275 | 1.65024 | 1.68676 |
| 5 | 20.002 | 0.33906 | 0.35285 | 1.6537 | 1.68699 |
| 6 | 30.002 | 0.3412 | 0.35292 | 1.6589 | 1.68716 |
| 7 | 40.001 | 0.34298 | 0.35294 | 1.66323 | 1.68721 |
| 8 | 50.011 | 0.34493 | 0.35295 | 1.66795 | 1.68724 |
| 9 | 60.033 | 0.34668 | 0.35296 | 1.67218 | 1.68725 |
| 10 | 70.056 | 0.34807 | 0.35296 | 1.67553 | 1.68726 |
| 11 | 80.053 | 0.35015 | 0.35296 | 1.68052 | 1.68727 |
| 12 | 90.092 | 0.3521 | 0.35297 | 1.6852 | 1.68727 |
| 13 | 100.11 | 0.35383 | 0.35297 | 1.68933 | 1.68728 |
| 14 | 110.12 | 0.35576 | 0.35297 | 1.69394 | 1.68728 |
| 15 | 120.14 | 0.35741 | 0.35297 | 1.69787 | 1.68728 |
| 16 | 130.16 | 0.35888 | 0.35297 | 1.70136 | 1.68728 |
| 17 | 140.18 | 0.35994 | 0.35297 | 1.70387 | 1.68728 |
| 18 | 150.13 | 0.36068 | 0.35297 | 1.70561 | 1.68728 |
| 19 | 160.2 | 0.36081 | 0.35297 | 1.70591 | 1.68728 |
| 20 | 170.21 | 0.36055 | 0.35297 | 1.7053 | 1.68728 |
| 21 | 180.22 | 0.35991 | 0.35297 | 1.7038 | 1.68728 |
| 22 | 190.23 | 0.35934 | 0.35297 | 1.70245 | 1.68729 |
| 23 | 200.24 | 0.35887 | 0.35297 | 1.70132 | 1.68729 |
| 24 | 210.23 | 0.3586 | 0.35297 | 1.70069 | 1.68729 |
| 25 | 220.16 | 0.35924 | 0.35297 | 1.70219 | 1.68729 |
| 26 | 230.24 | 0.36033 | 0.35297 | 1.70478 | 1.68729 |
| 27 | 240.26 | 0.36206 | 0.35297 | 1.70887 | 1.68729 |
| 28 | 250.25 | 0.3662 | 0.35297 | 1.71861 | 1.68729 |
| 29 | 260.26 | 0.37092 | 0.35297 | 1.72966 | 1.68729 |
| 30 | 270.24 | 0.36923 | 0.35297 | 1.72569 | 1.68729 |
| 31 | 280.17 | 0.34991 | 0.35297 | 1.67996 | 1.68729 |
| 32 | 290.24 | 0.37592 | 0.35297 | 1.74127 | 1.68729 |

Complex VL^N₂ (5)

MW = 673.1 g/mol, $\chi_{\text{dia}} = -415.10 \times 10^{-6} \text{ cm}^3 \text{ mol}^{-1}$
 m = 24.03 mg, H = 1.000 T

| No | T(K) | $\chi \cdot T_{\text{exp.}}$ | $\chi \cdot T_{\text{calc.}}$ | μ_{exp} | $\mu_{\text{calc.}}$ |
|----|--------|------------------------------|-------------------------------|--------------------|----------------------|
| 1 | 2.001 | 0.31949 | 0.3236 | 1.60527 | 1.61556 |
| 2 | 5.003 | 0.32919 | 0.333 | 1.62944 | 1.63886 |
| 3 | 10.003 | 0.33517 | 0.33505 | 1.6442 | 1.6439 |
| 4 | 15 | 0.33584 | 0.33602 | 1.64583 | 1.64628 |
| 5 | 20.002 | 0.33686 | 0.33683 | 1.64832 | 1.64826 |
| 6 | 30 | 0.33835 | 0.33834 | 1.65197 | 1.65195 |
| 7 | 39.999 | 0.33973 | 0.33981 | 1.65532 | 1.65552 |
| 8 | 50.009 | 0.34471 | 0.34126 | 1.66742 | 1.65907 |
| 9 | 60.035 | 0.34915 | 0.34272 | 1.67813 | 1.6626 |
| 10 | 70.047 | 0.34777 | 0.34417 | 1.6748 | 1.66611 |
| 11 | 80.067 | 0.34725 | 0.34562 | 1.67356 | 1.66962 |
| 12 | 90.08 | 0.34765 | 0.34707 | 1.67451 | 1.67312 |
| 13 | 100.12 | 0.34843 | 0.34852 | 1.67639 | 1.67662 |
| 14 | 110.14 | 0.34972 | 0.34997 | 1.67949 | 1.6801 |
| 15 | 120.1 | 0.35078 | 0.35141 | 1.68203 | 1.68355 |
| 16 | 130.16 | 0.35187 | 0.35286 | 1.68465 | 1.68703 |
| 17 | 140.18 | 0.35337 | 0.35431 | 1.68824 | 1.69049 |
| 18 | 150.19 | 0.35473 | 0.35576 | 1.69147 | 1.69394 |
| 19 | 160.19 | 0.35618 | 0.35721 | 1.69494 | 1.69738 |
| 20 | 170.2 | 0.35758 | 0.35865 | 1.69827 | 1.70081 |
| 21 | 180.22 | 0.35933 | 0.3601 | 1.70242 | 1.70424 |
| 22 | 190.23 | 0.36048 | 0.36155 | 1.70513 | 1.70766 |
| 23 | 200.15 | 0.36193 | 0.36298 | 1.70857 | 1.71105 |
| 24 | 210.24 | 0.3636 | 0.36444 | 1.71249 | 1.71448 |
| 25 | 220.24 | 0.36506 | 0.36589 | 1.71594 | 1.71788 |
| 26 | 230.24 | 0.36633 | 0.36733 | 1.71893 | 1.72127 |
| 27 | 240.26 | 0.36871 | 0.36878 | 1.72448 | 1.72466 |
| 28 | 250.26 | 0.36972 | 0.37023 | 1.72685 | 1.72803 |
| 29 | 260.26 | 0.3722 | 0.37167 | 1.73264 | 1.7314 |
| 30 | 270.25 | 0.37335 | 0.37312 | 1.73532 | 1.73476 |
| 31 | 280.26 | 0.37561 | 0.37456 | 1.74055 | 1.73812 |
| 32 | 290.25 | 0.37845 | 0.37601 | 1.74711 | 1.74147 |

Complex VL^{N1}₂ (6)

MW = 982.38 g/mol, $\chi_{\text{dia}} = -689.70 \times 10^{-6} \text{ cm}^3 \text{ mol}^{-1}$
m = 19.61 mg , H = 1.000 T

| No | T(K) | $\chi \cdot T_{\text{exp.}}$ | $\chi \cdot T_{\text{calc.}}$ | μ_{exp} | $\mu_{\text{calc.}}$ |
|----|--------|------------------------------|-------------------------------|--------------------|----------------------|
| 1 | 1.999 | 0.2096 | 0.33076 | 1.29473 | 1.62643 |
| 2 | 4.998 | 0.34585 | 0.34075 | 1.66312 | 1.65081 |
| 3 | 9.999 | 0.35217 | 0.34316 | 1.67824 | 1.65663 |
| 4 | 15.001 | 0.35366 | 0.34443 | 1.6818 | 1.6597 |
| 5 | 20.002 | 0.35487 | 0.34553 | 1.68467 | 1.66235 |
| 6 | 29.999 | 0.35647 | 0.34762 | 1.68845 | 1.66737 |
| 7 | 40.002 | 0.3579 | 0.34967 | 1.69184 | 1.67227 |
| 8 | 50.003 | 0.35999 | 0.3517 | 1.69678 | 1.67713 |
| 9 | 60.03 | 0.36158 | 0.35374 | 1.70052 | 1.68198 |
| 10 | 70.026 | 0.36411 | 0.35577 | 1.70646 | 1.68679 |
| 11 | 80.058 | 0.36707 | 0.3578 | 1.71337 | 1.6916 |
| 12 | 90.108 | 0.36914 | 0.35983 | 1.71821 | 1.69641 |
| 13 | 100.08 | 0.37068 | 0.36185 | 1.72179 | 1.70116 |
| 14 | 110.13 | 0.37214 | 0.36389 | 1.72517 | 1.70594 |
| 15 | 120.16 | 0.37389 | 0.36592 | 1.72924 | 1.71069 |
| 16 | 130.16 | 0.37517 | 0.36794 | 1.73219 | 1.71542 |
| 17 | 140.17 | 0.3767 | 0.36997 | 1.73572 | 1.72014 |
| 18 | 150.12 | 0.37778 | 0.37198 | 1.73819 | 1.72481 |
| 19 | 160.2 | 0.37934 | 0.37402 | 1.74178 | 1.72953 |
| 20 | 170.21 | 0.38005 | 0.37605 | 1.74341 | 1.73421 |
| 21 | 180.23 | 0.38089 | 0.37808 | 1.74534 | 1.73888 |
| 22 | 190.23 | 0.38249 | 0.3801 | 1.74899 | 1.74353 |
| 23 | 200.25 | 0.38368 | 0.38213 | 1.75171 | 1.74818 |
| 24 | 210.25 | 0.38605 | 0.38416 | 1.75713 | 1.7528 |
| 25 | 220.24 | 0.38847 | 0.38618 | 1.76261 | 1.75741 |
| 26 | 230.15 | 0.39035 | 0.38818 | 1.76688 | 1.76197 |
| 27 | 240.27 | 0.39427 | 0.39023 | 1.77573 | 1.76661 |
| 28 | 250.26 | 0.39859 | 0.39225 | 1.78542 | 1.77118 |
| 29 | 260.26 | 0.40311 | 0.39428 | 1.79553 | 1.77575 |
| 30 | 270.24 | 0.37328 | 0.3963 | 1.72782 | 1.78029 |
| 31 | 280.25 | 0.37532 | 0.39832 | 1.73252 | 1.78484 |
| 32 | 290.24 | 0.38057 | 0.40035 | 1.74461 | 1.78936 |

Complex [CrL^{Se}(μ-OMe)(MeOH)]₂ (9)

MW = 1205.31 g/mol, $\chi_{\text{dia}} = -745.42 \times 10^{-6} \text{ cm}^3 \text{ mol}^{-1}$
m = 15.45 mg ; H = 1.000 T

| No | T(K) | $\chi \cdot T_{\text{exp.}}$ | $\chi \cdot T_{\text{calc.}}$ | μ_{exp} | $\mu_{\text{calc.}}$ |
|----|--------|------------------------------|-------------------------------|--------------------|----------------------|
| 1 | 1.999 | 0.05457 | 7.06105E-6 | 0.66346 | 0.00755 |
| 2 | 5.002 | 0.09583 | 0.01574 | 0.87918 | 0.35635 |
| 3 | 10.003 | 0.24399 | 0.17736 | 1.40284 | 1.19603 |
| 4 | 14.999 | 0.43039 | 0.37243 | 1.86316 | 1.73316 |
| 5 | 20.002 | 0.61488 | 0.5593 | 2.22696 | 2.12393 |
| 6 | 30.001 | 0.96457 | 0.92066 | 2.78924 | 2.72501 |
| 7 | 39.999 | 1.27806 | 1.25468 | 3.21066 | 3.18115 |
| 8 | 50.006 | 1.55772 | 1.5445 | 3.54457 | 3.52949 |
| 9 | 60.022 | 1.78449 | 1.78633 | 3.79381 | 3.79576 |
| 10 | 70.044 | 1.96857 | 1.98522 | 3.98468 | 4.0015 |
| 11 | 80.067 | 2.12409 | 2.14871 | 4.13909 | 4.16301 |
| 12 | 90.081 | 2.254 | 2.28389 | 4.26378 | 4.29196 |
| 13 | 100.11 | 2.36522 | 2.39699 | 4.36771 | 4.39695 |
| 14 | 110.12 | 2.45778 | 2.49227 | 4.45236 | 4.48349 |
| 15 | 120.15 | 2.54022 | 2.57366 | 4.52641 | 4.55611 |
| 16 | 130.15 | 2.61001 | 2.64351 | 4.58817 | 4.61752 |
| 17 | 140.17 | 2.67425 | 2.70429 | 4.64429 | 4.6703 |
| 18 | 150.19 | 2.73077 | 2.7575 | 4.69311 | 4.71603 |
| 19 | 160.2 | 2.78188 | 2.80438 | 4.73683 | 4.75594 |
| 20 | 170.2 | 2.82961 | 2.84596 | 4.77729 | 4.79107 |
| 21 | 180.22 | 2.87128 | 2.88318 | 4.81234 | 4.8223 |
| 22 | 190.23 | 2.91226 | 2.91658 | 4.84656 | 4.85015 |
| 23 | 200.22 | 2.94749 | 2.94668 | 4.87578 | 4.87511 |
| 24 | 210.24 | 2.97631 | 2.97407 | 4.89956 | 4.89772 |
| 25 | 220.24 | 3.00592 | 2.99897 | 4.92388 | 4.91818 |
| 26 | 230.23 | 3.02971 | 3.02172 | 4.94332 | 4.9368 |
| 27 | 240.25 | 3.05629 | 3.04267 | 4.96496 | 4.95388 |
| 28 | 250.25 | 3.07794 | 3.06193 | 4.98251 | 4.96954 |
| 29 | 260.26 | 3.10061 | 3.07974 | 5.00083 | 4.98397 |
| 30 | 270.24 | 3.12552 | 3.0962 | 5.02088 | 4.99727 |
| 31 | 280.25 | 3.1598 | 3.11154 | 5.04833 | 5.00963 |
| 32 | 290.26 | 3.18983 | 3.12583 | 5.07227 | 5.02112 |

Complex $\text{Bu}_4\text{N}[\text{Cr}_2\text{L}^{\text{Se}}_2(\mu\text{-OMe})_2(\text{MeOH})(\text{OMe})]$ (10)

MW = 1446.77 g/mol, $\chi_{\text{dia}} = -947.30 \times 10^{-6} \text{ cm}^3 \text{ mol}^{-1}$
m = 16.08 mg ; H = 1.000 T

| No | T(K) | $\chi \cdot T_{\text{exp.}}$ | $\chi \cdot T_{\text{calc.}}$ | μ_{exp} | $\mu_{\text{calc.}}$ |
|----|--------|------------------------------|-------------------------------|--------------------|----------------------|
| 1 | 1.999 | 1.11407 | 0.1436 | 2.99761 | 1.07621 |
| 2 | 5.003 | 1.52311 | 0.63624 | 3.50497 | 2.26532 |
| 3 | 10.002 | 1.81832 | 1.35716 | 3.8296 | 3.30852 |
| 4 | 14.999 | 2.00471 | 1.85841 | 4.02109 | 3.87159 |
| 5 | 20.002 | 2.16639 | 2.18041 | 4.1801 | 4.1936 |
| 6 | 30 | 2.42895 | 2.54409 | 4.42617 | 4.52986 |
| 7 | 39.998 | 2.62097 | 2.73751 | 4.59779 | 4.6989 |
| 8 | 50.006 | 2.75964 | 2.85598 | 4.71785 | 4.7995 |
| 9 | 60.029 | 2.86334 | 2.93561 | 4.80568 | 4.86595 |
| 10 | 70.05 | 2.93796 | 2.9926 | 4.8679 | 4.91295 |
| 11 | 80.069 | 2.9976 | 3.03536 | 4.91706 | 4.94793 |
| 12 | 90.058 | 3.04222 | 3.06851 | 4.95352 | 4.97487 |
| 13 | 100.11 | 3.07958 | 3.09518 | 4.98384 | 4.99645 |
| 14 | 110.12 | 2.95438 | 3.11689 | 4.88148 | 5.01394 |
| 15 | 120.15 | 3.13519 | 3.13501 | 5.02864 | 5.02849 |
| 16 | 130.16 | 3.15539 | 3.15029 | 5.04481 | 5.04073 |
| 17 | 140.17 | 3.17608 | 3.16338 | 5.06132 | 5.05119 |
| 18 | 150.18 | 3.19343 | 3.17472 | 5.07513 | 5.06024 |
| 19 | 160.2 | 3.21258 | 3.18464 | 5.09032 | 5.06814 |
| 20 | 170.22 | 3.23014 | 3.19339 | 5.10422 | 5.0751 |
| 21 | 180.22 | 3.24487 | 3.20115 | 5.11584 | 5.08126 |
| 22 | 190.15 | 3.25984 | 3.20805 | 5.12763 | 5.08673 |
| 23 | 200.23 | 3.27401 | 3.21434 | 5.13876 | 5.09172 |
| 24 | 210.24 | 3.28814 | 3.21999 | 5.14984 | 5.09619 |
| 25 | 220.25 | 3.30031 | 3.22513 | 5.15936 | 5.10026 |
| 26 | 230.25 | 3.3108 | 3.22981 | 5.16755 | 5.10395 |
| 27 | 240.25 | 3.3202 | 3.2341 | 5.17488 | 5.10734 |
| 28 | 250.25 | 3.329 | 3.23805 | 5.18174 | 5.11046 |
| 29 | 260.26 | 3.33483 | 3.2417 | 5.18627 | 5.11334 |
| 30 | 270.24 | 3.348 | 3.24506 | 5.1965 | 5.11599 |
| 31 | 280.26 | 3.36175 | 3.2482 | 5.20716 | 5.11846 |
| 32 | 290.26 | 3.37468 | 3.25111 | 5.21717 | 5.12076 |

Complex [CrL^S(μ-OMe)(MeOH)]₂ (11)

MW = 1111.51 g/mol, $\chi_{\text{dia}} = -729.00 \times 10^{-6} \text{ cm}^3 \text{ mol}^{-1}$
m = 32.42 mg ; H = 1.000 T

| No | T(K) | $\chi \cdot T_{\text{exp.}}$ | $\chi \cdot T_{\text{calc.}}$ | μ_{exp} | $\mu_{\text{calc.}}$ |
|----|--------|------------------------------|-------------------------------|--------------------|----------------------|
| 1 | 1.998 | 0.06426 | 1.73699E-5 | 0.71991 | 0.01184 |
| 2 | 4.999 | 0.09933 | 0.02082 | 0.89507 | 0.40982 |
| 3 | 10.004 | 0.23412 | 0.18762 | 1.37416 | 1.23014 |
| 4 | 15 | 0.40797 | 0.37328 | 1.81397 | 1.73515 |
| 5 | 20.002 | 0.57893 | 0.55164 | 2.16089 | 2.10934 |
| 6 | 30.002 | 0.95502 | 0.89516 | 2.77539 | 2.68701 |
| 7 | 40.002 | 1.2052 | 1.20466 | 3.1178 | 3.1171 |
| 8 | 50.008 | 1.46144 | 1.46513 | 3.43328 | 3.43761 |
| 9 | 60.03 | 1.67309 | 1.67732 | 3.67348 | 3.67812 |
| 10 | 70.043 | 1.86486 | 1.84845 | 3.8783 | 3.8612 |
| 11 | 80.067 | 1.98964 | 1.98744 | 4.00595 | 4.00374 |
| 12 | 90.096 | 2.10681 | 2.10143 | 4.12222 | 4.11695 |
| 13 | 100.11 | 2.2087 | 2.19585 | 4.22072 | 4.20843 |
| 14 | 110.12 | 2.28694 | 2.27511 | 4.29483 | 4.2837 |
| 15 | 120.15 | 2.35831 | 2.34254 | 4.36133 | 4.34672 |
| 16 | 130.17 | 2.41753 | 2.40034 | 4.41575 | 4.40002 |
| 17 | 140.17 | 2.4874 | 2.45032 | 4.4791 | 4.44559 |
| 18 | 150.19 | 2.54472 | 2.49407 | 4.53042 | 4.48511 |
| 19 | 160.2 | 1.70321 | 2.53256 | 3.7064 | 4.51958 |
| 20 | 170.21 | 2.59611 | 2.56669 | 4.57594 | 4.54993 |
| 21 | 180.21 | 2.62922 | 2.59712 | 4.60502 | 4.57683 |
| 22 | 190.23 | 2.65912 | 2.62449 | 4.63113 | 4.60088 |
| 23 | 200.22 | 2.68568 | 2.6491 | 4.6542 | 4.6224 |
| 24 | 210.24 | 2.71149 | 2.67149 | 4.67652 | 4.64189 |
| 25 | 220.25 | 2.73301 | 2.69185 | 4.69504 | 4.65955 |
| 26 | 230.25 | 2.75504 | 2.71044 | 4.71392 | 4.67561 |
| 27 | 240.28 | 2.77569 | 2.72756 | 4.73155 | 4.69035 |
| 28 | 250.25 | 2.79296 | 2.74322 | 4.74625 | 4.7038 |
| 29 | 260.27 | 2.81196 | 2.75776 | 4.76237 | 4.71625 |
| 30 | 270.25 | 2.82968 | 2.77118 | 4.77735 | 4.72771 |
| 31 | 280.26 | 2.84681 | 2.78369 | 4.79179 | 4.73837 |
| 32 | 290.26 | 2.86095 | 2.79532 | 4.80367 | 4.74826 |

Complex $\text{Bu}_4\text{N}[\text{Cr}_2\text{L}^{\text{S}}_2(\mu\text{-OMe})_2(\text{MeOH})(\text{OMe})]$ (12)

MW = 1351.00 g/mol, $\chi_{\text{dia}} = -931.00 \times 10^{-6} \text{ cm}^3 \text{ mol}^{-1}$
 $m = 27.14 \text{ mg}$; $H = 1.000 \text{ T}$

| No | T(K) | $\chi \cdot T_{\text{exp.}}$ | $\chi \cdot T_{\text{calc.}}$ | μ_{exp} | $\mu_{\text{calc.}}$ |
|----|--------|------------------------------|-------------------------------|--------------------|----------------------|
| 1 | 1.999 | 1.1801 | 1.15838 | 3.08516 | 3.05664 |
| 2 | 4.999 | 2.36113 | 2.22137 | 4.36394 | 4.23281 |
| 3 | 10 | 2.74009 | 2.78146 | 4.70111 | 4.73647 |
| 4 | 15 | 2.85329 | 2.98296 | 4.79724 | 4.90503 |
| 5 | 20.003 | 2.93258 | 3.08467 | 4.86344 | 4.98796 |
| 6 | 30 | 3.04967 | 3.18616 | 4.95958 | 5.06935 |
| 7 | 40 | 3.13444 | 3.23669 | 5.02804 | 5.10939 |
| 8 | 50.01 | 3.1874 | 3.26691 | 5.07033 | 5.13319 |
| 9 | 60.029 | 3.2288 | 3.28701 | 5.10316 | 5.14895 |
| 10 | 70.041 | 3.26005 | 3.30132 | 5.12779 | 5.16015 |
| 11 | 80.078 | 3.2887 | 3.31205 | 5.15028 | 5.16853 |
| 12 | 90.082 | 3.31155 | 3.32036 | 5.16814 | 5.17501 |
| 13 | 100.11 | 3.32602 | 3.32701 | 5.17942 | 5.18019 |
| 14 | 110.13 | 3.33819 | 3.33244 | 5.18888 | 5.18441 |
| 15 | 120.16 | 3.34693 | 3.33696 | 5.19567 | 5.18793 |
| 16 | 130.17 | 3.35503 | 3.34078 | 5.20195 | 5.1909 |
| 17 | 140.18 | 3.35979 | 3.34405 | 5.20564 | 5.19344 |
| 18 | 150.19 | 3.36823 | 3.34689 | 5.21218 | 5.19564 |
| 19 | 160.2 | 3.37291 | 3.34936 | 5.2158 | 5.19756 |
| 20 | 170.21 | 3.37868 | 3.35155 | 5.22026 | 5.19926 |
| 21 | 180.15 | 3.38153 | 3.35348 | 5.22246 | 5.20075 |
| 22 | 190.23 | 3.38471 | 3.35523 | 5.22491 | 5.20211 |
| 23 | 200.25 | 3.38968 | 3.35679 | 5.22875 | 5.20332 |
| 24 | 210.25 | 3.39175 | 3.35821 | 5.23034 | 5.20442 |
| 25 | 220.25 | 3.39633 | 3.35949 | 5.23387 | 5.20541 |
| 26 | 230.25 | 3.40111 | 3.36066 | 5.23756 | 5.20632 |
| 27 | 240.26 | 3.40621 | 3.36174 | 5.24148 | 5.20715 |
| 28 | 250.25 | 3.4086 | 3.36273 | 5.24332 | 5.20792 |
| 29 | 260.28 | 3.41102 | 3.36364 | 5.24518 | 5.20863 |
| 30 | 270.27 | 3.41645 | 3.36448 | 5.24935 | 5.20928 |
| 31 | 280.27 | 3.42096 | 3.36527 | 5.25282 | 5.20989 |
| 32 | 290.25 | 3.42591 | 3.366 | 5.25662 | 5.21045 |

Complex [MnL^{Se}(μ-OMe)(MeOH)]₂ (13)

MW = 1211.20 g/mol, $\chi_{\text{dia}} = -746.04 \times 10^{-6} \text{ cm}^3 \text{ mol}^{-1}$
m = 18.21 mg ; H = 1.000 T

| No | T(K) | $\chi \cdot T_{\text{exp.}}$ | $\chi \cdot T_{\text{calc.}}$ | μ_{exp} | $\mu_{\text{calc.}}$ |
|----|--------|------------------------------|-------------------------------|--------------------|----------------------|
| 1 | 1.998 | 0.03401 | 0.04485 | 0.52377 | 0.60144 |
| 2 | 5 | 0.07172 | 0.0482 | 0.76059 | 0.62349 |
| 3 | 10 | 0.17799 | 0.13551 | 1.19817 | 1.04545 |
| 4 | 15.001 | 0.32847 | 0.29066 | 1.62767 | 1.53113 |
| 5 | 20.003 | 0.47964 | 0.44542 | 1.96687 | 1.8954 |
| 6 | 30.001 | 0.7676 | 0.74216 | 2.48821 | 2.44662 |
| 7 | 40.002 | 1.04509 | 1.03425 | 2.90332 | 2.88823 |
| 8 | 50.011 | 1.31771 | 1.32396 | 3.26008 | 3.2678 |
| 9 | 60.034 | 1.59896 | 1.60872 | 3.59118 | 3.60212 |
| 10 | 70.051 | 1.86981 | 1.88336 | 3.88344 | 3.89749 |
| 11 | 80.072 | 2.12424 | 2.1438 | 4.13924 | 4.15825 |
| 12 | 90.097 | 2.36469 | 2.38704 | 4.36722 | 4.38781 |
| 13 | 100.11 | 2.58979 | 2.61132 | 4.57036 | 4.58932 |
| 14 | 110.11 | 2.7947 | 2.81657 | 4.74773 | 4.76627 |
| 15 | 120.16 | 2.98434 | 3.0047 | 4.90617 | 4.92288 |
| 16 | 130.16 | 3.15462 | 3.17503 | 5.04419 | 5.06049 |
| 17 | 140.18 | 3.31122 | 3.33025 | 5.16788 | 5.18271 |
| 18 | 150.18 | 3.45411 | 3.47119 | 5.27821 | 5.29124 |
| 19 | 160.2 | 3.58427 | 3.59984 | 5.37674 | 5.3884 |
| 20 | 170.21 | 3.70607 | 3.71711 | 5.46733 | 5.47547 |
| 21 | 180.22 | 3.81429 | 3.82435 | 5.54658 | 5.55389 |
| 22 | 190.23 | 3.91752 | 3.92263 | 5.62113 | 5.6248 |
| 23 | 200.24 | 4.01132 | 4.01292 | 5.68803 | 5.68917 |
| 24 | 210.23 | 4.09935 | 4.0959 | 5.75011 | 5.74769 |
| 25 | 220.24 | 4.18385 | 4.17265 | 5.80907 | 5.80129 |
| 26 | 230.24 | 4.25902 | 4.24359 | 5.86102 | 5.85039 |
| 27 | 240.25 | 4.33093 | 4.30943 | 5.91029 | 5.8956 |
| 28 | 250.27 | 4.40091 | 4.37069 | 5.95785 | 5.93736 |
| 29 | 260.28 | 4.46168 | 4.42767 | 5.99884 | 5.97594 |
| 30 | 270.24 | 4.52353 | 4.4806 | 6.04028 | 6.01155 |
| 31 | 280.26 | 4.58244 | 4.53039 | 6.07948 | 6.04486 |
| 32 | 290.26 | 4.64057 | 4.57694 | 6.11792 | 6.07583 |

Complex Bu₄N[MnL^{Se}₂] (14)

MW = 1313.63 g/mol, $\chi_{\text{dia}} = -805.00 \times 10^{-6} \text{ cm}^3 \text{ mol}^{-1}$
m = 26.59 mg ; H = 1.000 T

| No | T(K) | $\chi \cdot T_{\text{exp.}}$ | $\chi \cdot T_{\text{calc.}}$ | μ_{exp} | $\mu_{\text{calc.}}$ |
|----|--------|------------------------------|-------------------------------|--------------------|----------------------|
| 1 | 1.999 | 1.80062 | 1.79038 | 3.79481 | 3.78401 |
| 2 | 4.998 | 2.54891 | 2.58516 | 4.51499 | 4.54698 |
| 3 | 10.005 | 2.85506 | 2.83871 | 4.77845 | 4.76475 |
| 4 | 15.003 | 2.92496 | 2.90251 | 4.83659 | 4.81799 |
| 5 | 20.004 | 2.94813 | 2.92708 | 4.85571 | 4.83834 |
| 6 | 30.002 | 2.96118 | 2.94554 | 4.86644 | 4.85358 |
| 7 | 40.001 | 2.96164 | 2.95222 | 4.86682 | 4.85908 |
| 8 | 50.007 | 2.96203 | 2.95537 | 4.86714 | 4.86167 |
| 9 | 60.034 | 2.96143 | 2.95709 | 4.86665 | 4.86308 |
| 10 | 70.028 | 2.9587 | 2.95814 | 4.86441 | 4.86395 |
| 11 | 80.071 | 2.95758 | 2.95882 | 4.86349 | 4.86451 |
| 12 | 90.074 | 2.962 | 2.95929 | 4.86712 | 4.86489 |
| 13 | 100.11 | 2.96056 | 2.95962 | 4.86594 | 4.86516 |
| 14 | 110.13 | 2.96224 | 2.95987 | 4.86732 | 4.86537 |
| 15 | 120.14 | 2.96103 | 2.96006 | 4.86632 | 4.86552 |
| 16 | 130.16 | 2.96152 | 2.96021 | 4.86672 | 4.86565 |
| 17 | 140.18 | 2.95971 | 2.96033 | 4.86524 | 4.86575 |
| 18 | 150.19 | 2.96166 | 2.96042 | 4.86684 | 4.86582 |
| 19 | 160.13 | 2.96035 | 2.9605 | 4.86576 | 4.86589 |
| 20 | 170.21 | 2.96318 | 2.96056 | 4.86809 | 4.86594 |
| 21 | 180.21 | 2.96371 | 2.96062 | 4.86852 | 4.86598 |
| 22 | 190.22 | 2.96233 | 2.96066 | 4.86739 | 4.86602 |
| 23 | 200.23 | 2.96365 | 2.9607 | 4.86847 | 4.86605 |
| 24 | 210.23 | 2.9609 | 2.96074 | 4.86621 | 4.86608 |
| 25 | 220.24 | 2.95916 | 2.96077 | 4.86478 | 4.86611 |
| 26 | 230.25 | 2.95663 | 2.96079 | 4.8627 | 4.86612 |
| 27 | 240.25 | 2.95119 | 2.96081 | 4.85823 | 4.86614 |
| 28 | 250.25 | 2.95191 | 2.96083 | 4.85882 | 4.86616 |
| 29 | 260.26 | 2.94659 | 2.96085 | 4.85444 | 4.86617 |
| 30 | 270.25 | 2.9437 | 2.96087 | 4.85206 | 4.86619 |
| 31 | 280.25 | 2.94619 | 2.96088 | 4.85411 | 4.8662 |
| 32 | 290.14 | 2.94383 | 2.96089 | 4.85217 | 4.86621 |

Complex [MnL^{Se}₂] (15)

MW = 1031.11 g/mol, $\chi_{\text{dia}} = -648.60 \times 10^{-6} \text{ cm}^3 \text{ mol}^{-1}$
m = 22.66 mg ; H = 1.000 T

| No | T(K) | $\chi \cdot T_{\text{exp.}}$ | $\chi \cdot T_{\text{calc.}}$ | μ_{exp} | $\mu_{\text{calc.}}$ |
|----|--------|------------------------------|-------------------------------|--------------------|----------------------|
| 1 | 1.999 | 1.1718 | 1.18637 | 3.0613 | 3.08027 |
| 2 | 4.997 | 1.49424 | 1.47533 | 3.45692 | 3.43498 |
| 3 | 10.002 | 1.6039 | 1.59098 | 3.58153 | 3.56707 |
| 4 | 15 | 1.63289 | 1.63214 | 3.61375 | 3.61292 |
| 5 | 20.001 | 1.64819 | 1.65383 | 3.63064 | 3.63685 |
| 6 | 30.001 | 1.66743 | 1.67736 | 3.65177 | 3.66263 |
| 7 | 40.001 | 1.68311 | 1.6909 | 3.6689 | 3.67738 |
| 8 | 50.009 | 1.70229 | 1.70044 | 3.68974 | 3.68774 |
| 9 | 60.035 | 1.71762 | 1.70797 | 3.70632 | 3.69589 |
| 10 | 70.046 | 1.71825 | 1.71433 | 3.707 | 3.70277 |
| 11 | 80.056 | 1.71952 | 1.71998 | 3.70837 | 3.70887 |
| 12 | 90.086 | 1.72673 | 1.72515 | 3.71614 | 3.71444 |
| 13 | 100.08 | 1.73125 | 1.72997 | 3.721 | 3.71962 |
| 14 | 110.13 | 1.73391 | 1.73457 | 3.72385 | 3.72456 |
| 15 | 120.17 | 1.73625 | 1.73898 | 3.72637 | 3.72929 |
| 16 | 130.16 | 1.73734 | 1.74323 | 3.72754 | 3.73385 |
| 17 | 140.18 | 1.74102 | 1.74738 | 3.73148 | 3.73829 |
| 18 | 150.19 | 1.74632 | 1.75144 | 3.73716 | 3.74263 |
| 19 | 160.21 | 1.75138 | 1.75543 | 3.74257 | 3.74689 |
| 20 | 170.21 | 1.75698 | 1.75936 | 3.74855 | 3.75108 |
| 21 | 180.21 | 1.76194 | 1.76323 | 3.75383 | 3.75521 |
| 22 | 190.22 | 1.76715 | 1.76706 | 3.75938 | 3.75928 |
| 23 | 200.15 | 1.771 | 1.77083 | 3.76347 | 3.76329 |
| 24 | 210.23 | 1.77585 | 1.77463 | 3.76862 | 3.76733 |
| 25 | 220.26 | 1.78151 | 1.77838 | 3.77462 | 3.77131 |
| 26 | 230.24 | 1.78523 | 1.78209 | 3.77856 | 3.77524 |
| 27 | 240.25 | 1.78774 | 1.78579 | 3.78122 | 3.77915 |
| 28 | 250.26 | 1.79195 | 1.78947 | 3.78567 | 3.78305 |
| 29 | 260.27 | 1.7942 | 1.79314 | 3.78804 | 3.78692 |
| 30 | 270.25 | 1.79423 | 1.79679 | 3.78807 | 3.79078 |
| 31 | 280.26 | 1.80058 | 1.80043 | 3.79477 | 3.79461 |
| 32 | 290.26 | 1.80759 | 1.80405 | 3.80215 | 3.79843 |

Complex [MnL^{Se}₂]*Fc (15Fc)

MW = 1257.14 g/mol, $\chi_{\text{dia}} = -779.66 \times 10^{-6} \text{ cm}^3 \text{ mol}^{-1}$
m = 14.48 mg ; H = 1.000 T

| No | T(K) | $\chi \cdot T_{\text{exp.}}$ | $\chi \cdot T_{\text{calc.}}$ | μ_{exp} | $\mu_{\text{calc.}}$ |
|----|--------|------------------------------|-------------------------------|--------------------|----------------------|
| 1 | 2.003 | 1.61773 | 1.6148 | 3.59693 | 3.59367 |
| 2 | 5.003 | 2.06369 | 2.05847 | 4.06258 | 4.05744 |
| 3 | 10.003 | 2.24245 | 2.2402 | 4.23488 | 4.23275 |
| 4 | 15 | 2.29716 | 2.30692 | 4.28623 | 4.29532 |
| 5 | 20.002 | 2.33272 | 2.34359 | 4.31927 | 4.32933 |
| 6 | 30.001 | 2.37392 | 2.38641 | 4.35725 | 4.3687 |
| 7 | 40 | 2.40302 | 2.41393 | 4.38387 | 4.39381 |
| 8 | 50.004 | 2.42622 | 2.43533 | 4.40499 | 4.41325 |
| 9 | 60.032 | 2.4481 | 2.4537 | 4.4248 | 4.42986 |
| 10 | 70.047 | 2.46771 | 2.47029 | 4.44249 | 4.44481 |
| 11 | 80.045 | 2.48663 | 2.48575 | 4.45949 | 4.4587 |
| 12 | 90.092 | 2.50497 | 2.50056 | 4.4759 | 4.47196 |
| 13 | 100.1 | 2.51971 | 2.51479 | 4.48905 | 4.48467 |
| 14 | 110.12 | 2.53612 | 2.52868 | 4.50365 | 4.49704 |
| 15 | 120.14 | 2.55016 | 2.54228 | 4.5161 | 4.50911 |
| 16 | 130.16 | 2.56475 | 2.55567 | 4.529 | 4.52097 |
| 17 | 140.17 | 2.57773 | 2.56888 | 4.54044 | 4.53264 |
| 18 | 150.18 | 2.59241 | 2.58195 | 4.55335 | 4.54416 |
| 19 | 160.13 | 2.60327 | 2.59484 | 4.56288 | 4.55549 |
| 20 | 170.21 | 2.61738 | 2.6078 | 4.57523 | 4.56685 |
| 21 | 180.2 | 2.62824 | 2.62058 | 4.58471 | 4.57802 |
| 22 | 190.21 | 2.63989 | 2.63331 | 4.59486 | 4.58913 |
| 23 | 200.23 | 2.65247 | 2.64601 | 4.6058 | 4.60018 |
| 24 | 210.23 | 2.66272 | 2.65863 | 4.61469 | 4.61114 |
| 25 | 220.24 | 2.67427 | 2.67123 | 4.62468 | 4.62205 |
| 26 | 230.23 | 2.6859 | 2.68376 | 4.63473 | 4.63288 |
| 27 | 240.24 | 2.69324 | 2.6963 | 4.64106 | 4.64369 |
| 28 | 250.24 | 2.70307 | 2.70879 | 4.64952 | 4.65444 |
| 29 | 260.25 | 2.7124 | 2.72127 | 4.65754 | 4.66515 |
| 30 | 270.24 | 2.72155 | 2.73371 | 4.66539 | 4.6758 |
| 31 | 280.24 | 2.73462 | 2.74614 | 4.67657 | 4.68641 |
| 32 | 290.22 | 2.74966 | 2.75852 | 4.68942 | 4.69697 |

Complex [MnL^S(μ-OMe)(MeOH)]₂ (16)

MW = 1117.40 g/mol, $\chi_{\text{dia}} = -730.00 \times 10^{-6} \text{ cm}^3 \text{ mol}^{-1}$
m = 24.56 mg ; H = 1.000 T

| No | T(K) | $\chi \cdot T_{\text{exp.}}$ | $\chi \cdot T_{\text{calc.}}$ | μ_{exp} | $\mu_{\text{calc.}}$ |
|----|--------|------------------------------|-------------------------------|--------------------|----------------------|
| 1 | 2 | 0.12487 | 0.03013 | 0.99934 | 0.49091 |
| 2 | 5.006 | 0.23999 | 0.05689 | 1.38539 | 0.67451 |
| 3 | 10.004 | 0.46054 | 0.26013 | 1.91916 | 1.44236 |
| 4 | 15 | 0.67617 | 0.48364 | 2.32545 | 1.9667 |
| 5 | 20.002 | 0.87293 | 0.69884 | 2.64222 | 2.36411 |
| 6 | 30 | 1.23904 | 1.12262 | 3.14791 | 2.99637 |
| 7 | 40.001 | 1.59271 | 1.53921 | 3.56901 | 3.50856 |
| 8 | 50.006 | 1.93396 | 1.93735 | 3.93281 | 3.93626 |
| 9 | 60.026 | 2.25521 | 2.30466 | 4.24691 | 4.29322 |
| 10 | 70.042 | 2.55207 | 2.63353 | 4.51779 | 4.58932 |
| 11 | 80.064 | 2.82814 | 2.92337 | 4.75587 | 4.83528 |
| 12 | 90.092 | 3.07744 | 3.17676 | 4.96106 | 5.04048 |
| 13 | 100.08 | 3.3016 | 3.39681 | 5.13856 | 5.21213 |
| 14 | 110.15 | 3.50112 | 3.59046 | 5.29155 | 5.35864 |
| 15 | 120.16 | 3.68143 | 3.75899 | 5.4261 | 5.48296 |
| 16 | 130.15 | 3.83805 | 3.90696 | 5.54032 | 5.58983 |
| 17 | 140.16 | 3.98281 | 4.03803 | 5.64383 | 5.68282 |
| 18 | 150.19 | 4.11126 | 4.15469 | 5.73412 | 5.76433 |
| 19 | 160.19 | 4.23273 | 4.25851 | 5.81821 | 5.83591 |
| 20 | 170.21 | 4.34405 | 4.35182 | 5.89423 | 5.8995 |
| 21 | 180.22 | 4.44091 | 4.43581 | 5.95958 | 5.95615 |
| 22 | 190.23 | 4.53113 | 4.51181 | 6.01981 | 6.00696 |
| 23 | 200.23 | 4.6104 | 4.58081 | 6.07224 | 6.05272 |
| 24 | 210.24 | 4.68682 | 4.64382 | 6.12236 | 6.09421 |
| 25 | 220.25 | 4.75479 | 4.70149 | 6.16659 | 6.13193 |
| 26 | 230.25 | 4.81619 | 4.75441 | 6.20628 | 6.16634 |
| 27 | 240.25 | 4.87718 | 4.80318 | 6.24545 | 6.19789 |
| 28 | 250.25 | 4.93391 | 4.84824 | 6.28167 | 6.22689 |
| 29 | 260.26 | 4.98909 | 4.89005 | 6.3167 | 6.25369 |
| 30 | 270.24 | 5.04494 | 4.92877 | 6.35195 | 6.2784 |
| 31 | 280.24 | 5.09752 | 4.96492 | 6.38497 | 6.30138 |
| 32 | 290.26 | 5.15792 | 4.99873 | 6.42269 | 6.3228 |

Complex [MnL^S₂] (17)

MW = 936.31 g/mol, $\chi_{\text{dia}} = -632.60 \times 10^{-6} \text{ cm}^3 \text{ mol}^{-1}$
m = 15.62 mg ; H = 1.000 T

| No | T(K) | $\chi \cdot T_{\text{exp.}}$ | $\chi \cdot T_{\text{calc.}}$ | μ_{exp} | $\mu_{\text{calc.}}$ |
|----|--------|------------------------------|-------------------------------|--------------------|----------------------|
| 1 | 2 | 1.2858 | 1.31191 | 3.20676 | 3.23915 |
| 2 | 5.01 | 1.64371 | 1.62364 | 3.6257 | 3.6035 |
| 3 | 10.003 | 1.77081 | 1.74287 | 3.76327 | 3.73346 |
| 4 | 15 | 1.7985 | 1.7838 | 3.79258 | 3.77705 |
| 5 | 20.002 | 1.81287 | 1.80444 | 3.8077 | 3.79884 |
| 6 | 30.002 | 1.82723 | 1.82524 | 3.82275 | 3.82067 |
| 7 | 39.998 | 1.83288 | 1.83579 | 3.82866 | 3.83169 |
| 8 | 50.006 | 1.83843 | 1.84223 | 3.83445 | 3.83841 |
| 9 | 60.031 | 1.84022 | 1.84663 | 3.83632 | 3.84299 |
| 10 | 70.047 | 1.84208 | 1.84984 | 3.83825 | 3.84633 |
| 11 | 80.051 | 1.84509 | 1.85233 | 3.84139 | 3.84892 |
| 12 | 90.089 | 1.84837 | 1.85433 | 3.8448 | 3.85099 |
| 13 | 100.12 | 1.84975 | 1.85598 | 3.84624 | 3.85271 |
| 14 | 110.13 | 1.8516 | 1.85739 | 3.84816 | 3.85417 |
| 15 | 120.16 | 1.85344 | 1.85861 | 3.85007 | 3.85544 |
| 16 | 130.16 | 1.85477 | 1.85968 | 3.85145 | 3.85655 |
| 17 | 140.18 | 1.85579 | 1.86065 | 3.85251 | 3.85755 |
| 18 | 150.19 | 1.85811 | 1.86152 | 3.85492 | 3.85845 |
| 19 | 160.13 | 1.8581 | 1.86231 | 3.85491 | 3.85927 |
| 20 | 170.21 | 1.86085 | 1.86306 | 3.85776 | 3.86005 |
| 21 | 180.22 | 1.86167 | 1.86375 | 3.85861 | 3.86076 |
| 22 | 190.22 | 1.86241 | 1.8644 | 3.85938 | 3.86144 |
| 23 | 200.22 | 1.86411 | 1.86501 | 3.86114 | 3.86207 |
| 24 | 210.24 | 1.86407 | 1.86559 | 3.8611 | 3.86267 |
| 25 | 220.25 | 1.8652 | 1.86615 | 3.86227 | 3.86325 |
| 26 | 230.24 | 1.86649 | 1.86668 | 3.8636 | 3.8638 |
| 27 | 240.24 | 1.86797 | 1.86719 | 3.86513 | 3.86433 |
| 28 | 250.25 | 1.86979 | 1.86768 | 3.86701 | 3.86483 |
| 29 | 260.24 | 1.86661 | 1.86816 | 3.86372 | 3.86533 |
| 30 | 270.14 | 1.87091 | 1.86862 | 3.86817 | 3.8658 |
| 31 | 280.24 | 1.88146 | 1.86907 | 3.87906 | 3.86627 |
| 32 | 290.25 | 1.88137 | 1.86951 | 3.87897 | 3.86673 |

Complex [FeL^{Se}(μ-OMe)(MeOH)]₂ (18)

MW = 1437.31 g/mol, $\chi_{\text{dia}} = -900.37 \times 10^{-6} \text{ cm}^3 \text{ mol}^{-1}$
m = 33.01 mg ; H = 1.000 T

| No | T(K) | $\chi \cdot T_{\text{exp.}}$ | $\chi \cdot T_{\text{calc.}}$ | μ_{exp} | $\mu_{\text{calc.}}$ |
|----|--------|------------------------------|-------------------------------|--------------------|----------------------|
| 1 | 1.999 | 0.11179 | 0.06582 | 0.94956 | 0.7286 |
| 2 | 4.999 | 0.15834 | 0.06728 | 1.1301 | 0.73666 |
| 3 | 10.003 | 0.21198 | 0.12759 | 1.30757 | 1.01445 |
| 4 | 14.999 | 0.31862 | 0.25999 | 1.60307 | 1.4481 |
| 5 | 20.002 | 0.44755 | 0.40034 | 1.89993 | 1.79693 |
| 6 | 30.001 | 0.70114 | 0.66806 | 2.37805 | 2.32128 |
| 7 | 39.998 | 0.94703 | 0.92969 | 2.76376 | 2.73834 |
| 8 | 50.006 | 1.19548 | 1.19007 | 3.1052 | 3.09817 |
| 9 | 60.032 | 1.44553 | 1.45022 | 3.41454 | 3.42007 |
| 10 | 70.047 | 1.6905 | 1.7093 | 3.69255 | 3.71302 |
| 11 | 80.068 | 1.93342 | 1.96704 | 3.94895 | 3.98313 |
| 12 | 90.091 | 2.17401 | 2.22204 | 4.18744 | 4.23345 |
| 13 | 100.11 | 2.41338 | 2.47255 | 4.41196 | 4.46571 |
| 14 | 110.13 | 2.64657 | 2.71701 | 4.62019 | 4.68127 |
| 15 | 120.13 | 2.87602 | 2.95345 | 4.81631 | 4.88071 |
| 16 | 130.16 | 3.10005 | 3.18183 | 5.00038 | 5.0659 |
| 17 | 140.18 | 3.32088 | 3.40036 | 5.17541 | 5.23698 |
| 18 | 150.19 | 3.53191 | 3.60857 | 5.33732 | 5.39493 |
| 19 | 160.19 | 3.73887 | 3.80626 | 5.49147 | 5.54074 |
| 20 | 170.2 | 3.93587 | 3.99385 | 5.63428 | 5.67563 |
| 21 | 180.21 | 4.12769 | 4.17132 | 5.76995 | 5.80036 |
| 22 | 190.22 | 4.31054 | 4.33899 | 5.89636 | 5.91579 |
| 23 | 200.24 | 4.48245 | 4.49743 | 6.01279 | 6.02283 |
| 24 | 210.24 | 4.65252 | 4.64662 | 6.1258 | 6.12191 |
| 25 | 220.25 | 4.81058 | 4.78751 | 6.22898 | 6.21403 |
| 26 | 230.24 | 4.95763 | 4.9202 | 6.32347 | 6.29955 |
| 27 | 240.26 | 5.10124 | 5.04581 | 6.4144 | 6.37946 |
| 28 | 250.24 | 5.23591 | 5.16396 | 6.49852 | 6.45371 |
| 29 | 260.27 | 5.37362 | 5.27615 | 6.58342 | 6.52344 |
| 30 | 270.24 | 5.49947 | 5.38161 | 6.66007 | 6.58832 |
| 31 | 280.26 | 5.62263 | 5.48191 | 6.73423 | 6.64943 |
| 32 | 290.26 | 5.74732 | 5.57671 | 6.80849 | 6.70668 |

Complex Bu₄N[FeL^{Se}₂] (19)

MW = 1273.48 g/mol, $\chi_{\text{dia}} = -857.65 \times 10^{-6} \text{ cm}^3 \text{ mol}^{-1}$
m = 23.29 mg ; H = 1.000 T

| No | T(K) | $\chi \cdot T_{\text{exp.}}$ | $\chi \cdot T_{\text{calc.}}$ | μ_{exp} | $\mu_{\text{calc.}}$ |
|----|--------|------------------------------|-------------------------------|--------------------|----------------------|
| 1 | 1.999 | 3.39818 | 3.30078 | 5.2353 | 5.15973 |
| 2 | 5.001 | 4.1735 | 4.19885 | 5.80188 | 5.81947 |
| 3 | 9.994 | 4.40423 | 4.48195 | 5.9601 | 6.01246 |
| 4 | 15.001 | 4.4721 | 4.56544 | 6.00584 | 6.0682 |
| 5 | 20.003 | 4.52358 | 4.6042 | 6.04031 | 6.0939 |
| 6 | 30 | 4.59064 | 4.64075 | 6.08492 | 6.11804 |
| 7 | 40 | 4.63716 | 4.65814 | 6.11567 | 6.12949 |
| 8 | 50.013 | 4.66604 | 4.6683 | 6.13469 | 6.13617 |
| 9 | 60.035 | 4.69062 | 4.67495 | 6.15083 | 6.14054 |
| 10 | 70.045 | 4.70266 | 4.67962 | 6.15872 | 6.14361 |
| 11 | 80.063 | 4.71345 | 4.6831 | 6.16578 | 6.14589 |
| 12 | 90.086 | 4.71697 | 4.68578 | 6.16808 | 6.14765 |
| 13 | 100.06 | 4.71978 | 4.6879 | 6.16992 | 6.14904 |
| 14 | 110.14 | 4.72047 | 4.68965 | 6.17037 | 6.15019 |
| 15 | 120.13 | 4.72195 | 4.69109 | 6.17133 | 6.15113 |
| 16 | 130.16 | 4.71779 | 4.6923 | 6.16861 | 6.15193 |
| 17 | 140.18 | 4.71781 | 4.69334 | 6.16863 | 6.15261 |
| 18 | 150.19 | 4.71461 | 4.69423 | 6.16654 | 6.15319 |
| 19 | 160.2 | 4.71434 | 4.69502 | 6.16636 | 6.15371 |
| 20 | 170.21 | 4.71199 | 4.6957 | 6.16482 | 6.15416 |
| 21 | 180.21 | 4.70932 | 4.69631 | 6.16307 | 6.15456 |
| 22 | 190.22 | 4.70802 | 4.69686 | 6.16222 | 6.15492 |
| 23 | 200.23 | 4.7016 | 4.69735 | 6.15802 | 6.15524 |
| 24 | 210.23 | 4.70069 | 4.69779 | 6.15743 | 6.15553 |
| 25 | 220.25 | 4.69692 | 4.6982 | 6.15496 | 6.15579 |
| 26 | 230.15 | 4.68936 | 4.69856 | 6.15 | 6.15603 |
| 27 | 240.25 | 4.69381 | 4.6989 | 6.15292 | 6.15625 |
| 28 | 250.25 | 4.68862 | 4.69921 | 6.14951 | 6.15646 |
| 29 | 260.26 | 4.68494 | 4.69949 | 6.1471 | 6.15664 |
| 30 | 270.23 | 4.68861 | 4.69976 | 6.14951 | 6.15682 |
| 31 | 280.24 | 4.69024 | 4.7 | 6.15058 | 6.15697 |
| 32 | 290.25 | 4.69243 | 4.70023 | 6.15201 | 6.15712 |

Complex Bu₄N[FeL^{Se}L^{Se'}] (20)

MW = 1069.17 g/mol, $\chi_{\text{dia}} = -709.00 \times 10^{-6} \text{ cm}^3 \text{ mol}^{-1}$
m = 25.51 mg, H = 1.000 T

| No | T(K) | $\chi \cdot T_{\text{exp.}}$ | $\chi \cdot T_{\text{calc.}}$ | μ_{exp} | $\mu_{\text{calc.}}$ |
|----|--------|------------------------------|-------------------------------|--------------------|----------------------|
| 1 | 1.998 | 2.48268 | 2.63414 | 4.47485 | 4.60933 |
| 2 | 5 | 3.61941 | 3.56061 | 5.40303 | 5.35896 |
| 3 | 10.003 | 4.0798 | 3.95819 | 5.73638 | 5.65024 |
| 4 | 14.999 | 4.18658 | 4.09853 | 5.81096 | 5.74953 |
| 5 | 20.002 | 4.23241 | 4.17024 | 5.84268 | 5.79961 |
| 6 | 30.001 | 4.26604 | 4.24349 | 5.86585 | 5.85032 |
| 7 | 39.999 | 4.28612 | 4.28148 | 5.87964 | 5.87645 |
| 8 | 50.009 | 4.29522 | 4.30535 | 5.88588 | 5.89281 |
| 9 | 60.02 | 4.30469 | 4.32215 | 5.89236 | 5.9043 |
| 10 | 70.051 | 4.31227 | 4.33492 | 5.89755 | 5.91301 |
| 11 | 80.07 | 4.32441 | 4.34514 | 5.90584 | 5.91998 |
| 12 | 90.088 | 4.33732 | 4.35368 | 5.91465 | 5.92579 |
| 13 | 100.11 | 4.34369 | 4.36104 | 5.91899 | 5.9308 |
| 14 | 110.12 | 4.35393 | 4.36754 | 5.92596 | 5.93522 |
| 15 | 120.1 | 4.35818 | 4.37338 | 5.92886 | 5.93919 |
| 16 | 130.17 | 4.3673 | 4.37878 | 5.93506 | 5.94285 |
| 17 | 140.17 | 4.37152 | 4.38375 | 5.93792 | 5.94622 |
| 18 | 150.19 | 4.38047 | 4.38842 | 5.944 | 5.94939 |
| 19 | 160.2 | 4.38624 | 4.39284 | 5.94791 | 5.95239 |
| 20 | 170.2 | 4.39301 | 4.39705 | 5.9525 | 5.95524 |
| 21 | 180.22 | 4.40038 | 4.40109 | 5.95749 | 5.95797 |
| 22 | 190.23 | 4.40468 | 4.40498 | 5.9604 | 5.9606 |
| 23 | 200.24 | 4.41427 | 4.40874 | 5.96689 | 5.96315 |
| 24 | 210.25 | 4.41899 | 4.41241 | 5.97008 | 5.96563 |
| 25 | 220.25 | 4.42335 | 4.41597 | 5.97302 | 5.96804 |
| 26 | 230.25 | 4.42938 | 4.41946 | 5.97709 | 5.97039 |
| 27 | 240.25 | 4.42925 | 4.42288 | 5.977 | 5.9727 |
| 28 | 250.26 | 4.42796 | 4.42624 | 5.97613 | 5.97497 |
| 29 | 260.26 | 4.42298 | 4.42954 | 5.97277 | 5.9772 |
| 30 | 270.25 | 4.47827 | 4.43279 | 6.00999 | 5.97939 |
| 31 | 280.17 | 4.42016 | 4.43598 | 5.97087 | 5.98154 |
| 32 | 290.25 | 4.43409 | 4.43918 | 5.98027 | 5.9837 |

Complex Bu₄N[FeL^SL^{S'}] (21)

MW = 957.37 g/mol, $\chi_{\text{dia}} = -693.00 \times 10^{-6} \text{ cm}^3 \text{ mol}^{-1}$
m = 32.05 mg, H = 1.000 T

| No | T(K) | $\chi \cdot T_{\text{exp.}}$ | $\chi \cdot T_{\text{calc.}}$ | μ_{exp} | $\mu_{\text{calc.}}$ |
|----|--------|------------------------------|-------------------------------|--------------------|----------------------|
| 1 | 1.998 | 2.70413 | 2.84056 | 4.65043 | 4.7663 |
| 2 | 5.006 | 3.83691 | 3.72874 | 5.5395 | 5.46085 |
| 3 | 10.003 | 4.17452 | 4.0751 | 5.77807 | 5.70885 |
| 4 | 15 | 4.24818 | 4.19696 | 5.82882 | 5.79358 |
| 5 | 20.001 | 4.28638 | 4.2625 | 5.85497 | 5.83864 |
| 6 | 30.002 | 4.33368 | 4.33808 | 5.88719 | 5.89017 |
| 7 | 40.001 | 4.36642 | 4.38639 | 5.90938 | 5.92288 |
| 8 | 50.008 | 4.39951 | 4.42399 | 5.93173 | 5.94821 |
| 9 | 60.031 | 4.42768 | 4.45631 | 5.95069 | 5.9699 |
| 10 | 70.045 | 4.45652 | 4.48559 | 5.97004 | 5.98948 |
| 11 | 80.04 | 4.48623 | 4.51295 | 5.98991 | 6.00772 |
| 12 | 90.089 | 4.52013 | 4.5392 | 6.0125 | 6.02517 |
| 13 | 100.12 | 4.54725 | 4.56453 | 6.03051 | 6.04195 |
| 14 | 110.13 | 4.57628 | 4.58917 | 6.04973 | 6.05824 |
| 15 | 120.15 | 4.60328 | 4.61337 | 6.06755 | 6.07419 |
| 16 | 130.16 | 4.62835 | 4.63719 | 6.08405 | 6.08985 |
| 17 | 140.18 | 4.65279 | 4.66075 | 6.10009 | 6.1053 |
| 18 | 150.19 | 4.68103 | 4.68405 | 6.11857 | 6.12055 |
| 19 | 160.13 | 4.70213 | 4.70701 | 6.13235 | 6.13553 |
| 20 | 170.21 | 4.73253 | 4.73014 | 6.15214 | 6.15058 |
| 21 | 180.22 | 4.75716 | 4.75299 | 6.16813 | 6.16542 |
| 22 | 190.23 | 4.77989 | 4.77573 | 6.18284 | 6.18015 |
| 23 | 200.24 | 4.80548 | 4.79838 | 6.19937 | 6.19479 |
| 24 | 210.25 | 4.82741 | 4.82095 | 6.2135 | 6.20934 |
| 25 | 220.25 | 4.85147 | 4.84343 | 6.22897 | 6.2238 |
| 26 | 230.26 | 4.87367 | 4.86588 | 6.2432 | 6.23821 |
| 27 | 240.25 | 4.89394 | 4.88823 | 6.25617 | 6.25252 |
| 28 | 250.26 | 4.91798 | 4.91058 | 6.27152 | 6.2668 |
| 29 | 260.27 | 4.93776 | 4.93289 | 6.28412 | 6.28102 |
| 30 | 270.25 | 4.95885 | 4.95511 | 6.29752 | 6.29515 |
| 31 | 280.26 | 4.98168 | 4.97735 | 6.312 | 6.30926 |
| 32 | 290.26 | 4.99992 | 4.99955 | 6.32355 | 6.32332 |

Complex $[\text{Ni}_4\text{L}^{\text{S}}_2(\mu\text{-OMe})_4(\text{MeOH})_4(\text{MeCN})_2]$ (22)

MW = 1450.54 g/mol, $\chi_{\text{dia}} = -888.22 \times 10^{-6} \text{ cm}^3 \text{ mol}^{-1}$
 m = 42.45 mg, H = 1.000 T

| No | T(K) | $\chi \cdot T_{\text{exp.}}$ | $\chi \cdot T_{\text{calc.}}$ | μ_{exp} | $\mu_{\text{calc.}}$ |
|----|--------|------------------------------|-------------------------------|--------------------|----------------------|
| 1 | 2.007 | 4.52147 | 4.59983 | 6.01339 | 6.06527 |
| 2 | 5.003 | 6.28015 | 6.08527 | 7.08703 | 6.97621 |
| 3 | 10.003 | 6.86601 | 6.96338 | 7.41023 | 7.46259 |
| 4 | 14.999 | 7.08199 | 7.16368 | 7.52588 | 7.56916 |
| 5 | 20.002 | 7.10419 | 7.11477 | 7.53766 | 7.54327 |
| 6 | 30.001 | 6.8709 | 6.83279 | 7.41287 | 7.39228 |
| 7 | 39.999 | 6.59895 | 6.5567 | 7.26469 | 7.24139 |
| 8 | 50.002 | 6.36667 | 6.33771 | 7.13568 | 7.11944 |
| 9 | 60.028 | 6.18662 | 6.16821 | 7.03406 | 7.02359 |
| 10 | 70.055 | 6.04476 | 6.036 | 6.95295 | 6.94791 |
| 11 | 80.068 | 5.93454 | 5.9311 | 6.88927 | 6.88727 |
| 12 | 90.094 | 5.84375 | 5.84607 | 6.83636 | 6.83772 |
| 13 | 100.08 | 5.76141 | 5.7763 | 6.78803 | 6.7968 |
| 14 | 110.15 | 5.70545 | 5.71746 | 6.75498 | 6.76209 |
| 15 | 120.13 | 5.64981 | 5.66803 | 6.72197 | 6.7328 |
| 16 | 130.17 | 5.60741 | 5.62537 | 6.6967 | 6.70741 |
| 17 | 140.18 | 5.56637 | 5.58852 | 6.67214 | 6.68541 |
| 18 | 150.18 | 5.53807 | 5.55631 | 6.65516 | 6.66611 |
| 19 | 160.2 | 5.51293 | 5.52785 | 6.64004 | 6.64902 |
| 20 | 170.13 | 5.48373 | 5.50279 | 6.62243 | 6.63393 |
| 21 | 180.22 | 5.47663 | 5.48003 | 6.61814 | 6.6202 |
| 22 | 190.23 | 5.45571 | 5.45973 | 6.60549 | 6.60792 |
| 23 | 200.24 | 5.44189 | 5.44139 | 6.59712 | 6.59682 |
| 24 | 210.25 | 5.42587 | 5.42473 | 6.5874 | 6.58671 |
| 25 | 220.24 | 5.41052 | 5.40957 | 6.57808 | 6.5775 |
| 26 | 230.23 | 5.39714 | 5.39568 | 6.56994 | 6.56905 |
| 27 | 240.26 | 5.38756 | 5.38286 | 6.5641 | 6.56124 |
| 28 | 250.26 | 5.38016 | 5.37107 | 6.55959 | 6.55405 |
| 29 | 260.28 | 5.37743 | 5.36015 | 6.55793 | 6.54738 |
| 30 | 270.26 | 5.36828 | 5.35005 | 6.55235 | 6.54121 |
| 31 | 280.27 | 5.35979 | 5.34063 | 6.54717 | 6.53545 |
| 32 | 290.25 | 5.34318 | 5.33187 | 6.53701 | 6.53009 |

Complex [Ni₄L^{Se}₂ (μ-OMe)₄(MeOH)₄(MeCN)₂] (23)

MW = 1544.34 g/mol, $\chi_{\text{dia}} = -904.20 \times 10^{-6} \text{ cm}^3 \text{ mol}^{-1}$
m = 39.08 mg, H = 1.000 T

| No | T(K) | $\chi \cdot T_{\text{exp.}}$ | $\chi \cdot T_{\text{calc.}}$ | μ_{exp} | $\mu_{\text{calc.}}$ |
|----|--------|------------------------------|-------------------------------|--------------------|----------------------|
| 1 | 1.999 | 2.74347 | 3.52544 | 4.68414 | 5.3099 |
| 2 | 5 | 5.52943 | 5.24009 | 6.64997 | 6.47364 |
| 3 | 10.003 | 6.19534 | 6.24308 | 7.03902 | 7.06608 |
| 4 | 15 | 6.37365 | 6.46786 | 7.13959 | 7.19217 |
| 5 | 20.002 | 6.39648 | 6.44442 | 7.15237 | 7.17912 |
| 6 | 29.997 | 6.22062 | 6.24094 | 7.05336 | 7.06487 |
| 7 | 40.004 | 6.03564 | 6.04708 | 6.9477 | 6.95428 |
| 8 | 50.01 | 5.88921 | 5.89757 | 6.8629 | 6.86777 |
| 9 | 60.041 | 5.77516 | 5.78373 | 6.79613 | 6.80117 |
| 10 | 70.041 | 5.68151 | 5.69604 | 6.7408 | 6.74941 |
| 11 | 80.083 | 5.62275 | 5.62649 | 6.70585 | 6.70808 |
| 12 | 90.082 | 5.5656 | 5.57064 | 6.67168 | 6.6747 |
| 13 | 100.09 | 5.52151 | 5.52469 | 6.6452 | 6.64712 |
| 14 | 110.14 | 5.4845 | 5.48617 | 6.6229 | 6.6239 |
| 15 | 120.19 | 5.45877 | 5.45356 | 6.60734 | 6.60419 |
| 16 | 130.16 | 5.42558 | 5.42582 | 6.58722 | 6.58737 |
| 17 | 140.17 | 5.40487 | 5.40169 | 6.57464 | 6.57271 |
| 18 | 150.13 | 5.38104 | 5.38068 | 6.56013 | 6.55991 |
| 19 | 160.19 | 5.36837 | 5.36197 | 6.5524 | 6.5485 |
| 20 | 170.21 | 5.35183 | 5.34543 | 6.5423 | 6.53839 |
| 21 | 180.21 | 5.33765 | 5.33067 | 6.53363 | 6.52936 |
| 22 | 190.23 | 5.32589 | 5.31738 | 6.52643 | 6.52121 |
| 23 | 200.23 | 5.31298 | 5.30538 | 6.51851 | 6.51385 |
| 24 | 210.25 | 5.3067 | 5.29447 | 6.51466 | 6.50715 |
| 25 | 220.24 | 5.29997 | 5.28454 | 6.51053 | 6.50104 |
| 26 | 230.24 | 5.29635 | 5.27543 | 6.5083 | 6.49544 |
| 27 | 240.25 | 5.30088 | 5.26706 | 6.51109 | 6.49028 |
| 28 | 250.24 | 5.30982 | 5.25934 | 6.51657 | 6.48552 |
| 29 | 260.26 | 5.30422 | 5.25219 | 6.51314 | 6.48111 |
| 30 | 270.25 | 5.30366 | 5.24557 | 6.51279 | 6.47703 |
| 31 | 280.26 | 5.3051 | 5.23939 | 6.51368 | 6.47321 |
| 32 | 290.26 | 5.31296 | 5.23364 | 6.5185 | 6.46966 |

Complex [Ni₅L^N₄ (μ₃-OH)₂(μ-H₂O)₂(EtOH)₂] (24)

MW = 1708.96 g/mol, $\chi_{\text{dia}} = -994.70 \times 10^{-6} \text{ cm}^3 \text{ mol}^{-1}$
m = 48.47 mg , H = 1.000 T

| No | T(K) | $\chi \cdot T_{\text{calc.}}$ | $\chi \cdot T_{\text{exp.}}$ | $\mu_{\text{calc.}}$ | $\mu_{\text{exp.}}$ |
|----|--------|-------------------------------|------------------------------|----------------------|---------------------|
| 1 | 5 | 7.90777 | 7.95918 | 7.95375 | 7.97957 |
| 2 | 10 | 9.09605 | 8.9475 | 8.53044 | 8.46049 |
| 3 | 15 | 9.11566 | 9.0792 | 8.53963 | 8.52253 |
| 4 | 20 | 8.91349 | 9.03196 | 8.4444 | 8.50033 |
| 5 | 30 | 8.47387 | 8.62679 | 8.23353 | 8.30748 |
| 6 | 40 | 8.14193 | 8.22758 | 8.07065 | 8.11299 |
| 7 | 50 | 7.90475 | 7.94064 | 7.95223 | 7.97026 |
| 8 | 60.02 | 7.73175 | 7.72024 | 7.86473 | 7.85888 |
| 9 | 70.05 | 7.60145 | 7.56276 | 7.79818 | 7.77831 |
| 10 | 80.07 | 7.50052 | 7.45928 | 7.74624 | 7.72491 |
| 11 | 90.07 | 7.42042 | 7.36827 | 7.70476 | 7.67764 |
| 12 | 100.11 | 7.35508 | 7.30022 | 7.67077 | 7.6421 |
| 13 | 110.1 | 7.30128 | 7.23764 | 7.64266 | 7.60928 |
| 14 | 120.16 | 7.25575 | 7.20167 | 7.61879 | 7.59035 |
| 15 | 130.16 | 7.21721 | 7.15451 | 7.59853 | 7.56545 |
| 16 | 140.17 | 7.18396 | 7.12456 | 7.58101 | 7.5496 |
| 17 | 150.19 | 7.155 | 7.09633 | 7.56571 | 7.53463 |
| 18 | 160.21 | 7.12957 | 7.07728 | 7.55225 | 7.52451 |
| 19 | 170.2 | 7.10713 | 7.05649 | 7.54036 | 7.51345 |
| 20 | 180.22 | 7.08707 | 7.03993 | 7.52972 | 7.50463 |
| 21 | 190.23 | 7.06911 | 7.02595 | 7.52017 | 7.49718 |
| 22 | 200.23 | 7.05294 | 7.01005 | 7.51156 | 7.48869 |
| 23 | 210.17 | 7.03836 | 6.99929 | 7.50379 | 7.48294 |
| 24 | 220.27 | 7.02488 | 6.99996 | 7.4966 | 7.48329 |
| 25 | 230.24 | 7.01272 | 6.99377 | 7.49011 | 7.47998 |
| 26 | 240.26 | 7.0015 | 6.99661 | 7.48412 | 7.4815 |
| 27 | 250.26 | 6.9912 | 6.99677 | 7.47861 | 7.48159 |
| 28 | 260.26 | 6.98167 | 6.99345 | 7.47351 | 7.47981 |
| 29 | 270.25 | 6.97286 | 6.9938 | 7.46879 | 7.48 |
| 30 | 280.25 | 6.96466 | 6.99308 | 7.4644 | 7.47961 |
| 31 | 290.25 | 6.95702 | 6.99851 | 7.46031 | 7.48252 |

Complex [Ni₆L^N₄ (μ-MeOH)(μ₃-OMe)₂(MeOH)₂(MeCN)₂] (25)

MW = 1816.04 g/mol, $\chi_{\text{dia}} = -1035.83 \times 10^{-6} \text{ cm}^3 \text{ mol}^{-1}$
m = 58.88 mg , H = 1.000 T

| No | T(K) | $\chi \cdot T_{\text{calc.}}$ | $\chi \cdot T_{\text{obs.}}$ | $\mu_{\text{calc.}}$ | $\mu_{\text{exp.}}$ |
|----|--------|-------------------------------|------------------------------|----------------------|---------------------|
| 1 | 2 | 1.17762 | 1.04719 | 3.06935 | 2.8944 |
| 2 | 5 | 1.97869 | 1.9895 | 3.97863 | 3.98948 |
| 3 | 10 | 2.50193 | 2.74923 | 4.47387 | 4.68975 |
| 4 | 15 | 2.97729 | 3.23265 | 4.8804 | 5.08539 |
| 5 | 20 | 3.4335 | 3.64278 | 5.24099 | 5.39836 |
| 6 | 30 | 4.23205 | 4.28804 | 5.81862 | 5.85699 |
| 7 | 40 | 4.84072 | 4.78324 | 6.223 | 6.18595 |
| 8 | 50 | 5.29115 | 5.18531 | 6.50609 | 6.44069 |
| 9 | 60.02 | 5.6291 | 5.51272 | 6.71065 | 6.64092 |
| 10 | 70.05 | 5.88873 | 5.78237 | 6.86366 | 6.8014 |
| 11 | 80.07 | 6.09292 | 6.00788 | 6.98164 | 6.93275 |
| 12 | 90.08 | 6.25717 | 6.18911 | 7.07512 | 7.03654 |
| 13 | 100.12 | 6.39224 | 6.3434 | 7.15108 | 7.12371 |
| 14 | 110.09 | 6.50424 | 6.46206 | 7.21345 | 7.19003 |
| 15 | 120.16 | 6.59998 | 6.57407 | 7.26635 | 7.25207 |
| 16 | 130.16 | 6.68141 | 6.65794 | 7.31104 | 7.29819 |
| 17 | 140.18 | 6.75208 | 6.73551 | 7.3496 | 7.34058 |
| 18 | 150.19 | 6.81379 | 6.8006 | 7.38311 | 7.37596 |
| 19 | 160.19 | 6.86814 | 6.86014 | 7.4125 | 7.40818 |
| 20 | 170.2 | 6.91646 | 6.91404 | 7.43852 | 7.43722 |
| 21 | 180.21 | 6.95964 | 6.95773 | 7.46171 | 7.46068 |
| 22 | 190.22 | 6.99846 | 7.00219 | 7.48249 | 7.48449 |
| 23 | 200.24 | 7.03358 | 7.03884 | 7.50124 | 7.50404 |
| 24 | 210.23 | 7.06538 | 7.07613 | 7.51818 | 7.5239 |
| 25 | 220.25 | 7.09448 | 7.11319 | 7.53365 | 7.54358 |
| 26 | 230.23 | 7.12103 | 7.14196 | 7.54773 | 7.55882 |
| 27 | 240.15 | 7.14529 | 7.1692 | 7.56058 | 7.57322 |
| 28 | 250.25 | 7.16807 | 7.19419 | 7.57262 | 7.5864 |
| 29 | 260.27 | 7.18898 | 7.21599 | 7.58365 | 7.59789 |
| 30 | 270.25 | 7.2083 | 7.24378 | 7.59384 | 7.61251 |
| 31 | 280.23 | 7.22627 | 7.27561 | 7.6033 | 7.62921 |
| 32 | 290.24 | 7.24309 | 7.30824 | 7.61214 | 7.6463 |

Complex [CuL^{Se}(Et₃N)] (26)

MW = 652.32 g/mol, $\chi_{\text{dia}} = -416.82 \times 10^{-6} \text{ cm}^3 \text{ mol}^{-1}$
m = 29.08 mg, H = 1.000 T

| No | T(K) | $\chi \cdot T_{\text{exp.}}$ | $\chi \cdot T_{\text{calc.}}$ | μ_{exp} | $\mu_{\text{calc.}}$ |
|----|--------|------------------------------|-------------------------------|--------------------|----------------------|
| 1 | 1.998 | 0.21065 | 0.23475 | 1.30347 | 1.376 |
| 2 | 5.001 | 0.33791 | 0.31256 | 1.6509 | 1.58777 |
| 3 | 10.003 | 0.36291 | 0.35049 | 1.71087 | 1.68135 |
| 4 | 15 | 0.3702 | 0.36511 | 1.72797 | 1.71605 |
| 5 | 20.002 | 0.37463 | 0.37286 | 1.73829 | 1.73417 |
| 6 | 30.001 | 0.37977 | 0.38092 | 1.75016 | 1.75281 |
| 7 | 40.002 | 0.38295 | 0.38508 | 1.75748 | 1.76235 |
| 8 | 50.003 | 0.38518 | 0.38762 | 1.76259 | 1.76815 |
| 9 | 60.03 | 0.38638 | 0.38933 | 1.76532 | 1.77206 |
| 10 | 70.052 | 0.38762 | 0.39057 | 1.76816 | 1.77487 |
| 11 | 80.068 | 0.38905 | 0.3915 | 1.77142 | 1.77699 |
| 12 | 90.063 | 0.39005 | 0.39223 | 1.77369 | 1.77865 |
| 13 | 100.11 | 0.39092 | 0.39282 | 1.77566 | 1.77998 |
| 14 | 110.13 | 0.39154 | 0.39331 | 1.77709 | 1.78108 |
| 15 | 120.15 | 0.39241 | 0.39371 | 1.77905 | 1.782 |
| 16 | 130.16 | 0.39281 | 0.39406 | 1.77996 | 1.78278 |
| 17 | 140.18 | 0.39359 | 0.39436 | 1.78173 | 1.78346 |
| 18 | 150.19 | 0.39418 | 0.39461 | 1.78306 | 1.78404 |
| 19 | 160.13 | 0.39465 | 0.39484 | 1.78413 | 1.78456 |
| 20 | 170.21 | 0.39544 | 0.39505 | 1.7859 | 1.78502 |
| 21 | 180.22 | 0.3958 | 0.39523 | 1.78671 | 1.78543 |
| 22 | 190.23 | 0.39621 | 0.39539 | 1.78764 | 1.7858 |
| 23 | 200.24 | 0.39649 | 0.39554 | 1.78829 | 1.78614 |
| 24 | 210.24 | 0.39665 | 0.39568 | 1.78865 | 1.78644 |
| 25 | 220.25 | 0.39681 | 0.3958 | 1.78901 | 1.78672 |
| 26 | 230.25 | 0.3964 | 0.39592 | 1.78807 | 1.78698 |
| 27 | 240.25 | 0.39691 | 0.39602 | 1.78922 | 1.78722 |
| 28 | 250.25 | 0.39631 | 0.39612 | 1.78787 | 1.78744 |
| 29 | 260.26 | 0.3958 | 0.39621 | 1.78672 | 1.78765 |
| 30 | 270.24 | 0.39681 | 0.3963 | 1.78901 | 1.78784 |
| 31 | 280.26 | 0.39598 | 0.39638 | 1.78712 | 1.78802 |
| 32 | 290.25 | 0.39775 | 0.39645 | 1.79111 | 1.78819 |

Complex [CuL^{Se}(Et₂NH)](27)

MW = 624.27 g/mol, $\chi_{\text{dia}} = -393.10 \times 10^{-6} \text{ cm}^3 \text{ mol}^{-1}$

m = 37.64 mg, H = 1.000 T

| No | T(K) | $\chi \cdot T_{\text{exp.}}$ | $\chi \cdot T_{\text{calc.}}$ | μ_{exp} | $\mu_{\text{calc.}}$ |
|----|--------|------------------------------|-------------------------------|--------------------|----------------------|
| 1 | 1.999 | 0.24893 | 0.28126 | 1.41097 | 1.49979 |
| 2 | 5.001 | 0.38629 | 0.35483 | 1.75767 | 1.68458 |
| 3 | 10.003 | 0.40424 | 0.38749 | 1.79804 | 1.76038 |
| 4 | 15 | 0.40904 | 0.39956 | 1.80868 | 1.7876 |
| 5 | 20.002 | 0.41217 | 0.40586 | 1.8156 | 1.80165 |
| 6 | 30.001 | 0.41638 | 0.41237 | 1.82483 | 1.81604 |
| 7 | 39.999 | 0.4192 | 0.41574 | 1.83101 | 1.82342 |
| 8 | 50.008 | 0.42124 | 0.41781 | 1.83545 | 1.82796 |
| 9 | 60.034 | 0.42222 | 0.41923 | 1.83759 | 1.83107 |
| 10 | 70.034 | 0.42319 | 0.42027 | 1.83971 | 1.83334 |
| 11 | 80.069 | 0.42378 | 0.42107 | 1.84099 | 1.83509 |
| 12 | 90.09 | 0.42387 | 0.42172 | 1.84118 | 1.8365 |
| 13 | 100.11 | 0.42333 | 0.42225 | 1.84 | 1.83766 |
| 14 | 110.14 | 0.42305 | 0.42271 | 1.83939 | 1.83865 |
| 15 | 120.14 | 0.42274 | 0.4231 | 1.83873 | 1.83949 |
| 16 | 130.11 | 0.4224 | 0.42344 | 1.83797 | 1.84024 |
| 17 | 140.18 | 0.42226 | 0.42375 | 1.83767 | 1.84091 |
| 18 | 150.19 | 0.42244 | 0.42402 | 1.83807 | 1.84151 |
| 19 | 160.2 | 0.42247 | 0.42428 | 1.83815 | 1.84206 |
| 20 | 170.22 | 0.42272 | 0.42451 | 1.83867 | 1.84257 |
| 21 | 180.22 | 0.42291 | 0.42473 | 1.83909 | 1.84304 |
| 22 | 190.25 | 0.42304 | 0.42493 | 1.83938 | 1.84348 |
| 23 | 200.24 | 0.42351 | 0.42512 | 1.84038 | 1.8439 |
| 24 | 210.14 | 0.42361 | 0.4253 | 1.8406 | 1.84428 |
| 25 | 220.25 | 0.42409 | 0.42547 | 1.84165 | 1.84466 |
| 26 | 230.24 | 0.4246 | 0.42564 | 1.84276 | 1.84502 |
| 27 | 240.25 | 0.42528 | 0.4258 | 1.84423 | 1.84536 |
| 28 | 250.25 | 0.42566 | 0.42595 | 1.84506 | 1.84569 |
| 29 | 260.27 | 0.42572 | 0.4261 | 1.84519 | 1.846 |
| 30 | 270.26 | 0.42616 | 0.42624 | 1.84614 | 1.84631 |
| 31 | 280.27 | 0.42889 | 0.42637 | 1.85205 | 1.84661 |
| 32 | 290.26 | 0.42941 | 0.42651 | 1.85318 | 1.8469 |

Complex [CuL^{Se}(^tBuNH₂)](28)

MW = 624.27 g/mol, $\chi_{\text{dia}} = -393.10 \times 10^{-6} \text{ cm}^3 \text{ mol}^{-1}$

m = 27.51 mg, H = 1.000 T

| No | T(K) | $\chi \cdot T_{\text{exp.}}$ | $\chi \cdot T_{\text{calc.}}$ | μ_{exp} | $\mu_{\text{calc.}}$ |
|----|--------|------------------------------|-------------------------------|--------------------|----------------------|
| 1 | 1.999 | 0.3761 | 0.37539 | 1.73432 | 1.73268 |
| 2 | 4.998 | 0.39615 | 0.39793 | 1.77996 | 1.78396 |
| 3 | 10.002 | 0.40465 | 0.40425 | 1.79895 | 1.79807 |
| 4 | 15 | 0.40636 | 0.40662 | 1.80274 | 1.80332 |
| 5 | 20.001 | 0.40796 | 0.40813 | 1.8063 | 1.80667 |
| 6 | 30.002 | 0.41041 | 0.41037 | 1.8117 | 1.81162 |
| 7 | 39.999 | 0.41234 | 0.41224 | 1.81597 | 1.81574 |
| 8 | 50.002 | 0.41449 | 0.41396 | 1.82069 | 1.81953 |
| 9 | 60.034 | 0.41679 | 0.41562 | 1.82574 | 1.82318 |
| 10 | 70.048 | 0.41755 | 0.41724 | 1.8274 | 1.82672 |
| 11 | 80.072 | 0.41901 | 0.41884 | 1.8306 | 1.83021 |
| 12 | 90.081 | 0.4207 | 0.42041 | 1.83428 | 1.83365 |
| 13 | 100.08 | 0.42204 | 0.42197 | 1.83721 | 1.83706 |
| 14 | 110.12 | 0.42361 | 0.42354 | 1.84062 | 1.84046 |
| 15 | 120.15 | 0.42518 | 0.42509 | 1.84402 | 1.84383 |
| 16 | 130.16 | 0.42655 | 0.42664 | 1.84698 | 1.84718 |
| 17 | 140.18 | 0.42786 | 0.42818 | 1.84982 | 1.85052 |
| 18 | 150.18 | 0.42952 | 0.42972 | 1.85341 | 1.85385 |
| 19 | 160.2 | 0.43097 | 0.43126 | 1.85653 | 1.85717 |
| 20 | 170.14 | 0.43266 | 0.43279 | 1.86017 | 1.86045 |
| 21 | 180.21 | 0.4342 | 0.43433 | 1.86349 | 1.86376 |
| 22 | 190.22 | 0.43556 | 0.43587 | 1.8664 | 1.86705 |
| 23 | 200.24 | 0.43733 | 0.4374 | 1.87019 | 1.87033 |
| 24 | 210.23 | 0.43849 | 0.43893 | 1.87266 | 1.87359 |
| 25 | 220.24 | 0.44023 | 0.44046 | 1.87638 | 1.87686 |
| 26 | 230.24 | 0.44161 | 0.44199 | 1.87931 | 1.88011 |
| 27 | 240.27 | 0.44243 | 0.44352 | 1.88105 | 1.88337 |
| 28 | 250.25 | 0.44473 | 0.44504 | 1.88593 | 1.8866 |
| 29 | 260.26 | 0.44686 | 0.44657 | 1.89045 | 1.88983 |
| 30 | 270.24 | 0.44819 | 0.44809 | 1.89327 | 1.89305 |
| 31 | 280.23 | 0.45007 | 0.44961 | 1.89723 | 1.89627 |
| 32 | 290.25 | 0.45255 | 0.45114 | 1.90245 | 1.89949 |

Complex [CuL^{Se}(PhCH₂NH₂)]₂ (29)

MW = 1334.59 g/mol, $\chi_{\text{dia}} = -789.2 \times 10^{-6} \text{ cm}^3 \text{ mol}^{-1}$
m = 42.13 mg , H = 1.000 T

| No | T(K) | $\chi \cdot T_{\text{exp.}}$ | $\chi \cdot T_{\text{calc.}}$ | μ_{exp} | $\mu_{\text{calc.}}$ |
|----|--------|------------------------------|-------------------------------|--------------------|----------------------|
| 1 | 1.999 | 0.35792 | 0.36102 | 1.69907 | 1.70641 |
| 2 | 5 | 0.65658 | 0.64892 | 2.30124 | 2.28777 |
| 3 | 10.004 | 0.74933 | 0.74644 | 2.45841 | 2.45366 |
| 4 | 15 | 0.77557 | 0.77739 | 2.50109 | 2.50402 |
| 5 | 20.002 | 0.79007 | 0.79285 | 2.52436 | 2.5288 |
| 6 | 30.002 | 0.80528 | 0.80894 | 2.54855 | 2.55433 |
| 7 | 40.003 | 0.81475 | 0.81786 | 2.56349 | 2.56838 |
| 8 | 50.009 | 0.82102 | 0.824 | 2.57333 | 2.57799 |
| 9 | 60.032 | 0.82551 | 0.82876 | 2.58035 | 2.58543 |
| 10 | 70.034 | 0.83039 | 0.83274 | 2.58796 | 2.59162 |
| 11 | 80.077 | 0.8357 | 0.83624 | 2.59623 | 2.59708 |
| 12 | 90.095 | 0.8398 | 0.83942 | 2.6026 | 2.60201 |
| 13 | 100.11 | 0.84341 | 0.84238 | 2.60818 | 2.60659 |
| 14 | 110.13 | 0.84684 | 0.84517 | 2.61348 | 2.61091 |
| 15 | 120.15 | 0.85026 | 0.84785 | 2.61874 | 2.61504 |
| 16 | 130.12 | 0.85219 | 0.85042 | 2.62172 | 2.61899 |
| 17 | 140.17 | 0.85478 | 0.85294 | 2.6257 | 2.62287 |
| 18 | 150.18 | 0.85706 | 0.85538 | 2.6292 | 2.62663 |
| 19 | 160.19 | 0.85932 | 0.85779 | 2.63266 | 2.63032 |
| 20 | 170.21 | 0.86253 | 0.86015 | 2.63758 | 2.63394 |
| 21 | 180.23 | 0.86487 | 0.86249 | 2.64115 | 2.63751 |
| 22 | 190.24 | 0.86707 | 0.86479 | 2.64451 | 2.64103 |
| 23 | 200.24 | 0.86887 | 0.86707 | 2.64726 | 2.64451 |
| 24 | 210.24 | 0.87062 | 0.86933 | 2.64991 | 2.64795 |
| 25 | 220.16 | 0.8718 | 0.87155 | 2.65172 | 2.65134 |
| 26 | 230.24 | 0.87426 | 0.8738 | 2.65545 | 2.65475 |
| 27 | 240.25 | 0.87587 | 0.87601 | 2.65789 | 2.65812 |
| 28 | 250.25 | 0.87786 | 0.87822 | 2.66092 | 2.66146 |
| 29 | 260.28 | 0.87884 | 0.88042 | 2.6624 | 2.66479 |
| 30 | 270.25 | 0.88045 | 0.8826 | 2.66484 | 2.66808 |
| 31 | 280.26 | 0.88143 | 0.88477 | 2.66631 | 2.67137 |
| 32 | 290.26 | 0.88421 | 0.88694 | 2.67052 | 2.67465 |

Complex [L^{Se}₂ (HL^{Se})Cu₃(μ-OH)(MeCN)](30)

MW = 1711.00 g/mol, $\chi_{\text{dia}} = -1015.00 \times 10^{-6} \text{ cm}^3 \text{ mol}^{-1}$
m = 28.22 mg , H = 1.000 T

| No | T(K) | $\chi \cdot T_{\text{exp.}}$ | $\chi \cdot T_{\text{calc.}}$ | μ_{exp} | $\mu_{\text{calc.}}$ |
|----|--------|------------------------------|-------------------------------|--------------------|----------------------|
| 1 | 2 | 0.28079 | 0.3805 | 1.49854 | 1.74445 |
| 2 | 4.998 | 0.39409 | 0.39349 | 1.77532 | 1.77397 |
| 3 | 9.993 | 0.39996 | 0.39625 | 1.7885 | 1.78018 |
| 4 | 15.001 | 0.40234 | 0.3975 | 1.7938 | 1.78299 |
| 5 | 20.002 | 0.40349 | 0.39852 | 1.79637 | 1.78527 |
| 6 | 30.002 | 0.4055 | 0.40041 | 1.80085 | 1.7895 |
| 7 | 39.999 | 0.40758 | 0.40224 | 1.80544 | 1.79358 |
| 8 | 50.009 | 0.40995 | 0.40406 | 1.8107 | 1.79763 |
| 9 | 60.02 | 0.41187 | 0.4059 | 1.81494 | 1.80172 |
| 10 | 70.05 | 0.41358 | 0.40785 | 1.81869 | 1.80605 |
| 11 | 80.071 | 0.41654 | 0.41008 | 1.8252 | 1.81098 |
| 12 | 90.087 | 0.41946 | 0.41284 | 1.83158 | 1.81706 |
| 13 | 100.1 | 0.42318 | 0.4164 | 1.83967 | 1.82487 |
| 14 | 110.12 | 0.42769 | 0.42102 | 1.84946 | 1.83498 |
| 15 | 120.1 | 0.43381 | 0.42688 | 1.86264 | 1.84771 |
| 16 | 130.16 | 0.44033 | 0.43418 | 1.87659 | 1.86344 |
| 17 | 140.18 | 0.44899 | 0.44288 | 1.89494 | 1.88201 |
| 18 | 150.19 | 0.45889 | 0.45295 | 1.91573 | 1.9033 |
| 19 | 160.2 | 0.46992 | 0.46432 | 1.9386 | 1.92702 |
| 20 | 170.21 | 0.48209 | 0.47684 | 1.96355 | 1.95283 |
| 21 | 180.22 | 0.49531 | 0.49034 | 1.9903 | 1.9803 |
| 22 | 190.05 | 0.50784 | 0.50441 | 2.01531 | 2.0085 |
| 23 | 200.24 | 0.52269 | 0.51965 | 2.04457 | 2.03862 |
| 24 | 210.23 | 0.53708 | 0.53509 | 2.07252 | 2.06868 |
| 25 | 220.25 | 0.55131 | 0.55091 | 2.0998 | 2.09903 |
| 26 | 230.25 | 0.56654 | 0.5669 | 2.12861 | 2.12927 |
| 27 | 240.26 | 0.58203 | 0.58299 | 2.1575 | 2.15928 |
| 28 | 250.25 | 0.59587 | 0.59903 | 2.18301 | 2.18879 |
| 29 | 260.27 | 0.61069 | 0.61503 | 2.20999 | 2.21782 |
| 30 | 270.26 | 0.62498 | 0.63081 | 2.2357 | 2.24609 |
| 31 | 280.24 | 0.64203 | 0.64635 | 2.26598 | 2.2736 |
| 32 | 290.26 | 0.65912 | 0.6617 | 2.29594 | 2.30043 |

Complex [L^{Se}₂ (HL^{Se})Cu₃(μ-OMe)(MeOH)] (31)

MW = 1802.31 g/mol, $\chi_{\text{dia}} = -1110.00 \times 10^{-6} \text{ cm}^3 \text{ mol}^{-1}$
m = 25.85 mg , H = 1.000 T

| No | T(K) | $\chi \cdot T_{\text{exp.}}$ | $\chi \cdot T_{\text{calc.}}$ | μ_{exp} | $\mu_{\text{calc.}}$ |
|----|--------|------------------------------|-------------------------------|--------------------|----------------------|
| 1 | 2.001 | 0.4091 | 0.42433 | 1.80881 | 1.84218 |
| 2 | 5.005 | 0.43219 | 0.43993 | 1.85916 | 1.87572 |
| 3 | 10 | 0.44277 | 0.44679 | 1.88178 | 1.8903 |
| 4 | 15.003 | 0.45075 | 0.45213 | 1.89865 | 1.90156 |
| 5 | 20.002 | 0.45821 | 0.45724 | 1.91431 | 1.91228 |
| 6 | 30.001 | 0.4709 | 0.4673 | 1.94063 | 1.9332 |
| 7 | 39.994 | 0.48174 | 0.4773 | 1.96285 | 1.95378 |
| 8 | 50.007 | 0.49223 | 0.4873 | 1.9841 | 1.97414 |
| 9 | 60.032 | 0.50374 | 0.49731 | 2.00716 | 1.99431 |
| 10 | 70.069 | 0.51596 | 0.50733 | 2.03136 | 2.01429 |
| 11 | 80.045 | 0.52722 | 0.51729 | 2.05341 | 2.03397 |
| 12 | 90.098 | 0.53763 | 0.52734 | 2.07358 | 2.05364 |
| 13 | 100.11 | 0.54587 | 0.5374 | 2.08941 | 2.07313 |
| 14 | 110.13 | 0.55045 | 0.54755 | 2.09816 | 2.09263 |
| 15 | 120.13 | 0.55467 | 0.55784 | 2.10618 | 2.11219 |
| 16 | 130.16 | 0.56284 | 0.56838 | 2.12163 | 2.13206 |
| 17 | 140.18 | 0.57299 | 0.57922 | 2.14068 | 2.15229 |
| 18 | 150.2 | 0.58447 | 0.59045 | 2.16203 | 2.17307 |
| 19 | 160.2 | 0.59667 | 0.60213 | 2.18447 | 2.19445 |
| 20 | 170.22 | 0.61094 | 0.61438 | 2.21043 | 2.21665 |
| 21 | 180.22 | 0.62386 | 0.62719 | 2.23369 | 2.23965 |
| 22 | 190.24 | 0.63865 | 0.64067 | 2.26002 | 2.26358 |
| 23 | 200.24 | 0.65381 | 0.65478 | 2.28669 | 2.28837 |
| 24 | 210.16 | 0.66984 | 0.66944 | 2.31454 | 2.31385 |
| 25 | 220.26 | 0.68669 | 0.68504 | 2.34348 | 2.34066 |
| 26 | 230.24 | 0.7032 | 0.70111 | 2.37148 | 2.36795 |
| 27 | 240.25 | 0.72048 | 0.71785 | 2.40043 | 2.39605 |
| 28 | 250.25 | 0.73508 | 0.73516 | 2.42463 | 2.42476 |
| 29 | 260.27 | 0.75359 | 0.75305 | 2.45497 | 2.45409 |
| 30 | 270.25 | 0.77095 | 0.77136 | 2.4831 | 2.48375 |
| 31 | 280.27 | 0.79673 | 0.79019 | 2.52426 | 2.51389 |
| 32 | 290.27 | 0.80882 | 0.80938 | 2.54335 | 2.54423 |

Complex Bu₄N[FeL^N₂] (33)

MW = 957.19 g/mol, $\chi_{\text{dia}} = -659.83 \times 10^{-6} \text{ cm}^3 \text{ mol}^{-1}$
m = 41.34 mg , H = 1.000 T

| No | T(K) | $\chi \cdot T_{\text{exp.}}$ | $\chi \cdot T_{\text{calc.}}$ | μ_{exp} | $\mu_{\text{calc.}}$ |
|----|--------|------------------------------|-------------------------------|--------------------|----------------------|
| 1 | 1.999 | 3.60042 | 3.49383 | 5.38884 | 5.30847 |
| 2 | 5.002 | 4.2564 | 4.19331 | 5.85922 | 5.81563 |
| 3 | 10.003 | 4.37485 | 4.32874 | 5.94018 | 5.9088 |
| 4 | 14.999 | 4.36763 | 4.35518 | 5.93528 | 5.92682 |
| 5 | 20 | 4.36504 | 4.36455 | 5.93352 | 5.93319 |
| 6 | 30 | 4.36191 | 4.37128 | 5.93139 | 5.93776 |
| 7 | 40 | 4.36017 | 4.37364 | 5.93021 | 5.93936 |
| 8 | 50.002 | 4.35657 | 4.37473 | 5.92776 | 5.9401 |
| 9 | 60.034 | 4.35333 | 4.37533 | 5.92556 | 5.94051 |
| 10 | 70.047 | 4.35207 | 4.37569 | 5.9247 | 5.94075 |
| 11 | 80.068 | 4.35572 | 4.37592 | 5.92718 | 5.94091 |
| 12 | 90.095 | 4.35782 | 4.37608 | 5.92861 | 5.94102 |
| 13 | 100.07 | 4.35724 | 4.37619 | 5.92822 | 5.94109 |
| 14 | 110.12 | 4.35734 | 4.37628 | 5.92828 | 5.94116 |
| 15 | 120.14 | 4.35941 | 4.37634 | 5.92969 | 5.9412 |
| 16 | 130.16 | 4.35716 | 4.37639 | 5.92816 | 5.94123 |
| 17 | 140.18 | 4.35798 | 4.37643 | 5.92872 | 5.94126 |
| 18 | 150.19 | 4.35901 | 4.37646 | 5.92942 | 5.94128 |
| 19 | 160.2 | 4.35838 | 4.37649 | 5.92899 | 5.9413 |
| 20 | 170.22 | 4.36221 | 4.37651 | 5.9316 | 5.94131 |
| 21 | 180.22 | 4.36104 | 4.37653 | 5.9308 | 5.94132 |
| 22 | 190.22 | 4.36261 | 4.37655 | 5.93187 | 5.94134 |
| 23 | 200.15 | 4.36005 | 4.37656 | 5.93013 | 5.94135 |
| 24 | 210.24 | 4.36354 | 4.37657 | 5.9325 | 5.94135 |
| 25 | 220.25 | 4.36493 | 4.37658 | 5.93345 | 5.94136 |
| 26 | 230.24 | 4.36504 | 4.37659 | 5.93352 | 5.94137 |
| 27 | 240.26 | 4.36766 | 4.3766 | 5.9353 | 5.94137 |
| 28 | 250.26 | 4.36891 | 4.3766 | 5.93615 | 5.94137 |
| 29 | 260.26 | 4.36832 | 4.37661 | 5.93575 | 5.94138 |
| 30 | 270.23 | 4.37131 | 4.37661 | 5.93778 | 5.94138 |
| 31 | 280.26 | 4.37102 | 4.37662 | 5.93758 | 5.94139 |
| 32 | 290.25 | 4.37072 | 4.37662 | 5.93738 | 5.94139 |

Complex [MnL^N₂] (34)

MW = 649.73 g/mol, $\chi_{\text{dia}} = -404.20 \times 10^{-6} \text{ cm}^3 \text{ mol}^{-1}$
m = 38.92 mg , H = 1.000 T

| No | T(K) | $\chi \cdot T_{\text{exp.}}$ | $\chi \cdot T_{\text{calc.}}$ | μ_{exp} | $\mu_{\text{calc.}}$ |
|----|--------|------------------------------|-------------------------------|--------------------|----------------------|
| 1 | 2 | 1.50576 | 1.62344 | 3.48495 | 3.61857 |
| 2 | 5 | 1.74042 | 1.78139 | 3.74667 | 3.79051 |
| 3 | 10.004 | 1.79942 | 1.80774 | 3.80965 | 3.81844 |
| 4 | 15 | 1.80463 | 1.81294 | 3.81516 | 3.82393 |
| 5 | 20.003 | 1.80902 | 1.81493 | 3.81979 | 3.82603 |
| 6 | 30.001 | 1.8114 | 1.81667 | 3.82231 | 3.82786 |
| 7 | 40.002 | 1.81332 | 1.81761 | 3.82433 | 3.82885 |
| 8 | 50.008 | 1.81449 | 1.81831 | 3.82557 | 3.82959 |
| 9 | 60.017 | 1.81462 | 1.81892 | 3.8257 | 3.83023 |
| 10 | 70.049 | 1.81546 | 1.81949 | 3.82659 | 3.83083 |
| 11 | 80.068 | 1.81732 | 1.82003 | 3.82855 | 3.8314 |
| 12 | 90.07 | 1.81988 | 1.82056 | 3.83124 | 3.83196 |
| 13 | 100.11 | 1.82005 | 1.82109 | 3.83142 | 3.83252 |
| 14 | 110.11 | 1.82178 | 1.8216 | 3.83324 | 3.83305 |
| 15 | 120.11 | 1.82175 | 1.82211 | 3.83321 | 3.83359 |
| 16 | 130.15 | 1.82288 | 1.82262 | 3.8344 | 3.83413 |
| 17 | 140.18 | 1.82288 | 1.82313 | 3.8344 | 3.83466 |
| 18 | 150.2 | 1.82464 | 1.82364 | 3.83625 | 3.8352 |
| 19 | 160.19 | 1.82565 | 1.82414 | 3.83731 | 3.83572 |
| 20 | 170.2 | 1.82712 | 1.82465 | 3.83886 | 3.83626 |
| 21 | 180.22 | 1.82883 | 1.82515 | 3.84065 | 3.83679 |
| 22 | 190.23 | 1.82937 | 1.82566 | 3.84122 | 3.83732 |
| 23 | 200.24 | 1.83132 | 1.82616 | 3.84327 | 3.83785 |
| 24 | 210.24 | 1.83174 | 1.82666 | 3.84371 | 3.83837 |
| 25 | 220.26 | 1.83324 | 1.82716 | 3.84528 | 3.8389 |
| 26 | 230.25 | 1.83391 | 1.82767 | 3.84598 | 3.83943 |
| 27 | 240.25 | 1.83295 | 1.82817 | 3.84498 | 3.83996 |
| 28 | 250.25 | 1.83331 | 1.82867 | 3.84535 | 3.84048 |
| 29 | 260.28 | 1.83358 | 1.82917 | 3.84564 | 3.84101 |
| 30 | 270.24 | 1.8346 | 1.82967 | 3.84671 | 3.84153 |
| 31 | 280.15 | 1.83669 | 1.83017 | 3.8489 | 3.84206 |
| 32 | 290.24 | 1.84074 | 1.83067 | 3.85314 | 3.84258 |

Complex Bu₄N[MnL^N₂] (35)

MW = 892.20 g/mol, $\chi_{\text{dia}} = -616.20 \times 10^{-6} \text{ cm}^3 \text{ mol}^{-1}$
m = 38.05 mg , H = 1.000 T

| No | T(K) | $\chi \cdot T_{\text{exp.}}$ | $\chi \cdot T_{\text{calc.}}$ | μ_{exp} | $\mu_{\text{calc.}}$ |
|----|--------|------------------------------|-------------------------------|--------------------|----------------------|
| 1 | 2 | 1.96879 | 2.48346 | 3.98491 | 4.47556 |
| 2 | 5.005 | 2.67305 | 2.84107 | 4.64325 | 4.78695 |
| 3 | 10.003 | 2.91702 | 2.90452 | 4.85052 | 4.84011 |
| 4 | 15.001 | 2.94529 | 2.91672 | 4.87396 | 4.85027 |
| 5 | 20.002 | 2.94469 | 2.92103 | 4.87347 | 4.85385 |
| 6 | 30 | 2.93295 | 2.92412 | 4.86374 | 4.85642 |
| 7 | 40.001 | 2.92176 | 2.9252 | 4.85446 | 4.85731 |
| 8 | 50.008 | 2.92192 | 2.9257 | 4.85459 | 4.85773 |
| 9 | 60.031 | 2.92741 | 2.92597 | 4.85915 | 4.85795 |
| 10 | 70.05 | 2.92772 | 2.92614 | 4.85941 | 4.85809 |
| 11 | 80.066 | 2.92248 | 2.92624 | 4.85505 | 4.85818 |
| 12 | 90.092 | 2.91859 | 2.92632 | 4.85182 | 4.85824 |
| 13 | 100.11 | 2.9136 | 2.92637 | 4.84767 | 4.85828 |
| 14 | 110.12 | 2.91345 | 2.92641 | 4.84755 | 4.85832 |
| 15 | 120.15 | 2.91259 | 2.92644 | 4.84683 | 4.85834 |
| 16 | 130.11 | 2.91095 | 2.92646 | 4.84547 | 4.85836 |
| 17 | 140.17 | 2.91144 | 2.92648 | 4.84588 | 4.85838 |
| 18 | 150.19 | 2.91364 | 2.92649 | 4.84771 | 4.85838 |
| 19 | 160.2 | 2.91418 | 2.92651 | 4.84816 | 4.8584 |
| 20 | 170.2 | 2.9152 | 2.92652 | 4.849 | 4.85841 |
| 21 | 180.21 | 2.91719 | 2.92652 | 4.85066 | 4.85841 |
| 22 | 190.22 | 2.91668 | 2.92653 | 4.85023 | 4.85842 |
| 23 | 200.23 | 2.91928 | 2.92654 | 4.8524 | 4.85843 |
| 24 | 210.24 | 2.92007 | 2.92654 | 4.85305 | 4.85843 |
| 25 | 220.24 | 2.9229 | 2.92655 | 4.8554 | 4.85843 |
| 26 | 230.26 | 2.92713 | 2.92655 | 4.85892 | 4.85843 |
| 27 | 240.25 | 2.92677 | 2.92655 | 4.85862 | 4.85843 |
| 28 | 250.25 | 2.92849 | 2.92656 | 4.86004 | 4.85844 |
| 29 | 260.27 | 2.92914 | 2.92656 | 4.86058 | 4.85844 |
| 30 | 270.26 | 2.92878 | 2.92656 | 4.86028 | 4.85844 |
| 31 | 280.27 | 2.93121 | 2.92656 | 4.8623 | 4.85844 |
| 32 | 290.27 | 2.93303 | 2.92657 | 4.86381 | 4.85845 |

Complex Bu₄N[CrL^N₂] (36)

MW = 889.26 g/mol, $\chi_{\text{dia}} = -616.17 \times 10^{-6} \text{ cm}^3 \text{ mol}^{-1}$
m = 32.25 mg, H = 1.000 T

| No | T(K) | $\chi \cdot T_{\text{exp.}}$ | $\chi \cdot T_{\text{calc.}}$ | μ_{exp} | $\mu_{\text{calc.}}$ |
|----|--------|------------------------------|-------------------------------|--------------------|----------------------|
| 1 | 1.999 | 1.66263 | 1.64865 | 3.66198 | 3.64655 |
| 2 | 5 | 1.80734 | 1.81202 | 3.81802 | 3.82296 |
| 3 | 10.003 | 1.84224 | 1.83961 | 3.85471 | 3.85196 |
| 4 | 15 | 1.84364 | 1.8453 | 3.85617 | 3.85791 |
| 5 | 20.001 | 1.84519 | 1.84769 | 3.85779 | 3.86041 |
| 6 | 29.999 | 1.84735 | 1.85013 | 3.86005 | 3.86295 |
| 7 | 40 | 1.84793 | 1.85175 | 3.86066 | 3.86464 |
| 8 | 50.008 | 1.85025 | 1.85312 | 3.86308 | 3.86607 |
| 9 | 60.024 | 1.85127 | 1.85439 | 3.86414 | 3.8674 |
| 10 | 70.031 | 1.85092 | 1.85562 | 3.86378 | 3.86868 |
| 11 | 80.07 | 1.85434 | 1.85683 | 3.86735 | 3.86994 |
| 12 | 90.097 | 1.85734 | 1.85802 | 3.87047 | 3.87118 |
| 13 | 100.1 | 1.8577 | 1.85921 | 3.87085 | 3.87242 |
| 14 | 110.12 | 1.86021 | 1.86039 | 3.87346 | 3.87365 |
| 15 | 120.16 | 1.86112 | 1.86156 | 3.87441 | 3.87487 |
| 16 | 130.16 | 1.86212 | 1.86273 | 3.87545 | 3.87609 |
| 17 | 140.17 | 1.86235 | 1.8639 | 3.87569 | 3.8773 |
| 18 | 150.18 | 1.86417 | 1.86507 | 3.87758 | 3.87852 |
| 19 | 160.19 | 1.86628 | 1.86623 | 3.87978 | 3.87972 |
| 20 | 170.13 | 1.86664 | 1.86739 | 3.88015 | 3.88093 |
| 21 | 180.22 | 1.86946 | 1.86856 | 3.88308 | 3.88215 |
| 22 | 190.22 | 1.8694 | 1.86973 | 3.88302 | 3.88336 |
| 23 | 200.23 | 1.87141 | 1.87089 | 3.88511 | 3.88457 |
| 24 | 210.24 | 1.87366 | 1.87205 | 3.88744 | 3.88577 |
| 25 | 220.25 | 1.87483 | 1.87322 | 3.88865 | 3.88698 |
| 26 | 230.25 | 1.8757 | 1.87438 | 3.88956 | 3.88819 |
| 27 | 240.24 | 1.87588 | 1.87554 | 3.88974 | 3.88939 |
| 28 | 250.24 | 1.87581 | 1.8767 | 3.88967 | 3.89059 |
| 29 | 260.27 | 1.87669 | 1.87786 | 3.89058 | 3.89179 |
| 30 | 270.24 | 1.87712 | 1.87902 | 3.89103 | 3.893 |
| 31 | 280.26 | 1.87932 | 1.88019 | 3.89331 | 3.89421 |
| 32 | 290.26 | 1.88041 | 1.88135 | 3.89444 | 3.89541 |

3) Curriculum Vitae

Personal:

Name: TAPAN KANTI PAINE
Date of Birth: 02.01.1976
Place of Birth: Simlapal, West Bengal, India
Nationality: Indian
Marital status: Married

Education:

1980-1984: Kustora Primary School, West Bengal, India
1984-1991: Dhangori Sammilani High School, West Bengal, India
1991-1993: Vivekananda College, Calcutta, India
1993-1996: New Alipore College, Calcutta, India
(Bachelor of Science in Chemistry)
1996-1998: Indian Institute of Technology, Kharagpur, India
(Master of Science, Organic Chemistry with Prof. Dr. T. K. Sarkar)
1998-1999: Post-M.Sc project work at National Chemical Laboratory, Pune, India
with Dr. M. K. Gurjar
August 1999-
November 1999: German language course at Goethe-Institut, Göttingen, Germany
From December
1999- : Doktorand at the Max-Planck-Institut für Strahlenchemie, Mülheim an der
Ruhr, Germany (with Prof. Dr. P. Chaudhuri and Prof. Dr. K. Wieghardt)

Scholarship:

1997: Qualified in the National Eligibility Test, eligible for the lectureship and
research fellowship (Govt. of India)
1998: Qualified in GATE (Graduate Aptitude Test in Engineering, Chemistry)
with 97.79 percentile
August 1999: Max-Planck-Fellowship for German language course
December 1999: DFG-Fellowship for Ph.D. work with Prof. Dr. P. Chaudhuri